To the Graduate Council:

I am submitting herewith a dissertation written by Timothy Alan Whitley entitled "Cooper Minima in the Photoelectron Dynamic Spectra of Small Molecules: Continuum Multiple Scattering X-alpha Calculations." I have examined the final copy of this dissertation for form and content and recommend that it be accepted in partial fulfillment of the requirements for the degree of Doctor of Philosophy, with a major in Chemistry.

F. A. Grimm, Major Professor

We have read this dissertation
and recommend its acceptance:

John E Bloor

Harold C. Schweinler

Accepted for the Council:

The Graduate School

COOPER MINIMA IN THE PHOTOELECTRON DYNAMIC SPECTRA OF SMALL MOLECULES: CONTINUUM MULTIPLE SCATTERING X-ALPHA CALCULATIONS

A Dissertation
Presented for the
Doctor of Philosophy
Degree
The University of Tennessee, Knoxville

Timothy Alan Whitley
June 1985

ACKNOWLEDGEMENTS

I would like to express my gratitude to Drs. F.A. Grimm and T.A. Carlson for sharing their knowledge and extending their patience over the course of my graduate studies.

I acknowledge with thanks both the indispensable aid provided by the Eastman Kodak Company in the form of a three year Kodak Fellowship and the unrequited support of the University of Tennessee Computing Center and staff in the form of resources and consultation.

Thanks are also due the following: the staff of the Synchrotron Radiation Center at Stoughton, Wisconsin, for their inexplicable trust in my laboratory technique, Dr. H. Schweinler for acting as mediator between theoretical physics and myself, and Dr. J.E. Bloor and Ron Sherrod whose antics and advice were an integral part of my graduate career.

Although the above are deserving of thanks, my greatest and warmest thanks are reserved for my wife, Leslie, both for her typing and for her acceptance of Archilocus' proverb: "The fox knows many things, the hedgehog only one--one big one."

ABSTRACT

Results of multiple scattering X-alpha calculations are presented for the photoionization cross sections and angular parameter as a function of energy from one-tenth to about five Ry. Systems presented are: the noble gases, argon, krypton, and xenon; the halogen atoms, chlorine, bromine, and iodine; the hydrogen halides, HCl, HBr, and HI; and the homonuclear dihalogens, Cl_2, Br_2, and I_2.

Particular attention is paid to energy regions of cross section minima (Cooper minima), and energy regions of cross section maxima (shape resonances). The effects of molecule formation on these cross section extrema are discussed.

The theoretical molecular results presented are compared with available experimental results.

A brief treatment of the concepts of angular resolved photoemission and a brief treatment of the multiple scattering X-alpha formalism are presented.

TABLE OF CONTENTS

Chapter Page

LIST OF TABLES

LIST OF FIGURES

Figure Page

Figure Page

Figure Page

Figure Page

LIST OF SYMBOLS

PI photoionization

PES photoelectron spectroscopy

PED photoelectron dynamics

β angular asymmetry parameter

σ_{tot} cross section

PED parameters σ_{tot} and β

CM Cooper minimum [minima]

SR shape resonance(s)

Xα-SW X-alpha scattered wave

MSXα multiple scattering X-alpha

A.O. atomic orbital(s)

M.O. molecular orbital(s)

LCAO linear combination of atomic orbitals

L = (l, m) angular momentum quantum numbers

s, p, d l = 0, 1, 2 orbital, channel, or partial wave

σ, π, δ m_l = 0, 1, 2 orbital, channel, or partial wave (m_l is labeled m in this work)

$\sum_i$ summation over full (suppressed) range of index "i"

X an arbitrary halogen atom

HX an arbitrary hydrogen halide molecule

X_2 an arbitrary dihalogen molecule

CHAPTER I

INTRODUCTION

The interaction of radiation with matter is of interest to basic as well as to practical or applied scientists. The concepts and theory of quantum scattering provide formalisms and experimental guidelines which reveal the structure of the target particles involved. Photoelectron spectroscopy may be viewed as a probe of radiation's interaction with matter which can be treated as a scattering process.

Photoelectron spectroscopy or dynamics, or simply photoemission, involves an atomic or molecular (or solid!) target beset by photons, which consequently emits outgoing electrons. "Photoelectron spectroscopy" (PES) is usually taken to denote either this entire field of research concerned with photoemission--the term "photoionization" (PI) spectroscopy is used similarly--or to specify an experiment which measures the variations in electron intensity with electron energy for an incident photon of constant energy (i.e., wavelength). This latter experiment is usually aimed at extraction of ionization energies or the energies of other processes and their relative intensities. The title "photoelectron dynamics" (PED) is given to studies which measure the variation with photon energy of parameters describing the photoelectrons' spatial distribution. (Recently, spin distributions have become measurable.) In spin-unresolved measurements, the energy variation of only two parameters suffices to describe the photoelectrons' spatial distribution. One parameter, the total photoionization cross section, is a measure of the intensity of emission of electrons. The other parameter, the angular distribution parameter, indicates how the photoelectron emission will be distributed in space. We shall call these two parameters together the PED parameters.

A major motivation for pursuing photelectron dynamics in particular is the same as that for pursuing spectroscopy in general: an historically successful theory, quantum theory, which purports to describe microscopic events and situations, has been found to suffer important tests when used to interpret or predict results of

spectroscopic experiments. We have a theory of which we ask detailed questions, and the success or failure of the answers affects future formulations of that theory.

The theoretical calculations presented in this dissertation are based on formalisms and concepts with extensive roots. We use a computer code for calculating the PED parameters which was written in large part by Davenport[1] based on a photoionization formalism of Dehmer and Dill[2,3] which was in turn based on the Xα bound state formalism (References 4, 5, 6, 7). Our particular implementation of these codes has been described by Grimm.[8]

The theoretical picture sufficient to successfully describe photoelectron dynamics must be good, at least, it must be better than that sufficient to successfully predict ionization energies. Applying Cooper's self-criticism[9] to the present work:

> However, the most important result of these calculations is not that they provide a method for computing cross sections [or angular parameters] to a fair degree of accuracy in any given spectral range, but that they give a reasonable estimate of the spectral shape [that is, energy dependence] of the cross section [and angular parameter] over a broad spectral range.

Although our idea of a "broad spectral range" (sometimes four rydbergs) may differ from Cooper's idea (usually ten rydbergs), the point of the comment is the same: the methods used provide a survey of molecules and trends of effects.

In this dissertation, we shall be concerned with the area above, but within 100 eV of, the ionization threshold. This is the region where cross sections are large (where most oscillator strength is concentrated) and where many interesting features are found. These include shape resonances and the so-called autoionization. Some may be described as one-electron processes, others may require electron interaction refinements. There exist a number of excellent treatments of photoemission (References 10, 11, 12, 13, 14).

Primarily, we shall be concerned here with describing only one of these features, the Cooper minimum. The description of the origins of Cooper minima is straightforward in atoms using independent particle nonrelativistic atomic concepts.

The Cooper minimum (CM) is named for John Cooper, who performed survey calculations[9] on atomic PED showing the widespread occurrence of cross section minima in the valence orbitals. The gist of his explanation is as follows. The cross section is a non-negative, measurable quantity which at a given incident photon energy indicates the intensity of emitted electrons which leave behind an ion in a specific state. This energy dependent cross section in turn is linked to the sum of squares of transition matrix elements in the theory. These matrix elements are signed quantities for which a change in sign with changing energy is possible. A change in sign requires that the matrix element pass through zero and thus that the cross section intensity quantity (which depends on the square of matrix elements) experience a minimum. This minimum is called the Cooper minimum, and rules for its appearance in atoms may be formulated.[15] Basically, a CM occurs for hydrogenic atomic orbitals (A.O.'s) whose radial part shows nodes (apart from the origin). This excludes the occurence of CM in the outermost subshell of each principal shell: 1s, 2p, 3d, and 4f. Any other A.O. may show a CM. Many surveys of atomic calculations have been published which confirm that the CM is a widespread phenomenon in atoms.

At this point, the uninitiated might ask, "If it is found in atoms, would it not be found in molecules (which are comprised of atoms)?" Because our understanding of the CM phenomenon depends upon hydrogenic A.O. concepts and the description of molecular orbitals is known to involve complications on A.O.'s due to separated nuclear charge, and bonding and lone pair considerations, we expect CM in molecules to be much more complicated than in atoms. Nevertheless, the answer is yes, CM were found in theoretical results on H_2S[16] but were confirmed by only a single, line source experimental point.[17] Full energy dependent PED experimental confirmation of molecular CM awaited the synchrotron source work on CS_2 by Carlson, et al.[18] (with associated theoretical calculations by Grimm[8]). In this and in companion studies on CCl_4[19] and Cl_2,[20] the authors noted (as did Roche, et al.[16]) that lone pair orbitals of the molecules show PED curves similar to those of the atomic orbitals which make up the M.O.'s. Carlson, et al., went on to show that bonding orbitals display different,

"weakened" behavior around the energy of the CM. They christened this behavior the "partial Cooper minimum." Workers since have held out the hope that the comparison of lone pair to bonding molecular orbitals in experiment and theory may elucidate and confirm the differences found in theory for these two types of M.O.

T.A. Carlson and M.O. Krause are investigators at Oak Ridge National Laboratory, and F.A. Grimm is a professor at University of Tennessee at Knoxville. They travel to Stoughton, Wisconsin, to perform experiments at the Synchrotron Radiation Center operated by University of Wisconsin at Madison. There they are joined by J.W. Taylor of University of Wisconsin's Chemistry department and by various guest scientists, graduate students, and staff of all the institutions involved. The ORNL/Wisconsin group has performed PED experiments on a number of molecules showing CM, including CS_2 and COS,[21,18] CCl_4,[19] Cl_2,[20] HCl,[22] HBr and CH_3Br,[23] HI and CH_3I,[24] $SiCl_4$,[25] the freons, CF_xCl_{4-x},[26] and $Cl_2C{=}CH_2$.[27] See Reference 28 for a recent review of this group's activities.

The calculations presented in this dissertation were begun in "support" of the Wisconsin experimental studies but were extended into a survey of some small group VIIA molecules: the hydrogen halides and homonuclear dihalogens. This dissertation demonstrates: the behavior of the CM in molecules with respect to its behavior in atoms; the behavior of CM among various molecules of the same and of different type; and the behavior of the CM among different orbitals in a given molecule or atom. Because we wish to present the dihalogen molecules, we must introduce the concept of a shape resonance (SR). These are widespread features which have been studied extensively in molecules as well as atoms.

Plan of Dissertation

A synopsis of this dissertation is as follows.

In Chapter II, the concepts and bases of photoionization are reviewed. The transition matrix element and its relation to the cross section are introduced. It is shown that the use of slit detectors demands that we consider the angular distribution of photoelectrons.

Chapter III presents the theoretical formalism and approximations of the X-alpha scattered wave (Xα-SW) model of both the initial bound and final continuum (unbound electron) states. For the most part, we follow the treatment and notation of Davenport.

In Chapter IV, we explain Cooper minima and shape resonances in terms of our independent electron model. Argon 3p is used as an example of atomic CM. Xenon 4d is used as an example of atomic SR, and N_2 as an example of molecular SR.

Chapter V contains the results of our calculations on the noble gas atoms, argon, krypton, and xenon, and on the halogen atoms, chlorine, bromine, and iodine. The results for the noble gases are not state-of-the-art but still may be compared to experiment by keeping in mind the limitations of the model used. For ease of comparison with the molecules, in our calculations on the halogen atoms, we ignored their open shell nature entirely. The results are unsuitable for comparison to experiment (for the effects of open shells are known to be important). By presenting both the noble gases and our "halogens," we may see the small differences between the two, we may compare the noble gases to experiment, and we may compare the "halogens" to our molecular calculations.

Chapters VI and VII contain the molecular calculational results for the hydrogen halides, HCl, HBr, and HI, and for the homonuclear dihalogens, Cl_2, Br_2, and I_2, respectively. Model calculations which elucidate the "partial Cooper minimum" also are discussed.

The five appendices present more details of our methods and results.

CHAPTER II

PHOTOIONIZATION CONCEPTS

As stated in the Introduction, photoionization (PI) is a spectroscopy of photon in/electron out; studies of different aspects and energy ranges are given distinct names. The concepts of PI have been treated excellently by several authors (References 10, 29, 11, 14, 12, 13). The microscopic physical situation involves a vacuum ultraviolet or higher energy photon ($h\nu$) impinging upon and being fully absorbed by a molecule or atom (M) in its ground electronic and vibrational state. This target then emits an electron (e^-) leaving behind an ion (M^+). We may schematize the event as a reaction:

$$M + h\nu \rightarrow M^+ + e^-. \qquad \text{Eq. II-1}$$

The "photoelectron" bears away a kinetic energy equal to the difference of the photon energy and the sum of the electron's binding and the ion's excitation energy. In other words, the energy of the photon is spent in unbinding the electron, sending it away with some kinetic energy, and possibly in exciting the ion left behind.

This energy balance is stated arithmetically in a modified form of the Einstein photoelectric relation for photoionization of a ground state molecule or atom:

$$h\nu = IE + KE + EE. \qquad \text{Eq. II-2}$$

$h\nu$ represents the energy of the photon, IE is the ionization energy for the orbital or process of interest (i.e., the "unbinding energy" for the electron),

$$IE = \begin{pmatrix}\text{total energy of the final} \\ \text{ion in its ground state}\end{pmatrix} - \begin{pmatrix}\text{total energy of the initial} \\ \text{molecule in its ground state}\end{pmatrix}$$

(IE is often called IP, for "ionization potential.") KE stands for the photoelectron's kinetic energy, and EE is the excitation energy (translational, rotational, and vibrational) of the resultant ion. Using this relation, we can understand the following basic PES experiment and begin to interpret its results.

The starting point of this experiment is a source of monochromatic light--perhaps from monochromatized synchrotron radiation or from an electric discharge line source. This light is generally collimated into a beam and caused to fall on the sample--in our case a sub-atmospheric pressure gas. If sufficient energy is absorbed, the gas will be ionized and electrons will be produced. In most modern experiments, in order to increase signal-to-noise and to ease data analysis, the electrons are collected over only a narrow kinetic energy band, and this band is swept over the entire range of interest. This form of data collection yields peaks in electron intensity at photoelectron kinetic energies which indicate processes of energy equal to IE + EE. As we sweep kinetic energy, when KE = hν - (IE + EE), electrons of binding energy IE + EE will be liberated from every molecule that absorbs a photon.

Rigorously speaking, the ionization energy is the energy difference between the initial ground state and the final ionized state. According to the approximation known as Koopmans' theorem, however, the IE for an orbital is equal in magnitude to the orbital's binding energy or energy eigenvalue ($-\varepsilon_j$):

$$IE_j = -\varepsilon_j. \qquad \text{Eq. II-3}$$

Koopmans' theorem assumes that the ion does not relax around the vacancy left by the outgoing photoelectron.

An example spectrum from a PES experiment for Cl_2 is shown in Figure II-1. The major processes have all been interpreted as resulting from single-electron direct photoionization and are labelled by the bound orbital from which the photoelectron originates.

Combining Koopmans' theorem with the Einstein photoelectric relation and noting that the photon energy is fixed in this type of experiment, we see

$$\varepsilon_j - EE = KE - h\nu. \qquad \text{Eq. II-4}$$

Orbital energies may now be extracted from the locations of the peaks in Figure II-1.

At higher resolution, each peak is seen to be a band of vibrational peaks, showing that the ion may be left in an electronic state with differing degrees of vibrational excitation. At the energy of the most intense point of each band is the most probable

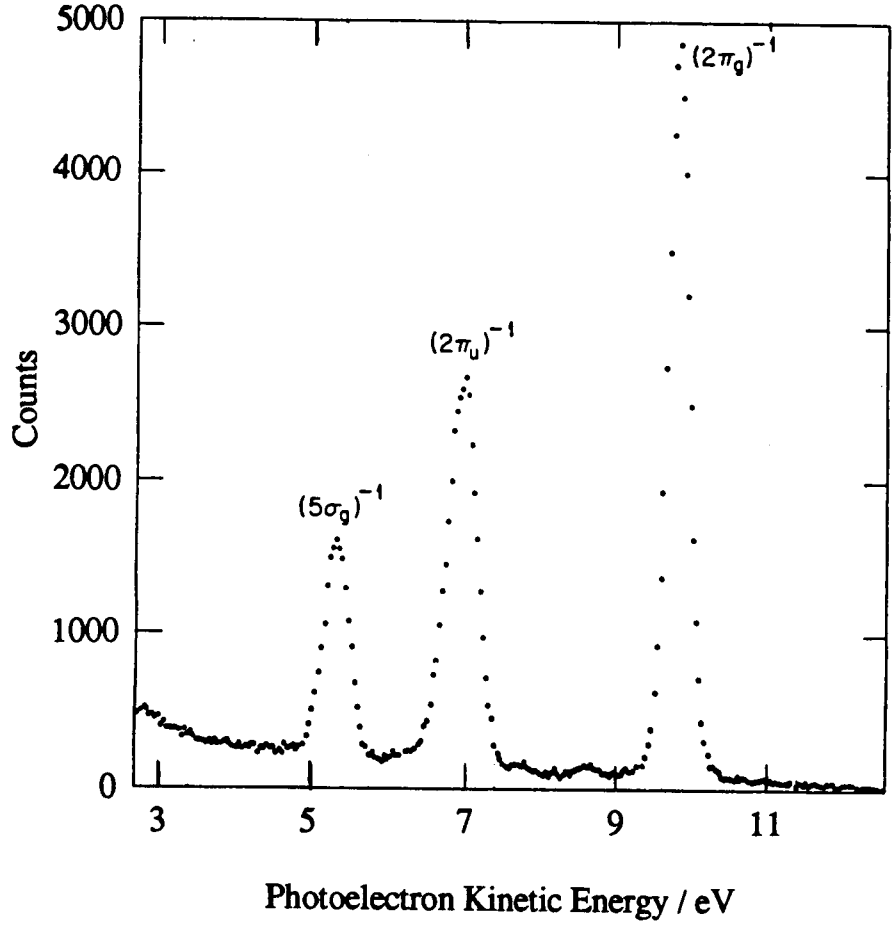

II-1. Photoelectron spectrum of Cl_2 at 21.2 eV incident photon energy. Spectrum was measured at the "magic angle," $\theta_m = 55.6°$.

transition (from the ground state to that particular vibrational state) for that electronic state of the ion. This is the energy often reported as the result of PES experiments, and it is called the "vertical ionization energy" (IE_v). The point where EE = 0 is called the "adiabatic ionization energy" (IE_a). IE_a is the minimum energy needed to ionize a molecule to a specific electronic state of the ion; IE_v is the energy needed to ionize the molecule to a vibrational level of a specific electronic state of the ion which has the maximum probability of being the result of photoionization.

If the time variation of the photon flux is known or is, at least, "well-behaved," then the number of electrons detected per unit time at a given photoelectron kinetic energy is related to the probability of the transition. In a causal account of the process, this probability should depend on the "nature" of the transition which should involve the starting and ending states and the means of transit. All this is summarized in the equation known as Fermi's Golden Rule derived from time dependent perturbation theory:[30]

$$W_{fi} = \frac{P_{fi}(t)}{t} = \frac{(2\pi)^2}{h} | V_{fi} |^2 \, n(h\nu). \qquad \text{Eq. II-5}$$

W_{fi} is the transition rate, the number of transitions from the initial state "i" to the final state "f" per unit time. $P_{fi}(t)$ is the probability that a molecule be found in state "f" at time "t" (or more accurately in the frequency picture of probability, it is the fraction of molecules in an "ensemble" that are found in "f" at "t," starting from "i"). V_{fi} is the matrix element of the transition matrix element of the perturbation--in Dirac notation, $\langle\psi_f|V_0|\psi_i\rangle$--when the perturbation hamiltonian is given by $H' = V_0 \times$ (a cyclic time function), and $|\psi_f\rangle$ and $|\psi_i\rangle$ are space functions. n(hν) is the number of states per unit energy in the neighborhood of hν.

If we are collecting electrons with a given kinetic energy--a specific final state--then n(hν) is proportional to a Dirac delta function, $\delta(E_f-E_i- h\nu)$. The matrix

element V_{fi} influences the difference in transition rate between states. Its influence will be the one of interest to us.

In a one-electron picture, this matrix element reduces from one containing the full wavefunctions to one dependent only on the orbital being ionized and the final free electron wavefunction. The initial orbital is described by a wavefunction in the usual sense: if the target molecule is in its ground state, |i> is bound and of molecular dimensions. |f> is a different case, however;[11] it describes an electron with an energy above the ionization limit. (This limit is known as the ionization threshold and is defined as ion plus zero kinetic energy electron an infinite distance away.) Thus, this positive energy electron is free or unbound and has appreciable probability amplitude throughout all space. This type of wavefunction is called a continuum wave, because solutions to the Schrödinger equation exist at all positive energies with any symmetry, and these solution form a continuum.

To find the form of the one-electron continuum wavefunction for an atom, we must solve the Schrödinger equation in Rydberg atomic units,

$$\{ \nabla^2 + (\varepsilon - V) \} \psi(\mathbf{r}) = 0 \qquad \text{Eq. II-6}$$

for $\varepsilon > 0$, and its radial part, after separation of variables,

$$\{ d^2/dr^2 - l(l+1)/r^2 + (\varepsilon - V) \} P_{\varepsilon l}(r) = 0. \qquad \text{Eq. II-7}$$

At large r from the nucleus, the r^{-2} term becomes small, as do the electron repulsion terms in V. This leaves a true wave equation whose solution is simply sinusoidal at large r. Near the nucleus, the coulombic interaction of the electron with other electrons and the nucleus are important and the wavefunction deviates from a pure sine wave. As the continuum electron's energy increases, its wavelength decreases as shown in Figure II-2.

The feature of having probability amplitude throughout all space makes analytical representation of these orbitals difficult; the common methods for solving the Schrödinger equation, those of separation of variables and partial wave expansion, require the retention of many terms (some corresponding to high angular momenta) which are cumbersome to handle.

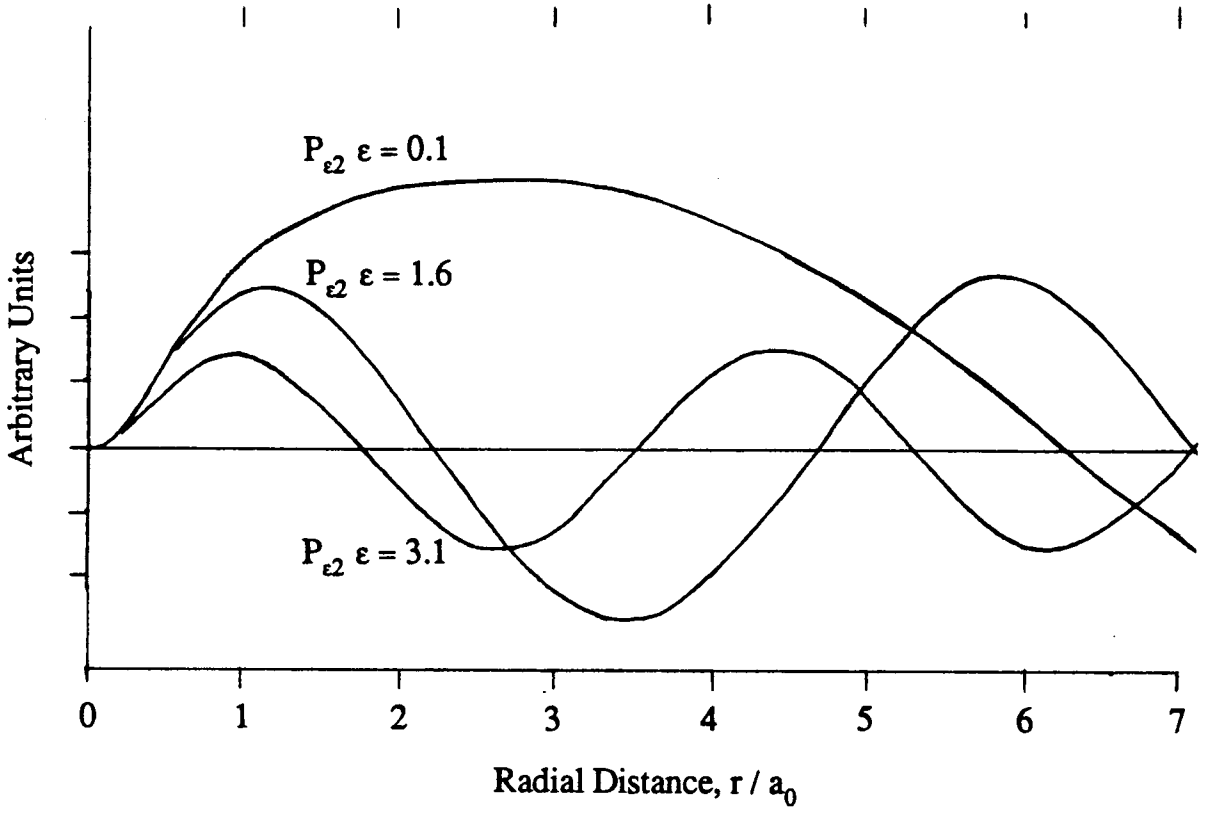

II-2. Continuum (l = 2) radial wavefunctions for argon at 0.1, 1.6, and 3.1 Ry photoelectron kinetic energy. Normalization has been ignored.

In this transition from bound to free electron at the low energies considered, the photon needs not be treated as a wave or a particle; it needs only be thought of as an electric field switched on and off with the passing of each photon. This is the dipole approximation--that the photon energy is low, and thus that its wavelength is large compared to molecular dimensions. Therefore the transient field on the transiting electron is small. The result of the dipole approximation is to render much easier the expansion of the transition operator. What was potentially an infinite series is only one term, the dipole term, after application of the approximation. This approximation serves very accurately for our purposes to about 1 keV photon energy.

The space in which our theoretical experiment takes place is permeated by the symmetry of the molecular potential. Hence, all wavefunctions and operators may be classified according to irreducible representations of the symmetry group of the molecule. Because we use calculus so extensively, integrals are quite common in theoretical work, and a certain result[31] of group theory is found to be useful. This result is, of course, that which gives us spectroscopic selection rules: the direct product of the representations of multiplied factors in the integrand must contain the totally symmetric representation, Γ_1, for the integral to be non-zero. Thus, if

$\Gamma(\langle f|Op|i\rangle) = \Gamma(\langle f|) \times \Gamma(Op) \times \Gamma(|i\rangle) = \Gamma_1$, then $\langle f|Op|i\rangle \neq 0$ by symmetry

($\langle f|Op|i\rangle$ may be zero accidentally). If $\Gamma(\langle f|Op|i\rangle) \neq \Gamma_1$, then $\langle f|Op|i\rangle = 0$.

As parenthetically mentioned earlier, the Schrödinger equation is soluble at any positive energy with any symmetry. Each of the symmetry types' solutions in this manifold may be considered as a channel in the photoionization process. [A channel is a possible exit mode for the outgoing particle.[32]] This is the method of symmetry channels. By allowing alternative symmetry solutions to serve as channels, we gain another theoretical causal handle on the situation; we may say, for instance, "the X process is due to a matrix element found in the Y channel." We cannot really say that the experiment recognizes symmetry channels, for it only records the collection or absence of an electron. We could never say that this electron is an "s" and that that is a "p" which have been collected from an experiment involving a multi-channel process.

By exploiting the symmetry of our molecule in the theory, we find that all eigen- functions, both initial and final, have definite symmetry representations (once we have defined our basis set). We deal with an independent electron theory, and we shall choose our basis so that each one-electron wavefunction is represented by a single irreducible representation of the group. Thus, the above "result of group theory" limits the final state symmetry channels by which the photoelectron may leave. The specific allowed channels are given by the selection rules for the process. [See Appendix I on selection rules.]

Cross Section

Referring again to Figure II-1 (page 8), the photoelectron spectrum for Cl_2, we note that the peak heights are different for each orbital, and thus that the probability of photoionization is also different; the more electrons emitted, the higher the probability. Here we introduce a new attribute, the cross section, which underlies this disparity in peak height and is conceptually related to the probability of photoemission.

Our experiment is closely analogous to scattering; we merely have distinct incident and scattered particles. In scattering (References 33, 32, 34, 30), the total cross section, σ_{tot}, is given in terms of the number of particles scattered per unit time, **N**, the number of incident particles per unit volume, P, the velocity of the incident beam, v, and the number of scattering centers, N, as

$$\sigma_{tot} = \mathbf{N}/\mathrm{PvN}. \qquad \text{Eq. II-8}$$

(Pv = J is the incident flux of particles.) The units of cross section are those of area. We express cross section in barns or megabarns. One barn equals 10^{-24} cm^2, so one megabarn, abbreviated Mb, equals 10^{-18} cm^2 or 10^{-2} $Å^2$. Again, in our case the incident particles are photons, the target is a gas of molecules, and the scattered particles are ionized photoelectrons. [As with other experiments involving quantum objects, there are problems with the interpretation of the cross section for a single

event (involving one photon and one photoelectron). Thus, we have and will continue to use "ensemble" or statistical pictures, although we shall not define our ensembles!]

The cross section measures the scattering power (amplitude) or collisional or reaction "area" of a process. In a process involving classical (non-quantum) objects, it is just the geometrical area that the target presents to the collimated incident beam. In the quantum situation of incident photons and exitting electrons, cross section is only qualitatively related to the spatial extent of the electron distribution.

Two influences upon the cross section stand out. Cross section depends upon the initial state occupation number; an orbital containing more electrons will more likely interact with an incoming photon than will one containing fewer electrons. Cross sections are also dependent on the energy of the exciting photon or, equivalently for a given orbital, the photoelectron kinetic energy. From a given initial state orbital, there are portions (energies) of the continuum that are more or less accessible to an emitted photoelectron, and thus it seems reasonable that the cross section might be energy dependent. We shall find that the energy dependence of the cross section is the more interesting influence, and that effects manifested in it will occupy most of our attention.

In most modern experiments,[10] we have the required collimated incident beam of photons, but seldom do we collect all the emitted electrons (analogous to scattered particles). Much more often, a detector which subtends a small solid angle is used. With this detector, only a fraction of the electrons emitted are collected, and these in only one direction in the lab frame. It is thus that we introduce the angular dependent or differential cross section, usually denoted $d\sigma/d\Omega|_{\Omega=\Omega 1}$.

The idea is the same as that for the total cross section: $N(\Omega_1)$ is the number per unit time of particles scattered into the solid angle, Ω_1, so

$$\left.\frac{d\sigma}{d\Omega}\right|_{\Omega=\Omega 1} = \frac{N(\Omega_1)}{PvN}, \qquad \text{Eq. II-9}$$

and thus,

$$\sigma_{tot} = \int_{\Omega'} (d\sigma/d\Omega)\, d\Omega. \qquad \text{Eq. II-10}$$

Just as the transition probability does, the cross section should depend upon theoretical quantities related to the initial state, the final state, and upon how the transition between them occurs. A theoretical expression fulfilling these expectations is that from Davenport[1] for the cross section per electron (in units of square Bohr radii):

$$\sigma = (\alpha k/ \pi \omega \varepsilon_{fi}^2) |\langle f| \mathbf{A}_\circ \nabla V |i\rangle|^2. \qquad \text{Eq. II-11}$$

$\alpha = e^2 2\pi/hc$ is the fine structure constant; $k = |\mathbf{k}|$ is the wave vector of the photoelectron (which has a numerical value equal to the square root of the photoelectron kinetic energy in rydbergs); ω is the photon frequency (which has a numerical value equal to the photon energy in rydbergs); $|f\rangle$ and $|i\rangle$ are the one-electron wavefunctions of the final state (per unit volume normalized) and initial state (unit normalized) orbitals, respectively; $\varepsilon_{fi} = \varepsilon_f - \varepsilon_{i,}$ where ε_f and ε_i are the energy eigenvalues of the final and initial state orbitals, respectively. Lengths are in terms of the Bohr radius of the hydrogen atom: $a_0 = h^2/(2\pi)^2 me^2 = 0.529$ Å. Energies are in rydbergs, and $1 \text{ Ry} = e^2/2a_0 = 13.6$ eV, and -e is the charge on, and m is the mass of, the electron.

The form of the operator is from Davenport. It follows from taking the electromagnetic field of the photon to be the vector potential

$$\tilde{\mathbf{A}} = \tilde{\mathbf{A}}_0 \cos(\mathbf{q}_\circ \mathbf{x} - \omega t), \qquad \text{Eq. II-12}$$

and the scalar potential $\phi = 0$ everywhere. $\tilde{\mathbf{A}}$, $\tilde{\mathbf{A}}_0$, $\mathbf{q}$, and $\mathbf{x}$ are vectors, and $\mathbf{A} = \tilde{\mathbf{A}}/|\tilde{\mathbf{A}}|$ is a unit vector in the direction of $\tilde{\mathbf{A}}$. To account for the effect of the photon, we make the substitution in the hamiltonian for the momentum:

$$\mathbf{p} \rightarrow \mathbf{p} + e\tilde{\mathbf{A}}/c \qquad \text{Eq. II-13}$$

where c is the speed of light.

We thus get the above form for the cross section by: taking into account that we are interested in ionization of gas phase molecules by a "low intensity" photon source, implementing the dipole approximation, and noting that for exact solutions to a hamiltonian, the dipole length, velocity, and acceleration forms of the dipole matrix element are equivalent.

We can see how final channels affect the cross section by the following. $|f(\Gamma_\alpha)>$, $|f(\Gamma_\beta)>$, etc., are the final symmetry channels by which the photoelectron may leave, as determined by the selection rules. The cross section for the photoionization process, $|i(\Gamma_i)> \rightarrow |f(\Gamma_\alpha)>$, is

$$\sigma_{i\alpha} \sim |<f(\Gamma_\alpha)| \mathbf{A}\circ\nabla V |i(\Gamma_i)>|^2 \qquad \text{Eq. II-14}$$

and likewise for the other allowed symmetry channels. In a large number of events, some fraction of the electrons in initial state $|i(\Gamma_i)>$ will leave by $|f(\Gamma_\alpha)>$, another fraction by $|f(\Gamma_\beta)>$, and so on. The relative likelihood is given by the cross section, and for the "ensemble"

$$\sigma_{tot} = \sum_{\gamma,sel} \sigma_{i\gamma} \qquad \text{Eq. II-15}$$

where the subscript "sel" means that the sum is to be taken only over final state symmetries allowed by the selection rule. Actually, all possible final state symmetries could be included (although we never include them), because those which are not symmetry allowed have cross sections equal to zero.

Now that we have the form of the cross section, we see that the dynamic energy dependence of the cross section is due in large part to the energy dependence of the continuum wavefunction. Its behavior will modulate the peaked background laid down by $k/(\omega(\varepsilon_f - \varepsilon_i)^2)$. [In many of our calculations, we take ε_i to be given by the Xα eigenvalue. Thus, ε_{fi} is the energy of the photon, and $k = \varepsilon_f^{1/2}$ (in magnitude, in Rydberg atomic units), so that $k/(\omega(\varepsilon_f - \varepsilon_i)^2)$ is at a maximum at $\varepsilon_f = -\varepsilon_i/5$.]

As does the transition probability, the cross section shows a dependence upon the square of a matrix element which involves the bound initial and continuum final wavefunctions. The operator is multiplicative, which means that it will modify the overlap of these wavefunctions to give the final value of the integral, but that this overlap is still a useful function to consider.

Angular Parameter

The question arises, "How is it that cross section can depend on the angle at which we place the detector?" Yang[35] proved a theorem for nuclear scattering events (reactions) which carries over to our case by its generality. It states:

> If only incoming waves of orbital angular momentum l contribute appreciably to the reaction, the angular distribution of the outgoing particles in the center of mass system is an even polynomial of $\cos\theta_z$ with maximum exponent not higher than $2 \times l$.

θ_z is the angle between the propagation directions of the incoming particle (traveling along the z-axis) and the outgoing particle. Since for photons in the dipole approximation, $l = 1$, this means

$$\left.\frac{d\sigma}{d\Omega}\right|_{\Omega=\Omega_1} = A + B\cos^2\theta_z . \qquad \text{Eq.II-17}$$

When this is written[10] as an expansion of Legendre polynomials multiplying the cross section per unit solid angle, we get

$$\left.\frac{d\sigma}{d\Omega}\right|_{\Omega=\Omega_1(\theta_z)} = \frac{\sigma_{tot}}{4\pi}\left[1 - \frac{\beta}{2}\left(\frac{3\cos^2\theta_z - 1}{2}\right)\right]. \qquad \text{Eq.II-17}$$

For a plane-polarized incident beam, application of trigonometric identities gives

$$\left.\frac{d\sigma}{d\Omega}\right|_{\Omega=\Omega_1(\theta)} = \frac{\sigma_{tot}}{4\pi}\left[1 + \beta\left(\frac{3\cos^2\theta - 1}{2}\right)\right], \qquad \text{Eq.II-18}$$

where now θ is the angle between the plane of polarization and the detector axis when the detector axis is placed perpendicular to the propagation direction of the light beam. Figure II-3 shows the relations among θ, θ_z, and the polarization and propagation directions of the photon.

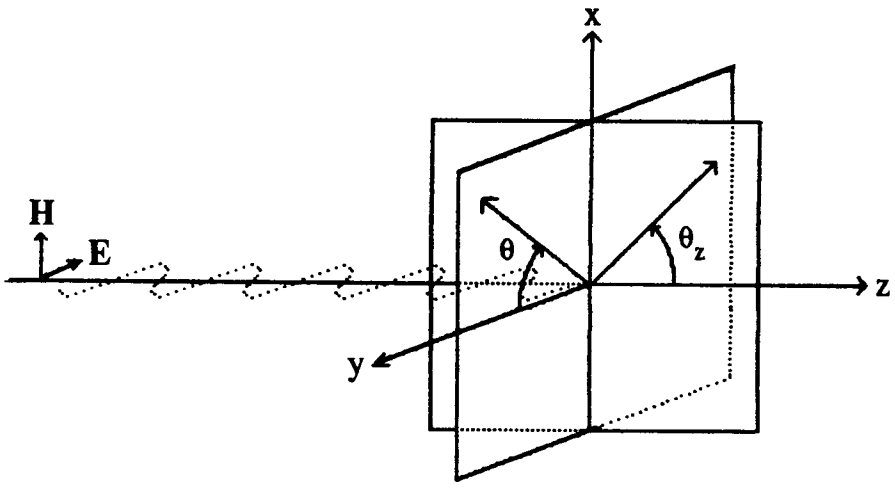

II-3. Angular relations between incident photons and outgoing electrons.

[For the case of elliptical polarization, Samson and Starace[36,10] obtain a relation from which the following may be derived.

$$\left.\frac{d\sigma}{d\Omega}\right|_{\Omega=\Omega_1(\theta)} = \frac{\sigma_{tot}}{4\pi}\left[1 + \frac{\beta}{4}(1 + 3p\cos 2\theta)\right], \qquad \text{Eq.II-19}$$

where $p = (I_x - I_y)/(I_x + I_y)$ is the polarization of the incoming light. $I_y/(I_x + I_y)$ and $I_x/(I_x + I_y)$ are the fractional intensities of light polarized parallel to the y- and x-axes, respectively, which make up the elliptically polarized beam. Synchrotrons emit elliptically polarized radiation--although strongly polarized along one axis.]

This last equation shows that the photoelectrons are emitted from a gas anisotropically according to a $\cos^2\theta$ dependence. This result should not produce the the shock that it does, for consider the effect of a plane-polarized photon on the microscopic level. The photon transfers angular momentum along the direction of its electric vector, that is, the photon imposes a unique lab frame direction on the molecule. Thus, even with a gaseous sample, the process is quantized with respect to this unique, imposed symmetry direction.

A useful rule of thumb is: "Quantum behavior (discrete energies and limited selection rules) is manifested when finite boundary conditions or symmetry are imposed." This is because we choose differential equations (D.E.'s) as our mathematical model, and the above statement applies to D.E.'s. We limit the number and kind of solutions to a D.E. by imposing boundary conditions and symmetry upon the D.E.

In another sense, we make measurements in the lab frame. The photon is in the lab frame already, but $|i\rangle$ and $|f\rangle$ are in the molecular frame. We have to average and "sum" the orientations of these wavefunctions to represent them in the lab frame.

This averaging and summing will smear at least some of their symmetry, leaving the representation of the photon dominant. [Because the partial cross section is proportional to $|\langle f|\text{photon}|i\rangle|^2$, however, this makes its representation $\mathbf{D}^2$ (in the pure rotation group), instead of $\mathbf{D}^1$. $\cos^2\theta$ is $\mathbf{D}^2$.]

Note also that the $\cos^2\theta$ dependence in all the above formulae is a result of only the dipole approximation--that the photon is represented by $l = 1$ (Reference 37).

In the experimental definition of the differential cross section, Equation II-9, because all the quantities on the right hand side are either positive or non-negative, the left must be non-negative. $\cos^2\theta_z$ has extrema at $\theta_z = 0$ (a maximum) and $\theta_z = \pi/2$ (a minimum). From Equation II-18 for a plane-polarized source,

$$\left.\frac{d\sigma}{d\Omega}\right|_{\Omega=\Omega_1(\theta)} = \frac{\sigma_{tot.}}{4\pi}\left[1 + \beta\left(\frac{3\cos^2\theta - 1}{2}\right)\right], \qquad \text{Eq.II-20}$$

$$= \frac{\sigma_{tot.}}{4\pi}\left[1 + \beta\right] \qquad \text{at } \theta = 0 \text{ and } \pi, \qquad \text{Eq.II-21}$$

$$= \frac{\sigma_{tot.}}{4\pi}\left[1 - \frac{\beta}{2}\right] \qquad \text{at } \theta = \pi/2. \qquad \text{Eq.II-22}$$

Thus, $-1 \le \beta \le 2$ in order for the differential cross section to remain non-negative.

In order to appreciate β's influence better, consider the angular distribution in the cases $\beta = 2, 1, 0$, and -1. For plane-polarization:

$$\left.\frac{d\sigma}{d\Omega}\right|^{(\beta=2)}_{\Omega=\Omega_1(\theta)} = \frac{\sigma_{tot.}}{4\pi}\left[3\cos^2\theta\right], \qquad \text{Eq.II-23}$$

$$\left.\frac{d\sigma}{d\Omega}\right|^{(\beta=1)}_{\Omega=\Omega_1(\theta)} = \frac{\sigma_{tot.}}{4\pi}\left[\frac{3\cos^2\theta + 1}{2}\right], \qquad \text{Eq.II-24}$$

$$\left.\frac{d\sigma}{d\Omega}\right|^{(\beta=0)}_{\Omega=\Omega_1(\theta)} = \frac{\sigma_{tot.}}{4\pi}, \qquad \text{Eq.II-25}$$

$$\left.\frac{d\sigma}{d\Omega}\right|^{(\beta=-1)}_{\Omega=\Omega_1(\theta)} = \frac{\sigma_{tot.}}{4\pi}\frac{3}{2}\left[1 - \cos^2\theta\right] = \frac{\sigma_{tot.}}{4\pi}\frac{3}{2}\left[\sin^2\theta\right]. \qquad \text{Eq.II-26}$$

Note that for positive β, the maximum photoelectron intensity is directed parallel to the axis of polarization of the photon source; for $\beta = 0$, the differential cross section is independent of the detector angle; for negative β, the maximum intensity is perpendicular to the polarization axis.

Cross sections are intensity quantities and thus may be broken into channels which sum to give a total. Angular parameters are directional quantities. As such, when subdivided into the same channels as the cross section, they do not add algebraically to give the overall β. Hence, though for some symmetry groups or for some special basis sets a kind of channelization can be achieved (the j_t basis), (References 38, 39, 2, 3) we do not consider subchannels of β in this thesis.

Even though we introduced the angular dependent cross section by demand of experimental considerations, we do not calculate this property; we calculate σ_{tot} and β. To compare with experiment, we measure $d\sigma/d\Omega|_{\Omega=\Omega 1}$ at a number of angles and then compute σ_{tot}(exp) and β(exp). [See Appendix II on the experimental techniques involved].

CHAPTER III

THEORETICAL FORMALISM

What we are trying to achieve is a representation or model of a molecule undergoing photoionization, and we are looking for quantitative results. The recent history of science teaches us that quantum theory is our best bet--if not our only bet--for spectroscopic models. For a case such as this, quantum theory prescribes that we write a classical hamiltonian--the sum of all pertinent kinetic and potential energies--and that we translate this classical energy into a quantum form of operators. We are told that when this Hamiltonian is used as an operator in an eigenequation, its eigenvalues will be interpretable as physically realizable total energies of the system described.

In certain systems we expect all the material parts or particles to remain for all time in the same region of space in a center-of-mass frame. These are called bound or stationary states of the system. When a system is bound, the energy eigenvalues are found to be discrete. When, however, the system has total energy greater than a value known as the ionization threshold, the energy eigenvalues form a continuum. The system is said to be free or unbound because one or more parts or particles may occupy any point in space, even in a center-of-mass frame. By convention, the ionization threshold is set as the "zero" of energy--we cannot calculate or measure meaningful absolute energies. With this convention, bound states have negative total energies--the absolute value of this energy for a given state is called its binding energy--and free states have positive total energies.

Were the problem as easy as writing a hamiltonian, writing an eigenequation, and recording the eigenvalues, then quantum theory would not be the enterprise it is today. To completely solve an eigenequation involves finding the eigenfunctions of the eigenoperator and then digging out the eigenvalues. By the way, the eigenfunctions we find in quantum theory are not physically interpretable! In quantum chemistry we usually work with the Schrödinger picture, so the operators

we use involve sums of second order derivatives and expressions of the Coulomb potential energies among nuclei and electrons. Thus do our eigenequations take on the form of differential equations, the solution of which yields the eigenfunctions and eigenvalues.

Hartree Fock treatments end up with a nonlocal exchange potential,[5] that is, one that is different for each electron. Nonlocality causes slow convergence to self consistency.

Since nonlocality is a difficulty resulting from an approximation, the one-electron approximation, and it is a difficulty bad enough to jeopardize the results of a calculation, Slater[5] decided that it would not be inappropriate to introduce a further approximation which removes nonlocality. This is the Xα approximation. From analysis of a free electron gas he found the exchange energy in Rydbergs to be approximated by

$$V_{X\alpha}(\mathbf{r}) = -6\alpha\,[(3/8\pi)\,\rho(\mathbf{r})]^{1/3} \qquad \text{Eq. III-1}$$

where $\mathbf{r}$ is the three-space position vector, and $\rho(\mathbf{r})$ is the electron density in units of electrons per cubic Bohr radius. (Note that electron correlation is still not explicitly included).[40] The parameter α equals one in Slater, two-thirds in Kohn and Sham[41] and Gaspar,[42] and is variable between two-thirds and one in Schwarz.[43]

The hamiltonian which results from this Xα approximation is easily solved in a central field (spherically symmetric) case. This leads us to another Slater introduction, the muffin tin potential approximation or model. Because central potential problems and their solutions are very well understood, space can be partitioned so that it consists of spherical regions each with a hamiltonian in Rydberg atomic units like:

$$\mathbf{H} = -\nabla_r^2 + V_C(r) + V_{X\alpha}(r), \qquad \text{Eq. III-2}$$

where $V_C(r)$ is the Coulomb potential. (The potential is a function of the radial distance only, because space has been broken into spherical regions.)

A sphere is drawn around each nucleus--this sphere is of such an extent to include all the atom's electron density but about two electrons' worth. An outer sphere is drawn which is tangent on the inside to as many of the atomic spheres as possible, i.e., its radius is as small as possible. There remains a troublesome inter sphere region whose treatment, although tricky, turns out to hold some keys to the solution of this model. Within this intersphere region, we make the potential constant, equal to an "average" over the spherical regions' potentials. Since we find that the potential at the surface of the atomic spheres does not equal that at the inner surface of the outer sphere, there will be a step in potential as we cross from any spherical region into the intersphere region. This is blatantly unphysical, and causes many purists to reject our model. Suffice it to say here that this unphysicality does come back to haunt us, but that by careful attention to the problems involved, we may satisfy the purists and achieve useful results.

Xα Bound State Method

We shall sketch Davenport's treatment[1] of the Xα-SW and photoionization (PI) formalism, sometimes called the "Continuum Scattered-wave Method" (CSM) or the "Multiple Scattering X-alpha" (MSXα) method. Many other treatments exist (References 2, 3, 4, 6, 44, 45, 7). Thus, Davenport's treatment is not definitive but is thorough and clear enough for this thesis. Note that we follow Davenport in not including symmetry; we feel the clarity of the presentation is degraded with such inclusion. Symmetry may be added at the end.[45]

First we make the muffin tin approximation--we break up space into spheres. We do this so that the hamiltonian becomes a sum over regions:

$$\mathbf{H}_{tot} = \mathbf{H}_{I} + \mathbf{H}_{II} + \sum_{i} \mathbf{H}_{i} \qquad \text{Eq. III-3}$$

$\mathbf{H}_{I}$ is for the outer sphere, $\mathbf{H}_{II}$ for the intersphere, and each $\mathbf{H}_{i}$ is for an atom of the

molecule. The hamiltonian in the j^{th} region is of the form

$$\mathbf{H}_j = -\nabla_j^2 + V(r_j)$$

$$= -\nabla_j^2 + V_C(r_j) + V_{X\alpha}(r_j), \qquad \text{Eq. III-4}$$

where $V_{X\alpha}(r_j) = -6\alpha_j [(3/8\pi)\,\rho(r_j)]^{1/3}$, from Equation III-1. Now, in the atomic spheres, $\lim_{r\to 0} V(r_i) = -2Z/r_i = V_C(r_i)$, the Coulomb potential, where Z is the atomic number of the nucleus in that sphere, and energy is in Rydbergs. This is to say that the Coulomb potential dominates at small r.

Bound Wavefunctions

Breaking up the hamiltonian this way leads to eigenfunctions which are sums over regions

$$\Psi(\mathbf{r}) = \Psi^I(\mathbf{r}_I) + \Psi^{II}(\mathbf{r}_{II}) + \sum_i \Psi^i(\mathbf{r}_i)\,. \qquad \text{Eq. III-5}$$

These are all N-electron wave functions. In the outer sphere and atomic spheres, the one electron eigenfunctions are well known. General solutions in the j^{th} sphere are of the form:

$$\psi(\mathbf{r}_j) = \sum_L [\,\mathbf{A}_L^j\, f_l^j(r_j) + \mathbf{B}_L^j\, g_l^j(r_j)\,]\; Y_L(r_j)\,, \qquad \text{Eq. III-6}$$

where L = (l ,m) is an abbreviation for the angular momentum quantum numbers; $r_j = \mathbf{r}_j/|\mathbf{r}_j|$, a unit vector in the direction of $\mathbf{r}_j$; $r_j = |\mathbf{r}_j|$; f_l is a regular or bounded (at the origin of its argument) radial function to be found from the radial Schrödinger equation, g_l is an irregular or unbounded radial function; Y_L is a spherical harmonic whose arguments are the spherical coordinate angles of r_j; and $\mathbf{A}_L$ and $\mathbf{B}_L$ are coefficients to be determined.

For bound states, these reduce to the eigenfunctions:

$$\psi(\mathbf{r}_I) = \sum_L \mathbf{B}_L^I\, g_l^I(r_I)\, Y_L(r_I)\,, \qquad \text{Eq. III-7}$$

and

$$\psi(\mathbf{r}_j) = \sum_L \tilde{\mathbf{A}}_L^j\, f_l^j(r_j)\, Y_L(r_j)\,, \qquad \text{Eq. III-8}$$

for the outer and atomic spheres, respectively. The tilde ~ indicates the initial state. These forms result from the boundary conditions: $\psi(r \to \infty) < \infty$, and $r\psi(r \to 0) = 0$.

The intersphere region's wavefunction is not nearly as simple. Davenport[1] and Johnson[4] show that it may be expressed in terms of expansions of functions on each site

$$\psi(r_{II}) = \sum_L \sum_{j \neq I} C_L^j \, n_l(kr_j) \, Y_L(r_j) + \sum_L C_L^I \, j_l(kr_I) \, Y_L(r_I) . \qquad \text{Eq. III-9}$$

n_l is a spherical Neumann function, j_l a spherical Bessel function (see Butkov[46]), $k = |\mathbf{k}|$ is the wave vector of the electron at the energy of the bound orbital under consideration, $E = k^2$, and the C's are coefficients to be determined. $\sum_{j \neq I}$ is a sum over atomic spheres only. $j \neq I$ means that the outer sphere is excluded from this sum; it is taken care of in the second term of Equation III-9.

Now we have compiled a list of wavefunctions in each of the regions of our model's space, each with undetermined coefficients. By imposing a constraint from the postulates of quantum mechanics--as many authors delineate them--we find the solution to the bound muffin tin Xα method. This constraint is that the wavefunction and its first derivative be everywhere continuous. This results in interrelations of the coefficients in the wavefunctions, since at the boundary between a sphere and the intersphere region the wavefunction [and first derivatives] in one sphere will be equal to that in the other. In this way, the intersphere region, for all its difficulty of representation, holds a key to the solution of the model: it carries "information" about the atomic spheres' solutions to the outer sphere and vice versa.

In the extended formal solution of the model, an entity known as the structure factor, $G_{LL'}^{ij}$, is introduced as the result of the wavefunction continuity constraint. Because wavefunctions and their derivatives are involved, certain Wronskians of the radial functions enter. [A Wronskian is a quantity from calculus defined by

$$[f,g] = fg' - gf' . \qquad \text{Eq. III-10}$$

f and g are functions of the same independent variable, and the prime indicates differentiation with respect to this variable[46]]. The result of the method is a secular equation involving these structure factors, Wronskians, and the coefficients of

wavefunctions (Johnson[4] equation II.60). The solutions to this secular equation are the molecular orbital energy eigenvalues.

Johnson's comments[4]--once he has reached the safety of the farther shore in his derivation of the formalism--demonstrate some of the advantages and features of this method. We shall paraphrase him as follows.

> Although the matrix elements of the secular equation may look complicated, they are relatively straightforward to compute efficiently. This is due, in part, to the dependence of these quantities only on radial functions and their first derivatives at sphere boundaries, and on "structure factors" which are functions of the internuclear vectors. Computer programs exist to perform the necessary numerical methods.
>
> Because the energy is a parameter occurring in all the matrix elements, the latter must be computed over a range of energies bracketing each orbital eigenvalue, and the determinant of the matrix involved in the secular equation must be interpolated to find its zeros. We have found that two or three partial waves (l = 0,1,2) per atom are sufficient in most polyatomics to yield convergence of orbital energies to ±0.001 Ry. With such rapid convergence, the typical secular array is much smaller than that of LCAO methods. Furthermore, the secular matrix can be partially factored by exploiting any symmetry which the molecule may possess. This leads to a smaller, faster solution.
>
> The SCF calculations are also easily carried out in spin unrestricted form using the unrestricted version
>
> $$V_{X\alpha}^{\uparrow}(r) = -6\alpha\,[(3/8\pi)\,\rho^{\uparrow}(r)]^{1/3}$$
> $$V_{X\alpha}^{\downarrow}(r) = -6\alpha\,[(3/8\pi)\,\rho^{\downarrow}(r)]^{1/3}$$
>
> of the Xα approximation to exchange correlation. This version is particularly valuable for developing a qualitative understanding of "open shell" molecules and crystals.

Photoionization Method

Bearing in mind that we want the transition matrix, <f| operator |i>, the final state wavefunction, |f>, and the "operator" need to be found. In the generalized theory of PI, <f| operator |i> means $\langle\Psi_f|$ operator $|\Phi_i\rangle$, where $|\Phi_i\rangle$ is the full ground

state N-electron wavefunction, and $|\Psi_f>$ is the full excited state (higher energy) wavefunction.

Since our method is an independent particle method, and we are primarily interested in direct photoionization, the final state wavefunction can be assumed to be a product of the N-1 electron wavefunction of the ion and the one electron wavefunction of the free electron. The ionic wavefunction obeys bound boundary conditions ($\Psi^{N-1} \rightarrow 0$ as $r \rightarrow \infty$), and the free wavefunction, the Coulomb boundary conditions (ψ is wave-like as $r \rightarrow \infty$, that is, $r\psi$ is sinusoidal at large r). In general, Ψ^{N-1} is not comprised of the same one electron functions as Φ^N; the ionized electron bears away some density causing the remaining orbitals to "relax", since they now experience a different effective nuclear charge.

Were we to calculate a different potential for the ground state and ion (at every final state energy!) we would have quite a job on our hands. The ionic orbitals, being eigenfunctions of a different hamiltonian from the ground state, would not necessarily be orthonormal to the ground state orbitals. . . .

As it is, before we go too far down this horrifying path, we side-step the problem by assuming that the ionic orbitals <u>are</u> eigenfunctions of the ground state hamiltonian, i.e., we use the same potential for the ground as for the ionic state. This is known as the frozen potential approximation. With it:

$$|\Psi_f^N> = |\Phi_f^N> = \prod_j^N |\phi_f^j> \qquad \text{Eq. III-11}$$

(ignoring antisymmetrization), where the $|\phi^j>$ are eigenfunctions of the ground state hamiltonian. Thus,

$$\begin{aligned} <\Psi_f^N| \, A_\circ \nabla V \, |\Phi_i^N> &= <\Phi_f^N| \, A_\circ \nabla V \, |\Phi_i^N> \\ &= <\prod_{j\neq k} \phi_f^j| \; <\phi_\varepsilon^k \,|\, A_\circ \nabla V \,|\, \phi_i^k> \; |\prod_{j\neq k} \phi_i^j> \\ &= \prod_{j\neq k}\prod_{j\neq k} <\phi_f^j \,|\, \phi_i^j> <\phi_\varepsilon^k \,|\, A_\circ \nabla V \,|\, \phi_i^k> \\ &= <\phi_\varepsilon^k \,|\, A_\circ \nabla V \,|\, \phi_i^k> \end{aligned} \qquad \text{Eq. III-12}$$

where $|\phi_\varepsilon^k\rangle$ is the one electron continuum wavefunction of the free electron of positive energy ε, and $|\phi_i^k\rangle$ is the one electron wavefunction of the active ground state electron. Recall that we are interested in direct photoionization, so that the operator, $A_o\nabla V$, is a single particle operator.

We see that not only do the ground and ionic states share the same potential, but that the same orbitals except one are occupied in both. This approximation causes a drastic reduction in the labor required--we have only one type of matrix element to evaluate, and this will be quite enough since molecular wavefunctions in the MSXα scheme are multi-termed.

Continuum Wavefunction

We may now find the final state wavefunction which we have been denoting $|f\rangle$ and now $|\phi_\varepsilon^k\rangle$. It is an eigenfunction of the same hamiltonian as we have seen in the spherical regions

$$\mathbf{H}_j = -\nabla_j^2 + V_C(r_j) + V_{X\alpha}(r_j), \qquad \text{Eq. III-13}$$

however, now the energy eigenvalue is positive and the boundary conditions are that for a scattered Coulomb wave.[32,33] It is "Coulomb," because the electron leaves behind a singly charged ion. It is "scattered," because even if the leaving electron comes from an orbital in an atomic sphere with well defined angular momentum (single *l*), as it "passes through" the intersphere region it is scattered into many angular momenta in the outer sphere where the Coulomb boundary condition is applied. This latter scattering arises from the continuity criterion discussed earlier and the resultant coupling of partial waves through the intersphere region. The "smearing" of angular momenta may also be accounted for by reference to the fact that the intersphere region results from the lack of spherical symmetry of the molecule. Although *l* is not a "good" quantum number for the molecule, we expand wavefunctions and scattering amplitudes in sums over *l* and thus have to accept that the result will be multi-termed or "multi-*l*" wavefunctions and scattering amplitudes.

First let us briefly present the pure Coulomb situation, then introduce the short range molecular potential. The following is paraphrased from Davenport[1] who refers to Messiah (Reference 33, Chapter X). The pure Coulomb Schrödinger equation in atomic units is:

$$[\nabla^2 + k^2 - 2\gamma k/r'] \psi(\mathbf{r}') = 0, \qquad \text{Eq. III-14}$$

where **k** is the wavevector of the leaving particle such that $k = |\mathbf{k}|$ and $k^2 = \varepsilon$, the positive photoelectron kinetic energy. $\gamma = Z_1 Z_2/k$, where Z_1 is the charge of the leaving particle (an electron, so $Z_1 = -1$), and Z_2 is that of the particle left behind.

Because of spherical symmetry, a partial wave expansion is applicable:

$$\psi(\mathbf{r}') = \sum_L (y_l(r')/r') Y_L(r'). \qquad \text{Eq. III-15}$$

Each term in this expansion is called a partial wave. Henceforth, we shall loosely call any term of a wavefunction which is indexed by l, the l^{th} partial wave.

The radial Schrödinger equation, for a given l, becomes

$$[d^2/dr'^2 + k^2 - 2\gamma k/r' - l(l+1)/r'^2] y_l(r') = 0. \qquad \text{Eq. III-16}$$

Its asymptotic ($r \to \infty$) solutions are

$$y_1(r') = F_l(\gamma,\rho') \sim \sin(\rho' - l\pi/2 - \gamma \ln(2\rho') + \sigma_l), \text{ and}$$

$$G_l(\gamma,\rho') \sim \cos(\rho' - l\pi/2 - \gamma \ln(2\rho') + \sigma_l), \qquad \text{Eq. III-17}$$

where $\rho' = kr'$, and $\sigma_l = \text{Arg } \Gamma(l + 1 + i\gamma)$ is the Coulomb phase shift. F_l is regular and G_l is irregular at the origin. We shall denote as θ_l the argument of the above trigonometric functions

$$\theta_l = \rho - l\pi/2 - \gamma \ln(2\rho) + \sigma_l. \qquad \text{Eq. III-18}$$

The term $l\pi/2$ arises due to the finite angular momentum, l, of the particle, $\gamma \ln(2\rho)$ is the shortening of its wavelength due to the Coulomb field, and σ_l denotes the phase shift due to the Coulomb field.

The general solution to the Coulomb radial Schrödinger equation is

$$\psi(\mathbf{r}') = \sum_L [\, \mathbf{A}_L f_l(r') + \mathbf{B}_L g_l(r') \,] Y_L(r'), \qquad \text{Eq. III-19}$$

where now $f_l(r') = F_l(\gamma,\rho')/\rho'$ and $g_l(r') = -G_l(\gamma,\rho')/\rho'$. Note that both the regular and irregular solutions appear. The full expansion of the pure Coulomb wave, unscattered by any other potential, with asymptotic boundary conditions is

$$\psi_C^{\pm}(\mathbf{r}') = \sum_L 4\pi i^l \, e^{\pm i\sigma_l} \, Y_L(r') \, Y_L^*(k') \, F_l(\gamma,\rho')/\rho', \qquad \text{Eq. III-20}$$

where $i = \sqrt{-1}$.

"The effect of the scattering potential is to shift the phase of each outgoing partial wave," says Messiah (Reference 33, p. 387). In the complete derivation of the formalism, an energy dependent matrix **K** is introduced which incorporates these scattering phase shifts due to the molecular potential.[32,34] In the outer sphere where we shall apply the boundary conditions for |f>, a solution of the Schrödinger equation with the molecular potential put in looks like

$$\psi_\Lambda(\mathbf{r}_I') \sim f_\lambda^I(r_I') \, Y_\Lambda(r_I') + \sum_L \mathbf{K}_{\Lambda L} \, g_l^I(r_I') \, Y_L(r_I'). \qquad \text{Eq. III-21}$$

[Note that **K** is diagonal for spherical potentials. It is the intersphere region which causes l to be smeared or coupled one to another, and the off-diagonal elements of **K** are the embodiment of this coupling. Because spherical potentials need no intersphere region, they have no off-diagonal elements in **K**.]

We may rewrite the above and indicate its asymptotic behavior by

$$\psi_\Lambda(\mathbf{r}_I') \sim \sum_L [\, \delta_{\Lambda L} f_l^I(r_I') + \mathbf{K}_{\Lambda L} g_l^I(r_I') \,] \, Y_L(r_I') \qquad \text{Eq. III-22}$$

$$\sim \sum_L [\, \delta_{\Lambda L} \sin\theta_l' - i\mathbf{K}_{\Lambda L} \cos\theta_l' \,] \, Y_L(r_I') \text{ as } r' \to \infty.$$

This helps to illustrate that **K** is a factor in the scattering of angular momentum, λ, into other angular momenta, l, and that it functions "to shift the phase of [otherwise pure] outgoing partial waves." The full wavefunction is normalized as a sum of partial waves like that in Equation III-22. It is then called "**K**-matrix normalized.

The result of the full derivation yields the wavefunction for the outer sphere which obeys asymptotic boundary conditions and shows proper normalization for

photoelectron kinetic energy $\varepsilon = k^2$:

$$\psi(\mathbf{r}_I') = \sum_{L'} \sum_{L''} 4\pi i^{l'} e^{-i\sigma_{l'}} Y_{L''}(r_I') Y_{L'}^*(k_I') \qquad \text{Eq. III-23}$$

$$\times \left[\left(1/ 1 - i\mathbf{K} \right)_{L'L''} f_{l''}(r_I') + \left(\mathbf{K}/ 1 - i\mathbf{K} \right)_{L'L''} g_{l''}(r_I') \right]$$

Again, primes on the arguments of functions indicate the molecular frame.

[Note: $\left(1/ 1 - i\mathbf{K} \right)_{L'L''} = \sum_{\Lambda} (1 - i\mathbf{K})_{L'\Lambda}^{-1} \delta_{\Lambda L''}$.]

When the continuity criterion and normalization has been carried through, the wavefunctions for the j^{th} atomic sphere looks like

$$\psi(\mathbf{r}_j') = \sum_{L'} \sum_{L''} 4\pi i^{l'} e^{-i\sigma_{l'}} Y_{L''}(r_j') Y_{L'}^*(k_I') \left(\mathbf{A}^j/ 1 - i\mathbf{K} \right)_{L'L''} f_{l''}(r_j'). \qquad \text{Eq. III-24}$$

We see that only the regular solution $f_{l''}$ is present because of the boundary condition at the nucleus: $r\,\psi \rightarrow 0$ as $r \rightarrow 0$. $\mathbf{A}^j$ is a coefficient determined by the continuity matching conditions. Note that **k**, the wave vector of the leaving electron, is measured from the center of the outer sphere. The wavefunctions for both the outer and atomic spheres must be found for each photoelectron energy considered; the wavefunction is parametrized by the photoelectron energy.

Photon Operator

Now that we have the initial and final state wavefunctions the operator is easy to express. $\mathbf{A}_o\nabla V$ is in the laboratory frame, but we have written the wavefunctions in the molecular frame. In this sense, it will be easiest to write the transition matrix in the molecular frame and then rotate it to the lab frame. The operator is

$$(\mathbf{A}_o\nabla V)^{mol} = (\mathbf{A}_o\mathbf{e}_r)^{mol}\, \partial V/\partial r', \qquad \text{Eq. III-25}$$

and

$$(\mathbf{A}_o\mathbf{e}_r)^{mol} = \sum_{\nu} 4\pi/3\ Y_{1\nu}^*(A') Y_{1\nu}(r'), \qquad \text{Eq. III-26}$$

where primes on independent variables indicate the molecular frame. ν is the z component angular momentum quantum number of the photon. Remember that A and **A** are both unit vectors in the direction of $\tilde{\mathbf{A}}$, but that we write A when we mean

to indicate the arguments of a spherical harmonic. $\mathbf{e}_r$ is the spherical coordinate three-space unit vector. Now we have the operator in the molecular frame:

$$(\mathbf{A}\circ\nabla V)^{mol} = \sum_v 4\pi/3\ Y_{1v}{}^*(A')\ Y_{1v}(r')\ \partial V/\partial r'. \qquad \text{Eq. III-27}$$

Because space has been broken into regions, the operator may be expressed as a sum of contributions from these regions (j)

$$(\mathbf{A}\circ\nabla V)^{mol} = \sum_{sites:\,j} (\mathbf{A}\circ\nabla V)_j^{mol}$$

$$= \sum_j \sum_v 4\pi/3\ Y_{1v}{}^*(A_j')\ Y_{1v}(r_j')\ \partial V/\partial r_j'. \qquad \text{Eq. III-28}$$

We can finally see an advantage of the constant intersphere potential. Again because we have broken up space into the regions of the muffin tin:

$$\langle f|\ \mathbf{A}\circ\nabla V\ |i\rangle = [\ \langle f_I| + \langle f_{II}| + \sum_j \langle f_j|\ ]\ [\ (\mathbf{A}\circ\nabla V)_I + (\mathbf{A}\circ\nabla V)_{II}$$

$$+ \sum_j (\mathbf{A}\circ\nabla V)_j\ ]\ [\ |i_I\rangle + |i_{II}\rangle + \sum_j |i_j\rangle\ ]. \qquad \text{Eq. III-29}$$

Since the regions are mutually exclusive, this reduces to

$$\langle f|\ \mathbf{A}\circ\nabla V\ |i\rangle = \langle f|\ \mathbf{A}\circ\nabla V\ |i\rangle_I + \langle f|\ \mathbf{A}\circ\nabla V\ |i\rangle_{II} + \sum_j \langle f|\ \mathbf{A}\circ\nabla V\ |i\rangle_j \qquad \text{Eq. III-30}$$

and since $\partial V/\partial r_{II}' = 0$ (because the intersphere potential is constant), only surface terms survive from the region II integral.[47] Thus, we have rid ourselves of the hardest integrals we faced.

Matrix elements

Putting in all the parts, we find the expression for the matrix element

$$\langle f|\ \mathbf{A}\circ\nabla V\ |i\rangle = \sum_{L'} \sum_v 4\pi/3\ Y_{1v}{}^*(A_j')\ \mathbf{F}(L',v,\varepsilon)\ Y_{L'}(k_I'), \qquad \text{Eq. III-31}$$

where the "amplitude matrix" is

$$\mathbf{F}(L',v,\varepsilon) = \sum_j \mathbf{F}_j(L',v,\varepsilon) + \mathbf{F}_I(L',v,\varepsilon) \qquad \text{Eq. III-32}$$

$$= 4\pi\ e^{i\sigma_{l'}}\ (-i)^{l'} \sum_L \sum_{L''} I(L,1v,L'')\ \{\sum_j (\mathbf{A}^j/\ 1 - i\mathbf{K})_{L'L''}\ \tilde{\mathbf{A}}_L{}^j\ \mathbf{R}_{l''}{}^j$$

$$+ \mathbf{B}_L{}^I\ [\ (1/\ 1 - i\mathbf{K})_{L'L''}\ \mathbf{R}_{l''}{}^{Ia}\ \delta_{l'l''} + (\mathbf{K}/\ 1 - i\mathbf{K})_{L'L''}\ \mathbf{R}_{l''}{}^{Ib}\ ]\}.$$

$\tilde{\mathbf{A}}_L^j$ and $\mathbf{B}_L^I$ are initial state coefficients on the outer and atomic spheres, respectively, $\mathbf{A}^j$ is the atomic sphere final state coefficient.

The Gaunt integrals, I(L,L',L"), are tabulated and are merely the coefficients of $Y_{l''m''}$ expressed as the product of Y_{lm} and $Y_{l'm'}$, that is, $Y_L Y_{L'} = \sum_{L''} I(L,L',L'')Y_{L''}$ (Reference 37). The Gaunt integral is given by

$$I(L,L',L'') = \iint d^2r\ Y_L(r)\, Y_{L'}(r)\, Y_{L''}(r)^*, \qquad \text{Eq. III-33}$$

$$= [\ (2l+1)(2l'+1)/\ 4\pi\ (2l''+1)\ ]^{1/2}\, C(l,l',l'' \mid m,m',m'')\ C(l,l',l'' \mid 0,0,0).$$

(Equation III-33), where $C(l,l',l'' \mid m,m',m'')$ is a Clebsch-Gordan or vector addition coefficient. Because of the relation $C(l,l',l'' \mid m,m',m'') = 0$, unless $m'' = m + m'$, we may drop the last index (it is always given by the sum of the two which precede it) and write instead $C(l,l',l'' \mid m,m')$. The integral in the expression is taken over all angles, θ and ϕ.

The radial integrals are

$$\mathbf{R}_{ll''}^{Ia} = \int_{RI}^{\infty} dr_I\, r_I^2\, (\partial V/\partial r_I)\, g_l^I\, f_{l''}^I + R_I^2\, g_l^I(R_I)\, f_{l''}^I(R_I)\, (V(R_I) - V_{II}),$$

$$\mathbf{R}_{ll''}^{Ib} = \int_{RI}^{\infty} dr_I\, r_I^2\, (\partial V/\partial r_I)\, g_l^I\, g_{l''}^I + R_I^2\, g_l^I(R_I)\, g_{l''}^I(R_I)\, (V(R_I) - V_{II}),$$

$$\mathbf{R}_{ll''}^{j} = \int_0^{Rj} dr_j\, r_j^2\, (\partial V/\partial r_j)\, f_l^j\, f_{l''}^j + R_j^2\, f_l^j(R_j)\, f_{l''}^j(R_j)\, (V_{II} - V(R_j)). \qquad \text{Eq. III-34}$$

These integrals are non-zero only for $l' = l \pm 1$, because each region is spherical, and we have used the dipole approximation (in its acceleration form).

In all the above, L or l labels the initial state, and L' or l' and L" or l'' label the final state. Any function or matrix (except the Clebsch-Gordan coefficient) labeled prime or double-prime is thus energy dependent.

We have not put primes on the arguments in the Gaunt integral or in the radial integrals because these arguments are "integrated out," that is, the result of integration is just a number, not a function of r. In fact, with regard to the space of the molecule, $\mathbf{F}(L',\nu,\varepsilon)$ is itself just a number. $\mathbf{F}(L',\nu,\varepsilon)$ is the "scattering" or response amplitude matrix, indexed by an outer sphere L' of the leaving electron and the azimuthal

quantum number of the photon, $\nu = 0, \pm 1$, and the continuous kinetic energy, ε, of the photon. **F** holds information about the final angular momentum states into which the incident photon causes the outgoing electron to be "scattered."

The matrix element above is still in the molecular frame, but experiments are carried out in the laboratory frame. For a randomly oriented molecule (in the gaseous phase, for instance) the matrix element must be rotated from the body frame to the laboratory frame and then squared, since the cross section depends on the square of the matrix element. When this is carried out, and account is taken of finite detector size (the quantities are all expressed in terms of those in Equation II-18), we find:

$$\sigma_{tot}(\varepsilon) = (4\,\alpha\,k/\,9\,\omega\,\varepsilon_{fi}^{2})\ \Sigma_{L}\,\Sigma_{\nu}\ |\,\mathbf{F}(L,\nu,\varepsilon)\,|^{2}, \qquad \text{Eq. III-35}$$

and

$$\beta(\varepsilon) = [\,5\,\Sigma_{L}\,\Sigma_{\nu}\ |\,\mathbf{F}(L,\nu,\varepsilon)\,|^{2}]^{-1} \times \Sigma_{L}\,\Sigma_{\nu}\,\Sigma_{L'}\,\Sigma_{\nu'}\ \{\,[(2l+1)(2l'+1)]^{1/2}\,\mathbf{F}(L,\nu,\varepsilon)\,\mathbf{F}^{*}(L',\nu',\varepsilon') \times \mathbf{C}(l,l',2\,|\,m,-m')\,\mathbf{C}(l,l',2\,|\,0\,0)\,\mathbf{C}(1,1,2\,|\,\nu,-\nu')\,\mathbf{C}(1,1,2\,|\,0\,0)\}. \qquad \text{Eq. III-36}$$

The $P_0(\cos\theta)$ and $P_2(\cos\theta)$ terms are the only ones to survive in Equation II-18 because of the occurrence in the derivation of a Clebsch-Gordan coefficient: $\mathbf{C}(1,1,l''\,|\,0\,0) \neq 0$, only for $l'' = 0, 2$. This factor occurs because the photon operator is represented by $l = 1$, which results from the application of the dipole approximation.

[In electron scattering, any l is possible in the operator--since it is an electron of continuously variable energy and hence angular momentum--and the final expression for cross section contains terms in $P_{l''}(x)$ for all l''. This series must be arbitrarily truncated.]

Eigenphase Sum

The coefficients, $\mathbf{K}_{\Lambda L}$, of the cosine term in Equation III-22 form a real, symmetric matrix. This "**K** matrix" supervises the coupling between different angular momenta due to the nonspherical molecular potential. As such, it summarizes the electron-molecule interaction. Because extensive coupling of angular momenta is

the rule in molecular photoionization, no pure phase shift exists to describe the process. Nevertheless, a useful quantity known as the eigenphase sum may be extracted from the **K** matrix for each channel. This eigenphase sum is a fingerprint in multichannel (scattering-like) processes which indicates the presence of rapid changes in phase of major components of the final wavefunction. It is defined[48,49] (modulo 1) by

$$\mu_{sum} = \pi^{-1} \delta_{sum} = \pi^{-1} \sum_L \tan^{-1}(\mathbf{U}^+ \mathbf{K}\, \mathbf{U})_{LL} \qquad \text{Eq. III-37}$$

where **U** is the (real) unitary matrix that diagonalizes **K**. Like the **K** matrix, μ_{sum} depends on the final state energy.

[Continuum resonances called shape resonances, which we shall discuss in Chapter 4, are accompanied by rises in μ_{sum} of about one unit for atoms,[50] less than one unit for molecules. This is due to a loop in the final state wavefunction traversing a potential barrier, near the origin, and becoming trapped inside this barrier, thus causing the phase shift (which is defined far out from the origin) to "rotate" by about π radians.]

μ_{sum} is a condensation of the information contained in **K**,[51] but at a cost. We may see in μ_{sum} only dramatic changes in phase shift--small features are lost by diagonalization and the taking of a trace. Appendix III contains μ_{sum} for all the channels of the molecules studied in this work.

CHAPTER IV

COOPER MINIMA AND SHAPE RESONANCES

It has been observed that for low photoelectron energies, the energy dependence of the PI cross section for complex atoms is often distinctly non-hydrogenic (References 9, 15, 11). Hydrogenic behavior includes a maximum at threshold and monotonic decrease above threshold. Often cross sections show minima (thus subsequent maxima at higher energy) or delayed maxima (in the region above threshold) or both. These features which modulate an otherwise smooth spectral shape are what we are interested in investigating for molecules.

Minima in the cross section are due to zeros in the spectral behavior of the dipole matrix elements. These are usually referred to as "Cooper minima"--abbreviated CM in this work. Delayed maxima are due to extrema (maximum amplitude) in the spectral behavior of the dipole matrix elements. These in turn are due to potential barrier effects in our independent particle picture. Delayed maxima are usually called shape resonances--abbreviated SR here.

Although these features have been treated exhaustively for atoms, experimentally as well as theoretically, we present here a brief discussion of some salient points about each using our calculations on the noble gases.

Cooper Minima

We have seen that the cross section is proportional to the square of the dipole matrix element. This makes the cross section non-negative as experimental definitions and our understanding of cross section require. The dipole matrix element may be positive, negative, or zero, however, and is energy dependent. This means that it may attain negative and positive values at different energies for a given initial state and final channel.

Based on his survey calculations of PI from outer atomic orbitals, Cooper[9] found that "the PI cross sections from atomic subshells whose radial wavefunctions are nodeless have, in general, a different spectral shape than those from subshells whose radial wavefunctions have nodes". He went on to elaborate this difference. It is due to the noded wavefunctions' $l \rightarrow l+1$ radial matrix elements being negative (with the convention that the wavefunctions have positive value near the origin) at threshold ($\varepsilon = 0$) but becoming positive in the limit of high energy. The $l \rightarrow l+1$ matrix element is generally dominant (that is, at most energies) over that for $l \rightarrow l-1$ by an order of magnitude (Bethe and Salpeter[52]). Thus at the energy where the $l \rightarrow l+1$ matrix element changes sign and becomes zero, the cross section is at a minimum.

We shall encounter cases where the $l \rightarrow l-1$ or corresponding cross section is changing sufficiently rapidly with respect to the broadness of the $l \rightarrow l+1$'s minimum, that the total cross section will not show a minimum. This does not affect our explanation, however; the $l \rightarrow l+1$ channel still undergoes a matrix element zero.

Fano and Cooper[15] state a more refined rule concerning the occurrence of negative radial matrix elements (R<0):

(1) R<0 for $l' = l+1$ only, since ($n' = n$, $l' = l-1$) is always occupied when (nl) is; this rule excludes only a minor fraction of the total oscillator strength.

(2) R<0 for $n > l+1$ only, since ($n' = n = l+1$, $l' = l+1$) does not exist; this rule excludes He and Ne for which $n = l+1$ altogether as well as the 1s, 2p, 3d, and 4f subshells of all atoms.

These rules exclude the 1s, 2p, 3d and 4f subshells and limit the occurrence of sign changes to the $l \rightarrow l+1$ rather than the $l \rightarrow l-1$ matrix element, since the $n(l-1)$ subshell is always occupied in the ground state of the atom. Also, the Fano-Cooper rule allows for matrix element sign changes in the discrete region of the atom's spectrum, although this would not be seen as a PI cross section minimum. With our method and model, the outermost ns orbitals of the noble gases and halogens show CM

at or below threshold, in the discrete part of the spectrum. Their cross sections rise from minima at threshold to maxima in the continuum due to CM near threshold.

For ground initial state PI, only one CM is possible per orbital, if any. It has been found that multiple minima occur in some excited initial state orbitals (References 53, 54, 55). These are due to matrix elements which are positive at threshold, go negative, and then positive again. They are possible only in more diffuse excited state orbitals.

An example for argon 2p and 3p is now given. In Figure IV-1 are the cross section and angular parameter for argon 2p as a function of photoelectron kinetic energy, in Figure IV-2 are those for argon 3p. [For this calculation it is necessary to use a different potential for 2p than for 3p as Kennedy and Manson showed.[56]] The channel breakdown in these Figures will be discussed in Chapter V.

The 2p is excluded from a matrix element zero by the above generalizations, and its cross section is "hydrogenic" or monotonically decreasing. The total cross section for 3p has a minimum at 1.9 Ry and a subsequent maximum at 4.1 Ry after which it is also monotonically decreasing. β also behaves differently between these two orbitals. For 3p a sharp dip appears around the energy of the cross section minimum, while β for 2p is shallow and undramatic.

The channel cross sections confirm that the 3p$\rightarrow$ kd channel underlies the minimum in argon 3p. Figure IV-3 shows the matrix elements 3p$\rightarrow$ ks and 3p$\rightarrow$ kd as a function of energy, and the wavefunctions involved in the 3p$\rightarrow$ kd matrix elements are shown in Figure IV-4 for a few final energies.

[Note: These are solutions to Schrödinger equations like

$$[\, d^2/dr^2 - l(l+1)/r^2 + (E - V)\,]\, P_{nl}(r) = 0 \qquad \text{Eq. IV-1}$$

for bound orbitals ($E < 0$) with bound boundary conditions and unit normalization, and

$$[\, d^2/dr^2 - l'(l'+1)/r^2 + (\varepsilon - V)\,]\, P_{\varepsilon l'}(r) = 0 \qquad \text{Eq. IV-2}$$

for continuum orbitals ($\varepsilon > 0$) with free particle boundary conditions and **K** matrix

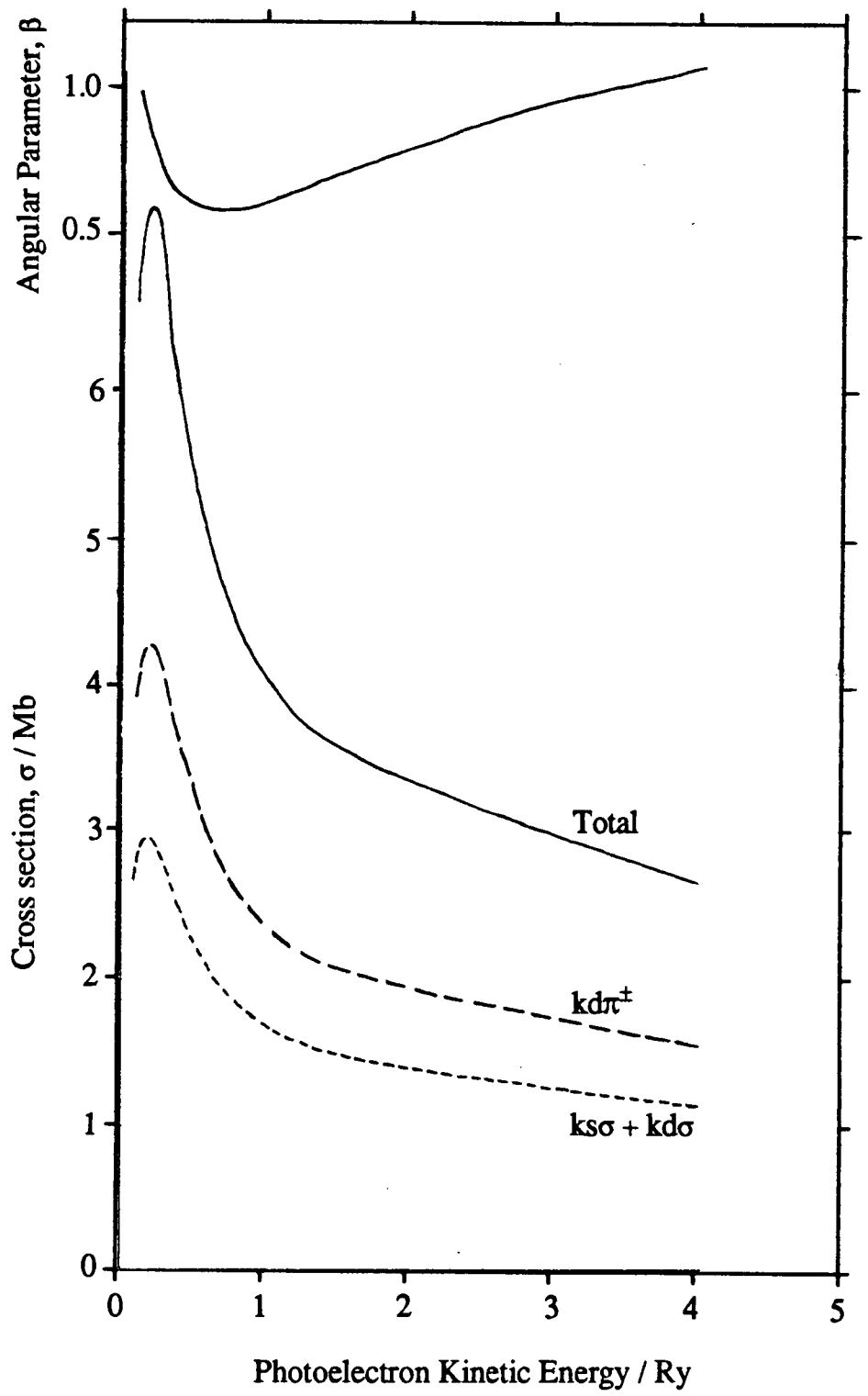

IV-1. Calculated cross section and angular parameter as a function of photoelectron energy for argon 2p.

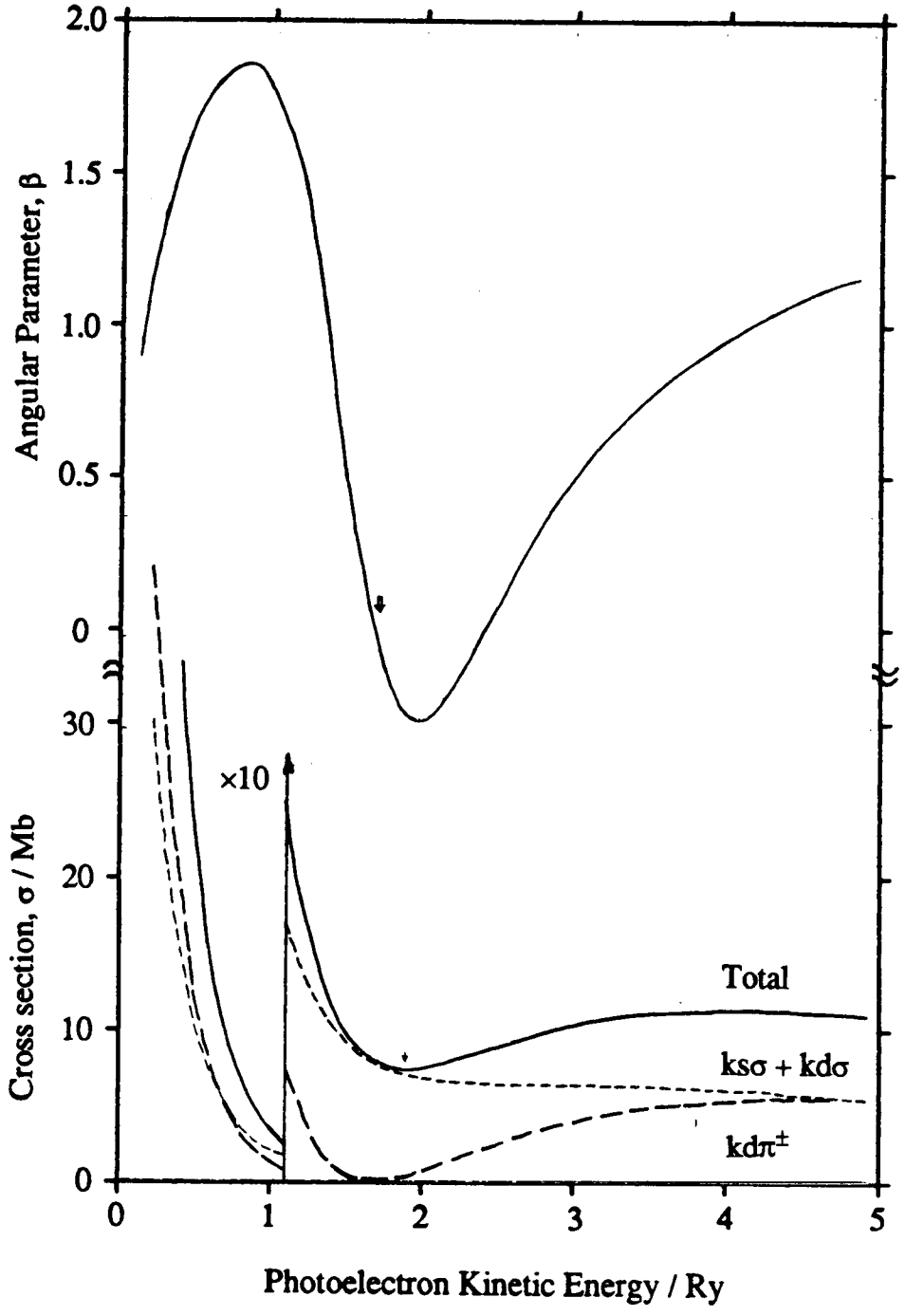

IV-2. Calculated cross section and angular parameter as a function of photoelectron energy for argon 3p.

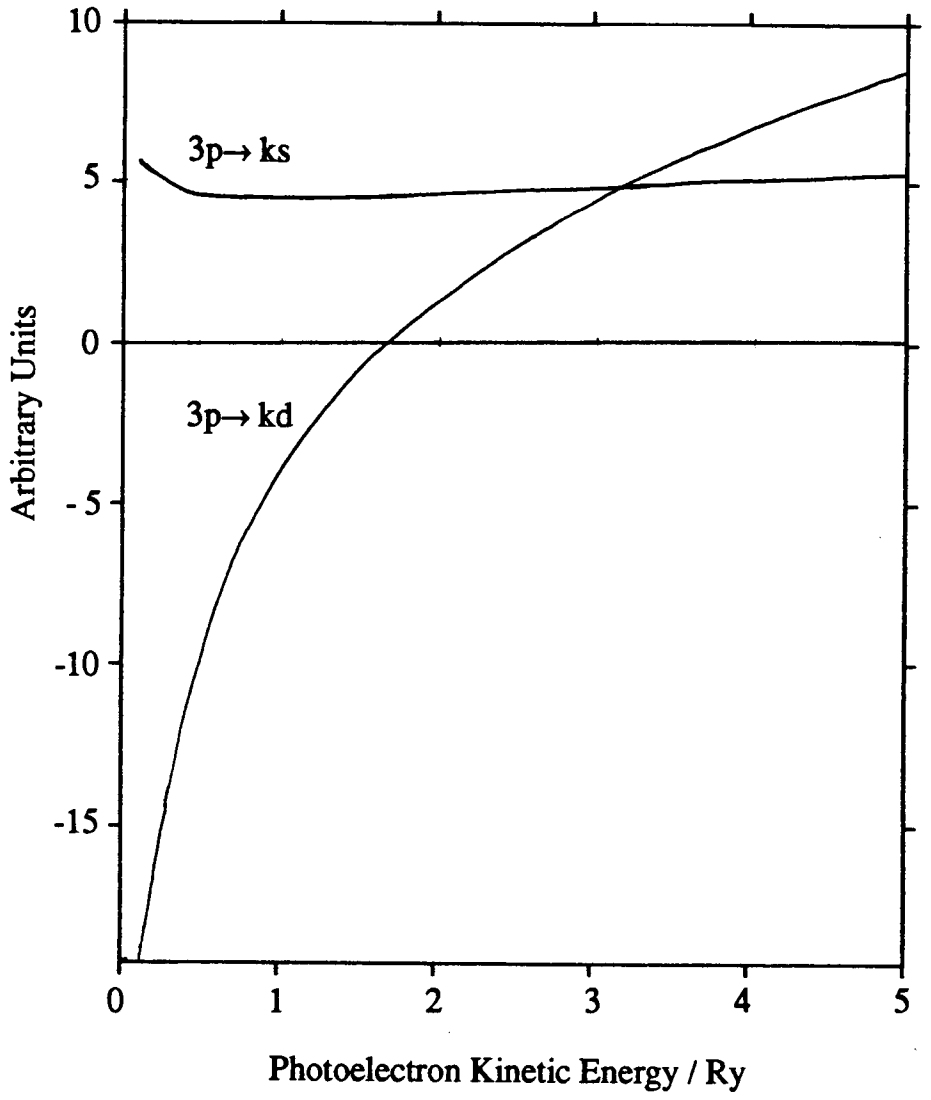

IV-3. Dipole matrix elements as a function of photoelectron energy for argon 3p.

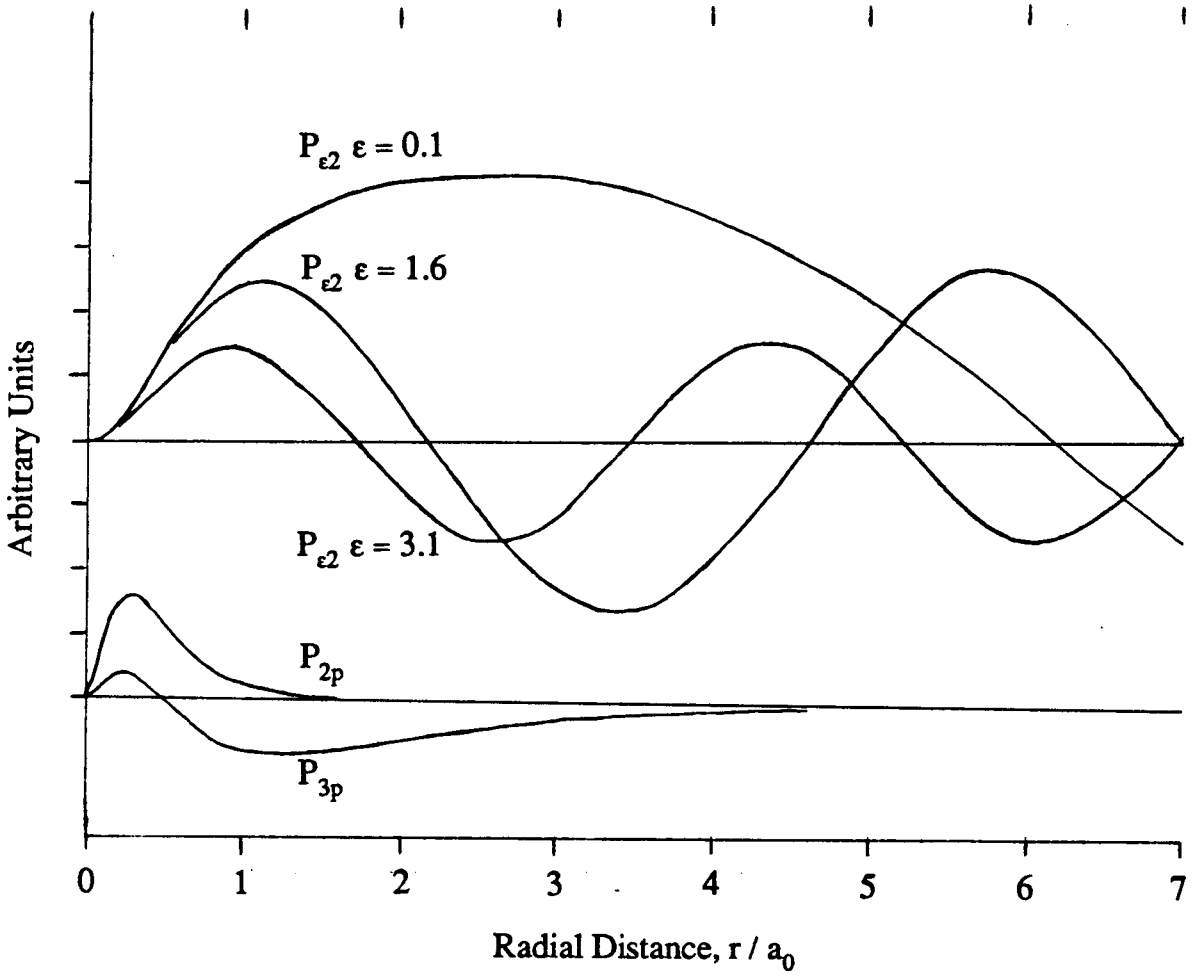

IV-4. Initial 2p and 3p (l = 1), and continuum (l = 2) radial wavefunctions for argon at 0.1, 1.6, and 3.1 Ry photoelectron kinetic energy.

normalization. The radial matrix elements are

$$\mathbf{R}_{l,l'}(\varepsilon) = \int_0^\infty P_{nl}(r)\, r\, P_{\varepsilon l'}(r)\, dr \qquad \text{Eq. IV-3}$$

with these functions. Usually chemists use $\psi_{nl} = P_{nl}/r$ and thus the "volume element" in the integral is r^2dr. Also note that $\lim_{r\to 0} P_{nl} = 0$ even for $l = 0$, whereas $\lim_{r\to 0} \psi_{ns} \neq 0$.]

At 0.1 Ry, near threshold, the extended negative loop in P_{3p} overlaps the positive loop of $P_{\varepsilon d}$, making the integral negative. (Remember that the product of $P_{\varepsilon d}$ and P_{3p} needs to be multiplied by r to get the integrand.) As ε increases, the "wavelength" of $P_{\varepsilon d}$ decreases, bringing more nodes (where $P_{\varepsilon d}$ crosses from positive to negative) closer to the origin (the nucleus). Since the product $P_{\varepsilon d}\, P_{3p}$ is predominantly negative inside the first loop of $P_{\varepsilon d}$, and alternates in sign in each subsequent loop of $P_{\varepsilon d}$, this bringing in of $P_{\varepsilon d}$'s loops with increasing energy causes first partial then complete cancellation of the first loop's negative contribution to the integral. At energies above that at which the integral changes sign, the various loops' contributions combine to leave the integral positive. At still higher energies, so many loops of $P_{\varepsilon d}$ have been crammed into the area where P_{3p} is appreciable that all these loops' contributions begin to cancel and the integral again decreases with increasing energy. We take the view that the cross section for argon 3p shows a maximum near threshold and another at 4.1 Ry not because of two separated regions of good "overlap" but because of a region between these of poor (zero!) "overlap."

Manson[57] discusses β's behavior near the CM by reference to the Cooper-Zare expression for β in atoms:[58]

$$\beta_l(\varepsilon) = \frac{l(l\text{-}1)\, \mathbf{R}_{l\text{-}1}(\varepsilon)^2 + (l\text{+}1)(l\text{+}2)\, \mathbf{R}_{l+1}(\varepsilon)^2 - 6\, l(l\text{+}1)\, \mathbf{R}_{l\text{-}1}(\varepsilon)\, \mathbf{R}_{l+1}(\varepsilon) \cos \Delta(\varepsilon)}{(2l\text{+}1)\, [\, l\, \mathbf{R}_{l\text{-}1}(\varepsilon)^2 + (l\text{+}1)\, \mathbf{R}_{l+1}(\varepsilon)^2\,]} \qquad \text{Eq. IV-4}$$

and specifically for p orbitals:

$$\beta_p(\varepsilon) = \frac{\mathbf{R}_d(\varepsilon)^2 - 2\,\mathbf{R}_s(\varepsilon)\,\mathbf{R}_d(\varepsilon)\cos\Delta(\varepsilon)}{\mathbf{R}_d(\varepsilon)^2 + (1/2)\,\mathbf{R}_s(\varepsilon)^2}, \qquad \text{Eq. IV-5}$$

where $\Delta(\varepsilon) = [\,\delta_{l+1} + \sigma_{l+1}] - [\,\delta_{l-1} + \sigma_{l-1}]$, the difference in the energy dependent phase shifts (δ is the short range potential phase shift, and σ the coulomb phase shift). $\mathbf{R}_{l\pm1}(\varepsilon)$ is the radial matrix element we shall label $\mathbf{R}_{l,l\pm1}(\varepsilon)$; Manson's form of writing the matrix element assumes the selection rule $l \rightarrow l'$, where $l' = l\pm1$, so the initial state l is supressed. From this expression, when $\mathbf{R}_d \rightarrow 0$, $\beta \rightarrow 0$. [Actually $\mathbf{R}_d = 0$ is just one solution for $\beta = 0$, the other being $\mathbf{R}_d = 2\,\mathbf{R}_s \cos\Delta$. We observe that the $\mathbf{R}_d = 0$ solution always occurs at lower energy than the other solution.] This result may be considered in another light. When $\mathbf{R}_d \rightarrow 0$, only the totally symmetric s channel is left and totally symmetric angular distribution is given by $\beta = 0$, as we found at the end of the last section.

Manson goes on to parametrize β near the CM where $\mathbf{R}_s(\varepsilon) >> \mathbf{R}_d(\varepsilon)$. We define $\gamma(\varepsilon) = \mathbf{R}_d(\varepsilon)/\,\mathbf{R}_s(\varepsilon)$, so

$$\beta_p(\varepsilon) = \frac{2\,\gamma(\varepsilon)\,\{\,\gamma(\varepsilon) - 2\cos\Delta(\varepsilon)\,\}}{1 + 2\,\gamma(\varepsilon)^2}, \qquad \text{Eq. IV-6}$$

which for $\gamma(\varepsilon) << 1$ yields $\beta_p(\varepsilon) = -4\,\gamma(\varepsilon)\cos\Delta(\varepsilon)$. Thus, in a restricted region around the CM, if γ goes from -0.2 to +0.2 and $\cos\Delta(\varepsilon)$ remains approximately constant (it does) at about 0.5, β_p will change by 0.8. This is a very rapid change in β, whose range is only 3 units. Of course, the above is only intended to indicate the trend of β_p, not to represent any actual case.

The above parametrization indicates further that β_p becomes negative at an energy immediately above that of the CM. This is common among p orbitals which

show CM. For atoms, there occurs a term in the expression for β involving the cross product of the $l \rightarrow l+1$ and $l \rightarrow l-1$ matrix elements. This term bears a negative sign which expresses itself as negative overall β_p at certain energies. (For negative β in the molecular case of HCl, see Thiel[59]). The $\mathbf{R}_d(\varepsilon) = 0$ root of the expression for $\beta_p(\varepsilon)$ always occurs at a lower energy than the other root, $\mathbf{R}_d = 2\,\mathbf{R}_s \cos\Delta$, and β_p is negative until the energy of this root is reached.

Energy Location of the Cooper Minimum

The total cross section of argon shows a minimum at 1.9 Ry, tempting us to place the CM at this energy. The σ_{tot}'s for krypton and xenon, among others, do not show minima, frustrating attempts to find their CM. Manson notes the experimental problem of locating CM and suggests using the sinuosity of β. He states:[57]

> The rapidity of the variation of β with energy in the vicinity of a Cooper minimum has an important possible application. It is generally very difficult to pinpoint the exact energy at which a Cooper minimum for a given subshell occurs from a *total absorption measurement* due to interference from other subshells so that the minimum is often washed out completely or just a very small dip percentagewise. Further, while looking at the *total photoelectron production cross section* for the subshell is somewhat better and abnegates this difficulty, it still suffers from the fact that the minimum is usually fairly broad making the determination of the zero point rather difficult. Measurement of the angular distribution of photoelectrons, however, is much more sensitive; the rapid variation of β near the zero [in cross section] means that only slightly above or below the zero the angular distribution differs measurably from isotropic, i.e., β is rather different from zero. Thus photoelectron angular distribution measurements have the capability of providing very accurate information on the position of the Cooper minimum which is of great importance in assessing theoretical treatments of photoionization. [Italics are added.]

Some workers have seemed to interpret this as meaning that the energy of the CM is at the minimum in β. This is not Manson's meaning, nor does it carry over to

theoretical calculations. The Figures show the situation. The minimum in β for argon, for instance, is at 2.0 Ry yet the kd channel is at its lowest at 1.7 Ry, where β is zero, as it must be. Further clouding the placement, we find the minimum total cross section at 1.9 Ry.

In the theory, it is easy to choose among these alternatives. Since it is the disappearance (or drastic diminution) of one or more channels which lies at the heart of the whole phenomenon, the energy at which this disappearance occurs is the energy of the CM. In atoms this is also where $\beta = 0$--within 0.1 Ry, the mesh or resolution in our calculations.

In molecules, the point where a channel is at a minimum and the point where $\beta = 0$ (if it does) may be separated by more than our resolution due to the multi-*l* makeup of molecular wavefunctions and cross sections. In this case, the channel cross section minimum is to be preferred as the location of the CM.

In experiment, we cannot observe symmetry channels to find their minima, and total cross sections sometimes yield broad or even no minima, as Manson points out. Thus have the above mentioned workers turned to the β curve to find CM. Since often β does not obtain zero in p orbital experiments, they have futher turned to the minimum β, β_{min}, as an indicator of energy of CM. We should like to suggest an alternative.

The rapidly changing part of the β curve occurs before the CM, and the minimum in our calculations occurs after the CM--even for molecules! An energy lying between the energies of these two portions is more reasonable than the energy of β_{min}. [That theory goes through zero while experiment does not is not due to an error in the theory but is probably due to our lack of understanding of the process of and corrections involved in the comparison of a model calculation with experiment.]

As the location of the CM in p-like orbitals, we suggest the midpoint of the interval bounded on the right by β_{min} and on the left by the "most rapid change" in β.

To find the most rapidly changing part of the β curve, calculating the greatest slope is difficult with typical experimental data, and using the energy midpoint of the maximum β and the minimum β is hazardous due to scatter of the experimental data along the ordinate. We shall suggest a method which seems to be needlessly complex, but is actually easy to perform with typical data.

1. Determine an "average" maximum β and an "average" minimum β.
2. Find the value of β lying at the midpoint between these:

$$\beta' = (\beta_{max} + \beta_{min})/ 2.$$

3 Find the energy where the experimental β curve seems to be equal to β'. This is ε'.
4. The energy midpoint between ε' and $\varepsilon(\beta_{min})$--the energy at which the β curve is lowest--is ε_{CM}.

Let us stress that there is no mystical truth contained in this procedure for finding ε_{CM}. It is merely a reproducible method for bringing ε_{CM} down from the too high values it has when found by looking for β_{min}. When applied to our theoretical results for np-like orbitals for atoms and molecules, the proposed method places the CM within 0.1 Ry of the energy where the np→ kd (or analogous 1π→ kδ) channel cross section shows a minimum.

An example of this procedure is given in Figure IV-5 for HBr 1π (from Reference 23). β_{max} is about 1.73, β_{min} is about -0.05, and β' = 0.84 is halfway between these. The experimental curve seems to cross β' = 0.84 at ε' = 52 eV (photon energy), and β_{min} is around $\varepsilon(\beta_{min})$ = 68 eV. Halfway between these is 60 eV where we shall place the CM. IE for HBr 1π is 11.9 eV, so our CM lies at about 48 eV photoelectron energy.

Carlson, et al.,[23] have published a graph showing the positions of the experimental and theoretical CM for the outermost np orbital of the noble gases

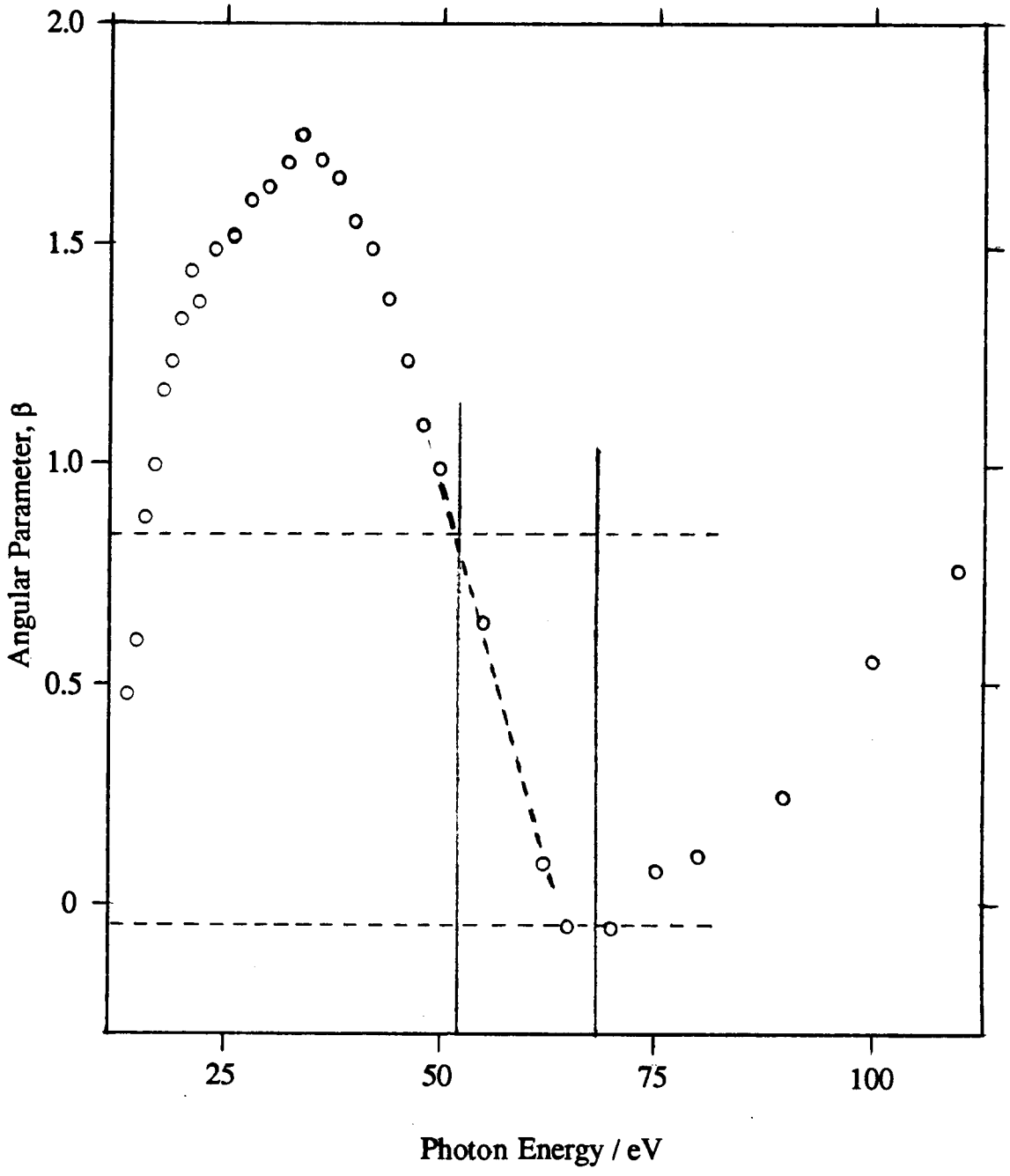

IV-5. Experimental angular parameter as a function of photon energy for the 1π orbital of HBr.

argon, krypton, and xenon, and the outermost 1π of the hydrogen halides, HCl, HBr, and HI. In Figure IV-6a, we present this graph which uses the β_{min} method. In Figure IV-6b, we show this graph using the same sources (References 22, 24, 60, 61, 62, 57, 63, 64) but with our method for locating the CM.

Carlson has this to say[23] about the graph we call Figure IV-6a.

> In Figure IV-6a are plotted the values of the photoelectron energy corresponding to the minimum in the β parameter for the π orbital arising from the effects of the Cooper minimum. Results are also plotted for the rare gases, (References 62, 60, 61) which are isoelectronic with the corresponding hydrogen halides. It has been noted before that the lone-pair orbitals of the halides closely mimic the behavior of the corresponding rare gas (Z + 1) with regards to the Cooper minimum (References 24, 19). It was also noted that the variation in the energy position of the Cooper minimum lone-pair orbitals of different molecular orbitals is much smaller (a few electron volts) than the difference between the different halides (References 22, 24, 19, 20). It can be seen from Figure IV-6a that there is a close parallel between the experimental behavior of the rare gases and the corresponding hydrogen halides. It is also to be noted from Figure IV-6a that the calculated energies of the minimum position in β for the rare gases using Hartree-Slater potentials (Reference 57) are nearly the same as our MSXα calculations on the hydrogen halides. This is not too surprising since the MSXα method uses a Hartree-Slater atomic potential for the starting point in the calculations and treats exchange in the same manner as the Hartree-Slater calculation for atoms.
>
> It is interesting to evaluate the effects of improving the atomic calculations. In Figure IV-6a results from atomic calculations are plotted for the rare gases, first improving the treatment of exchange and adding relativistic effects (Dirac-Fock, Reference 63) and then employing, in addition, many-body effects (Reference 64). In the latter case good agreement was finally obtained between experiment and theory. Presumably, if the same improvements could be applied to the molecular situation, good agreement between experiment and calculations on the hydrogen halides would also be achieved.

It is pleasantly ironic that after we apply our (not uninvolved) proposed method, all we have achieved is a minor rearrangement and shift downward by about 7 eV of the curves given by the β_{min} method. All of the comments by Carlson, et al., apply to our graph as well as his.

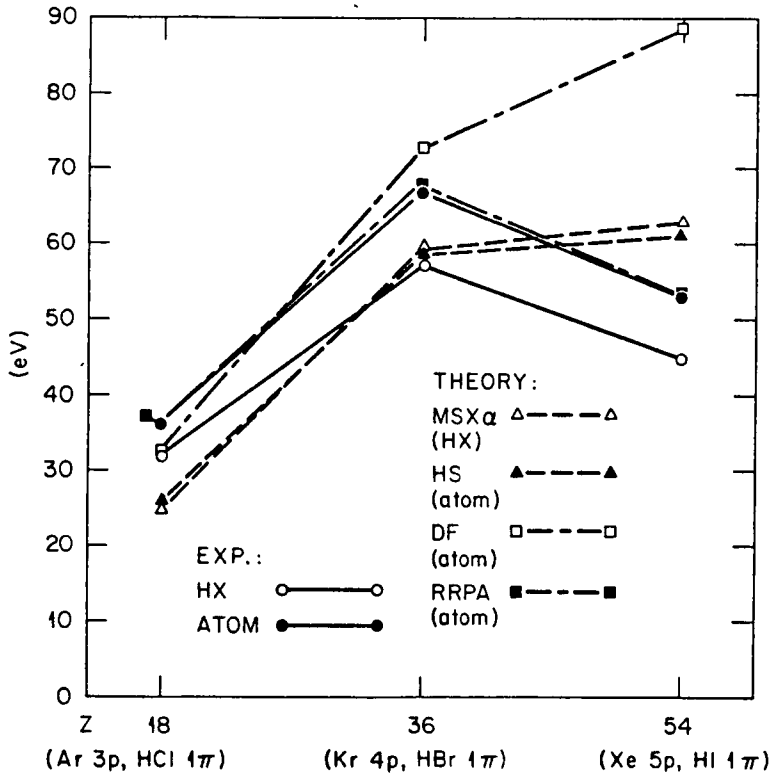

IV-6a. Comparison of the minimum position in the plots of β vs. photoelectron energy as a function of atomic number.

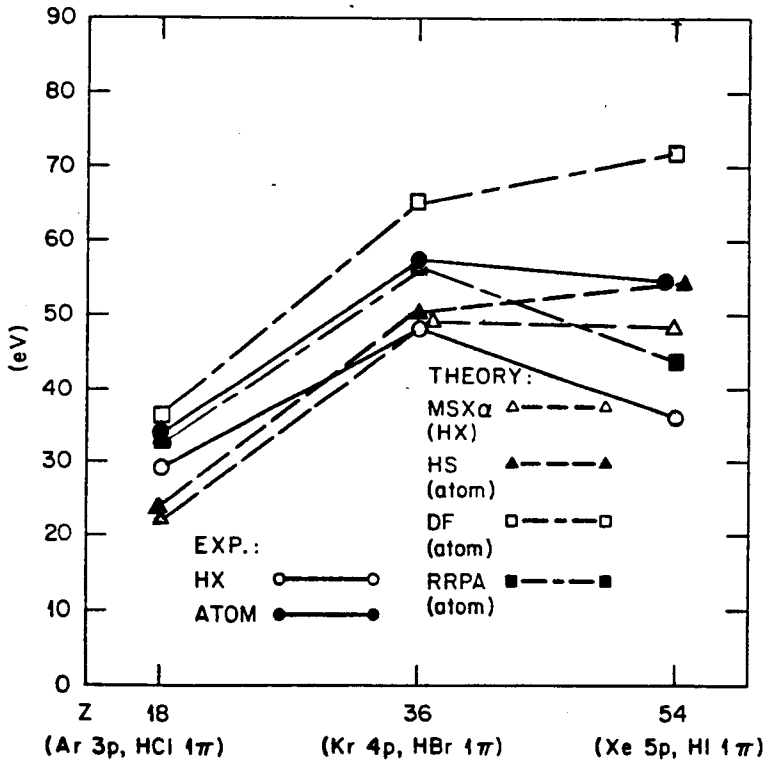

IV-6b. Comparison of the position of "most rapid change in β" in the plots of β vs. photoelectron energy as a function atomic number.

This is good for the experimentalists who want to assign the energy of the CM by the β_{min} method. They may do so with impunity (at least from us). Nevertheless, we still labor under the conviction that the Cooper minimum found by the β_{min} method is too high in energy, by an amount that depends on the broadness of the minimum.

[We shall discuss the practice of comparing hydrogen halides to their isoelectronic noble gases at the end of Chapter V.]

Shape Resonances

A shape resonance (SR) is manifested in a manner opposite to a CM. Instead of channel cross sections going through minima as in CM, SR show maxima due to a particularly large rise in matrix element magnitude over a small energy range (References 9, 15, 11).

Shape resonances show up in the $l \geq 2$ subshells in atoms of medium to high Z. The shape resonance in xenon 4d is shown in Figure IV-7 as an example. The maximum in cross section at 0.8 Ry is a shape resonance and the minimum near 6 Ry is a CM, to be discussed with the atomic results. From the channel cross sections, the kf channel is seen to underlie this resonant behavior.

In the radial Schrödinger equations IV-1 and IV-2, if we take the effective potential to be

$$V_{eff}(r) = V(r) + l(l+1)/r^2 \qquad \text{Eq. IV-7}$$

then at some r for high l, the second term dominates causing a positive energy potential "barrier." V_{eff} for $l = 3$ for xenon is shown in Figure IV-8. The $l = 3$ double well potential shows us that there cannot be an f bound solution deeper than - 6 Ry. More importantly, there is a hump in the potential from about $1a_0$ to $5a_0$ which in effect "raises the ionization energy for $l = 3$ photoelectrons."[11]

The initial 4d, the unoccupied 4f, and three $l = 3$ radial wavefunctions are presented in Figure IV-9. [In plotting these functions we have ignored their relative

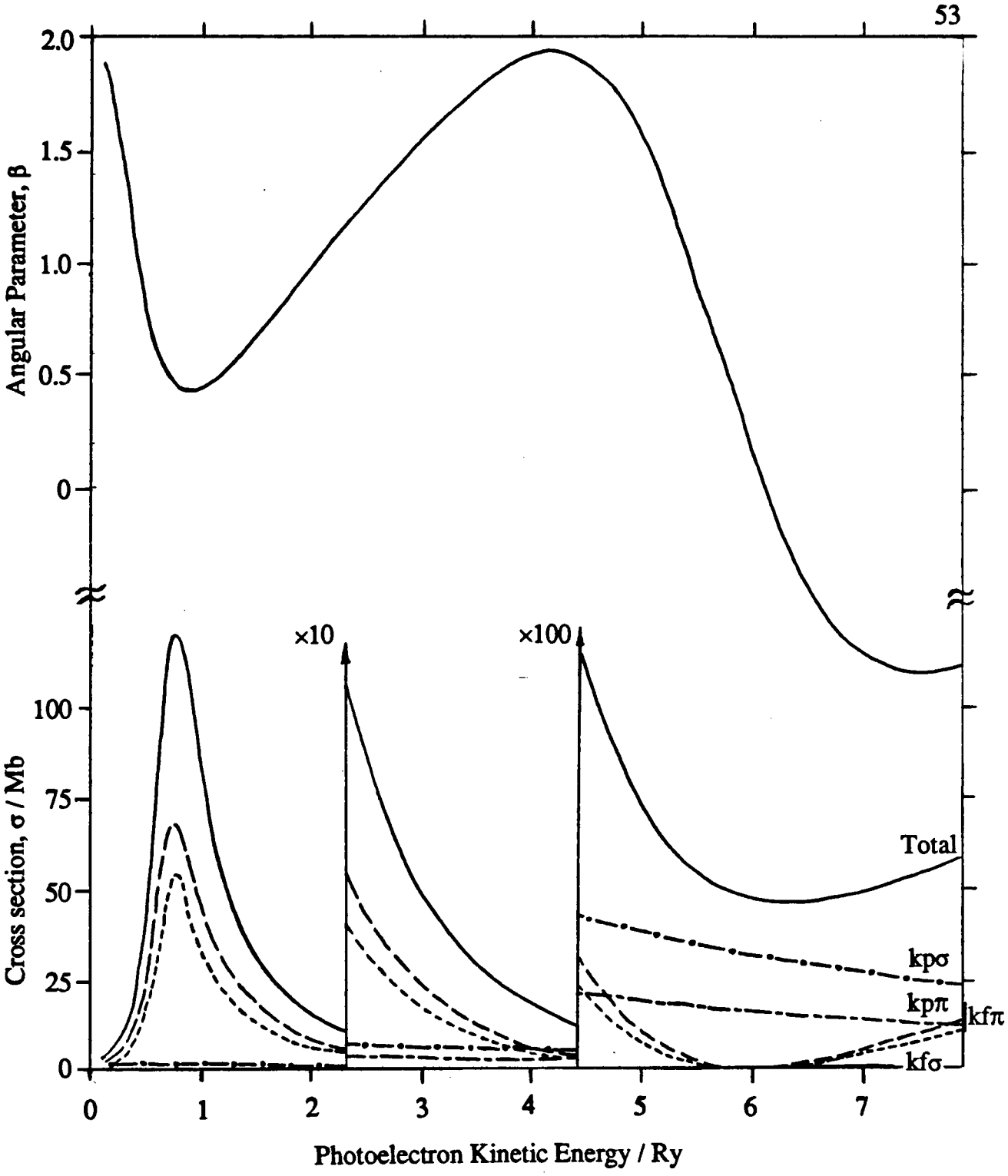

IV-7. Calculated cross section and angular parameter as a function of photoelectron kinetic energy for xenon 4d. The kpσ channel cross section is twice that for kpπ. The kfπ channel cross section is 4/3 that for kfσ.

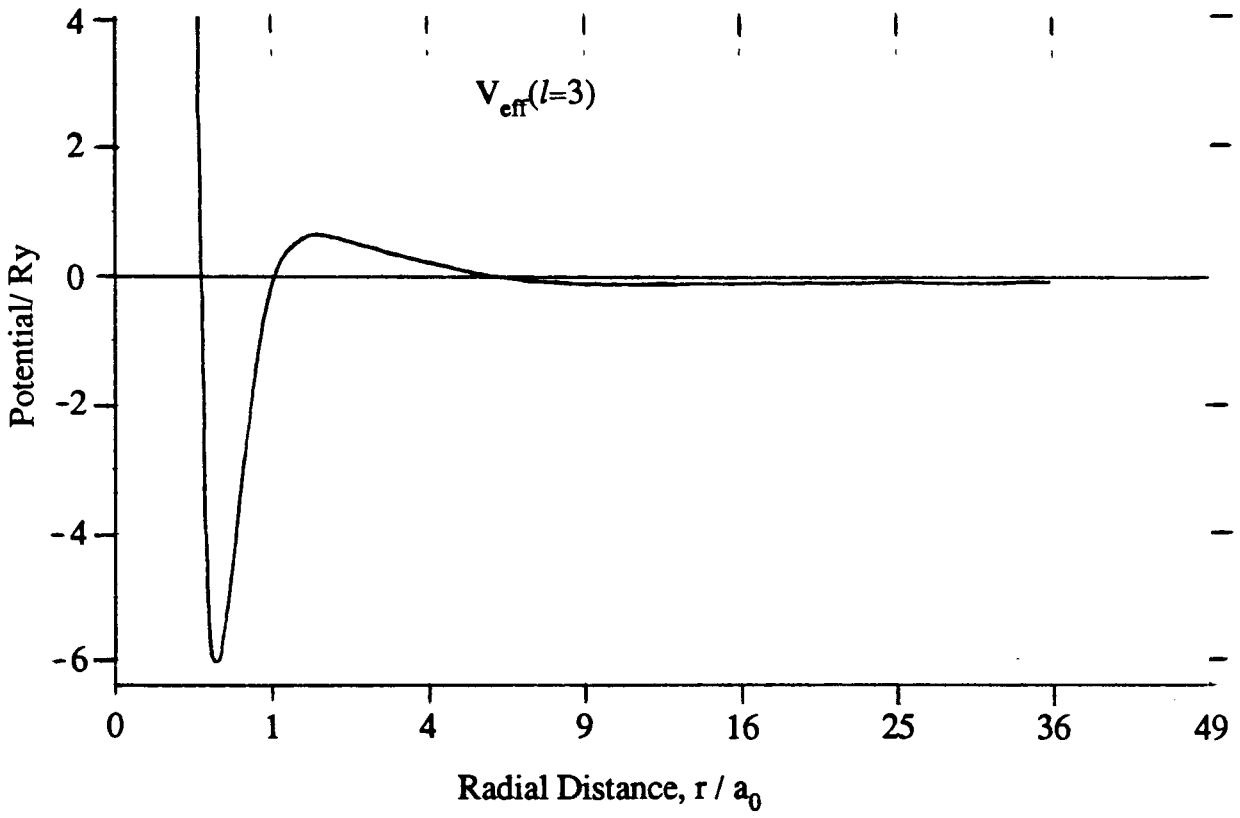

IV-8. Effective $l = 3$ potential for xenon.

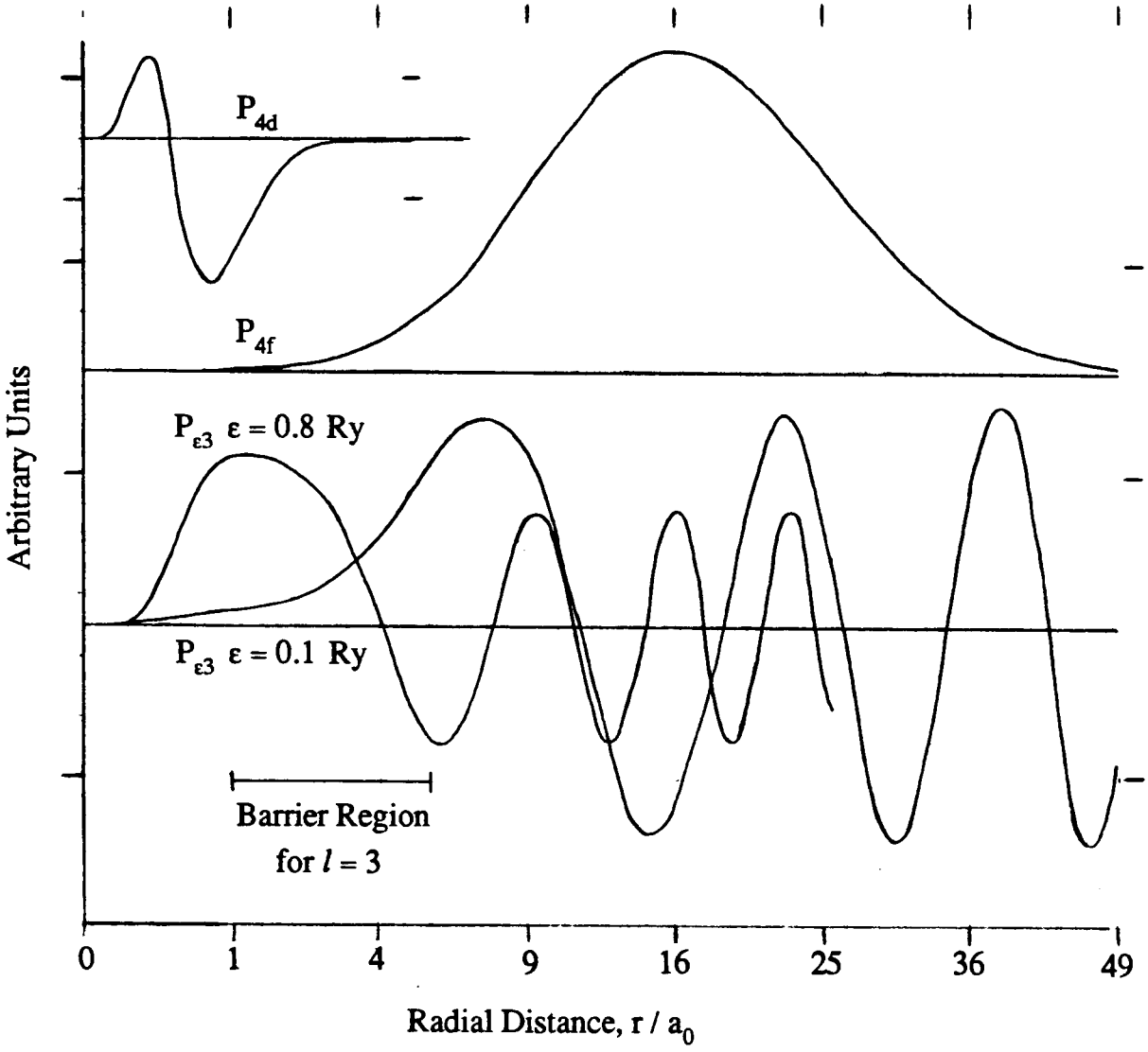

IV-9. Initial 4d (l = 2), 4f (l = 3, IE = -0.0625 Ry), and continuum (l = 3) radial wavefunctions for xenon at 0.1 and 0.8 Ry photoelectron kinetic energy. The l = 3 barrier region from Figure IV-8 is indicated.

normalization. We wish simply to indicate the radial behavior of each.] The barrier region has been indicated. Note that the $\varepsilon = 0.1$ Ry and the 4f wavefunctions have low amplitude inside the potential barrier, but the $\varepsilon = 0.8$ Ry wavefunction has quite substantial amplitude inside it.

We might say that 4f and $\varepsilon = 0.1$ Ry are "eigenfunctions" of the outer $l = 3$ well, and 4d is an "eigenfunction" of the $l = 2$ potential, but that the $\varepsilon = 0.8$ Ry solution is an "eigenfunction" of both the outer and inner $l = 3$ well. The amplitude in the inner well generally reaches its maximum at photoelectron energies comparable to the height of the barrier, so the inner well amplitude decreases with increasing energy from about 0.8 Ry.

Naturally, the dipole matrix element and subsequently the cross section are affected by this behavior of the wavefunction. At threshold, where the continuum electron's amplitude is low inside the barrier region, the overlap between P_{4d} and $P_{\varepsilon f}$ will be poor (the inner well position for $l = 3$ and the well in 4d are at approximately the same position). As the energy increases, and $P_{\varepsilon f}$ has a loop pushed into the inner well (making the phase shift jump by π),[50] the overlap improves as the continuum wavefunction's amplitude soars within the inner well, and the matrix element thus undergoes a great increase in magnitude. Eventually, the energy of the continuum photoelectron increases to a point where the barrier cannot "trap" amplitude any more, and the matrix element and cross section return to low values.

In a sense, SR matrix element enhancement (which underlie the cross section enhancement) are traceable to an enhancement in the coefficient(s) on the wave(s) in the region inside the barrier. We may find solutions to the Schrödinger equation at any positive energy for this region inside the barrier, but at some energies--the energies of SR--the coefficient(s) responsible for matching this solution to that outside the barrier grow large and "resonate." Manson and Cooper[65] discuss this as follows. The matrix element is describable as $\mathbf{R}_{l,l'}(\varepsilon) = C_{l'}(\varepsilon)\, \underline{\mathbf{R}}_{l,l'}(\varepsilon)$, where $C_{l'}(\varepsilon)$ is a final state normalization coefficient, and $\underline{\mathbf{R}}_{l,l'}(\varepsilon)$ is thus an unnormalized matrix

element. [In full,

$$\underline{\mathbf{R}}_{l,l'}(\varepsilon) = \int_0^{\infty} P_{nl}(r)\, r\, \underline{P}_{\varepsilon l'}(r)\, dr, \qquad \text{Eq. IV-8}$$

where

$$P_{\varepsilon l'}(r) = C_{l'}(\varepsilon)\, \underline{P}_{\varepsilon l'}(r) \qquad \text{Eq. IV-9}$$

is the solution of Equation IV-2. $C_{l'}(\varepsilon)$ for atoms is found so that $P_{\varepsilon l'}(r)$ acts asymptotically as

$$P_{\varepsilon l'}(r) = C_{l'}(\pi x)^{-1/2} \sin \theta_{l'} \qquad \text{Eq.IV-10}$$

where $x = \partial\theta/\partial r$, as Cooper descibes in Appendix A of Reference 9.] For core subshells, $\underline{\mathbf{R}}_{l,l'}(\varepsilon)$ does not vary much with energy, so $C_{l'}(\varepsilon)$ must be responsible for resonances.

As with CM, the $l \rightarrow l$-1 channel provides only a small contribution throughout. In the case of the CM, it keeps the cross section from achieving zero at the CM; here, it keeps the cross section above zero at threshold. Cooper[9] discusses these potential barrier effects, and Starace[11] provides a review of the atomic literature to 1978.

It is hard to analyze a general case for β around a SR, because SR involve unknown and untypical values of the matrix elements and the phase shifts. We can parametrize β_d around SR in the manner in which Manson did for β_p around CM. Let $\gamma(\varepsilon) = \mathbf{R}_p(\varepsilon)/\, \mathbf{R}_f(\varepsilon)$, and from the Cooper-Zare formula:[58]

$$\beta_d = \frac{2\,\gamma(\varepsilon)^2 + 12 - 36\,\gamma(\varepsilon)\cos\Delta(\varepsilon)}{10\,\gamma(\varepsilon)^2 + 15} \qquad \text{Eq. IV-11}$$

This equation shows the difficulty in describing a "typical SR": the largest coefficient, that on the last term in the numerator, multiplies the fast changing $\gamma(\varepsilon)$ and the factor involving the phase shift. Suffice it to say that β can undergo variations as drastic near a SR as it does near a CM. Figure IV-7 showed that as the xenon 4d SR is approached from below, β changes by 1.4 (from about 1.9 down to 0.5). Again, this is a very large change for a parameter whose range is only three units.

Molecular Shape Resonance

Dehmer and Dill[48,49] note that K-shell photoionization of N_2 shows a resonance at around 1 Ry photoelectron energy. "Not only," they continue,[48] "is this [cross section] enhancement non-hydrogenic, but it has no counterpart in either the spectra of the constituent atoms or the spectra of the united atom." This means that the resonance is due to the molecular nature of the potential, i.e., spatial extent (separated nuclei) and anisotropy (less than spherical symmetry) of the molecular potential. In atomic physics, it is known that high-l partial waves are "excluded" from the core, but Dehmer and Dill[51] show the N_2 resonance to be primarily due to an $l = 3$ partial wave. Thus the formation of the molecular potential has caused the introduction of, and coupling to, high-l components in the continuum wavefunctions. As we saw with xenon 4d, high-l waves experience effective potential barriers which give rise to resonant behavior. To quote Dehmer and Dill on the N_2 case:[49]

> The essence of this phenomenon can be described in mechanistic terms as follows. The electric dipole interaction, localized within the atomic K-shell, produces a photoelectron with angular momentum $l = 1$. As this p-wave electron escapes to infinity, the anisotropic molecular field can scatter it into the entire range of angular momentum states contributing to the allowed σ- and π-ionization channels ($\Delta\lambda = 0, \pm 1$). In addition, the spatial extent of the molecular field of the two atoms, separated by 1.1 Å, enables the $l = 3$ component of the σ continuum wavefunction to overcome its centrifugal barrier and penetrate into the molecular core at a kinetic energy of ~0.8 Ry. This penetration is rapid, a phase shift of ~π occurring over a range of ~0.3 Ry. These two circumstances combine to produce a dramatic enhancement of photoelectron current at ~0.8 Ry kinetic energy, with predominantly f-wave character.

While it is not in general helpful or possible to graph the effective potentials in molecules (because of the discontinuities introduced with the muffin tin approximation and overlapping spheres), we still believe that the effective trapping of high-l partial waves into regions of space near the molecule by centrifugal barriers is a useful picture of near-threshold molecular resonances.

Because the distribution of nuclear charge over more than one site is inherent to (or definitive of) all molecules, Dehmer and Dill's analysis establishes the possibility that centrifugal barrier phenomena are likely in molecules other than N_2. Indeed, when we discuss the valence orbitals of the dihalogen molecules, we shall see that shape resonances near threshold are the rule. The dipole matrix elements for valence initial orbitals vary much more with energy than those for core orbitals (due to the weaker local field which valence electrons experience). These energy effects will appear alongside the resonant features in the valence orbitals.

In molecules, the eigenphase sum does not always change by an entire unit at SR, as does the phase at atomic SR.[48,66] (Remember that the eigenphase sum has π radians divided out and is unitless; it is not quite a phase.) Often the "rotation" is by as little as one-quarter unit where distinguishable resonant behavior is apparent in the cross section. This is a result of the multi-*l* nature of molecular wavefunctions (and "scattering" amplitude) as evidenced by the sum over L in Equation III-37, the definition of the eigenphase sum.

CHAPTER V

ATOMIC RESULTS

In this chapter, we present the results of our calculations on atoms. First come the noble gases argon, krypton, and xenon, which provide a benchmark to other workers' calculations. They have been extensively studied both theoretically and experimentally, because they are easy to handle gases and are closed shell atoms. Second in this chapter come the halogen atoms chlorine, bromine, and iodine, which serve as a link between the much studied inert gases and the halide molecules which are the heart of this thesis. These molecules will be presented in the next two chapters, halogen acids, homonuclear dihalogens.

The data are presented in Figures. Note the following.

Energies are given as electron kinetic energy in rydbergs; one rydberg equals 13.6 eV. Rydbergs are more natural in theoretical work than eV. Since we do not optimize our calculations to give the best ionization energies, these reported kinetic energies may be considered as the next best thing to photon energies, i.e., they may be added to any calculated or experimental IE to find the photon energy. [There is, however, some question about this procedure.]

We approach threshold no closer than 0.1 Ry. Our model does not include polarization terms in the outer sphere region which are known to influence the exiting electron at energies near threshold.

Energy scales for Z = 17 and 18 are different from Z = 35, 36, 53 and 54. The features we are interested in lie within 4 Ry of threshold for Z = 17 and 18, but farther out for the higher Z. Results are shown to 8 Ry for these "high" atomic numbers.

We draw smooth, continuous curves through the data, although we calculate at intervals of 0.1 or 0.2 Ry. We have found strict belief in these curves to be unjustified, because the complicated mix of numerical methods in our photoionization program tends to misbehave at some energies. These energies vary with choice of

molecule and choice of options and parameters such as the sphere sizes. Some step in the calculation such as the inversion of a matrix begins to cause problems, and cross section, eigenphase sum, and asymmetry parameter are all sharply affected.

The resulting "features" resemble resonances and occur more often in molecules than in atoms, and more often in the larger molecules (consisting of atoms with higher atomic number and larger sphere size) than in the smaller. Some workers believe these to be "real" resonances, that is, not artifacts of the method. (There are no references in the molecular PES literature, however.) Our limited attempts to find an absolute cause for these features have been unsuccessful. Thus, in plotting the Figures, we smooth over these rough spots, which practice does not affect the major trends we shall discuss.

The precision of our energy "mesh" (0.1 or 0.2 Ry) also affects the accuracy with which we may locate the energies of features. We state this accuracy to be 0.05 Ry in most cases.

Continuum channel cross sections for atomic orbitals are reported in terms of the $C_{\infty v}$ subgroup of the full rotation-reflection group, K_h, to which the atoms belong (in our nonrelativistic method). This facilitates comparison of atomic results with molecular results. The np orbitals of the atoms were calculated using np_0 (or $np\sigma$) and an occupation number of six for the noble gases and five for the halogens. Thus, the PI process is schematically given by

$$np\sigma \rightarrow ks\sigma + kd\sigma + kd\pi^+ + kd\pi^-. \qquad \text{Eq. V-1}$$

In the Figures for the np orbitals, channel cross sections are presented as $k\sigma = ks\sigma + kd\sigma$, and $k\pi = kd\pi^+ + kd\pi^-$. This channel breakdown suffices for comparison with molecular σ orbitals involving the np_0 atomic orbital (A.O.) on the molecules constituent atoms, but is not suited to comparison with molecular π orbitals which involve the $np_{\pm 1}$ A.O.'s. The process for PI of $np_{\pm 1}$ ($np\pi^+$) is given by

$$np\pi^+ \rightarrow ks\sigma + kd\sigma + kd\pi^+ + kd\delta^+ + kd\delta^-. \qquad \text{Eq. V-2}$$

We shall not present the channel cross sections for PI from npπ orbitals in the Figures; the npπ$^+$ channel cross sections are related to those of npσ arithmetically. These relations are given as follows. Equal channel cross sections are connected by lines.

$$\begin{array}{ccccccccc} np\sigma & \rightarrow & ks\sigma & + & kd\sigma & + & kd\pi^+ & + & kd\pi^-. \\ & & | & & / \ \backslash & & | & & | \\ np\pi^+ & \rightarrow & ks\sigma & + & kd\sigma & + & kd\pi^+ & + & kd\delta^+ \ + \ kd\delta^-. \end{array} \qquad \text{Eq. V-3}$$

If we denote a channel cross section for a particular process as, say, $\sigma(np\pi^+ \rightarrow kd\sigma)$ for the process $np\pi^+ \rightarrow kd\sigma$, then together (a), the following two relations between channel cross sections of the npπ$^+$ initial state, and (b), the above relations between channel cross sections of npπ$^+$ and npσ, suffice to allow one to find any accessible channel cross section for either initial state:

$$\sigma(np\pi^+ \rightarrow kd\sigma) = (1/3)\ \sigma(np\pi^+ \rightarrow kd\pi^{\pm}), \qquad \text{Eq. V-4}$$

$$\sigma(np\pi^+ \rightarrow kd\pi^{\pm}) = \sigma(np\pi^+ \rightarrow kd\delta^{\pm}).$$

For the reader's ease, we present the following relations between the channels of npσ

$$\sigma(np\sigma \rightarrow kd\sigma) = (4/3)\ \sigma(np\sigma \rightarrow kd\pi^{\pm}),$$

$$\sigma(np\sigma \rightarrow ks\sigma) = \sigma(np\sigma \rightarrow k\sigma) - \sigma(np\sigma \rightarrow kd\sigma),$$

and relations between channels of npσ and those of npπ$^{\pm}$,

$$\sigma(np\pi^+ \rightarrow ks\sigma) = \sigma(np\sigma \rightarrow ks\sigma),$$

$$\sigma(np\pi^+ \rightarrow kd\pi^+) = \sigma(np\sigma \rightarrow kd\pi^{\pm}),$$

$$\sigma(np\pi^+ \rightarrow kd\sigma) = (1/4)\ \sigma(np\sigma \rightarrow kd\sigma),$$

$$\sigma(np\pi^+ \rightarrow kd\delta^{\pm}) = \sigma(np\sigma \rightarrow kd\pi^{\pm}).$$

These relations result from the appearance and behavior of the Gaunt integrals in **F**. They may be derived from Equations V-3 and V-4

Initial state *l*-type analyses and the parameters used in the calculations for all atoms and molecules studied are presented in the tables of Appendix V.

Noble Gas Atoms

The noble gas atoms which show CM in which we are interested and which are appropriate to calculate with our method are argon, krypton, and xenon. Neon has a CM in only the 2s which is, to say the least, not pronounced. Radon is so large that relativistic effects cannot be ignored, and thus it is not appropriate to study here.

The noble gases have been studied by Manson and others (References 9, 65, 57, 67, 68, 69, 63, 56, 64, 70) using a variety of theoretical techniques. We include our own calculations of noble gas properties to provide consistency in our work, and to illustrate the Cooper minimum clearly. Also, experimentalists are fond of comparing their results for each of the hydrogen halides with its isoelectronic noble gas--argon with HCl,[22] krypton with HBr,[23] and xenon with HI.[24] Because of this practice, our treatment might seem incomplete without results for the noble gases. In addition, the noble gas calculations may be compared directly to noble gas experiments, as our halogen atoms' results cannot. Let us stress that better calculations exist for these atoms. We have performed the atomic calculations using our model and method so as to better understand and interpret our results for molecules.

Figures V-1, V-2, and V-3 contain the photoelectron dynamics results for argon, krypton, and xenon, respectively, and subfigures subdivide these atoms into their outermost p, s, and d orbitals. Each subfigure contains graphs of the asymmetry parameter, total cross section, and symmetry channel cross sections. The energies of local minima and maxima are indicated by arrows, the energy of the CM by double, labeled arrows.

We take up the orbitals of the noble gases in order of type, i.e., outermost p, outermost s and, finally, d.

Noble Gas Outermost p Subshells

The selection rule for photoionization from a ground state orbital ($n\ell$) in non-relativistic, self consistent field atoms is $\Delta\ell = \pm 1$, and $n \rightarrow k$. k stands for the wave vector of the wave of energy $h^2k^2/2m$, or just k^2 in Rydberg atomic units. It may also

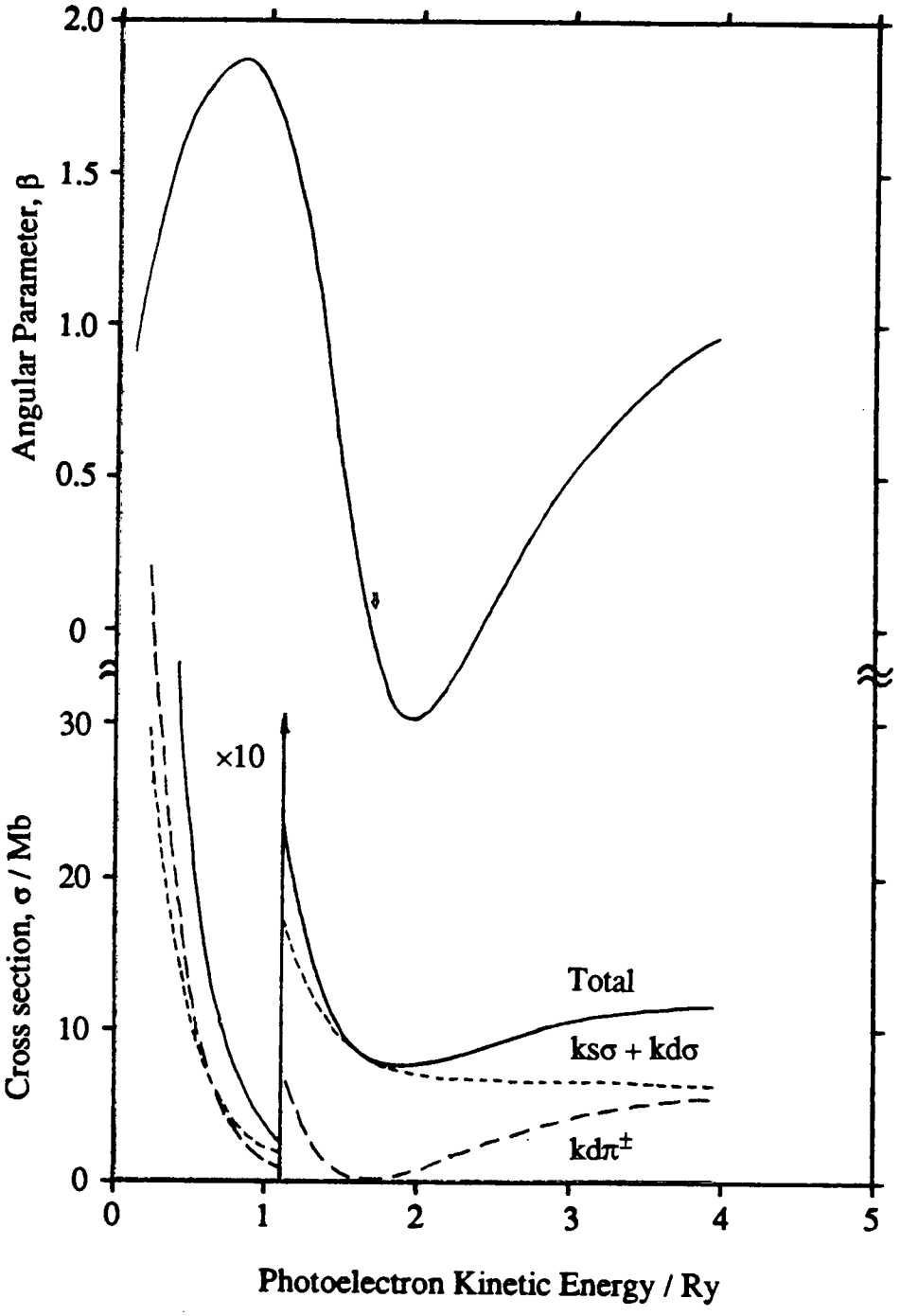

V-1a. Calculated total and channel cross sections and angular parameter as a function of photoelectron kinetic energy for argon 3p.

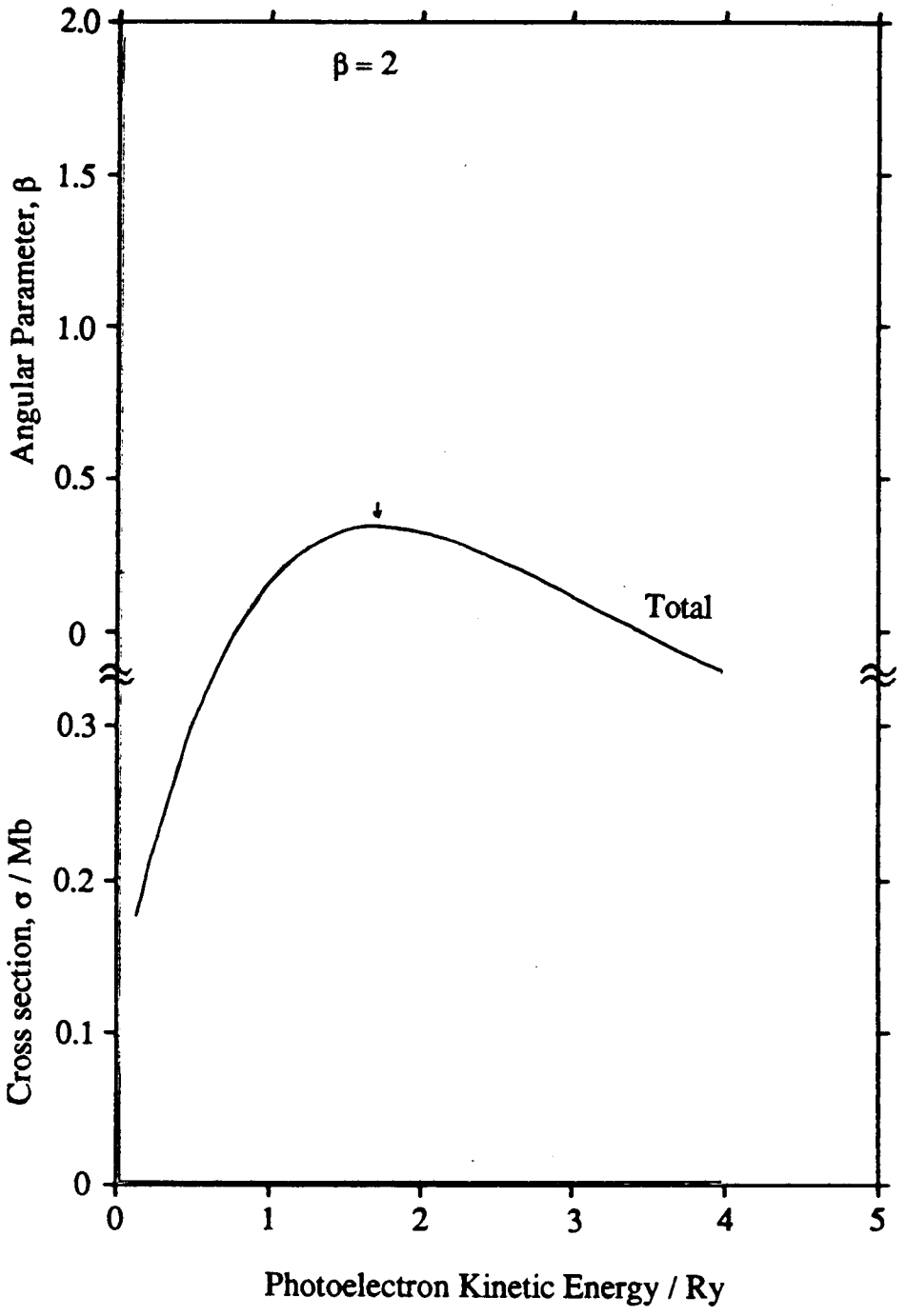

V-1b. Calculated total and channel cross sections and angular parameter as a function of photoelectron kinetic energy for argon 3s. The kpσ channel cross section is equal to 1/3 σ_{tot}. The kp$\pi^{\pm}$ channel cross section is equal to 2/3 σ_{tot}.

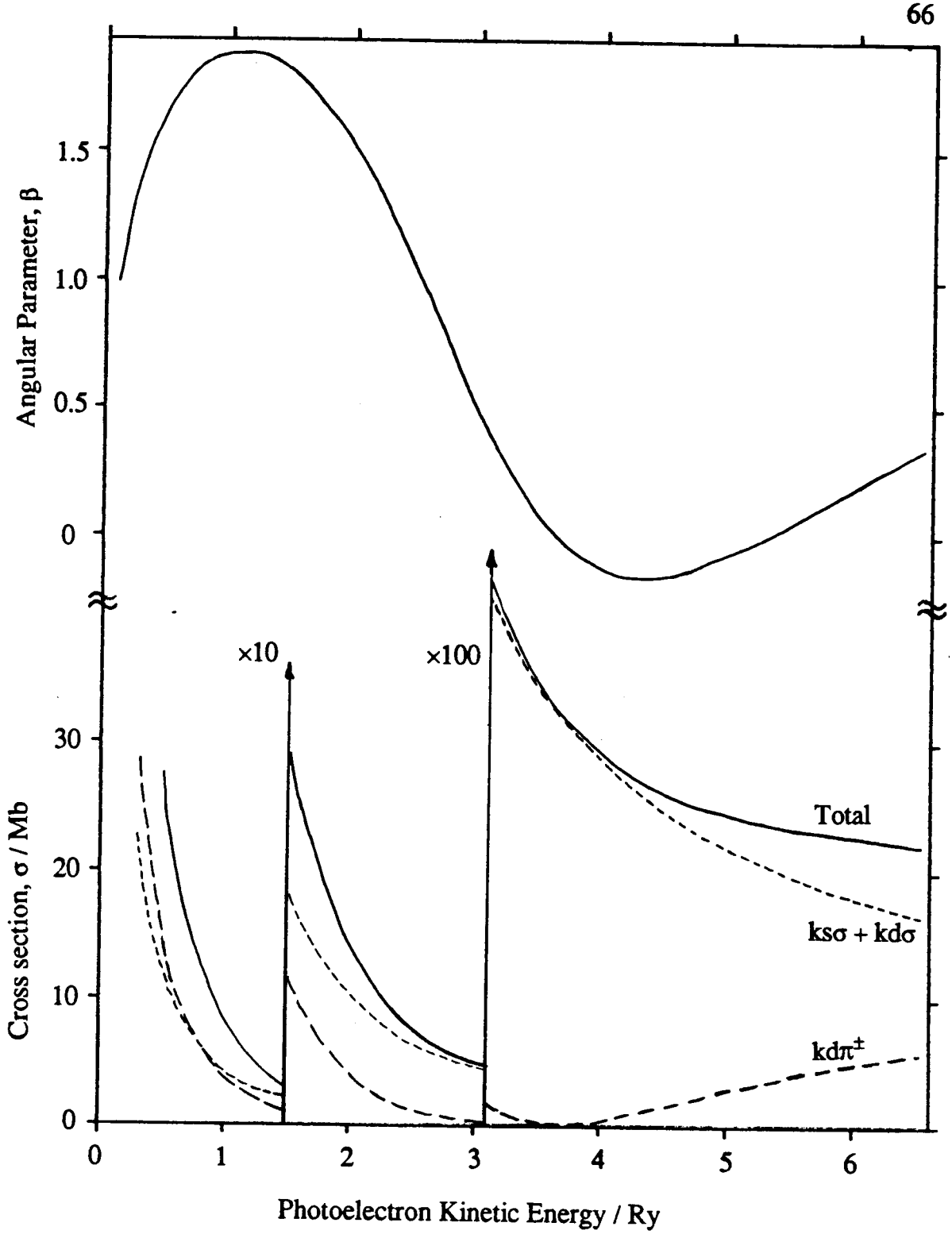

V-2a. Calculated total and channel cross sections and angular parameter as a function of photoelectron kinetic energy for krypton 4p.

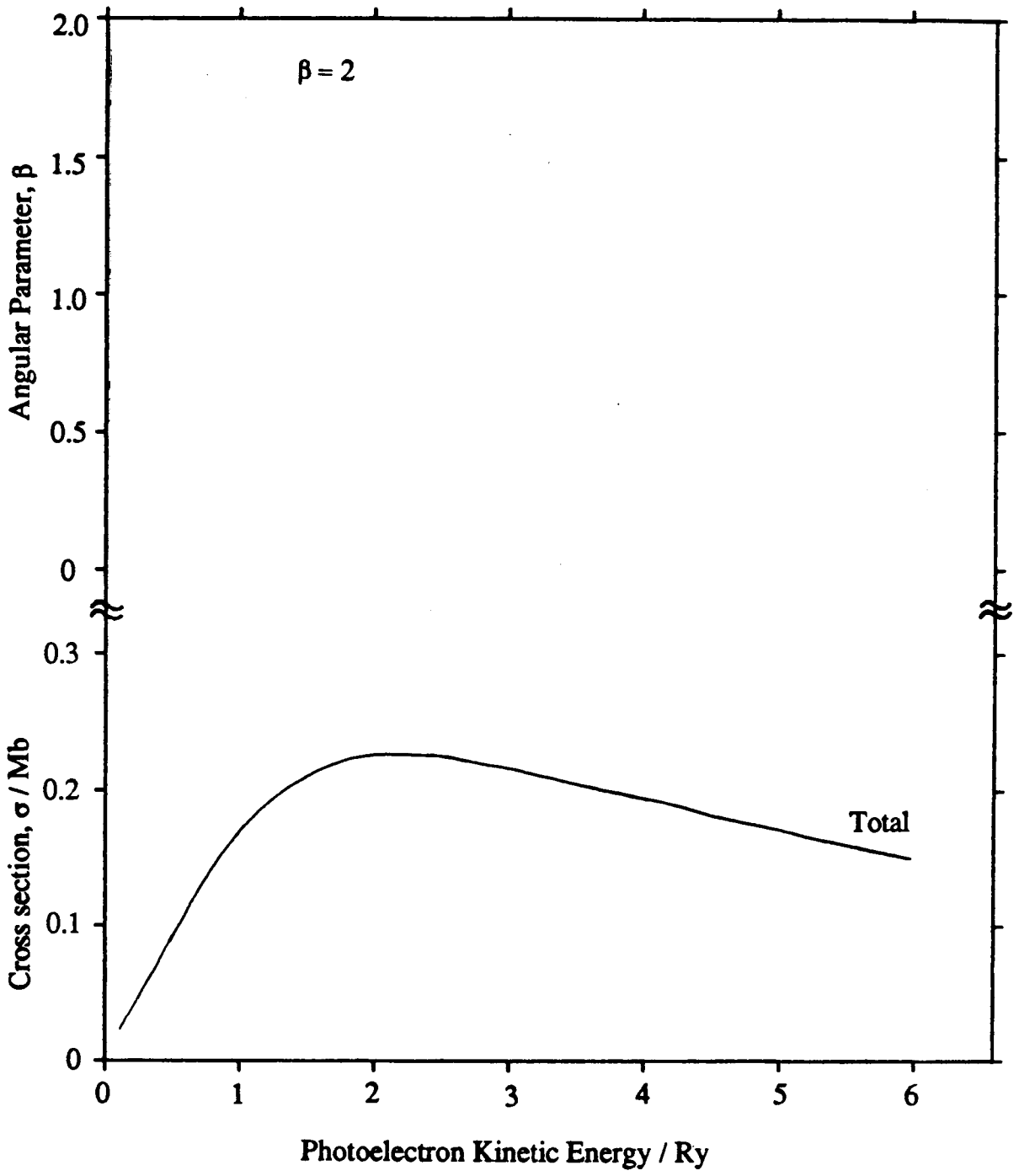

V-2b. Calculated total and channel cross sections and angular parameter as a function of photoelectron kinetic energy for krypton 4s. The kpσ channel cross section is equal to 1/3 σ_{tot}. The kp$\pi^{\pm}$ channel cross section is equal to 2/3 σ_{tot}.

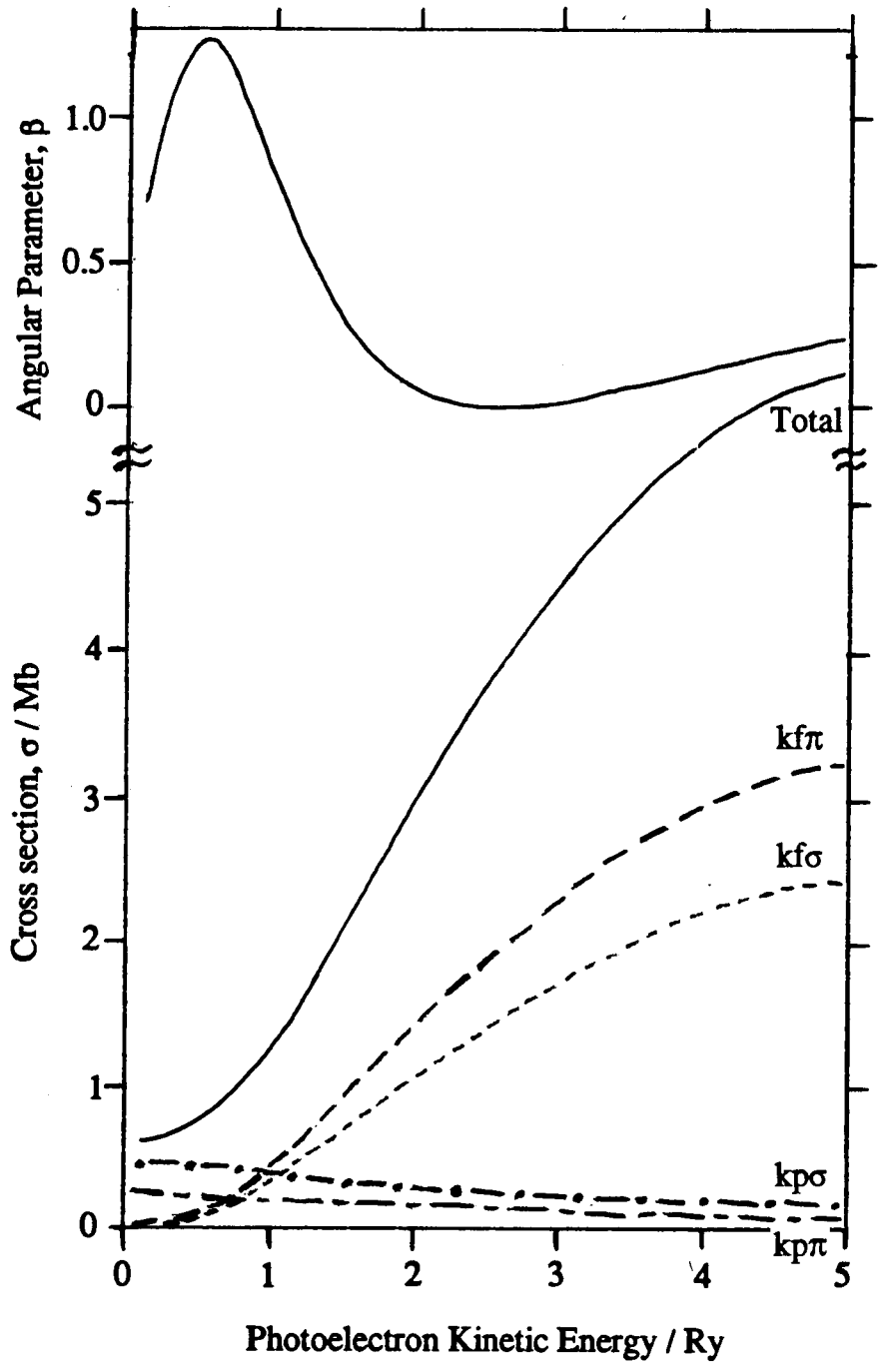

V-2c. Calculated total and channel cross sections and angular parameter as a function of photoelectron kinetic energy for krypton 3d. The kpσ channel cross section is twice that for kpπ. The kfπ channel cross section is 4/3 that for kfσ.

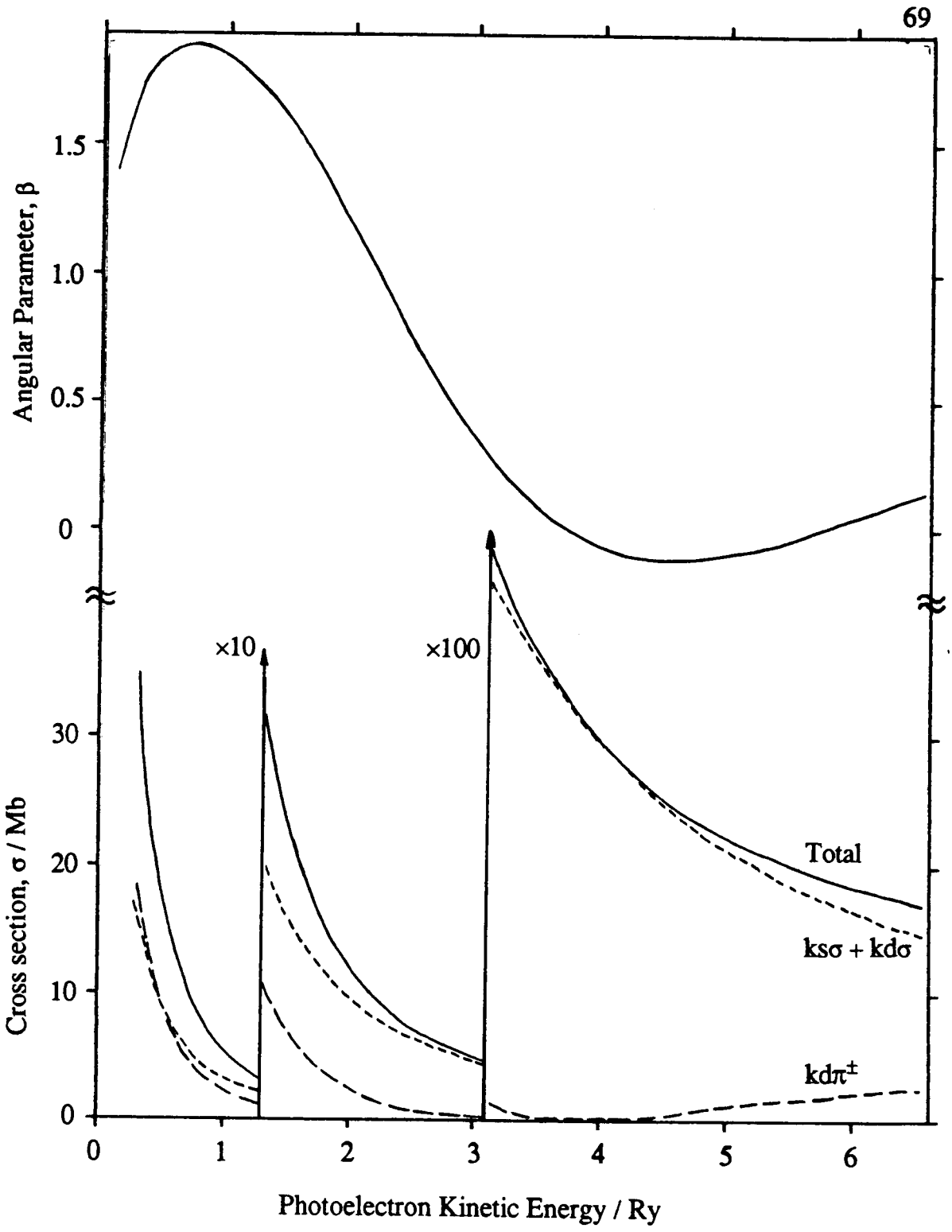

V-3a. Calculated total and channel cross sections and angular parameter as a function of photoelectron kinetic energy for xenon 5p.

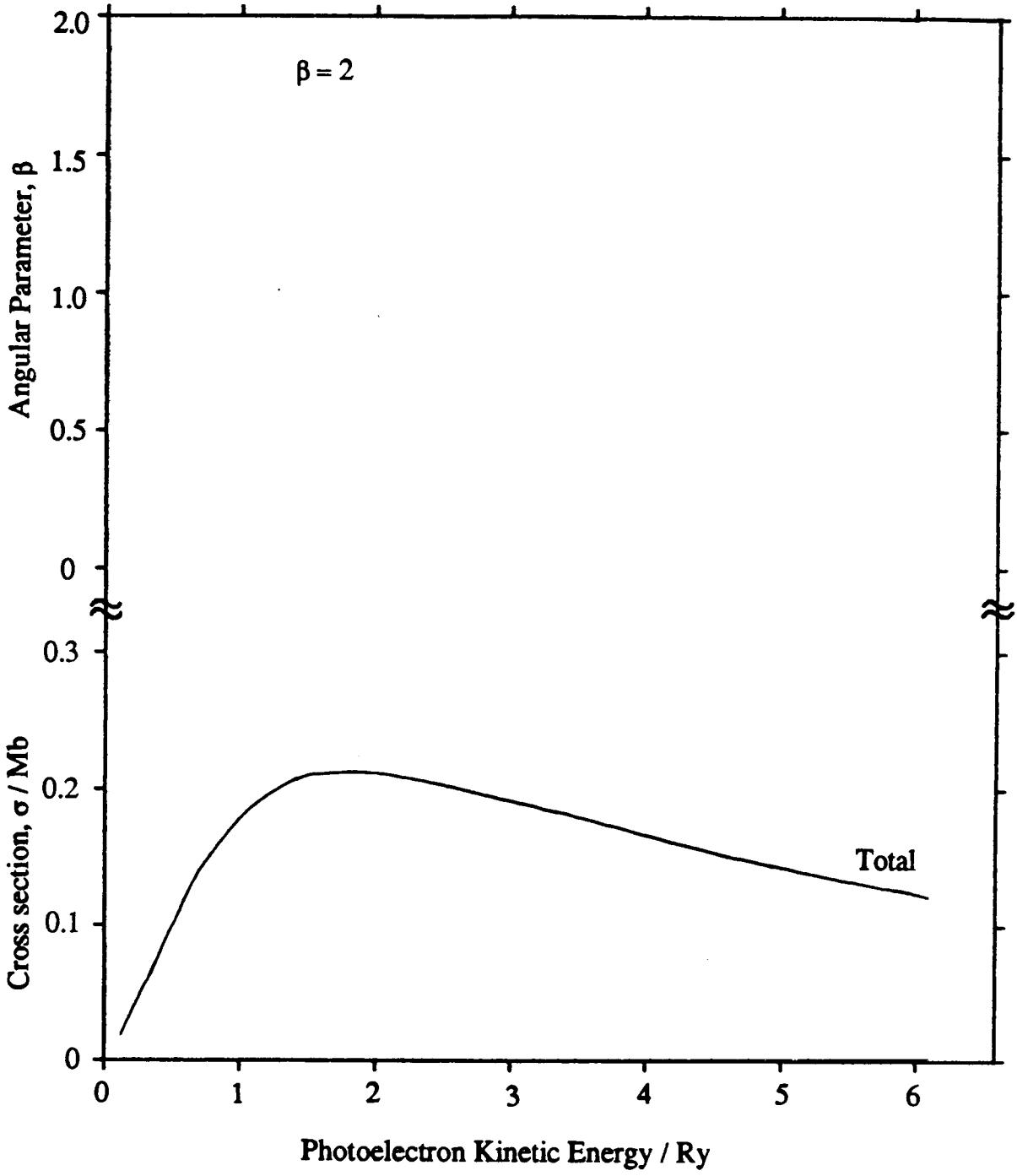

V-3b. Calculated total and channel cross sections and angular parameter as a function of photoelectron kinetic energy for xenon 5s. The kpσ channel cross section is equal to 1/3 σ_{tot}. The kp$\pi^{\pm}$ channel cross section is equal to 2/3 σ_{tot}.

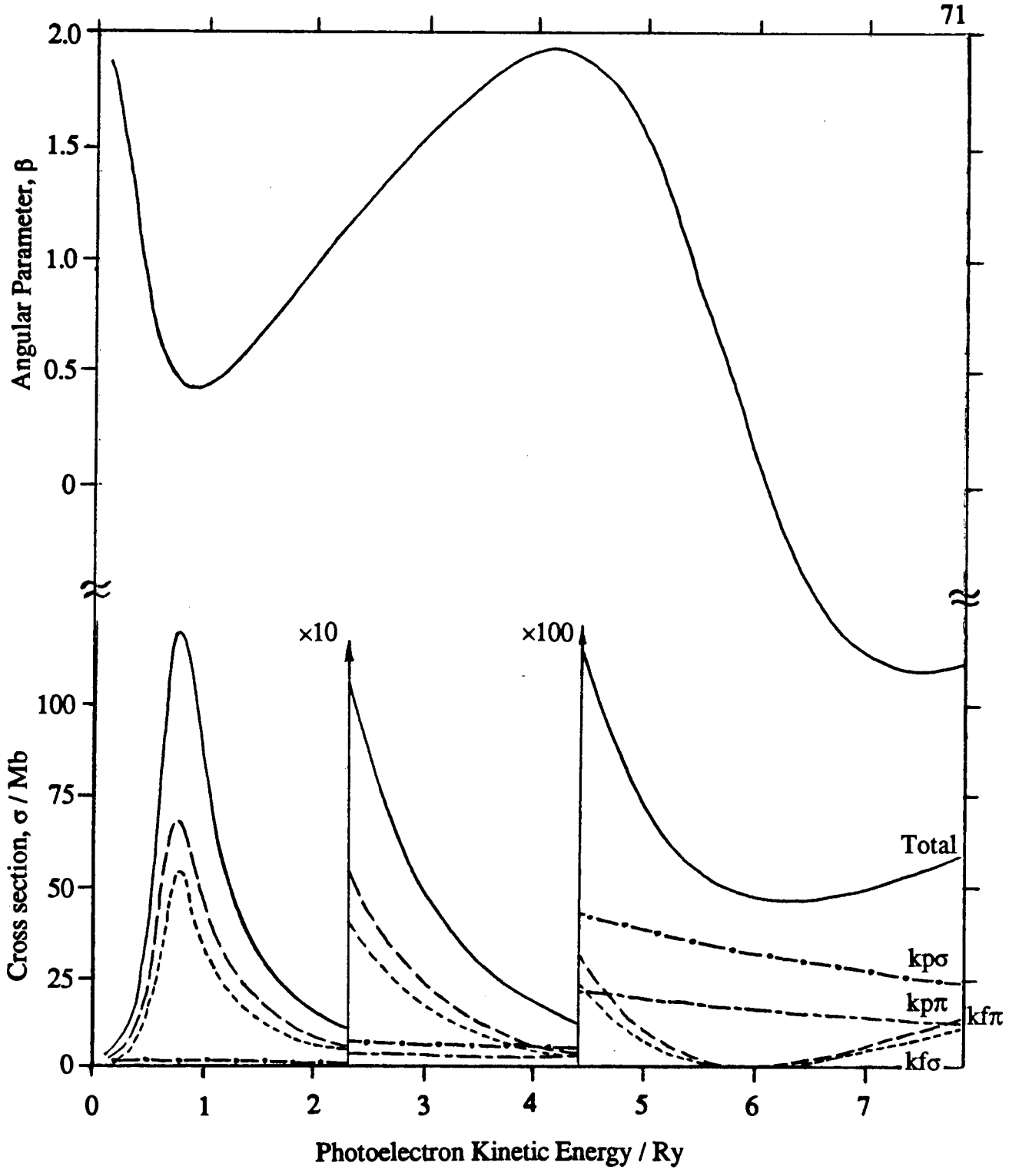

V-3c. Calculated total and channel cross sections and angular parameter as a function of photoelectron kinetic energy for xenon 4d. The kpσ channel cross section is twice that for kpπ. The kfπ channel cross section is 4/3 that for kfσ.

be thought of as standing for "continuum." Some authors prefer ε--for energy--to k. We use k to label continuum channels, so that a parallel with the bound state principal quantum number, n , is apparent. We use ε to label quantities which involve continuum wavefunctions, such as $\mathbf{R}_{l,l\pm1}(\varepsilon)$ and $P_{\varepsilon l}$, so that we are reminded that these are continuous functions of the continuously variable photoelectron energy.

The selection rule may also be written for initial state p electrons as

$$np \rightarrow ks + kd. \qquad \text{Eq. V-5}$$

This form emphasizes the channel concept for the scattering-like process.

As discussed in the chapter on CM, the spectral behavior of the cross section for each of these orbitals (argon 3p, krypton 4p, and xenon 5p) is affected by the CM. Their σ_{tot}'s measure in the tens of Mb at threshold and drop to the ones of Mb at 1.0 to 1.5 Ry kinetic energy. Their kd channel cross sections dip to zero where the np→ kd radial matrix element changes sign. The β curves are sinuous; they climb to maxima of about β = 1.9 at around 1 Ry and then plunge to negative values which have become associated with CM in p orbitals. This behavior is due to the np→ kd matrix element which is negative at threshold and must pass through zero to reach its high energy positive value.

Note that krypton's and xenon's total cross sections do not show minima. Reference to the channel cross sections helps us to understand this. Near the CM, the kd channel in these atoms has a broad shallow minimum which must be added to the dominant ks channel to obtain the total cross section. The shallowness of the kd's minimum and the monotonic, sufficiently rapid decrease of the ks channel conspire to leave the total without a minimum. We have not found a successful analysis of the total cross section alone which extracts the energy of the minimum in such cases. Such an analysis might prove useful in locating experimental CM more exactly.

Other studies of photoionization in p subshells are by Ong and Manson,[63] Manson,[57] and Kennedy and Manson.[56] Our results agree with those published previously.

Noble Gas Outermost s Subshells

The selection rule for photoionization of s electrons in a nonrelativistic atom is:

$$ns \rightarrow kp. \qquad \text{Eq. V-6}$$

Non-relativistic s subshell PI does not profit from channelization; there is only one possible channel!

Manson and Starace[68] show that for a one channel process, β is not energy dependent. From the Cooper-Zare expression[58] for β (Equation IV-4), since there is no $\mathbf{R}_{l-1}$ for $l = 0$,

$$\beta(\varepsilon) = 2\,\mathbf{R}_p^2/\,\mathbf{R}_p^2 = 2. \qquad \text{Eq. V-7}$$

Thus, for inert gas (s^2p^6) atom s photoionization, β = 2, and the CM has no effect on these β curves.

The cross sections of all these inert gases are similar, rising from a small value at threshold to a maximum near 1.5 to 2.0 Ry. This maximum is around 0.2 Mb for krypton and xenon but is twice as large, 0.4 Mb, for argon. Argon's potential near the edge of the atom (where the 3p wavefunction begins to die off) is shallower than krypton's near its edge. Argon's kp wavefunction has a larger amplitude here than krypton's kp, and the ns→ kp radial integral is larger for argon 3s than for either krypton 4s or xenon 5s. This phenomenon is present when comparing 3s orbital cross sections for Z = 17, 18 to 4s and 5s orbital cross sections for Z = 35, 36, 53, and 54. It occurs in molecules as well as in atoms. Our cross section calculations agree with Manson and Cooper's to tolerances which probably arise from the use of different methods and parameters used.

As Kennedy and Manson[56] show, the CM in these subshells are at or "just below" threshold with the HS (in our case, Xα) method of calculation. These cross section minima are true cross section zeros since this is a one channel process. Our calculations show low σ_{tot} at threshold due to CM. The energy placement of the CM in these calculations do not agree with experimental placement. Houlgate, et. al.,[71] and Fahlman, et. al., (References 72, 73, 74) show noble gas outermost ns orbitals' CM to

lie above threshold usually by 10 eV. Calculations which include many-body interactions[64] give much more accurate CM energies than do independent particle calculations using the Slater Xα exchange.

Ong and Manson,[69] and Manson and Starace[68] include relativitistic interactions in their calculations on ns photoionization so that spin may be included. With spin included, the modified selection rule is

$$ns_{1/2} \rightarrow kp_{1/2} + kp_{3/2}. \qquad \text{Eq. V-8}$$

The minimum number of channels is always two (spin up and spin down), and β can no longer be strictly energy independent.

Noble Gas d Subshells

The selection rule for d orbitals of inert gases may be written

$$nd \rightarrow kp + kf. \qquad \text{Eq. V-9}$$

The circumstances for the CM in d subshells are not quite the same as those for CM in p subshells; here, the nd→ kf radial matrix element changes sign. From the Cooper-Zare[58] formula for β(ε) (Equation IV-4),

$$\beta_d(\varepsilon) = \frac{2\,\mathbf{R}_p(\varepsilon)^2 + 12\,\mathbf{R}_f(\varepsilon)^2 - 36\,\mathbf{R}_p(\varepsilon)\,\mathbf{R}_f(\varepsilon)\cos\Delta_{fp}}{5\,[\,2\,\mathbf{R}_p(\varepsilon)^2 + 3\,\mathbf{R}_f(\varepsilon)^2\,]}. \qquad \text{Eq. V-10}$$

Thus, $\beta_d = 0.2$ at the CM, where $\mathbf{R}_f \rightarrow 0$. [Only when

$$\mathbf{R}_p(\varepsilon)^2 + 6\,\mathbf{R}_f(\varepsilon)^2 - 18\,\mathbf{R}_p(\varepsilon)\,\mathbf{R}_f(\varepsilon)\cos\Delta_{fp} = 0, \qquad \text{Eq. V-11}$$

does $\beta_d = 0$, but this is too complicated a relation about which to make generalizations.]

The Figures for the d's, particularly krypton's 3d, show that not every minimum in β is a CM, in addition to the lesson of the p's, that not every CM corresponds to a minimum in total cross section (specifically, for krypton 4p and xenon 5p).

Manson and Cooper (Reference 65, p.132) discuss the rapid rise of xenon's 3d→ kf cross section in terms of the initial and final wavefunctions. They show it to be due to a potential barrier effect, as for xenon 4d.

Halogen Atoms

We now present the photoionization calculation results for the halogen atoms. These serve as a link between the molecules which we wish to present and the noble gases which, for completeness, we must present. As we shall discuss at the end of this section, experimentalists favor the noble gases, whereas we, as theorists, will want to use the halogen atoms for comparison with molecular results.

Our method of calculation is spin-restricted, that is, the effects of electron spin are not included except that we allow only two electrons to occupy each spatial orbital, as Pauli exclusion requires. Because of this lack of sophistication in our methods, we may blindly attack such monstrous problems as the photoionization of the open shell halogens:

$$ns^2 np^5 \rightarrow ns^2 np^4 + e^-. \qquad \text{Eq. V-12}$$

The handling of unpaired spins is a complication which we do not attempt to address. Instead, we present results, for example, for chlorine atom with the electron configuration, $1s^2\ 2s^2\ 2p^6\ 3s^2\ 3p^5$, that is, we consider a subshell to be complete and degenerate with the occupation number shown. We do this because the atomic results which we present are meant only as useful models for the molecular discussion to come. They are not meant to model PI in atoms for close comparison with experiment; we recognize that better calculations exist for the atoms we treat.

As an example of the molecules presented later, take HCl with the configuration, $1\sigma^2_{Cl,1s}\ 2\sigma^2_{Cl,2s}\ 3\sigma^2_{Cl,2p}\ 1\pi^4_{Cl,2p}\ 4\sigma^2_{Cl,3s}\ 5\sigma^2_{H\text{-}Cl}\ 2\pi^4_{Cl,3p}$. All the molecules we shall present will be closed shell and will allow analysis in terms of their orbitals' constituent atomic orbital (A.O.) makeup. See Appendix V. (Although the Xα method is not an LCAO method, there exist population analyses which "correspond" to the A.O. breakdown of LCAO treatments.)

Although the population analysis for orbitals such as HCl's 2π indicate that it is primarily chlorine 3p, the effect of residual non-chlorine or non-"l=1" density upon the PED parameters, σ_{tot} and β, is unknown at this point in our discussion. We shall

compare HCl 2π to the chlorine 3p calculated as if it were closed shell--without spin coupling. By elimination, the source of any difference is due to the formation of the molecular potential. In this way, we shall pursue the molecular effects on CM.

Our format here is the same as that for the noble gases: p, s, then d orbitals. Figures V-4, V-5, and V-6 present the results.

Halogen Atom p Subshells

The selection rule for halogen (s^2p^5) PI in our model is the same as that for the noble gases (s^2p^6). The selection rule is repeated for convenience here

$$np \rightarrow ks + kd. \qquad \text{Eq. V-13}$$

The PI data for the halogen np's is presented in figures V-4a, V-5a, and V-6a. Comparing these results to those for the noble gases, we note exactly the same trends: the dropping total cross sections, chlorine (like argon) with a minimum; the kd channels showing minima; and the sinuous β curves.

In fact, the only significant differences in the noble gases and the halogens are the locations of the CM. Argon's CM is 0.2 Ry higher than chlorine's; krypton's CM is 0.1 Ry higher than bromine's; but xenon's CM is (within our "resolution") at the same energy as iodine's. If we may be allowed to speak qualitatively, we believe this to be due to the differing spatial extents of the initial state p orbitals for the halogens with respect to the nobles. Argon's higher nuclear charge "pulls in" the 3p orbital so that its radial nodes lie closer to the nucleus than those of chlorine 3p. Since the CM involves a zero in the radial matrix element which involves the continuum wavefunction whose nodes move toward the nucleus with increasing energy, the zero in $np \rightarrow kd$ radial matrix element will occur at a higher energy for a contracted initial state. Since the difference in atomic number (hence contracting power) between the groups VIIA and VIIIA decreases percentagewise with increasing atomic number, the effect of the noble gases' higher atomic number is negligible by the time we reach iodine and xenon.[57]

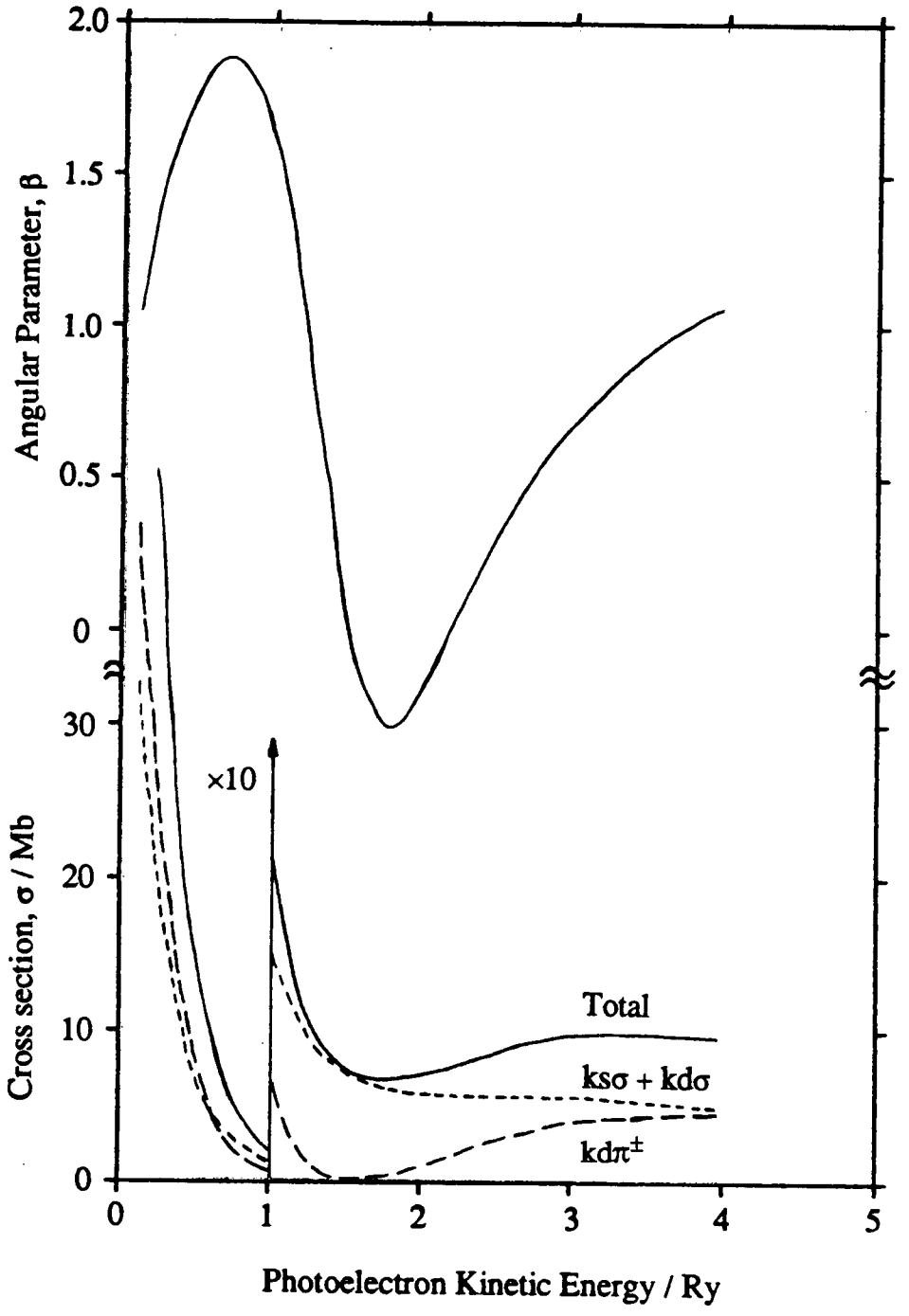

V-4a. Calculated total and channel cross sections and angular parameter as a function of photoelectron kinetic energy for chlorine 3p.

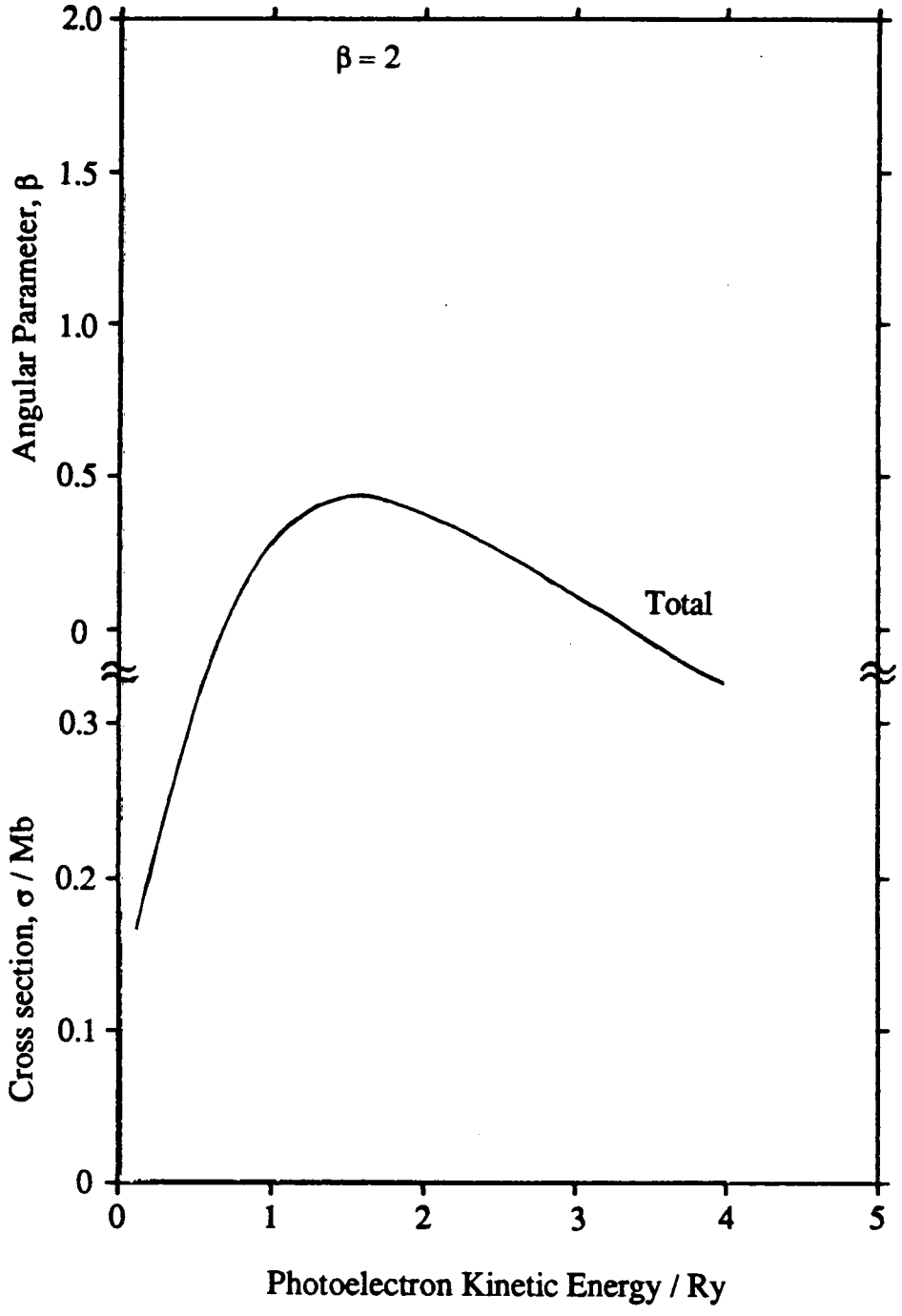

V-4b. Calculated total and channel cross sections and angular parameter as a function of photoelectron kinetic energy for chlorine 3s. The kpσ channel cross section is equal to 1/3 σ_{tot}. The kp$\pi^{\pm}$ channel cross section is equal to 2/3 σ_{tot}.

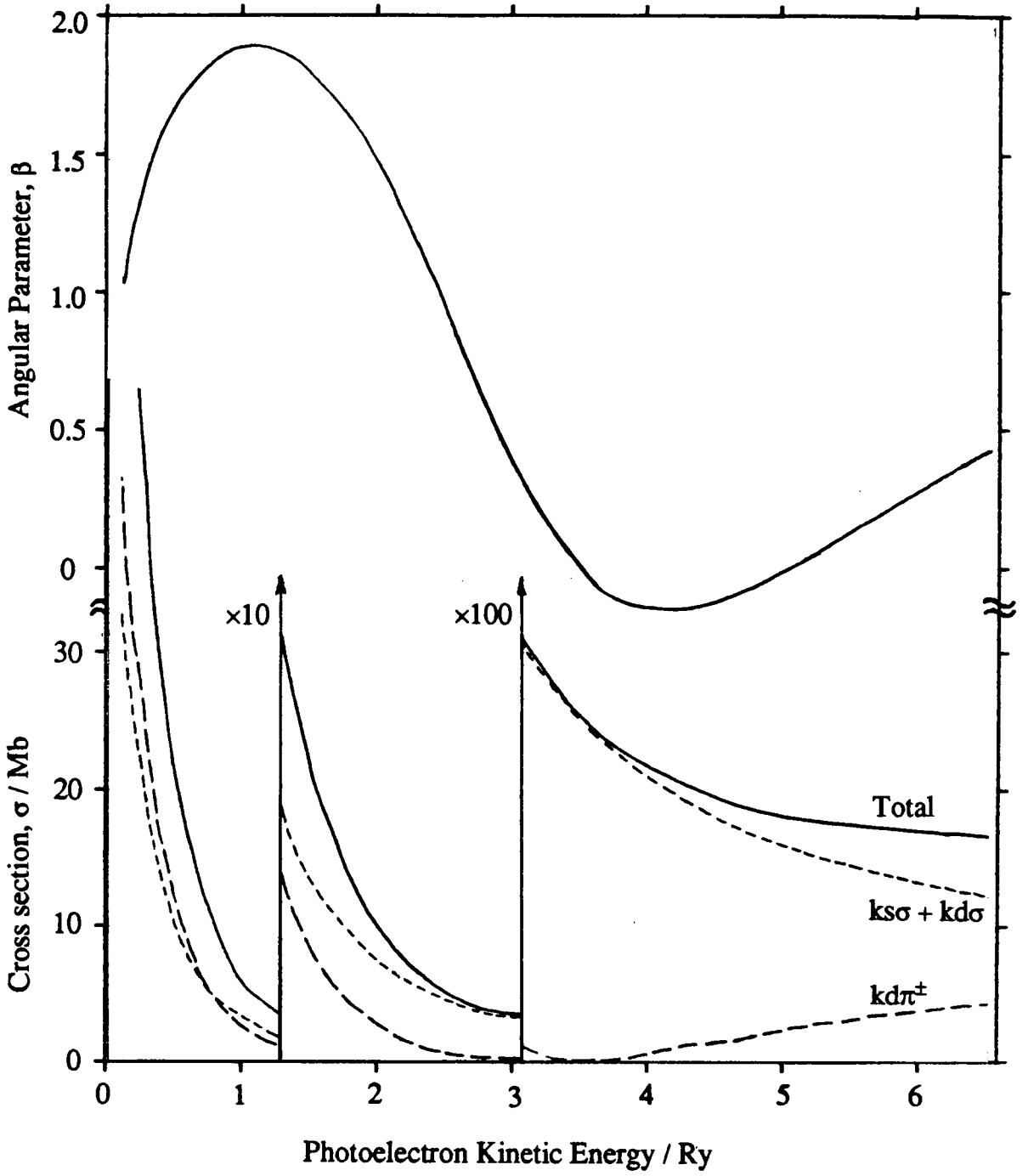

V-5a. Calculated total and channel cross sections and angular parameter as a function of photoelectron kinetic energy for bromine 4p.

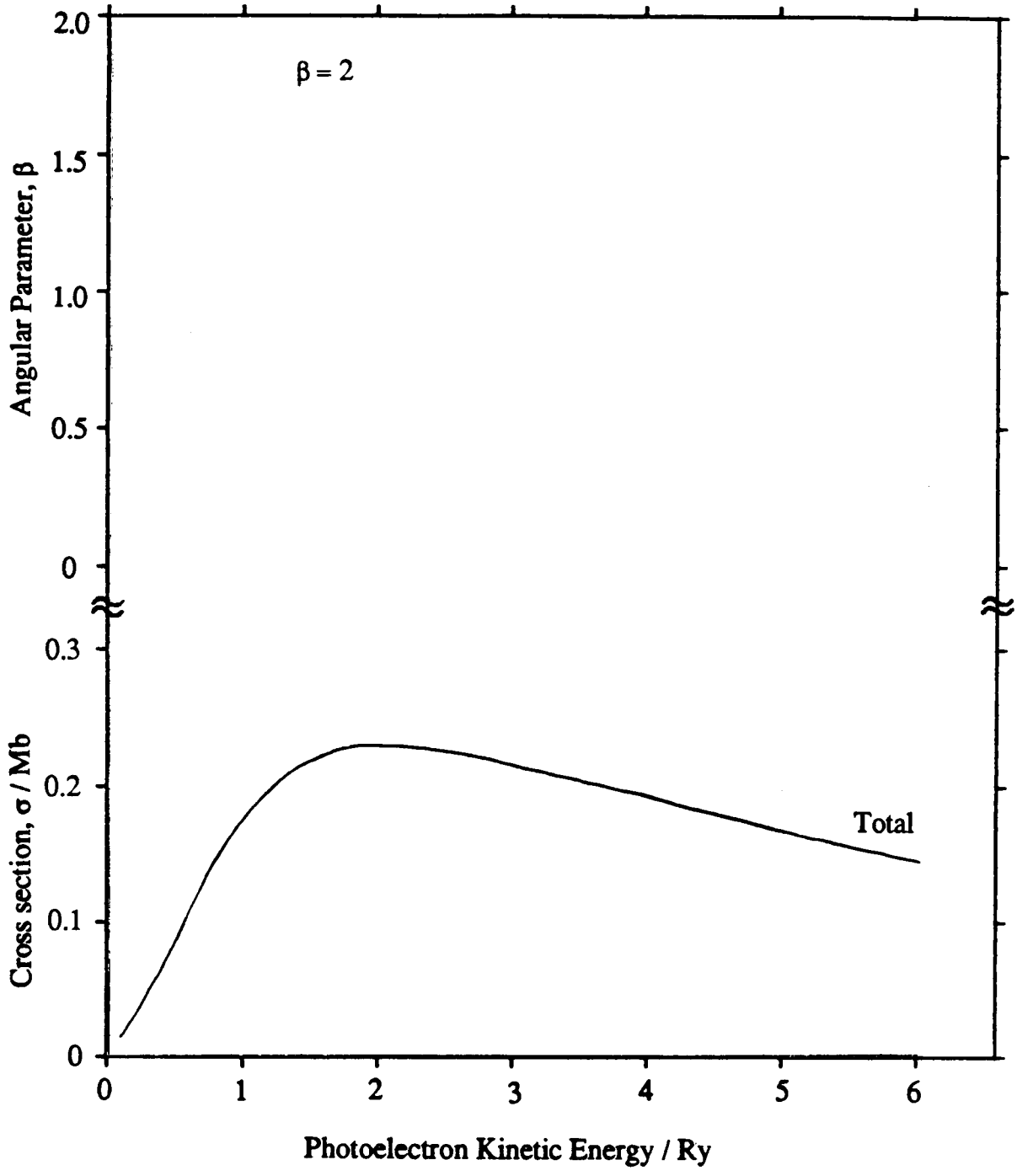

V-5b. Calculated total and channel cross sections and angular parameter as a function of photoelectron kinetic energy for bromine 4s. The kpσ channel cross section is equal to 1/3 σ_{tot}. The kp$\pi^{\pm}$ channel cross section is equal to 2/3 σ_{tot}.

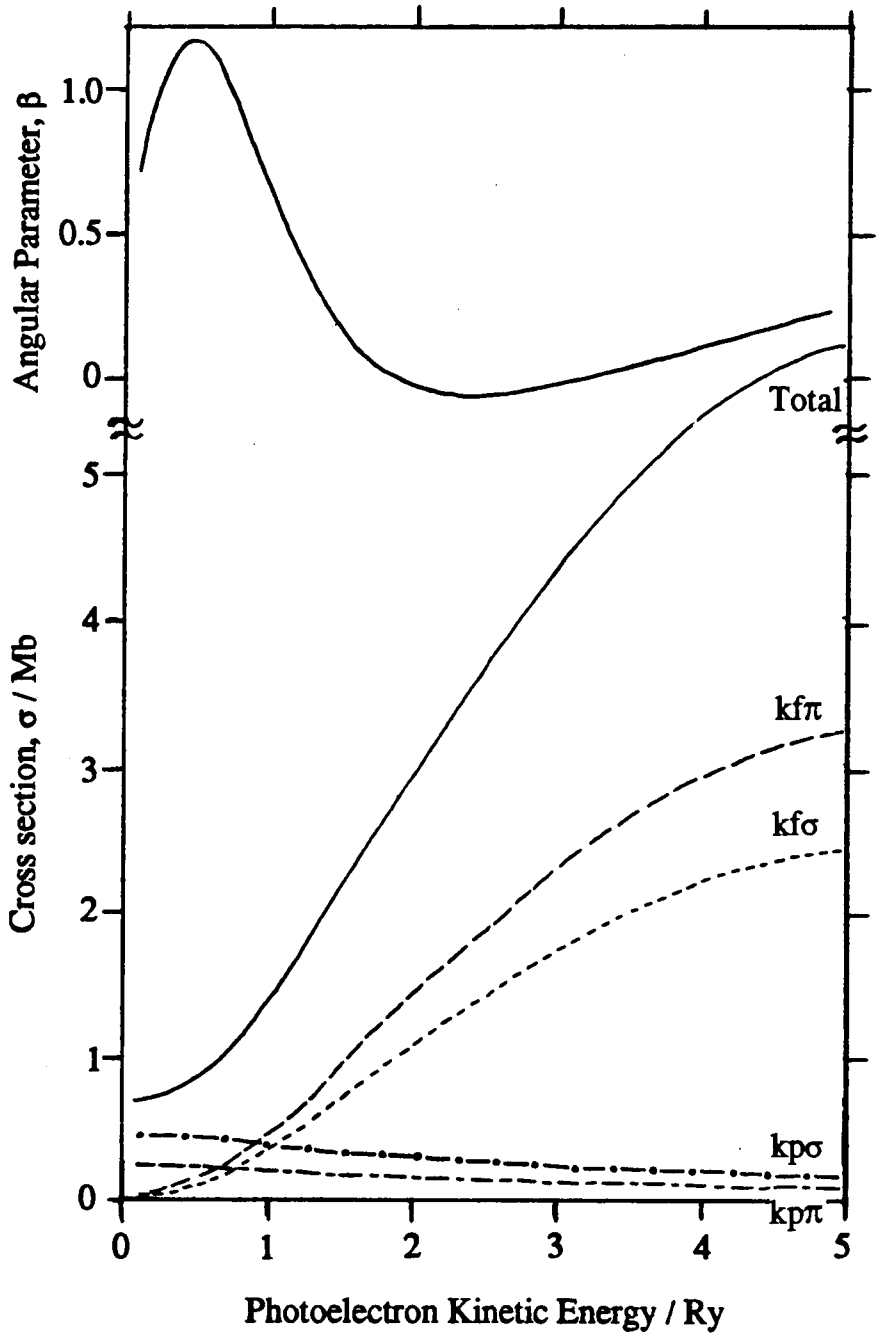

V-5c. Calculated total and channel cross sections and angular parameter as a function of photoelectron kinetic energy for bromine 3d. The kpσ channel cross section is twice that for kpπ. The kfπ channel cross section is 4/3 that for kfσ.

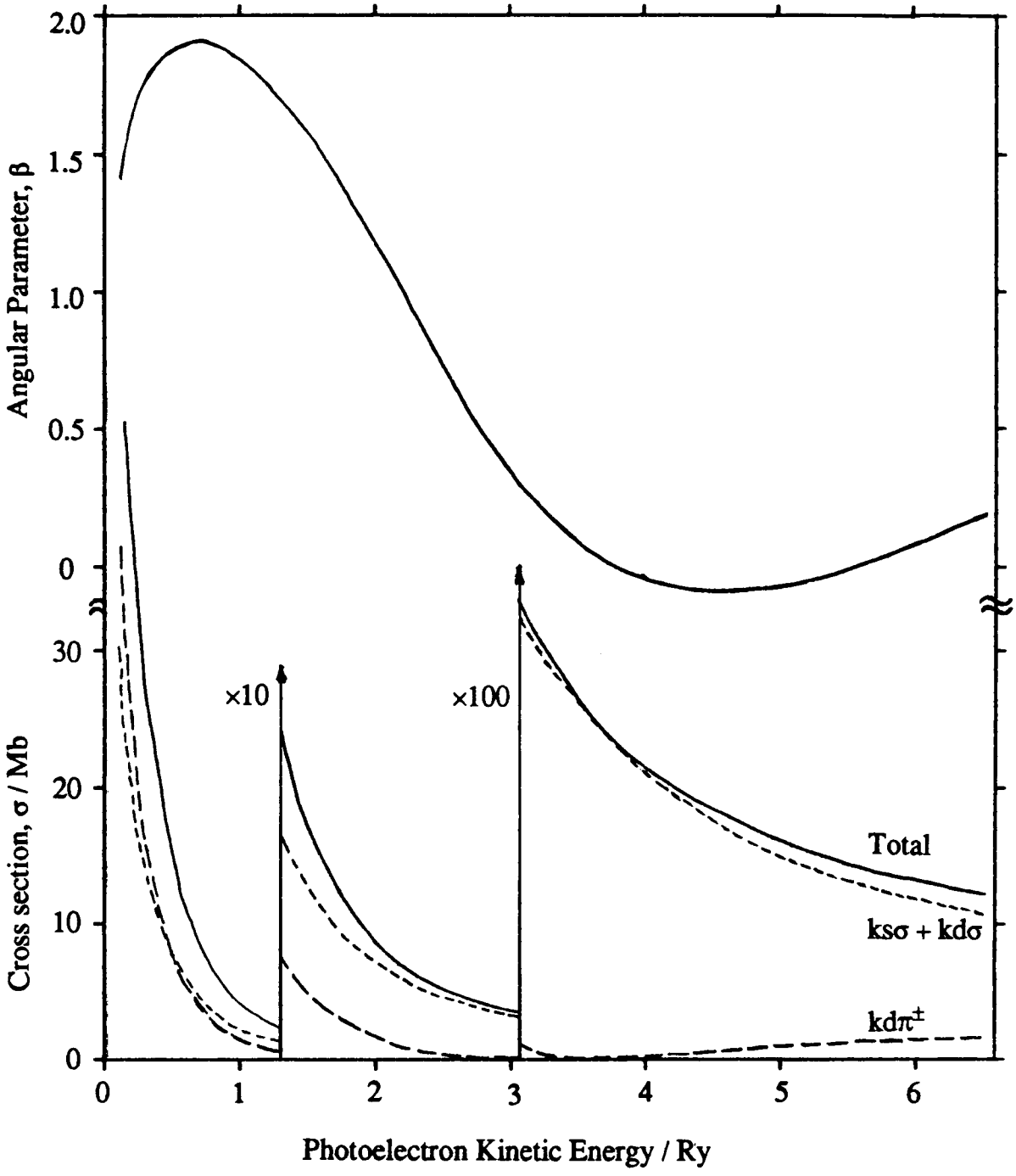

V-6a. Calculated total and channel cross sections and angular parameter as a function of photoelectron kinetic energy for iodine 5p.

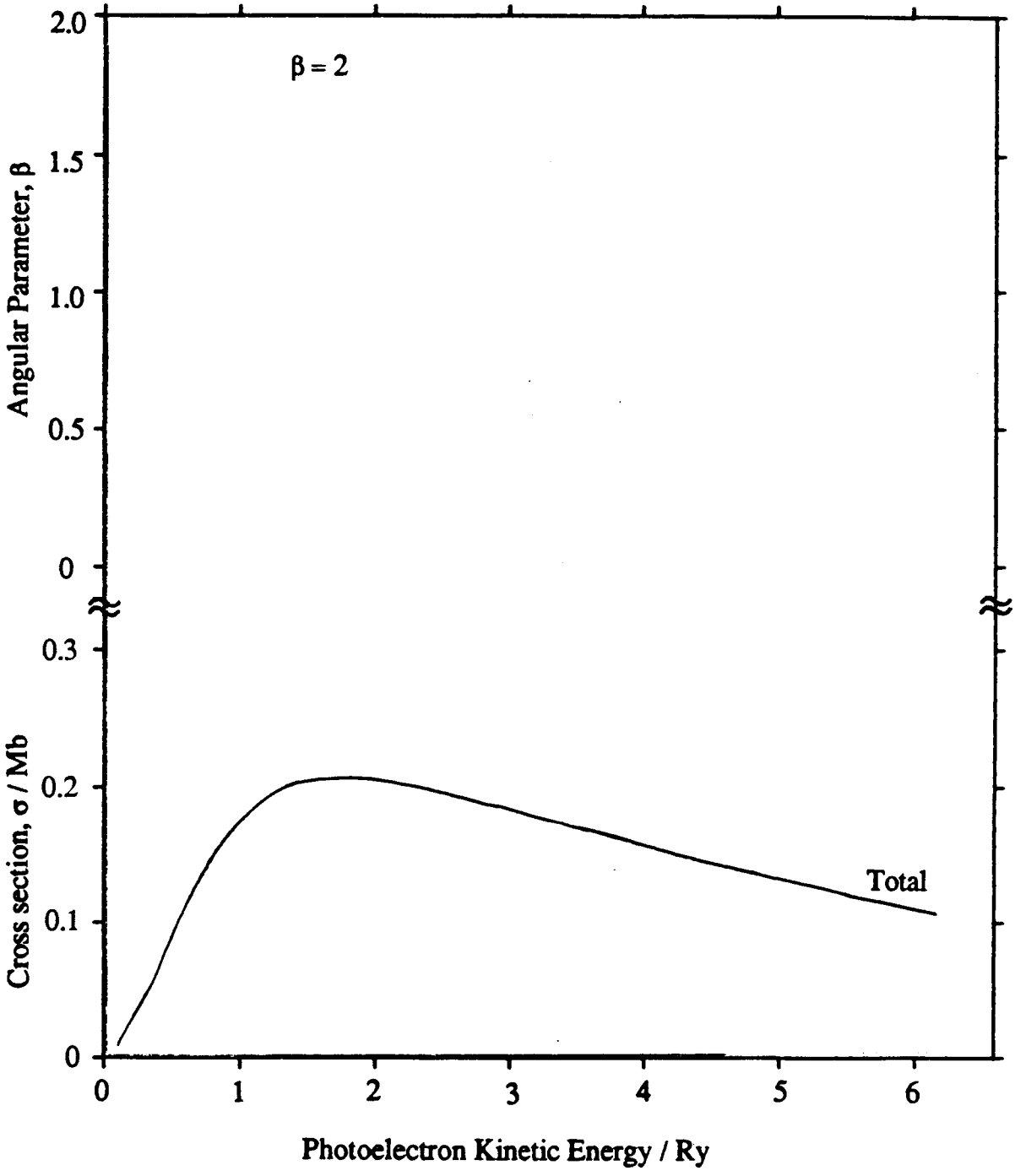

V-6b. Calculated total and channel cross sections and angular parameter as a function of photoelectron kinetic energy for iodine 5s. The kpσ channel cross section is equal to 1/3 σ_{tot}. The kp$\pi^{\pm}$ channel cross section is equal to 2/3 σ_{tot}.

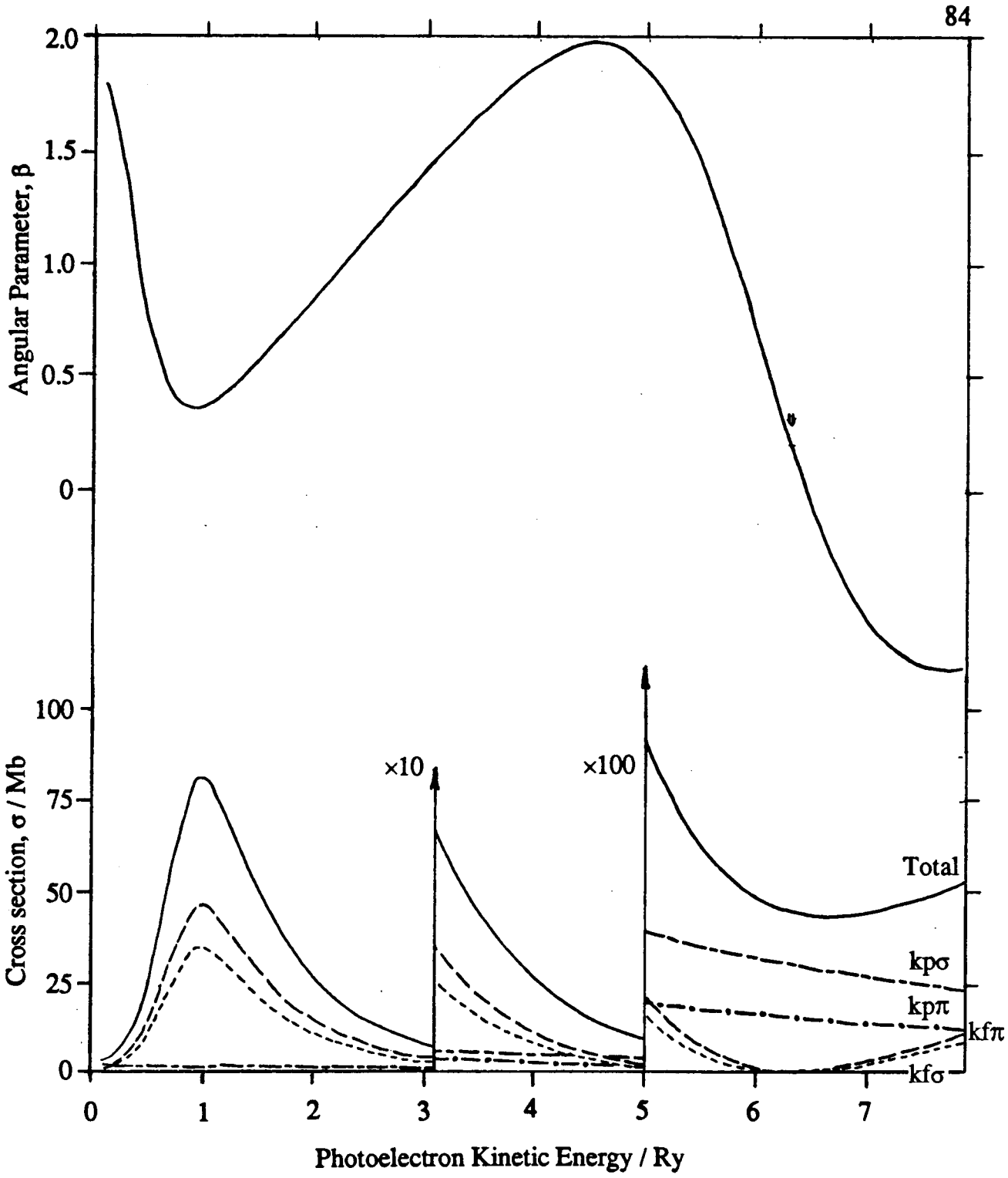

V-6c. Calculated total and channel cross sections and angular parameter as a function of photoelectron kinetic energy for iodine 4d. The kpσ channel cross section is twice that for kpπ. The kfπ channel cross section is 4/3 that for kfσ.

Halogen Atom s Subshells.

Again the selection rule for ns PI is:

$$ns \rightarrow kp. \qquad \text{Eq. V-14}$$

As with the np's, the halogen ns's are similar in trend to the noble gas ns's: cresting cross sections, and $\beta = 2$. The slight differences in cross section arise from the noble gases' contracted initial-states. Because the CM is below threshold, we cannot analyze the effect on it of increasing atomic number.

Note again that the chlorine 3s total cross section at its peak is nearly twice that for bromine 4s or iodine 5s as was the case with the noble gases (argon 3s twice krypton 4s or xenon 5s).

Halogen Atom d Subshells

With selection rule

$$nd \rightarrow kp + kf, \qquad \text{Eq. V-15}$$

the halogens' d orbitals show no unusual behavior when compared to the noble gases'.

Comparison of Atomic and Molecular Experimental Results

Carlson, et al.,[23] claim that, with respect to the CM, each hydrogen halide may be compared to the noble gas with which it is isoelectronic. Faegri and Kelly[75] performed single center *ab initio* calculations on HCl and stated that they expected that "the results should relate to the isoelectronic inert-gas atom--argon--in the same manner as the results from a previous calculation on HF (Reference 76) relate to Ne." Why the noble gases rather than the halogen atoms?

The preceding presentation has shown that the results for the halogens closely follow those of the nobles, that is, that trends are similar even if energy placement of features is different. (Manson[57] demonstrated that the overall appearance of the energy dependent β curve changes slowly with atomic number; the curves for atoms of adjacent atomic number are quite similar.) Noble gases are much more easy to deal

with experimentally (they are "inert gases") than the halogen atoms. With our theoretical method, since open shell systems are as easy to calculate as closed (by the adoption of some drastic simplifications), we may compare the hydrogen halides to either halogen or noble gas atoms, as we please.

We shall find that we discuss lone pair orbitals frequently, that is, orbitals whose electrons feel the influence of only one nucleus. Molecular orbitals primarily associated with a halogen atom in the molecule will be more accurately compared to the halogen atom than to the associated noble gas atom. For the low energy processes on ground state valence orbitals of the hydrogen halides considered here, the largest contribution to the transition integrals comes from the spatial region close to the nuclei. Here the electrons feel the influence of each individual atom (halogens) rather than the influence of the united atom (noble gases).

We do not mean to disparage the practice of reference to the noble gases, for there are experimental constraints which recommend that practice. (It is more difficult to produce halogen atoms than noble gas atoms. Also, different open shell final state electron configurations have different energies, complicating the analysis of halogen atom results.) In fact, the close theoretical agreement of the noble gases' and halogen atoms' behavior should encourage experimentalists in their practice of using noble gases for comparison with hydrogen halides.

CHAPTER VI

HYDROGEN HALIDE MOLECULE

RESULTS

The stated purpose of this dissertation is to investigate the manifestation in molecules of an atomic effect--the Cooper minimum. The next two chapters present our theoretical results for the halogen acids and diatomic halogens. All the notes concerning the format of the Figures in the atoms' section pertain for these chapters. All orbitals of one molecule will be treated (from the outermost inward) before moving on to the next molecule, and all of a class, for example, the halogen acids, will be treated before moving on to the next class and chapter.

We consider only the three outermost valence orbitals of the hydrogen halides. In keeping with recent usage[23] (but using a different convention), we number the valence orbitals of HX: 1σ, 2σ, and 1π. This facilitates intercomparison of the molecules. For the readers' ease, we present a table of correlations of the significations of these orbitals of HX (Table VI-1).

Table VI-1. Correlation of HX valence orbitals.

	1σ	2σ	1π
HCl	$4\sigma^2_{Cl,3s}$	$5\sigma^2_{H\text{-}Cl}$	$2\pi^4_{Cl,3p}$
HBr	$7\sigma^2_{Br,4s}$	$8\sigma^2_{H\text{-}Br}$	$4\pi^4_{Br,4p}$
HI	$10\sigma^2_{I,5s}$	$11\sigma^2_{H\text{-}I}$	$6\pi^4_{I,5p}$

When we speak of the 1σ orbital of HCl with respect to valence PES, we mean the 4σ, not the chlorine 1s. Chlorine 1s is referred to as the K-shell and is too deep to be studied by valence PES methods. Appendix V contains *l*-type analyses for the initial state orbitals of the hydrogen halides as calculated by the Xα-SW method.

To motivate these assignments of orbital symmetry, consider the following. As is conventional, the nuclei of our model linear molecule lie on the z-axis of our coordinate system, making it the principal symmetry axis. The 1s orbital of hydrogen, which is responsible for most of the bonding in which hydrogen takes part, is represented in $C_{\infty v}$ point group by Σ^+. Thus it will be involved in either the 1σ or 2σ, and the 1π will be a lone "pair" (actually two pairs) on the halogen. In fact, the assignments are as follows. 1σ is primarily the ns of the outermost shell on the halogen, 2σ is the admixture of 1s on hydrogen and np on the halogen forming the single bond holding the molecule together, and 1π is a nonbonding orbital of np's on the halogen. The 1π is often visualized as two lone pairs which are mutually perpendicular and are perpendicular to the single bond. These gross "A.O." assignments are indicated for each orbital in Table VI-1 as subscripts and are supported by the *l*-type analyses of Appendix V. "H-X" means that this orbital is a bond.

Since the CM is explained by reference to atomic orbitals, we should not be surprised if the 1π orbitals display atomic-like CM, and the 2σ bond has a somewhat different behavior due to the mixing with hydrogen 1s. This is not to say that we should not be pleased, for when our expectations are fulfilled, it is good, but that surprise is inappropriate, because we were forewarned.

Hydrogen Chloride: HCl

Figure VI-1a presents the results for the 1π orbital of HCl. Figure VI-1b presents the results for 2σ, the bonding orbital. Figure VI-1c shows the results for 1σ, which is mostly made up of chlorine 3s.

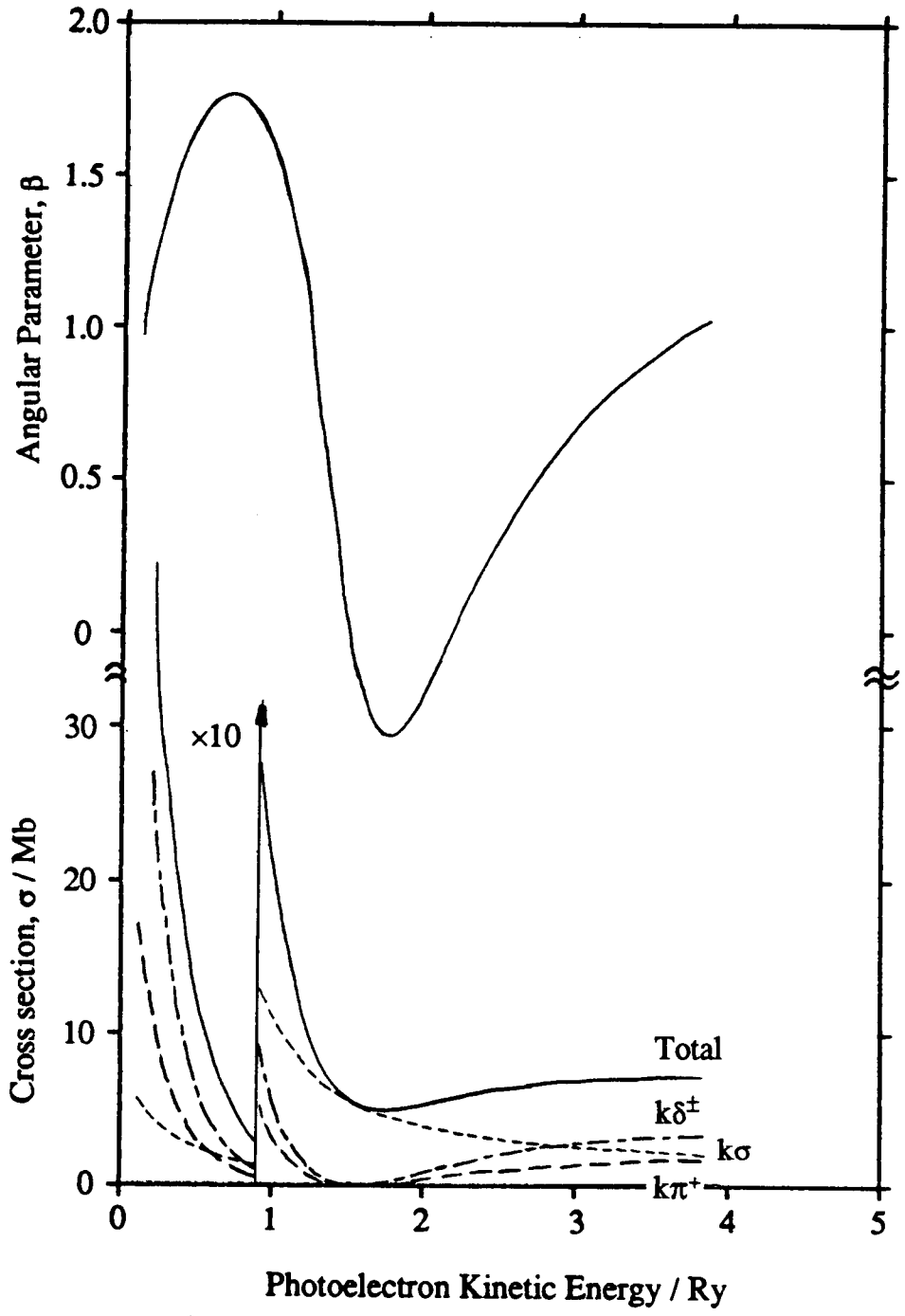

VI-1a. Calculated total and channel cross sections and angular parameter as a function of photoelectron kinetic energy for HCl 1π.

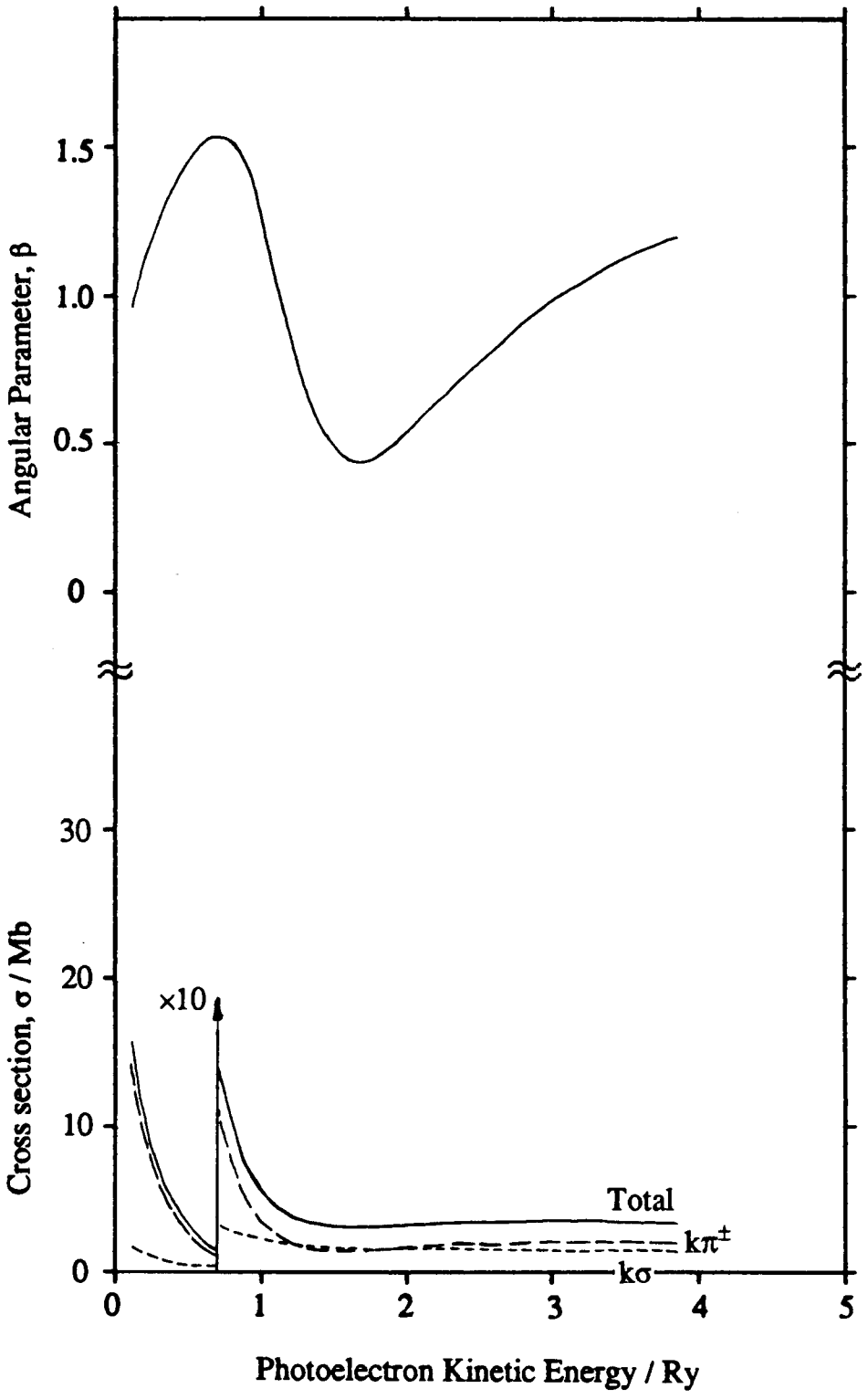

VI-1b. Calculated total and channel cross sections and angular parameter as a function of photoelectron kinetic energy for HCl 2σ.

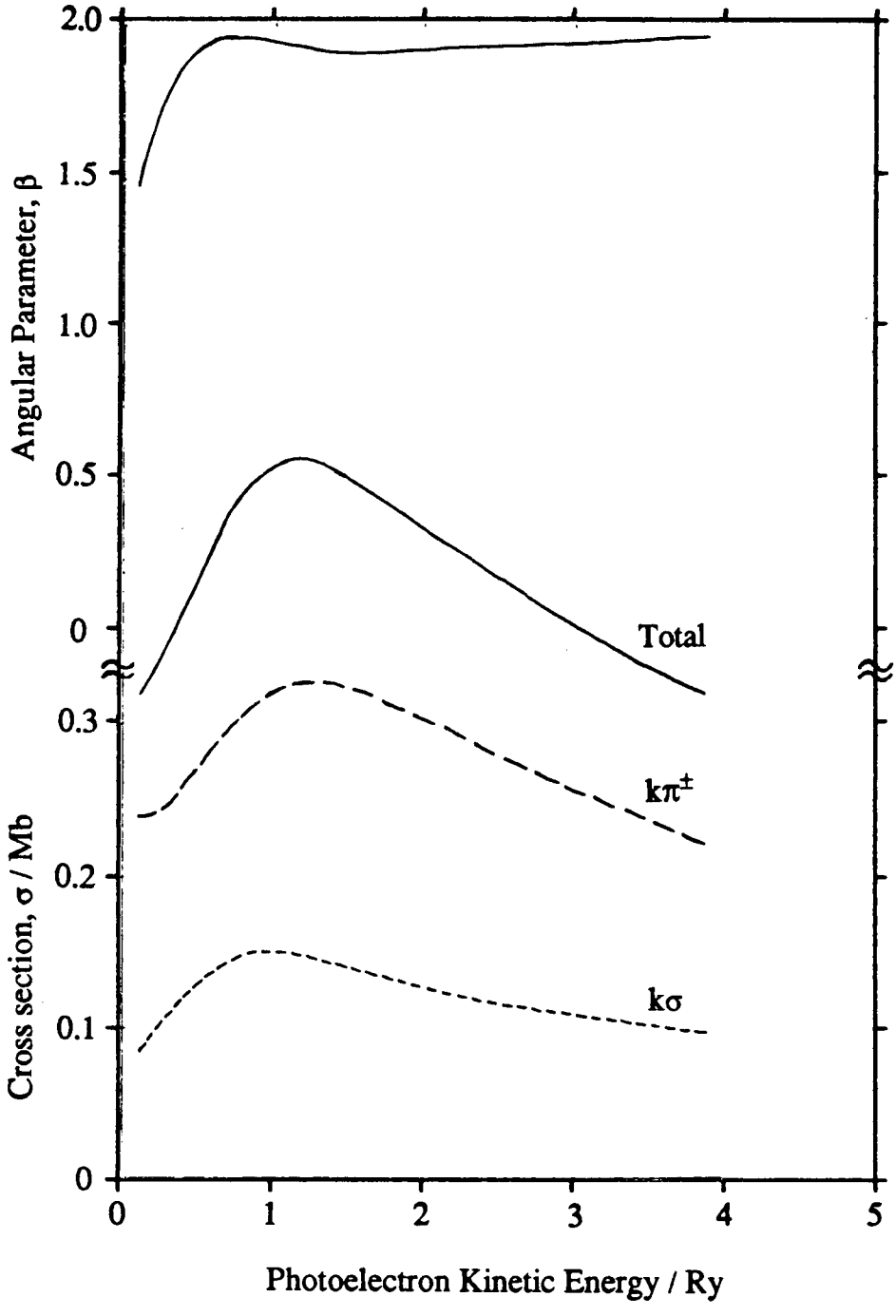

VI-1c. Calculated total and channel cross sections and angular parameter as a function of photoelectron kinetic energy for HCl 1σ.

HCl 1π

The selection rule for PI from this orbital (from Appendix I) is

$$1\pi^{+} \rightarrow k\sigma + k\pi^{+} + k\delta^{+} + k\delta^{-}. \qquad \text{Eq. VI-1}$$

As postulated above, the spectral features of this orbital behave virtually atomically; the β curve is almost indistinguishable from that of our chlorine 3p (not that of argon 3p). The cross section is about four-fifths of that for chlorine 3p along its whole energy range. This is due to the differing occupation numbers for HCl 1π and chlorine 3p, i.e., $n(1\pi_{HCl})/\, n(3p_{Cl}) = 4/5$.

That the above occupation number explanation is successful, and that the β curve is nearly interchangable with that of chlorine 3p, are further justifications for denoting HCl 1π as lone pairs.

We see that the $k\delta$ cross section is at a minimum at 1.5 Ry, the $k\pi$ at 1.6 Ry, the σ_{tot} at 1.8 Ry. $\beta = 0$ at 1.5 Ry, again showing that channel cross sections are preferable to β or σ_{tot} minima for locating CM. Reference to the channel cross sections shows that the $k\sigma$ is dominant at the CM, where $k\pi$ and $k\delta$ undergo minima. We regard this as due to the fact that $k\sigma$ contains $l = 0$, whereas $k\pi$ and $k\delta$ start with $l = 1$ and $l = 2$, respectively. The $(l = 1)_i \rightarrow (l = 0)_f$ matrix element in the atomic spheres is the major contributor to the amplitude matrix at the CM. It is analogous to the ks channel in chlorine atom $3p_{\pm 1}$.

HCl 2σ

The selection rule is

$$2\sigma \rightarrow k\sigma + k\pi^{+} + k\pi^{-}. \qquad \text{Eq. VI-2}$$

Note the much narrower traverse of β's oscillations compared to 1π's. Here again the cross section is diminished--it is less than half that for the 1π. The occupation numbers are $n(2\sigma) = 2$ and $n(1\pi) = 4$. When we take this into account, though, we still have a shallower minimum for 2σ than for 1π.

This weakening of the effect of the CM in bonding with respect to nonbonding orbitals is "typical," has been noted experimentally, and is referred to as a "partial" CM[19]. It is sometimes ascribed to the multi-*l* makeup of molecular wavefunctions. What we should note here in this regard are the channels' cross section behavior. kσ is more suppressed than the occupation numbers can account for, and kπ does not attain zero although it does show a minimum at 1.6 Ry around where the chlorine 3p and the HCl 1π show CM.

It is at this point that the multi-*l* nature of the wavefunction is often invoked. We reason that, because there is a minimum in the kπ cross section (and the associated β plunge), surely some partial wave making up kπ has a matrix element changing sign. kπ does not attain zero, because other partial waves are "interfering," that is, the channel is a sum of many partial waves. This reasoning is sound as far as it goes, but we shall find a more enlightening way to look at the partial CM in a later chapter. We shall show there that the cause can also be assigned as the presence of the bond, meaning finite wavefunction amplitude, and hence cross section, in the hydrogen sphere which is not present in HCl 2π or chlorine 3p.

HCl 1σ

The selection rule is the same as that for any σ orbital

$$1\sigma \rightarrow k\sigma + k\pi^{+} + k\pi^{-}. \qquad \text{Eq. VI-3}$$

We note that now, in a molecular environment, it is not true that $\beta = 2$. In fact, at threshold, β dips down to below 1.5. As with the atoms, the CM lies at or just below threshold, indicated by the drop in β. β is not necessarily aiming for zero--the value it takes for totally symmetric angular distributions--but since β is bounded above by two, and at high energy it will approach the atomic value of two, it has to fall from two to reach any other value near threshold.

The total cross section curve is similar in shape to that of chlorine 3s, and the occupation numbers for both are equal: $n(2\sigma_{HCl}) = n(3s_{Cl}) = 2$. In the atom, by our

method, the kσ channel's cross section is strictly equal to 1/3 σ_{tot}, the kπ's to 2/3 σ_{tot}, and $\beta = 2$. For HCl 1σ, the kπ cross section is enhanced with respect to 2/3 σ_{tot}, and kσ's is diminished with respect to 1/3 σ_{tot}. Where the molecule's channels approach one-third and two-thirds σ_{tot} most closely, at about 0.7 Ry, β approaches two most closely.

Hydrogen Bromide: HBr

Figure VI-2a presents the data on HBr 1π, the bromine 4p lone pairs. The selection rule is the same as that for HCl 1π (Equation VI-1). Figure VI-2b shows our results for the 2σ bonding orbital. The 1σ, mostly bromine 4s, results are presented in Figure VI-2c. Their selection rule is that for any σ orbital (Equations VI-2 and VI-3).

HBr 1π

As with HCl 1π and chlorine 3p, this orbital is nearly indistinguishable from bromine 4p once the differing occupation numbers have been taken into account.

β is at a minimum at 4.3 Ry but goes through zero at 3.6 Ry where the kδ and kπ channels both are at minima. Compare this with bromine 4p where $\beta = 0$ and kd is minimal, at 3.5 Ry--the same energy, given our "resolution."

HBr 2σ

Again, as with HCl, note that σ_{tot} shows no minimum, nor does the kπ channel (which is strangely enhanced at the expense of the kσ). The β curve for this orbital is one of the most unusual we have encountered (relative, of course, to one's appreciation of a "usual" β curve). Its traverse is limited between about 1.5 and 0.8 as is usual

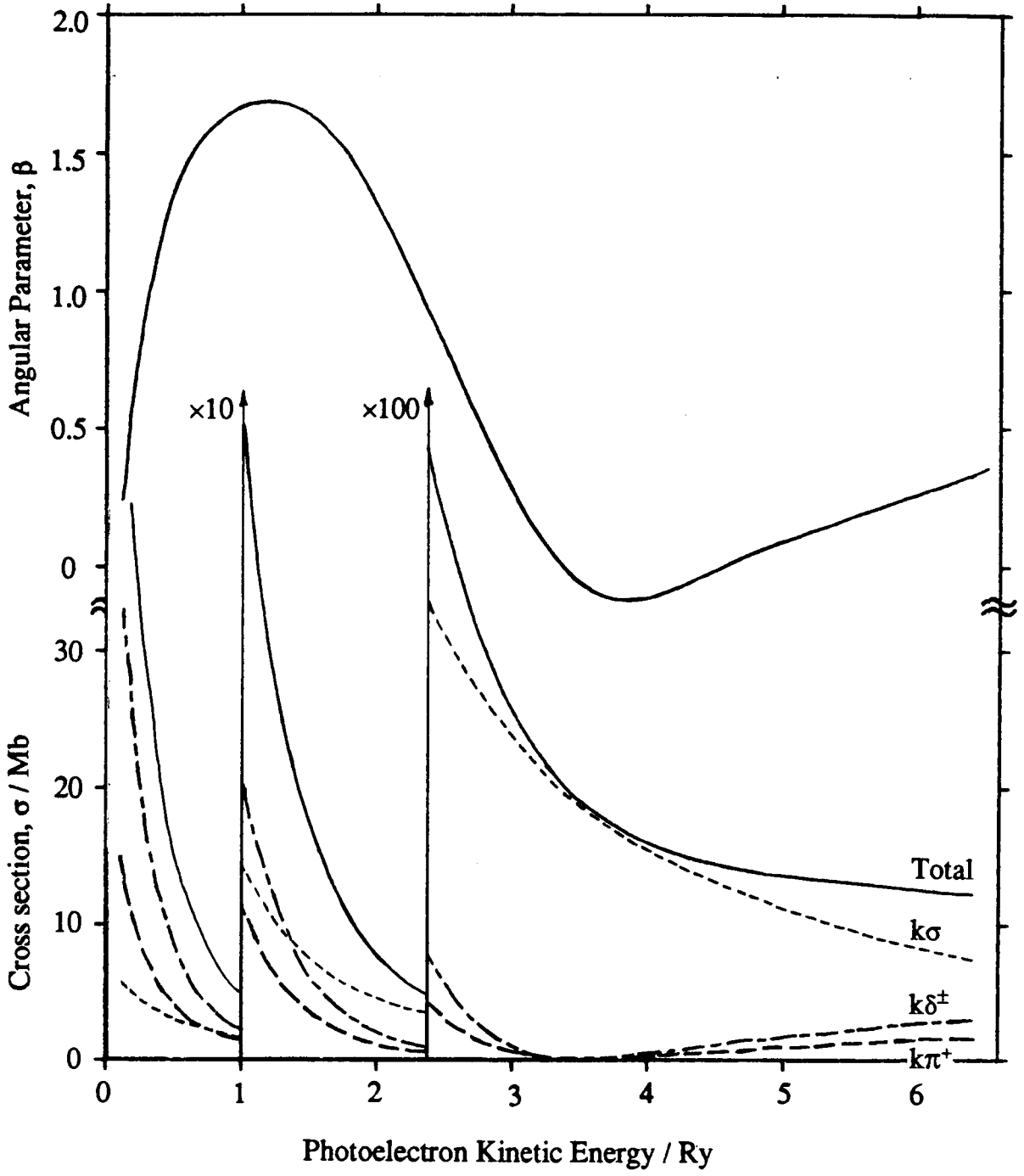

VI-2a. Calculated total and channel cross sections and angular parameter as a function of photoelectron kinetic energy for HBr 1π.

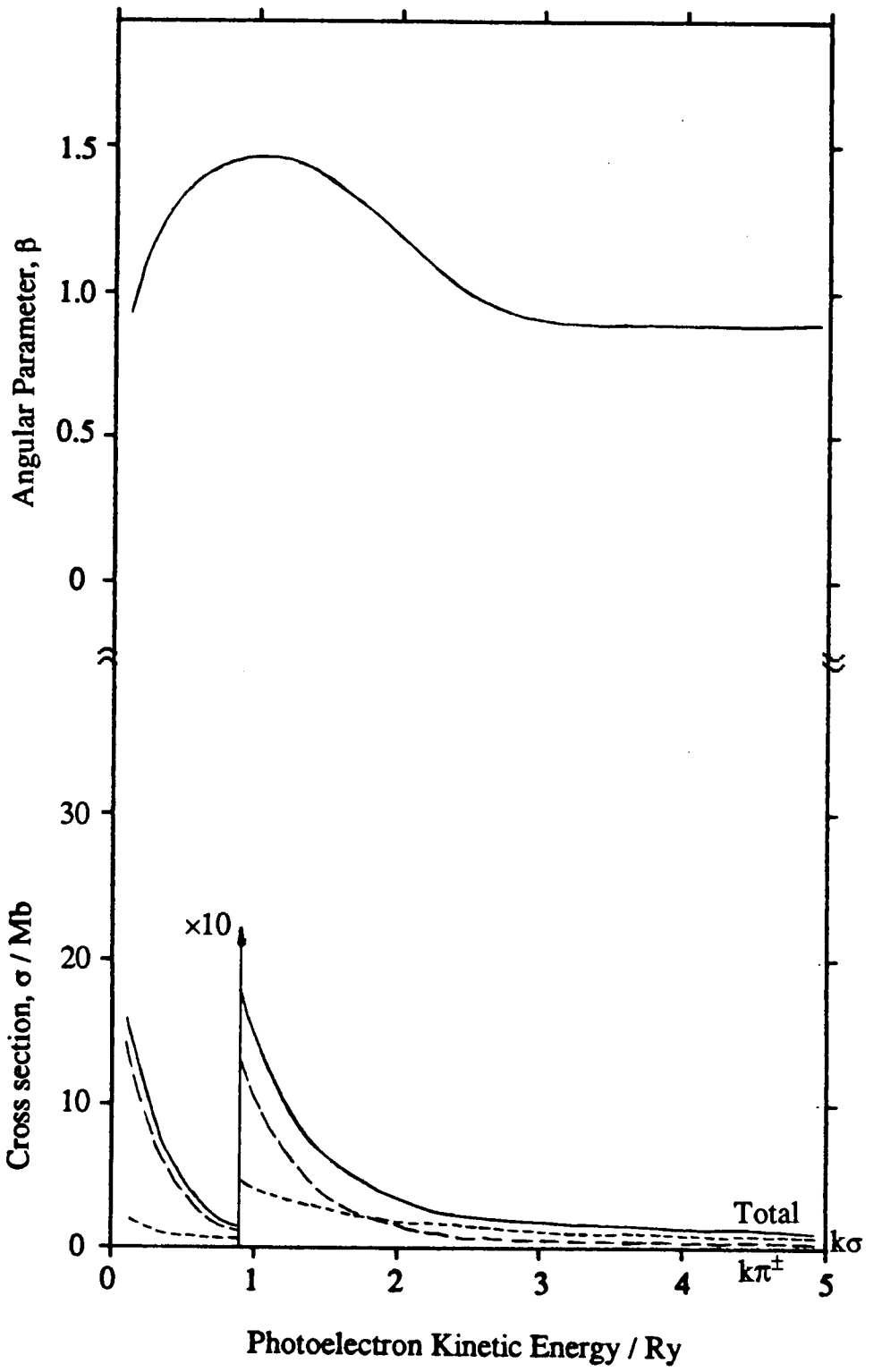

VI-2b. Calculated total and channel cross sections and angular parameter as a function of photoelectron kinetic energy for HBr 2σ.

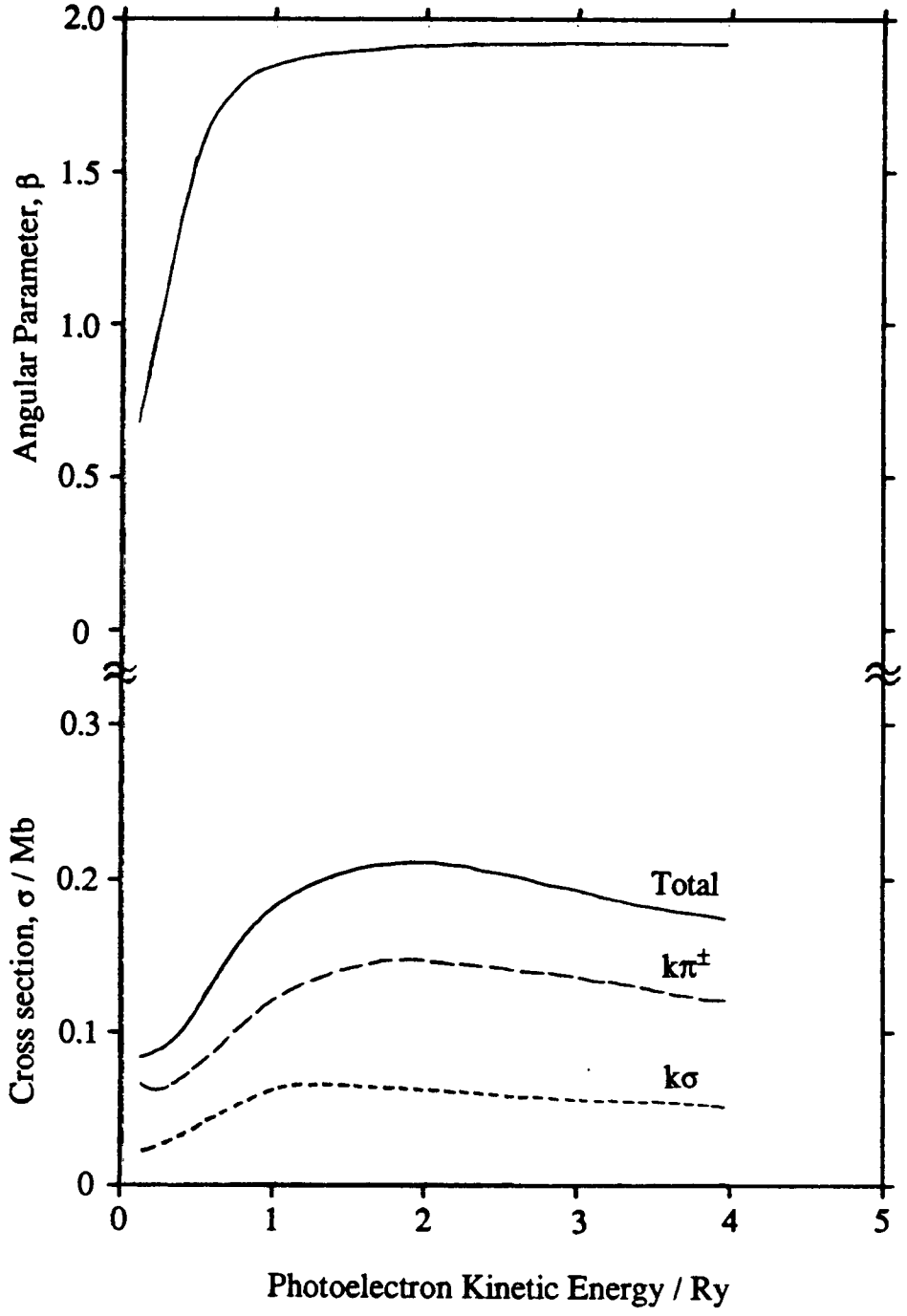

VI-2c. Calculated total and channel cross sections and angular parameter as a function of photoelectron kinetic energy for HBr 1σ.

for a partial CM, but past about 3.0 Ry it varies but slightly from the value $\beta = 0.88$ out to 6.0 Ry. In other words, it straightens to a horizontal line upon which it is difficult to distinguish a minimum. What we are trying to indicate is that β is a complicated function of energy (very much so for a bonding orbital such as this), and that for such a complicated function to revert to a straight (horizontal!) line over a large range after a period of relatively large variation, that for all this to be true is a bit shocking (again, relative to ones reactions to "usual" β curves). Were this behavior to be manifested in experiment--were only the relative traverse of β at high energy to be reduced compared to other hydrogen halides' 2σ's--a triumph of our calculational model should be declared. This behavior of the 2σ β curve is, in all seriousness, merely a long, broad minimum associated with the partial CM. It is longer and broader than most but is nonetheless just the manifestation of this same basic behavior.

HBr 1σ

HBr 1σ has the usual "ns" behavior. The CM is near threshold, and β dips to less than 0.7 there.

Hydrogen Iodide: HI

With HI, we reach a point in the periodic chart where it is questionable to disregard relativistic effects. The expectation value of the radial velocity of the K-shell electrons goes as Z a.u. (see Pyykkö[77]). Thus, the K electrons of HI are going $(Z/137) \times 100 = (53/137) \times 100 = 39\%$ of the speed of light. At this speed, the mass-velocity and Darwin terms of the relativistic hamiltonian are appreciably large and should be included. It has been found, however, that at these intermediate Z's (Z = 53 for iodine), the electron density around the atom is such that many-body effects begin to play an important role. Carlson, et al., (Reference 23 and references therein) by

use of the graph we call Figure IV-6a, show that inclusion of relativistic effects by the Dirac-Fock method results in wrong energy placement of the CM for xenon 5p (HI's united atom). Indeed, the non-relativistic Hartree-Fock or Herman-Skillman methods reproduce the rough experimental cross section and angular parameter energy trends and actually (fortuitously) place the CM at energies closer to those found in experiment than do relativistic treatments. Our preliminary molecular calculations using the Scalar Relativistic Approximation with the MSXα method (References 78, 79, 80, 81) have shown this same behavior. For these reasons, we shall present our non-relativistic calculations for molecules containing iodine and will only analyze trends, since ideally relativistic and many-body effects should be included.

Figure VI-3a presents the HI 1π, the nonbonding lone pairs, Figure VI-3b shows the graph of 2σ's dynamic features, and Figure VI-3c presents the results for 1σ, the bond.

HI 1π

HI 1π shows the behavior we have come to expect from a lone pair which has a CM. It is similar to iodine 5p: kπ and kδ show minima at 3.9 Ry where $\beta = 0$. kσ decreases too rapidly, relative to kπ and kδ's broad minima, for σ_{tot} to have a minimum. β in this energy range reaches up to 1.9 and down to -0.1 at its lowest.

HI 2σ

The behavior here is typical of bonding orbitals involving atomic orbitals which show CM. Note the broad valley in the β curve with its minimum at 5.9 Ry. This is different from HBr, remember, where the β curve flattens to a horizontal line. This is an extreme example of the failure of the method of finding the CM by looking for a minimum in β; the minimum β is at 5.9 Ry, but the CM is at 3.9 Ry, that is, this is the energy where the p$\rightarrow$ kd (and d$\rightarrow$ kp) matrix element changes sign.

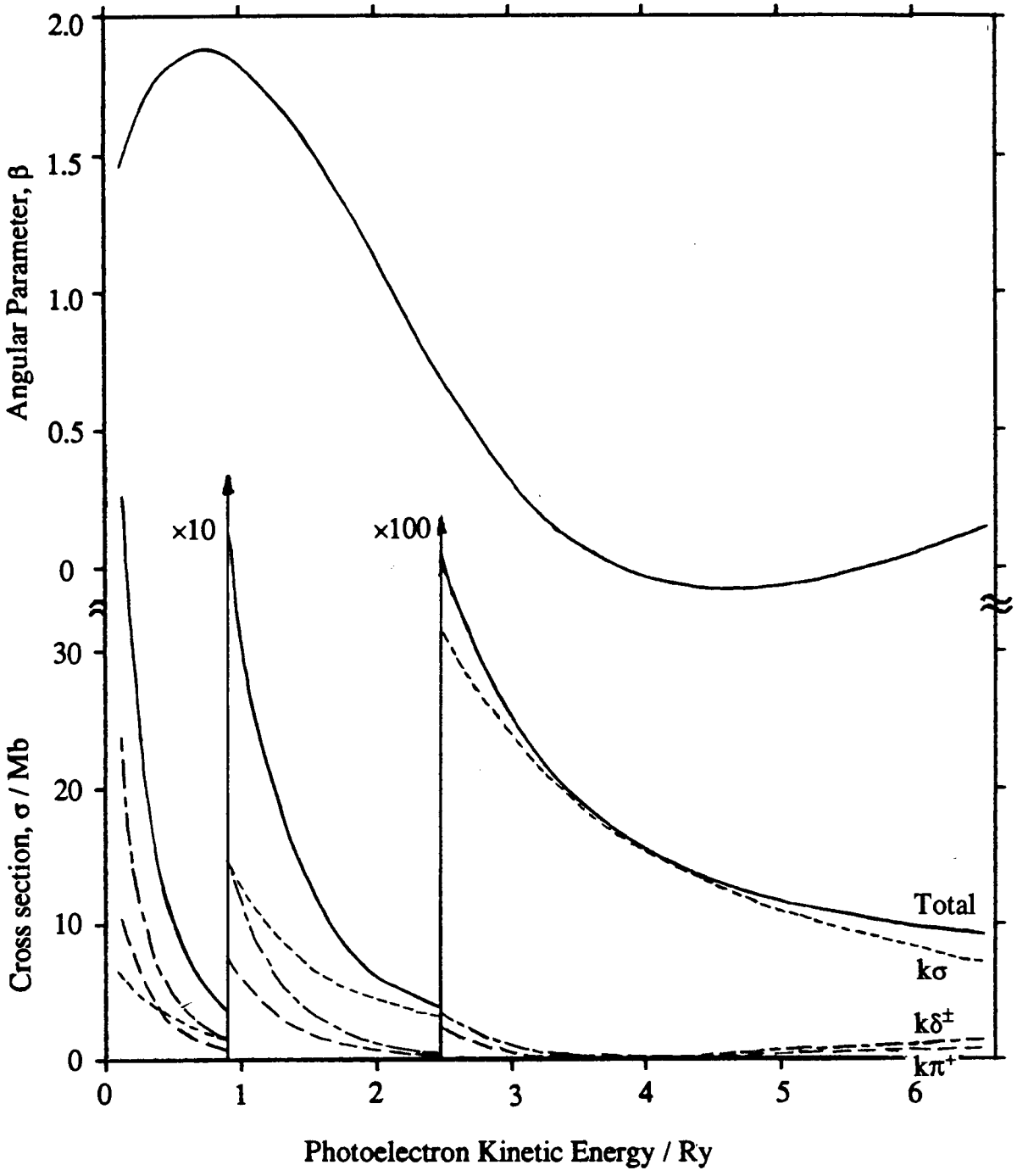

VI-3a. Calculated total and channel cross sections and angular parameter as a function of photoelectron kinetic energy for HI 1π.

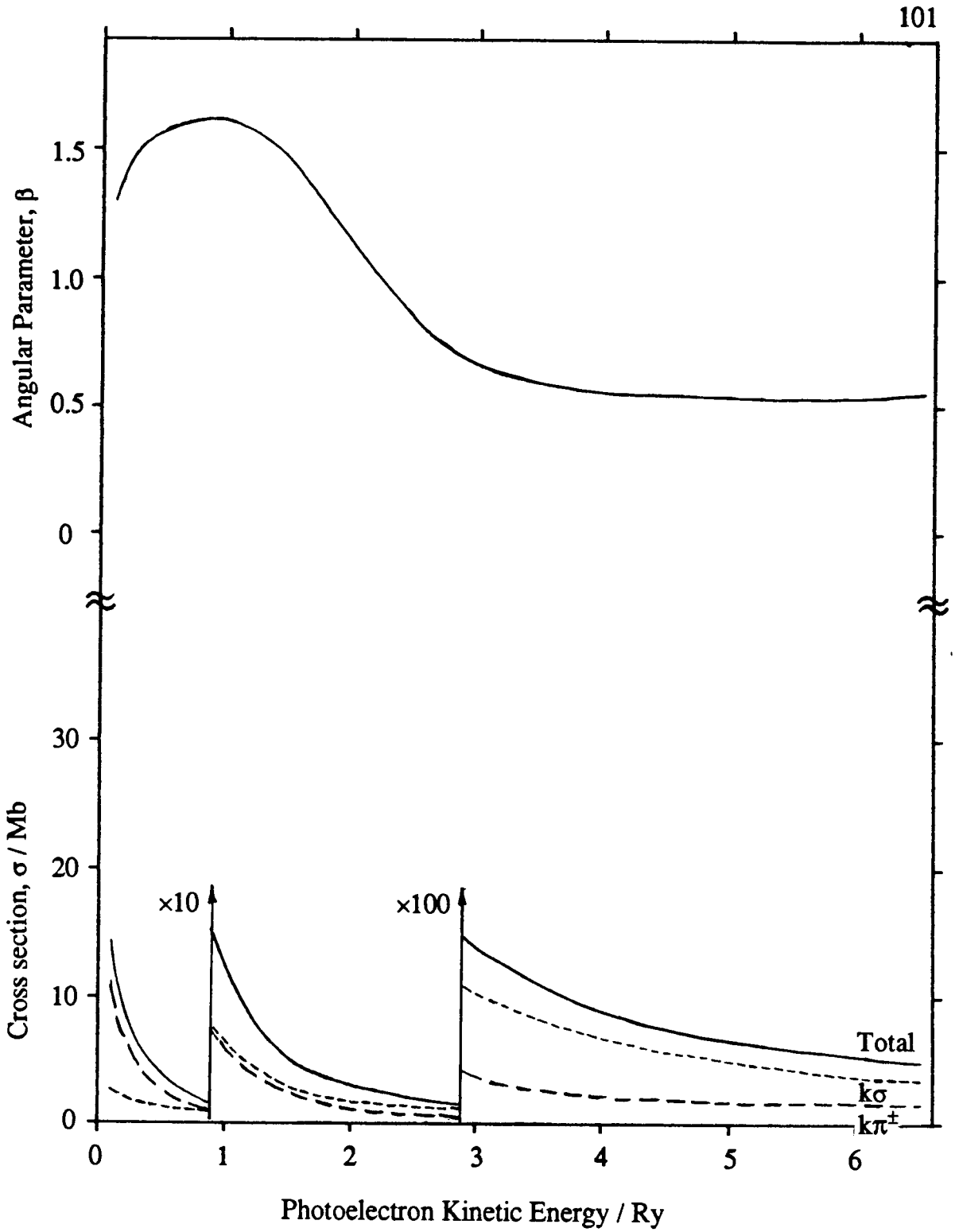

VI-3b. Calculated total and channel cross sections and angular parameter as a function of photoelectron kinetic energy for HI 2σ.

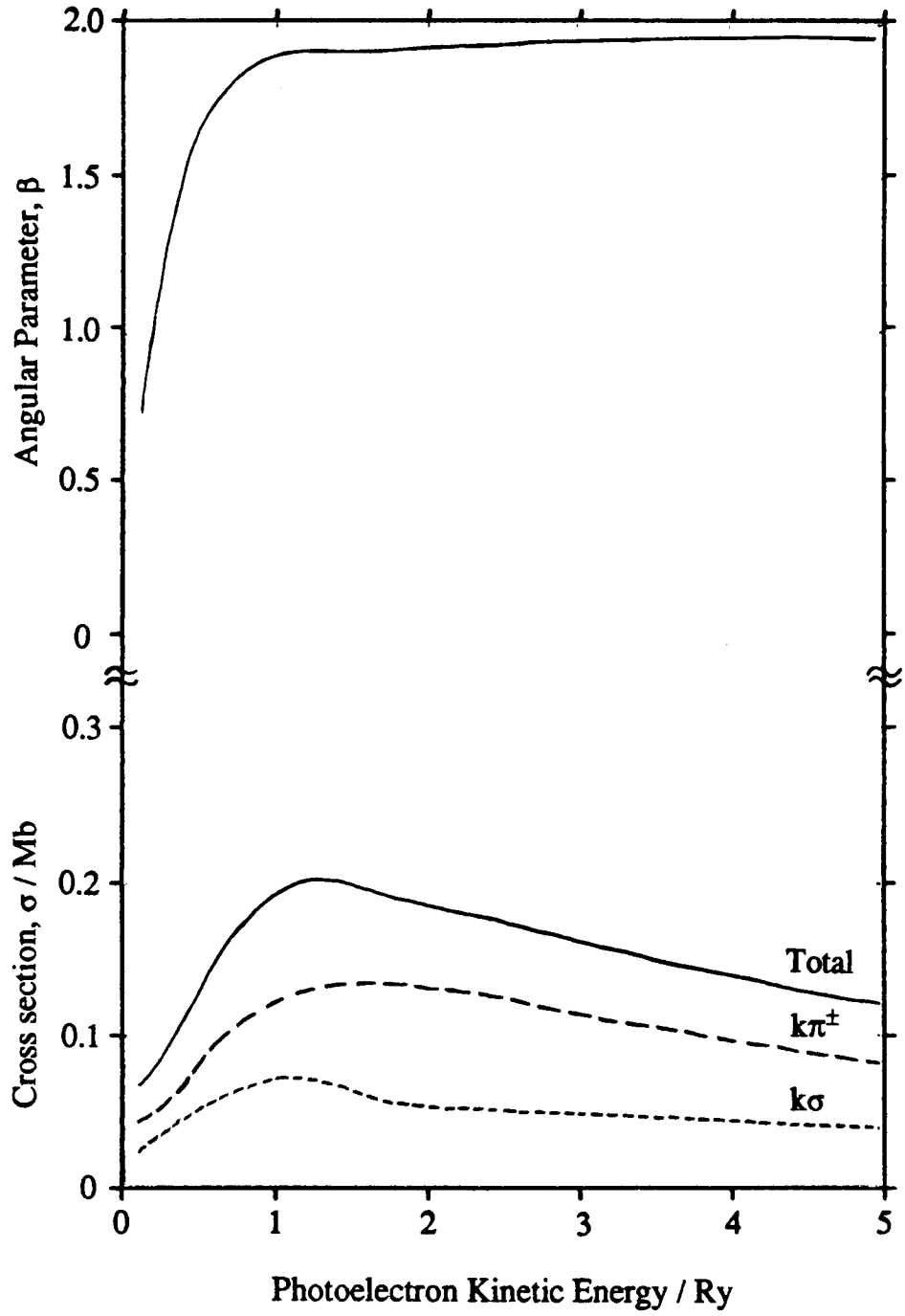

VI-3c. Calculated total and channel cross sections and angular parameter as a function of photoelectron kinetic energy for HI 1σ.

Unlike the 2σ bonding orbitals of other hydrogen halides, HI 2σ's $k\sigma$ channel remains dominant over the $k\pi$ well past the CM. This probably is a result of the diminished relative contribution of the hydrogen sphere in HI.

HI 1σ

Like HI's other orbitals, the 1σ displays typical behavior. The CM is near threshold where β and the cross section both fall off (that they both fall off is coincidence).

This orbital is unusual in one way; the $k\sigma$ channel cross section has a slightly pronounced bump at 1.1 Ry. The bump seems to be a shape resonance, since the eigenphase sum oscillates at this energy. None of the other HX orbitals shows any sign of shape resonance, even though the HI $k\pi$ and $k\delta$ channels' eigenphase sums also wiggle at 1 Ry. We believe that these resonances are so weak that they do not appear in the total or channel cross sections when these are large, as for 1π and 2σ. Only in the relatively small 1σ can it surface.

Summary of Results

It is remarkable how closely the molecular channels resemble the atomic channels. In HX, $k\sigma$ is recognizable as ks, $k\pi$ as kp, and $k\delta$ as kd. The difference in occupation number between the HX molecules' 1σ and 1π orbitals and X atoms' ns and np orbitals successfully explains the difference in their cross sections. This, and the fact that the β curves for these orbitals are nearly identical, argue that the hydrogen atom is a negligible perturbation. Of course, the hydrogen atom makes a difference in the bonding orbital where its presence is felt through the electron density it distorts in forming the bond.

Apparently the hydrogen atom does not cause a large enough perturbation on the X atom's potential for molecular shape resonance behavior to be manifested

(except in the case of HI's 1σ orbital). In Dehmer and Dill's terms,[49] although nuclear charge is separated in "forming HCl from the united atom," high-*l* partial waves are still excluded from the cores in HCl. This suggests that simple separation of nuclear charge is not enough to cause shape resonances. Sufficient charge must be separated to incite the high-*l* components into participating. Thus, molecules involving only hydrogen and another species normally do not show shape resonant behavior.[82]

Thiel's decomposition of β allows him to explain the general appearance of its energy dependency curve.[59,83] For instance, he traces the initial rapid rise in β to low energy changes in the Coulomb phase shifts of the continuum waves.[83,84] His methods are often capable of quickly locating such causes, where our methods require much analysis. At present, however, his method is limited to linear molecules, and ours is not.

Partial Cooper Minima

In experiment and theory on the 2σ orbitals of the hydrogen halide molecules, an effect is seen which has been dubbed the "partial Cooper minimum."[19,20] Partial CM are identified by comparison of molecular σ_{tot} and β with the σ_{tot} and β of the X atoms comprising the HX molecules.

Partial CM in HX 2σ (a bonding orbital involving mostly hydrogen 1s and X np_0) are marked by the following.

1. β traverses a narrower range than it does in X np.
2. The valley in σ_{tot} in 2σ of HX (near the energy of the CM in X np) is shallower than the valley in σ_{tot} in X np.
3. The kπ channel cross section in HX 2σ does not achieve zero as it does for kdπ in X np. kπ in HX 2σ does go through a minimum, but its cross section at this minimum is about equal to kσ's.

Points 1. and 2. apply to the experimental as well as the theoretical results, whereas, of course, point 3. applies only to the theory.

In order to understand better the causes of partial CM effects, we have carried out model calculations on the 2σ orbital of HCl and related species. We say "model" and "species," because the calculations are not meant to correspond with any real physical system or molecule. We have taken advantage of parameters and options in our program to tweak the calculations and find out the factors responsible for this weakened or partial CM.

At the outset of this discussion, we note that point 1. above can be qualitatively understood by reference to point 3. Recall the rough similarity of the spectral behaviors of the HX channel cross sections to the X atom channel cross sections. $k\sigma$ in HX roughly corresponds to $ks\sigma + kd\sigma$ in X atom, and $k\pi$ in HX to $kd\pi$ in X atom np_0.[75,76] Also, recall that β changes most rapidly where a channel cross section experiences dramatic change. At SR, channels show peaks, and β shows wiggles; at CM, channels show deep valleys, and β changes rapidly. Since HX $k\pi$ channels in the 2σ "spectra" show less pronounced valleys, β's dip is also less drastic than in X atom np "spectra." Because point 2. above is also due to point 3., it remains to be discovered what causes point 3., the enhancement of the $k\pi$ channel in HX 2σ.

For reference, Figure VI-4 presents the results for chlorine atom $3p_0$. σ_{tot} goes through a minimum at 1.7 Ry and $kd\pi$ is zero at 1.5 Ry, the shift being due to the falling $ks\sigma$ cross section.

The first model calculation, called "chlorine off-origin," is a modification (as are all the others) of the HCl overlapping spheres model (see Appendix V) using the same sphere sizes, positions, and values for α. This calculation is for chlorine atom moved off-origin (with a converged potential). It may also be viewed as an HCl calculation with hydrogen's atomic number set to zero. Its sphere remains but the potential inside it does not become large and negative toward the nucleus--there is no

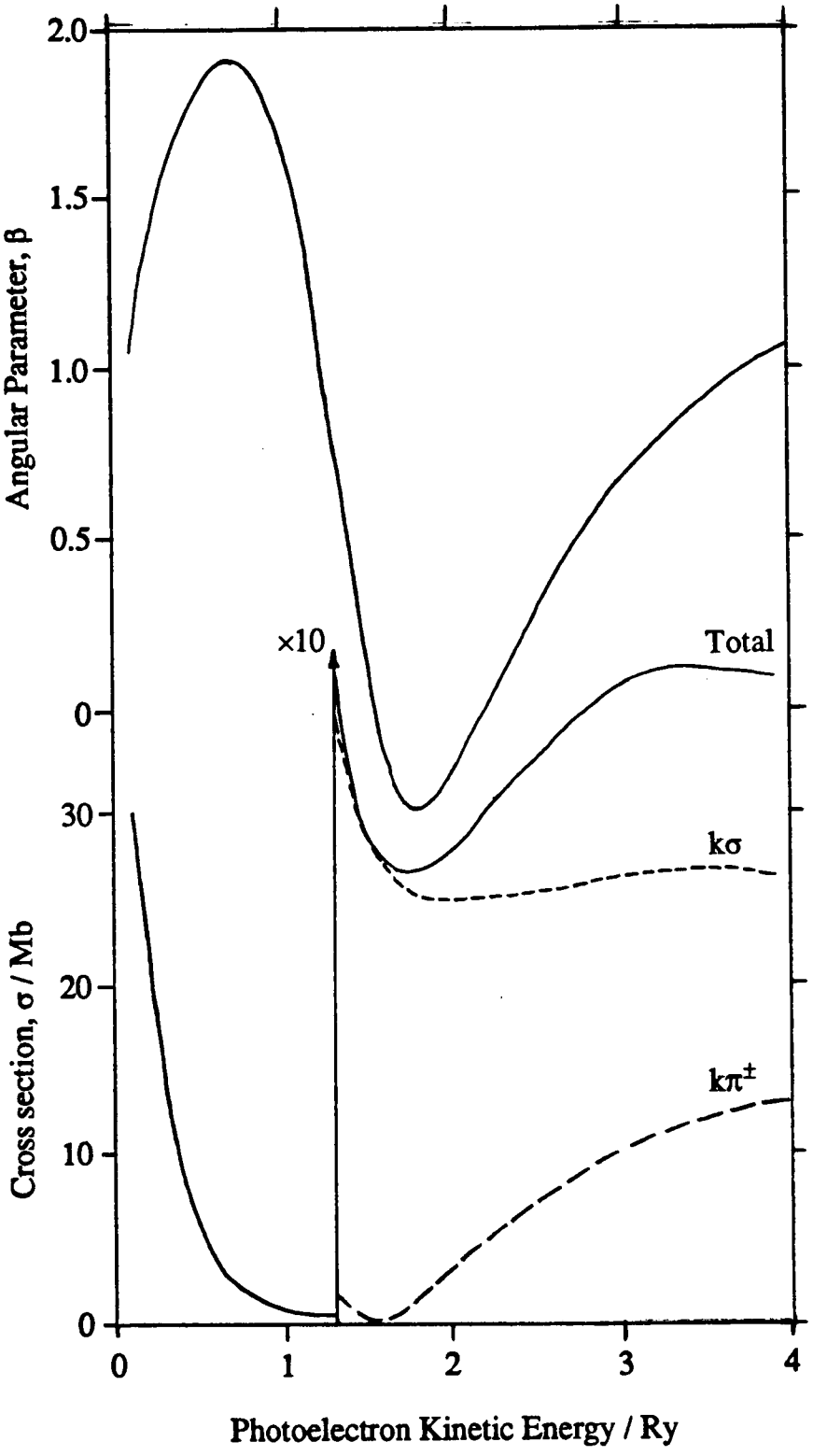

VI-4. Calculated total and channel cross sections and angular parameter as a function of photoelectron kinetic energy for chlorine atom $3p_0$.

nucleus. Instead, the potential inside the hydrogen sphere is nearly constant at around -0.9 Ry. We performed this calculation to find the effect of moving the chlorine atom off origin in forming HCl. Is it possible that this translation affects $3p_0$ in such a way to produce partial CM? As seen from Table VI-2, the initial state 2σ ($3p_0$) is still virtually all $l = 1$, and from Figure VI-5, translating the chlorine has only a small effect on cross sections and β.

Table VI-2. Initial State Molecular Orbitals' "l-type" analysis for model calculations. See the introduction to Appendix V for a full explanation of the entries in this Table.

		Cl $3p_0$	Cl off-origin	Hydrogen Neglected	HCl 2σ
Orbital energies/Ry:		-0.99	-1.01	-0.98	-1.10
Halogen sphere	$l = 0$	--	0.3	0.8	4.5
	$l = 1$	100	99.7	99.2	94.1
	$l = 2$	--	n	--	1.3
percent charge		(74.5)	(66.8)	(61.0)	(54.7)
"Hydrogen" sphere	$l = 0$	--	95.0	--	98.5
	$l = 1$	--	5.0	--	1.4
	$l = 2$	--	--	--	0.1
percent charge		--	(0.7)	--	(6.9)
Outer sphere	$l = 0$	--	0.2	n	0.1
	$l = 1$	100	90.1	90.1	97.2
	$l = 2$	--	9.2	8.6	1.4
	$l = 3$	--	0.5	0.6	1.3
	$l = 4$	--	n	--	n
percent charge		(21.2)	(17.9)	(20.2)	(19.3)
Intersphere percent charge		(4.4)	(14.6)	(18.8)	(19.0)

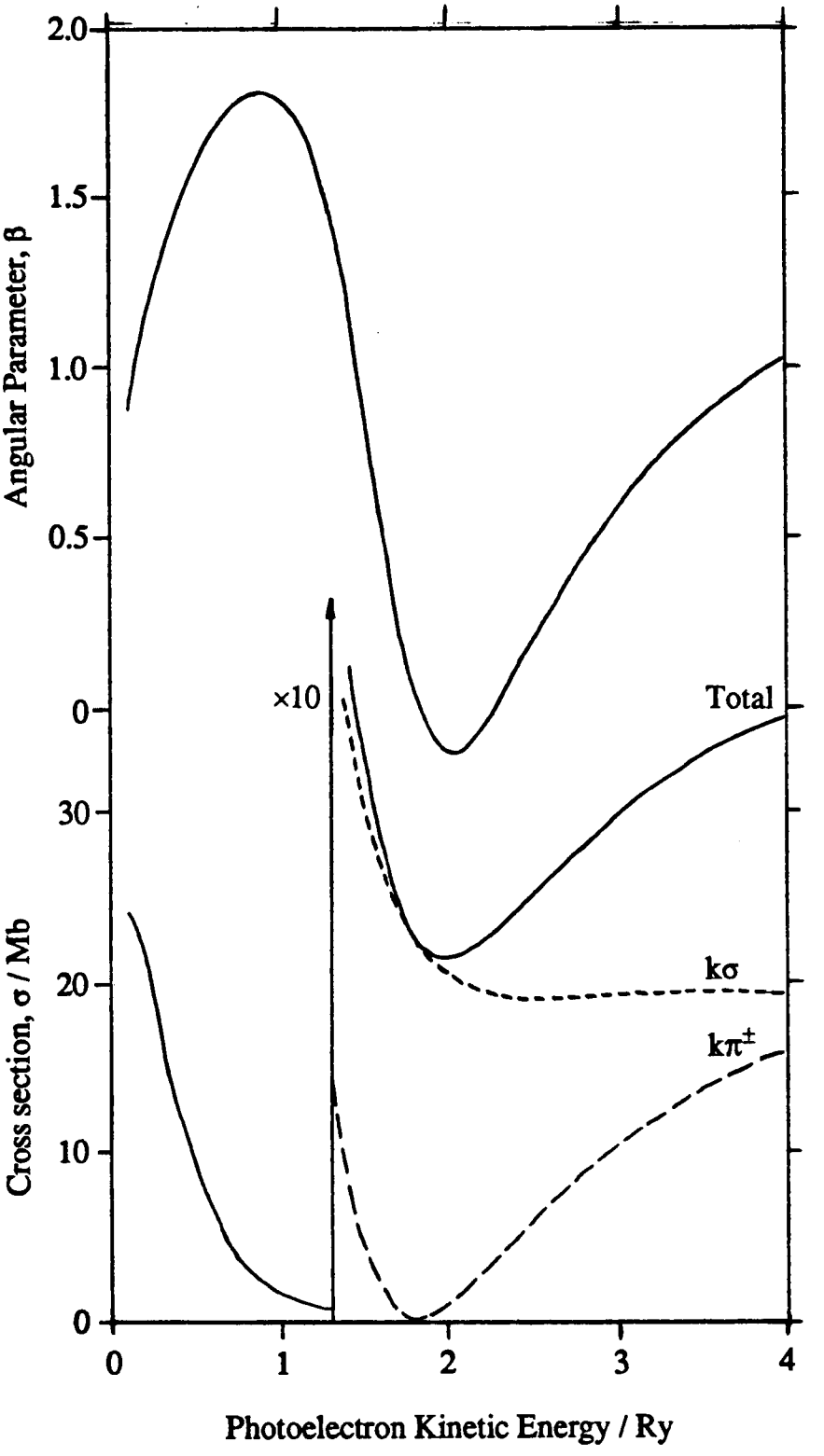

VI-5. Calculated total and channel cross sections and angular parameter as a function of photoelectron kinetic energy for "chlorine off-origin" 2σ model calculation.

In "chlorine off-origin," the CM is shifted to higher energies, σ_{tot} is minimal at 2.0 Ry, and $k\pi$ at 1.8 Ry. This sort of shift is seen elsewhere in our work simply by changing sphere sizes or using overlapping rather than tangent spheres. (The chlorine sphere has a radius of 2.30 a_0 in the normal atomic calculation but a radius of 1.901 a_0 in the "chlorine off-origin" calculation.)

This calculation shows that a converged off-origin atom (with an empty "counter sphere" and a large intersphere region) does not show partial CM. Partial CM must be a molecular effect, that is, must stem from the formation of the molecule.

[This model calculation further shows that our adoption of a "blatantly unphysical" constant potential intersphere region is not a hindrance to consistent qualitative results. An atomic calculation (in which this region is negligible) gives roughly equivalent results to a calculation involving a large intersphere region. This is encouraging.]

The second model calculation, called "hydrogen neglected" uses the converged HCl molecular potential. To find out the effect of molecule formation on chlorine atom's potential, and to screen out any confounding contributions of the hydrogen, we left out hydrogen's potential and calculated β and σ_{tot} only for the chlorine and outer spheres in the HCl potential. Table VI-2 shows that ignoring the hydrogen sphere in the initial state leaves the chlorine almost entirely as $l = 1$. Figure VI-6 shows that the results are virtually those of the chlorine atom $3p_0$ but for a tiny rise in $k\pi$'s cross section at the CM amounting to 0.006 Mb, up from 0.002 Mb for $k\pi$ in "chlorine off-origin" at its CM. [We also note that the minimum σ_{tot} is at 1.8 Ry, and minimum $k\pi$ is at 1.6 Ry as in the atom.]

This calculation is a measure of hydrogen's effect on the potential in chlorine's sphere and the outer sphere, while neglecting any amplitude arising from the hydrogen sphere. That the results resemble those of the atom shows that the effect of hydrogen on the chlorine through the potential is small.

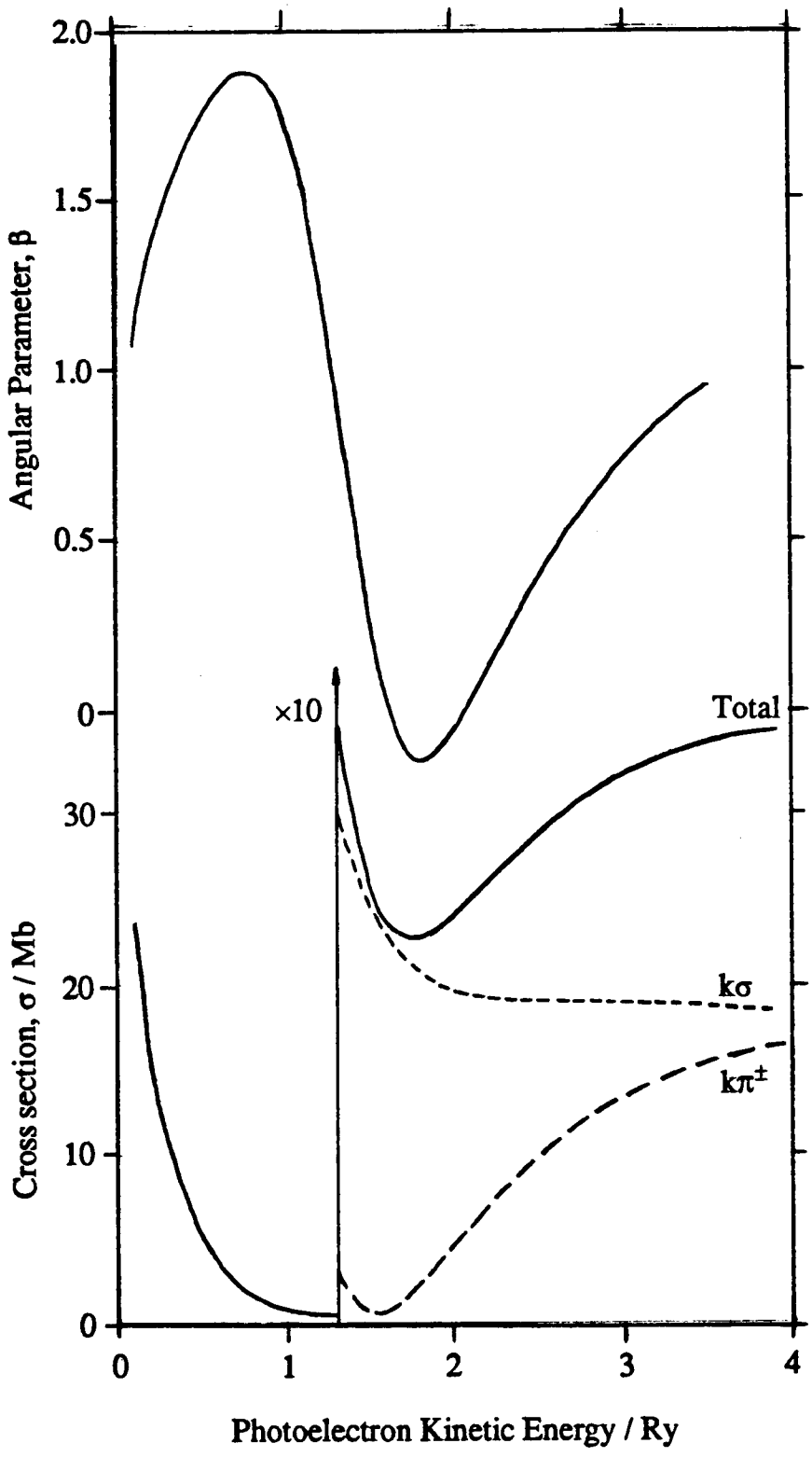

VI-6. Calculated total and channel cross sections and angular parameter as a function of photoelectron kinetic energy for "hydrogen neglected" 2σ model calculation.

Note from Table VI-2, however, that in the full initial state, inclusion of hydrogen arouses a noticeable $l = 0$ component in the chlorine sphere. Since we did not see this in "chlorine off-origin" or in the "hydrogen neglected" initial states, this effect must propagate through the wavefunction coefficients. Is this $l = 0$ contribution to the initial state responsible for the partial CM?

Our third (and final) model calculation, called "hydrogen final state neglected," investigates this by using the proper HCl 2σ initial state (with the proper converged HCl potential) but setting the final state hydrogen symmetry coefficients to zero. This allows hydrogen to influence and evoke the $l = 0$ initial state contribution in the chlorine sphere but then snatches out the hydrogen sphere amplitude contribution. All radial matrix elements in the **F** matrix in the hydrogen sphere may as well be zero in this calculation.

Figure VI-7 presents the results for "hydrogen final state neglected." The $k\pi$ cross section has been enhanced to 0.012 Mb at 1.6 Ry, and β no longer achieves zero. In fact, about half of the (partial CM) shift in β near the CM has been accounted for by this artifice of ours. (At its minimum, β in 2σ of HCl equals 0.42; in chlorine atom $3p_0$, $\beta = -0.3$ at its lowest; and here, in "hydrogen final state neglected," β bottoms out at 0.13.) Thus, we find our first real "cause" of the partial CM: the formation of a molecule by "putting two atoms together" produces an initial state effect of multi-l form of the wavefunction around the constituent atoms. This should not be too surprising, for we knew already that l is not a "good" quantum number in molecules. We might have suspected that it would not be good even <u>within</u> an atomic sphere in our model.

We again show the results for HCl 2σ in Figure VI-8, revealing the full "partial Cooper minimum." As stated at the beginning of this section, the $k\pi$ channel has risen to 0.146 Mb, and β reaches a minimum of 0.42, both much higher than in chlorine atom $3p_0$. This full, "realistic" calculation of HCl 2σ differs from "hydrogen final state neglected" in that this calculation now includes amplitude from the hydrogen

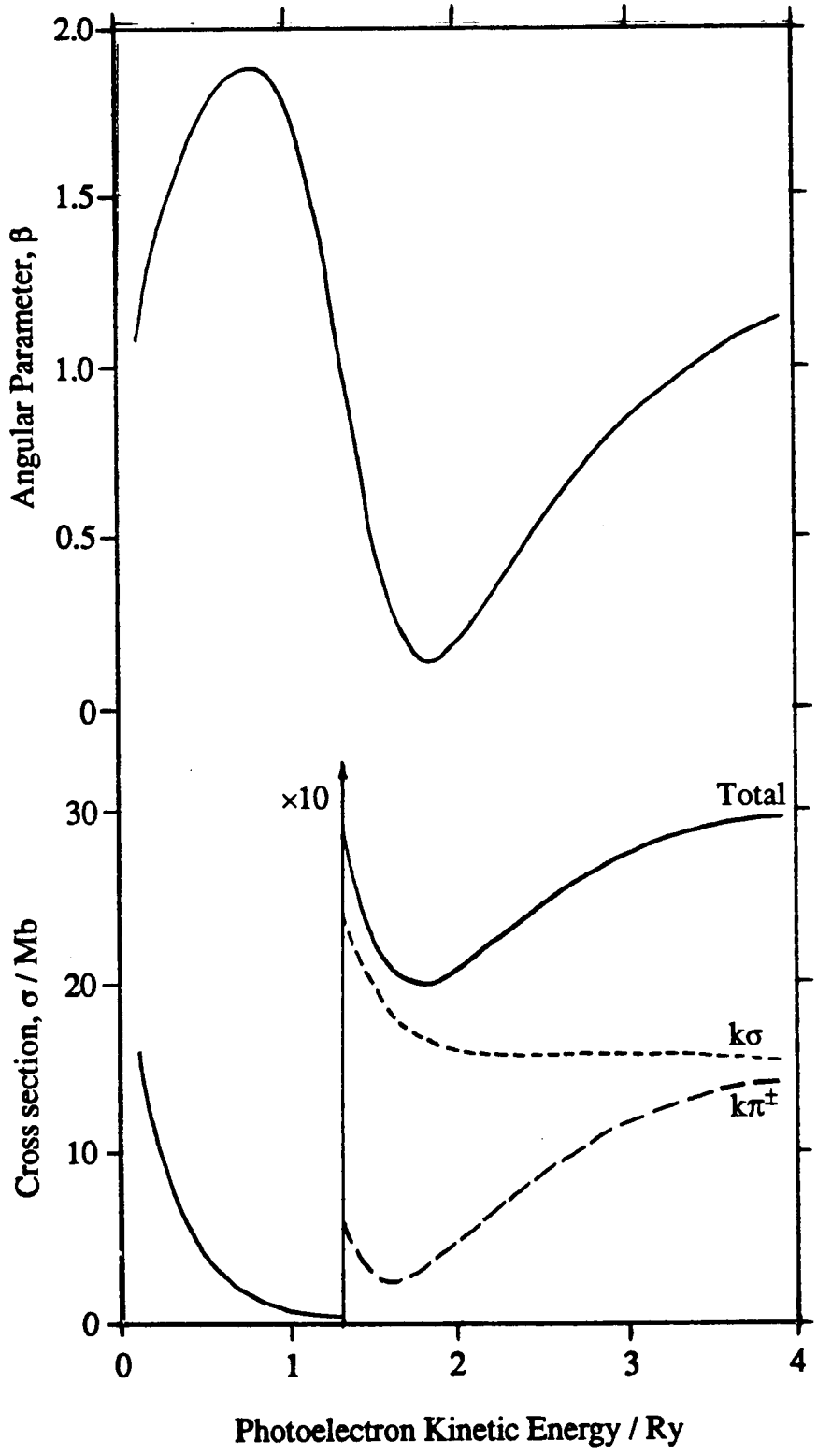

VI-7. Calculated total and channel cross sections and angular parameter as a function of photoelectron kinetic energy for "hydrogen final state neglected" 2σ model calculation.

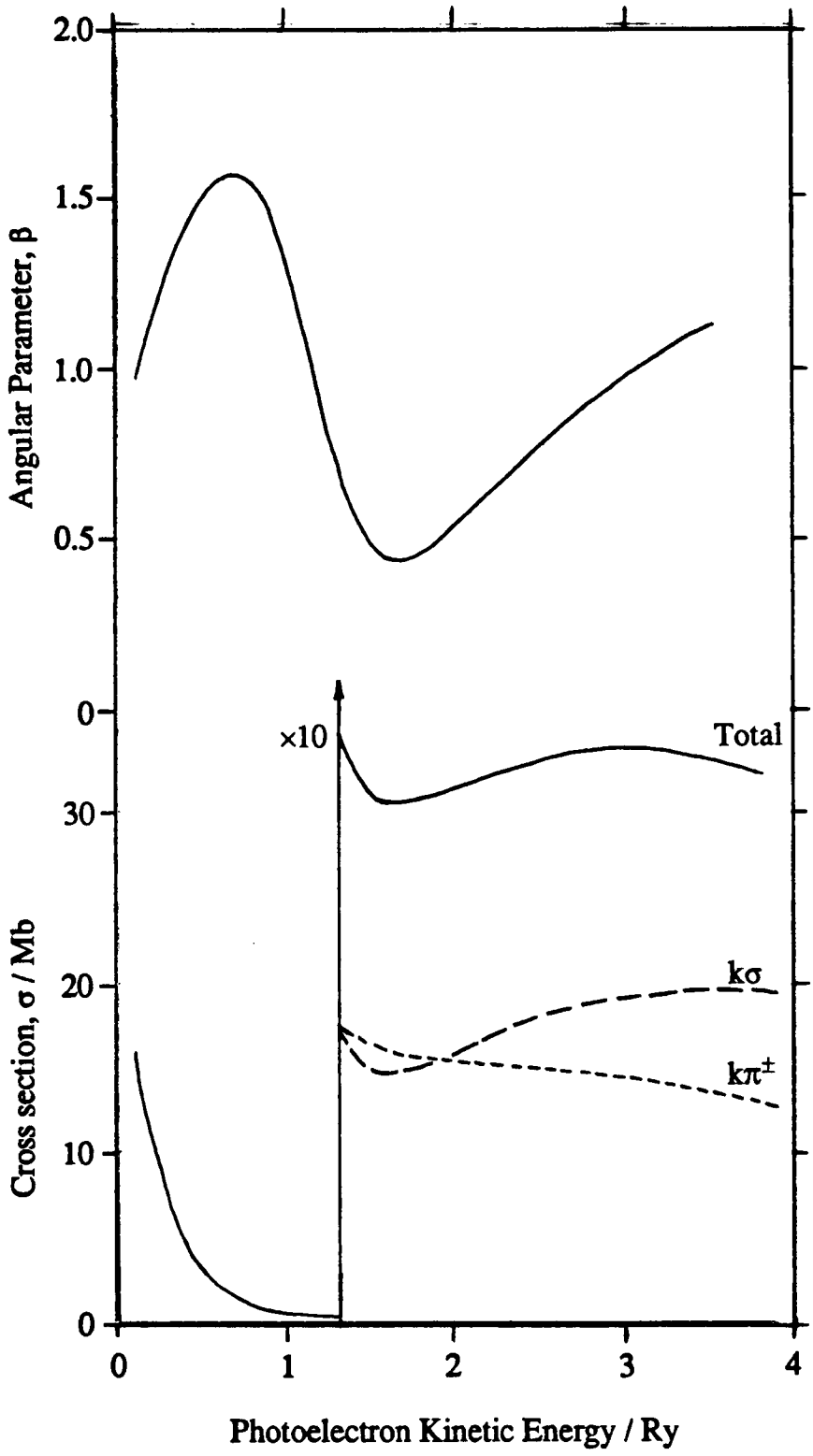

VI-8. Calculated total and channel cross sections and angular parameter as a function of photoelectron kinetic energy for HCl 2σ.

sphere. This amplitude results mostly from $(l = 0)_i \rightarrow (l = 1)_f$ radial matrix elements which contribute to the $k\pi$ channel.[59]

Summary

Figure VI-9 is a schematic summary of the model calculations. In HCl's 2σ bonding orbital, we see a smaller cross section minimum and a weaker β oscillation than in either the HCl 1π or in chlorine atom 3p. In "chlorine off-origin," we reconverged the HCl potential with the hydrogen sphere empty (Z = 0), thus simulating a chlorine atom whose nucleus had been moved off-origin. We were pleased that the results for "chlorine off-origin" were similar to those for the chlorine atom $3p_0$. (The differences are attributed to differing sphere sizes, as Figure VI-9 shows.) In "hydrogen neglected," we used the HCl potential but excluded the hydrogen sphere from the initial and final states. This was meant to measure the effect of the hydrogen on the chlorine during the process of converging the HCl potential (bringing it to self-consistency). Again the results closely resemble those for the chlorine $3p_0$; hydrogen does not "distort" chlorine's atomic potential in our model in a way which significantly affects the PED parameters. When the $X\alpha$ method is granted its full flexibility to find the proper initial state 2σ orbital of HCl, however, the matching of wavefunction coefficients at boundaries introduces a significant $l = 0$ contribution to the chlorine sphere; the presence of hydrogen has distorted the otherwise purely $l = 1$ wavefunction (of the chlorine $3p_0$). However significant this initial state effect may seem, if we perform the PI calculation with this proper initial state, but snatch out the hydrogen sphere's contribution to the **F** amplitude matrix before σ_{tot} and β are calculated, we see only a small effect. This is what we have done in the calculation called "hydrogen final state neglected." Thus, by elimination of causes, the contribution of hydrogen to the "scattering" or response amplitude matrix, **F**, adds to the chlorine atomic contribution, thus softening the pure atomic CM into a molecular partial CM.

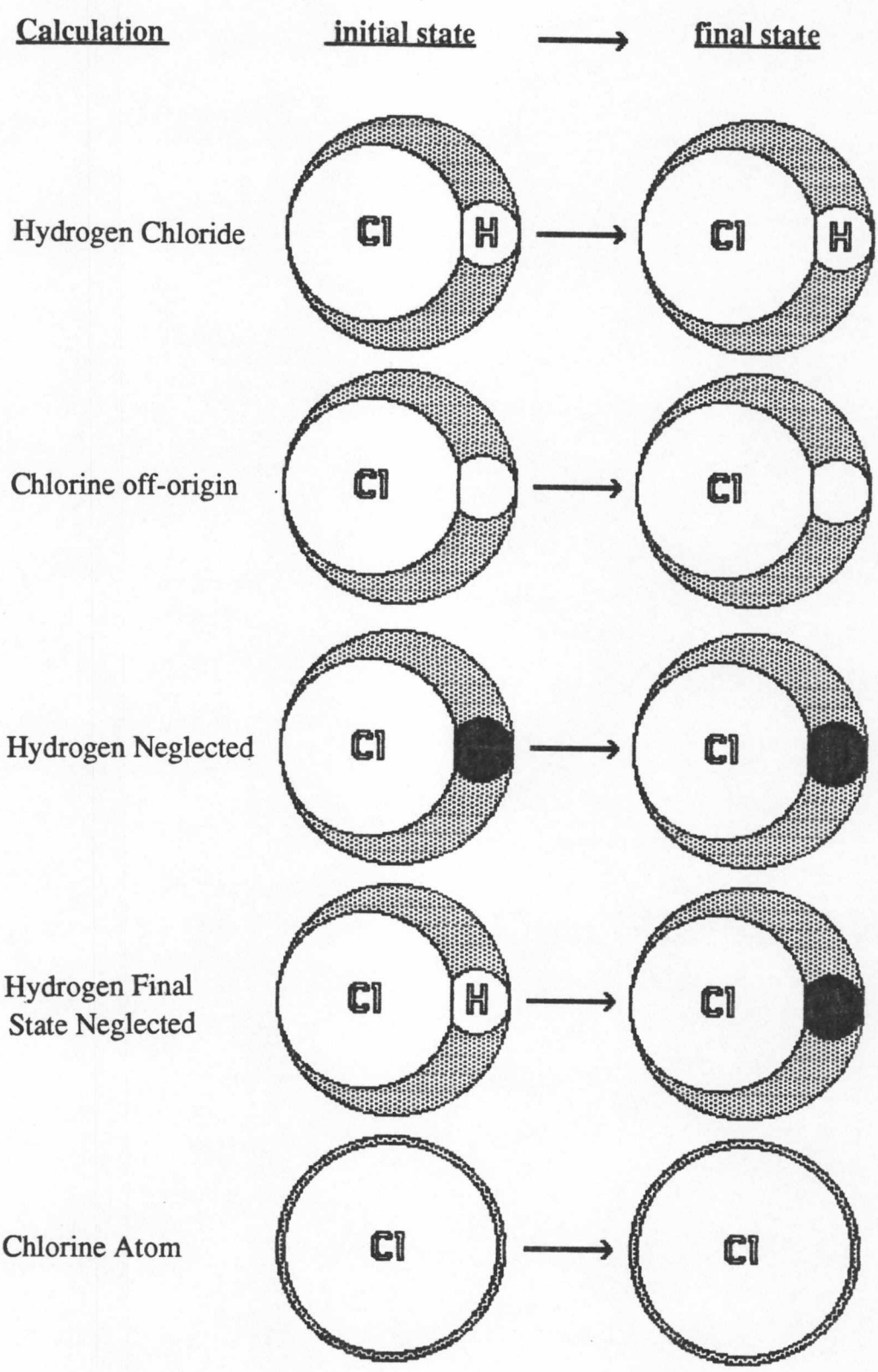

VI-9. Schematic summary of model calculations.

Comparison with Experimental Results

The PED of hydrogen halides has been extensively studied (compared to other classes of molecules). The cross sections of the two outermost orbitals of HCl have been treated theoretically by Faegri and Kelly using *ab initio* methods,[75] and their angular parameters by Thiel using his unique parametrization of MSXα calculations.[59]

Carlson, et. al.,[23] compare Faegri and Kelly's results to those presented here, and Thiel favorably compares his results to ours. But for some spurious remarks concerning the treatment of exchange in our method, Carlson's remarks are good. He shows that the *ab initio* method places the energy of the CM closer to the experimental value than does our MSXα method. (Thiel casts doubt on Faegri and Kelly's results, however, by noting that they were found with a basis set with an upper bound of $l = 2$ for the final state channels. Thiel found $l = 3$ to 5 to be important contributors around the CM.) Absolute cross section comparison of the theories with experiment is not particularly successful--measurement of these is difficult, and our calculations are not "optimized" for such comparison. More importantly, the authors show that the theories yield σ_{tot} and β trends in excellent agreement with experiment; there is one-to-one correspondence of features. The three methods (Faegri and Kelly's, Thiel's, and ours), as different as they are, all find the same basic behavior.

The experimental and theoretical trends for HBr are in disconcertingly good agreement.[23] The cross section results are in such good agreement as to compel the authors to resort to the unorthodox practice of presenting theory and experiment in the same graph. Compared to its behavior in HCl and HI 2σ orbitals, β in the 2σ of HBr shows a flat profile past 3 Ry in the experiment. As stated above, this is remarkable behavior for such a complicated parameter, and MSXα's prediction of it is encouraging.

Carlson, et. al.,[24] report experimental results for HI and discuss the comparison of these with our theoretical results. Our method produces much broader minima at

higher energies than are found in experiment. Elsewhere, Carlson[23] presents the graph which we have labeled Figure IV-6a, which shows that nonrelativistic, independent particle methods tend to find too high energies for the CM of heavier systems, but that relativistic, independent particle methods fare worse still.

In Reference 23, all the work on HX of Carlson, et. al., is compiled and compared with our calculations. Aside from absolute energy placement of the CM and agreement of absolute cross sections, they show that the MSXα method can predict the features of the experimental σ_{tot} and β curves.

HCl and HBr have also been studied by dipole (e,2e) spectroscopy.[85,86] (See Reference 87 for a recent review.) (e,2e) spectroscopy is a coincidence technique involving a "knockout reaction" in which a single incident electron knocks out a second, target electron from the system of interest so that one starts with one electron and ends with two; hence, (e,2e). Dipole (e,2e) uses low momentum transfer by the incident to the knocked out electron to simulate the photon in PES. A photoionization cross section is one result of dipole (e,2e) measurements.

The (e,2e) results for HCl and HBr agree excellently with those from PES, considering that the two experimental techniques differ vastly. The (e,2e) experiments have not been carried out to high enough energies to see the Cooper minima, but the cross sections tend towards low values at higher energies as do the PES results.

None of the third bands of HX have been studied experimentally over wide energy ranges by PI methods due to their low cross sections. Two points for the 1σ band of HBr have been reported.[23] β shows the expected high values (nearly equal to two), but σ_{tot} is discrepant between experiment and theory. We do not anticipate that our independent particle calculations will fare well in comparison with experiments on the third bands, in light of the results of such comparison for the ns orbitals of the noble gases (References 60, 72, 74, 73, 65, 88, 69). Our calculations place the CM at or below threshold, but experiment and more considered calculations find the CM in the area of about 10 eV into the continuum. Nevertheless, we look forward to these experiments as they will provide still further insight into "molecular effects" on CM.

Brion, et. al.,[85,86] have studied the "third bands" of HCl and HBr by (e,2e) spectroscopy. The cross section results have the same humped shape as our results, but are an order of magnitude larger. We use quotes on "third bands," because the third bands of HX are composed of (mostly unresolvable) many electron transitions, making comparison with our independent particle calculations hazardous.

CHAPTER VII

HOMONUCLEAR DIHALOGEN MOLECULE

RESULTS

This chapter presents our theoretical results for the diatomic halogens, X_2. All the notes concerning the format of the Figures in the atoms' section obtain for this chapter. All orbitals of one molecule will be treated (from the outermost inward) before moving on to the next molecule.

We consider the five outermost valence orbitals of the homonuclear halogens. Again in keeping with recent usage, we number the valence orbitals of X_2: $1\sigma_g$, $1\sigma_u$, $2\sigma_g$, $1\pi_u$, and $1\pi_g$; this facilitates intercomparison of the molecules. For the readers' ease, we present a table of correlations of the significations of these orbitals of X_2 (Table VII-1). Appendix V contains *l*-type analyses for these orbitals as calculated by the Xα-SW method.

Table VII-1. Correlation of X_2 Valence Orbitals.

	$1\sigma_g$	$1\sigma_u$	$2\sigma_g$	$1\pi_u$	$1\pi_g$
Cl_2	$4\sigma_g^2{}_{Cl,3s}$	$4\sigma_u^2{}_{Cl,3s}$	$5\sigma_g^2{}_{Cl\text{-}Cl}$	$2\pi_u^4{}_{Cl,3p}$	$2\pi_g^4{}_{Cl,3p}$
Br_2	$7\sigma_g^2{}_{Br,4s}$	$7\sigma_u^2{}_{Br,4s}$	$8\sigma_g^2{}_{Br\text{-}Br}$	$4\pi_u^4{}_{Br,4p}$	$4\pi_g^4{}_{Br,4p}$
I_2	$10\sigma_g^2{}_{I,5s}$	$10\sigma_u^2{}_{I,5s}$	$11\sigma_g^2{}_{I\text{-}I}$	$6\pi_u^4{}_{I,5p}$	$6\pi_g^4{}_{I,5p}$

The homonuclear dihalogen molecules belong to the $D_{\infty h}$ point group. Consider that the nuclei reside on the z-axis of our coordinate system. As with the hydrogen halides, we may make guesses as to the A.O. makeup of the orbitals. (Because they are made with hindsight these guesses are roughly correct.) The $np_{\pm 1}$ (or np_x and np_y) orbitals are virtually lone pairs represented as $1\pi_u$ and $1\pi_g$. The single bond of the molecule is made up of np_0 (or np_z, if you will) orbitals on the constituent atoms and is represented by $2\sigma_g$ (the $2\sigma_u$. is unoccupied). The outermost ns orbitals of the X atoms are represented by $1\sigma_g$ and $1\sigma_u$. These rough assignments are indicated in Table VII-1.

With the experience we have gained from the hydrogen halides, we may anticipate the behavior of the CM in the dihalogens: the lone pair orbitals, $1\pi_u$ and $1\pi_g$, will likely show atomic behavior; the outermost s orbitals, $1\sigma_g$ and $1\sigma_u$, will behave basically like their constituent ns's but will deviate in cross section and β due to mixing of $l = 1$ in the initial state; the $2\sigma_g$ bonding orbitals will display weakened or "partial" CM due to the mixing of $l = 0$ into the initial state, as with the hydrogen halides' 2σ.

These CM effects can be explained basically in terms of the atoms present, but the formation of a molecule (of the size of these we are considering) gives rise to phenomena not present in the atoms. These are, of course, shape resonances (SR). These lie in the region just above threshold to about 2 Ry kinetic energy, although one will occasionally sneak out to 3 Ry. As mentioned in Chapter 4, the barriers which underlie these resonances cannot easily be pictured due to the discontinuities of the muffin tin approximation and overlapping spheres. Nevertheless, by analyzing our symmetry channel breakdown of the cross section, we may label SR by channel. Further, by analyzing the partial wave cross sections within a symmetry channel, partial wave labels may be assigned to particular channel SR. SR are signaled by a

change in eigenphase sum, μ_{sum}. Molecular SR often involve changes as small as one-quarter unit. With practice, it becomes easy to distinguish potential resonant behavior from "normal" rises in μ_{sum}. (See References 48, 49, 51 for a description of the N_2 K-shell resonance and discussions of molecular resonances in general.)

In what follows, we indicate this by statements such as: "The SR in the X continuum channel of the Y initial state is mostly l = m, n, o" (where m, n, and o will be integers). Please take this to mean that, since a shape resonance is manifested as a (rapid) rise in cross section over a small energy range, the m, n, and o partial waves on the outer sphere were found to be most responsible for this rise. (Thus, a monotonically decreasing partial wave cross section is not listed, even if it dominates.) They are listed in the order of decreasing percentage contribution except in some unrankable cases when two components contribute almost equally.

We emphasize that these are partial wave labels for the continuum wavefunction in the outer sphere, because numerous partial waves (of differing l) in the atomic spheres are coupled to a single partial wave in the outer sphere. This coupling makes it possible for $l = 0$ to appear in our list of SR active partial waves, although from our picture of potential barriers, the effective potential for $l = 0$ cannot be repulsive [$V_{eff}(l=0) = V(r)$]. In such a case, the SR must occur in the atomic spheres and be coupled to $l = 0$ on the outer sphere.

The shape resonances do not occur in the same energy regions as the CM for the dihalogens. Most SR are near threshold; CM are out past 1.5 Ry.

As discussed for atoms in Chapter 4, a shape resonance will strongly affect β because it involves a single channel becoming rapidly large. Thus in addition to the cross section, the β curves for the dihalogens should not be expected to resemble those for the halogen atoms of Chapter V. We do hope to make plausible explanations for the differences, though.

Chlorine Molecule: Cl_2

Referring to Appendix III, we see that the $k\sigma_g$ and $k\pi_g$ channels show particularly sharp rises in eigenphase sum about 0.4 Ry and 0.7 Ry, respectively, although all the channels seem to hold the potential for resonant behavior.

Figures VII-1a through VII-1e present the cross section and β results for the five outermost orbitals of Cl_2. Table VII-2 contains a summary of the shape resonances found in these orbitals and the partial waves responsible for them.

Table VII-2. Energy positions in rydbergs of shape resonances in chlorine molecule. Numbers in parentheses indicate responsible partial waves. "n" means "no resonance in this channel."

	$k\sigma_g$	$k\pi_g$	$k\delta_g$	$k\sigma_u$	$k\pi_u$	$k\delta_u$
$1\sigma_g$	-.-	-.-	-.-	1.0 (1)	.n	-.-
$1\sigma_u$	0.3 (0,4)	0.6 (2)	-.-	-.-	-.-	-.-
$2\sigma_g$	-.-	-.-	-.-	1.0 (1,5)	.n	-.-
$1\pi_u$	0.6 (4,2)	0.65 (4)	.n	-.-	-.-	-.-
$1\pi_g$	-.-	-.-	-.-	1.2 (?)	.n	0.2 (3)

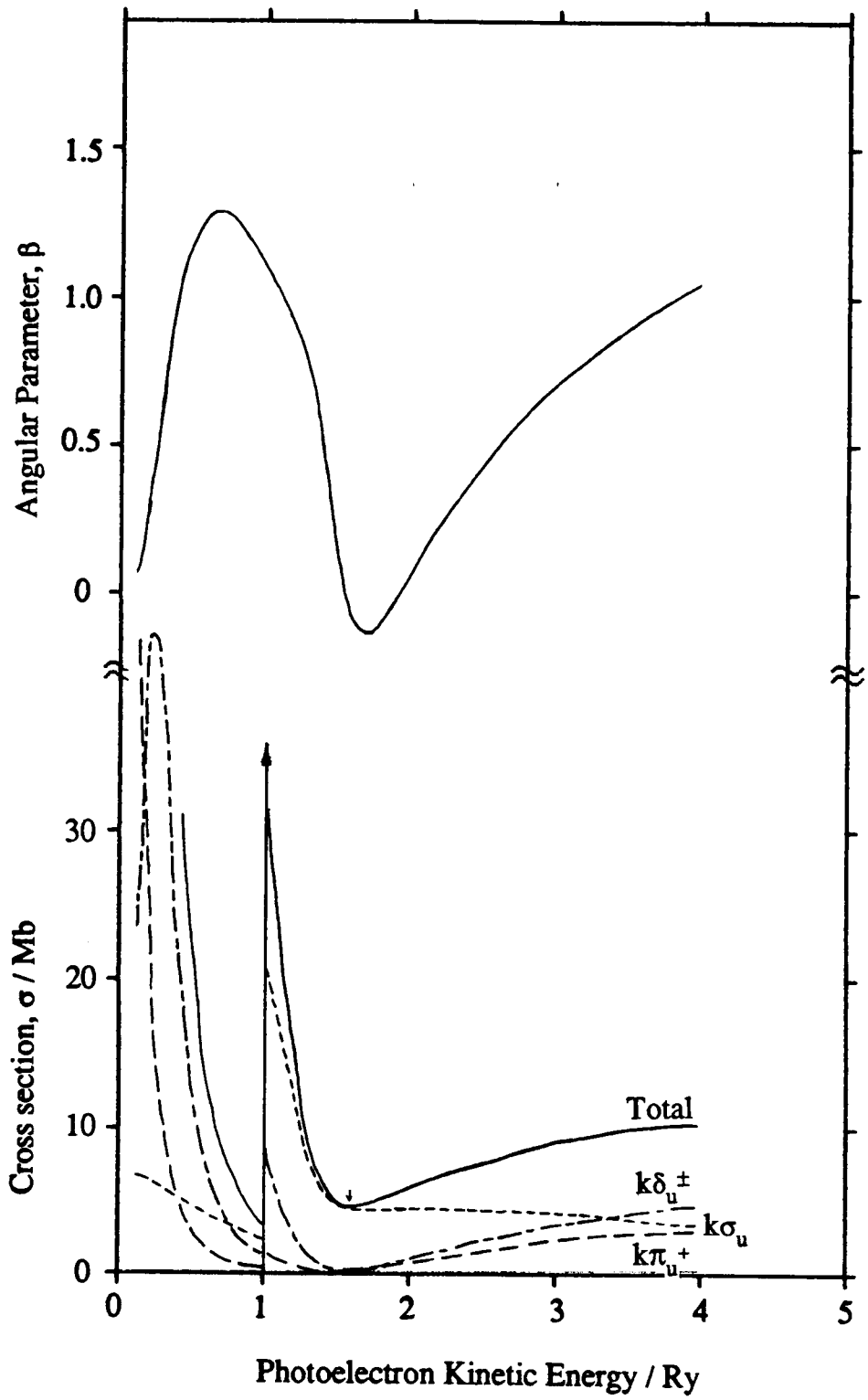

VII-1a. Calculated total and channel cross sections and angular parameter as a function of photoelectron kinetic energy for Cl_2 $1\pi_g$.

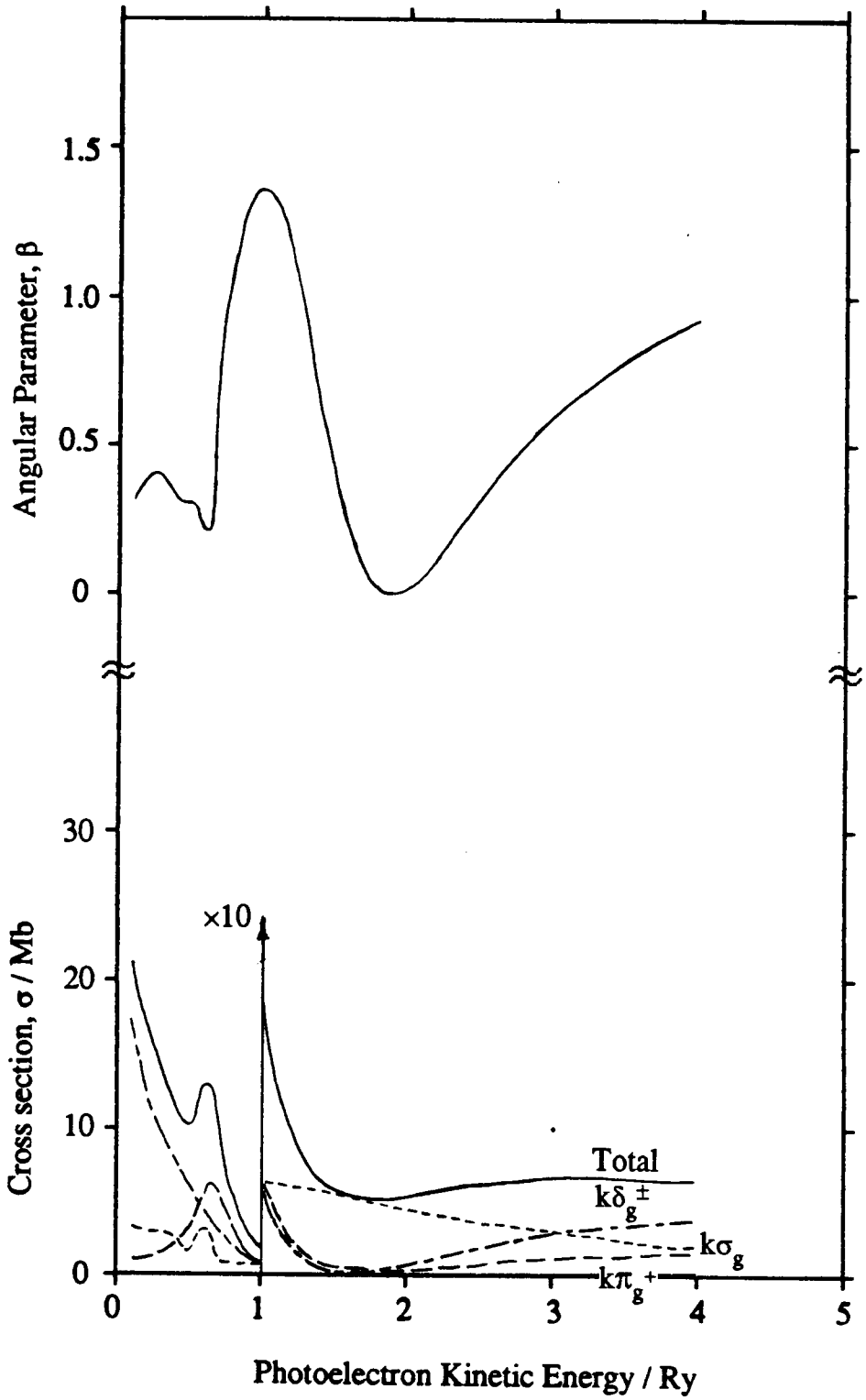

VII-1b. Calculated total and channel cross sections and angular parameter as a function of photoelectron kinetic energy for Cl_2 $1\pi_u$.

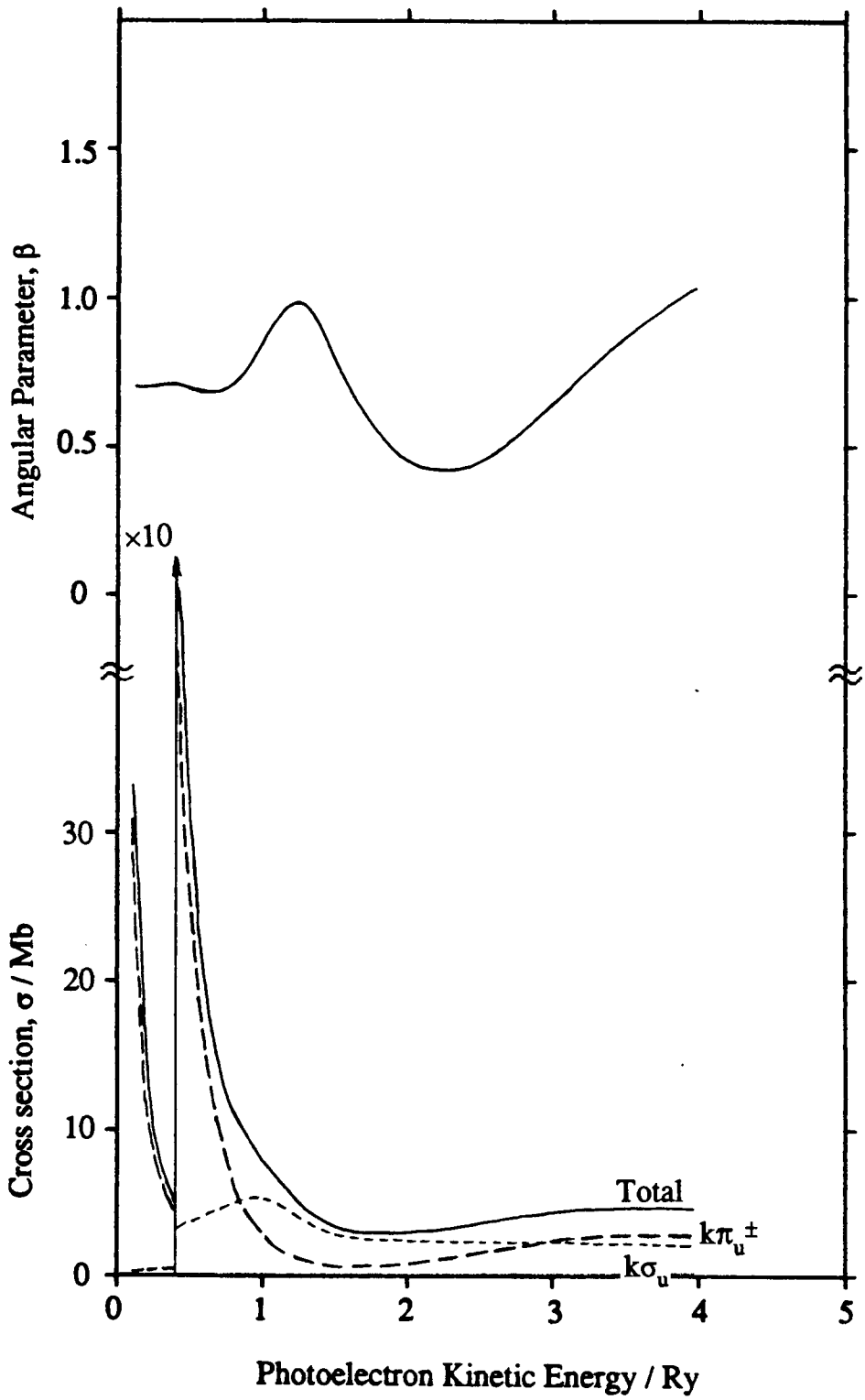

VII-1c. Calculated total and channel cross sections and angular parameter as a function of photoelectron kinetic energy for Cl_2 $2\sigma_g$.

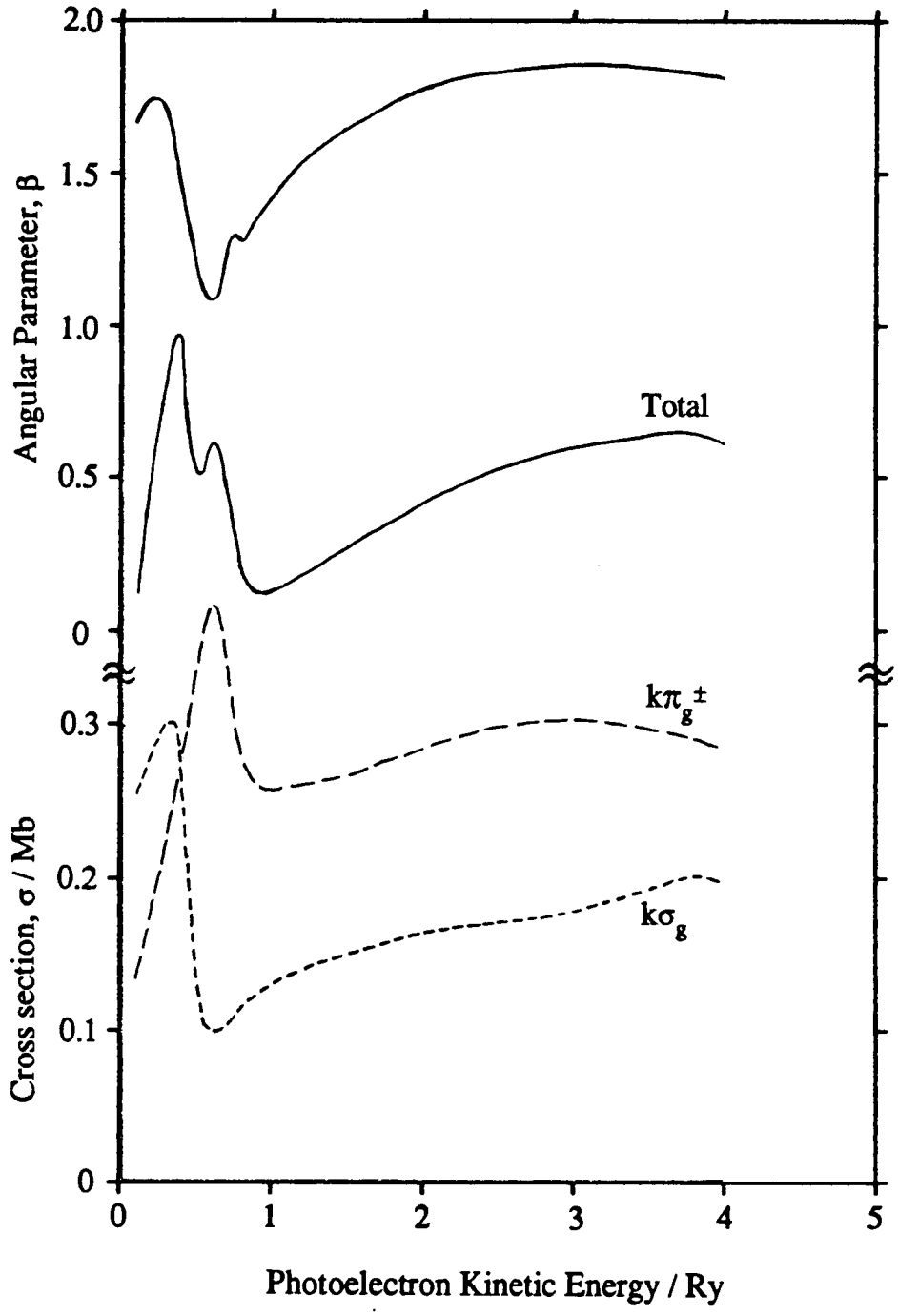

VII-1d. Calculated total and channel cross sections and angular parameter as a function of photoelectron kinetic energy for Cl_2 $1\sigma_u$.

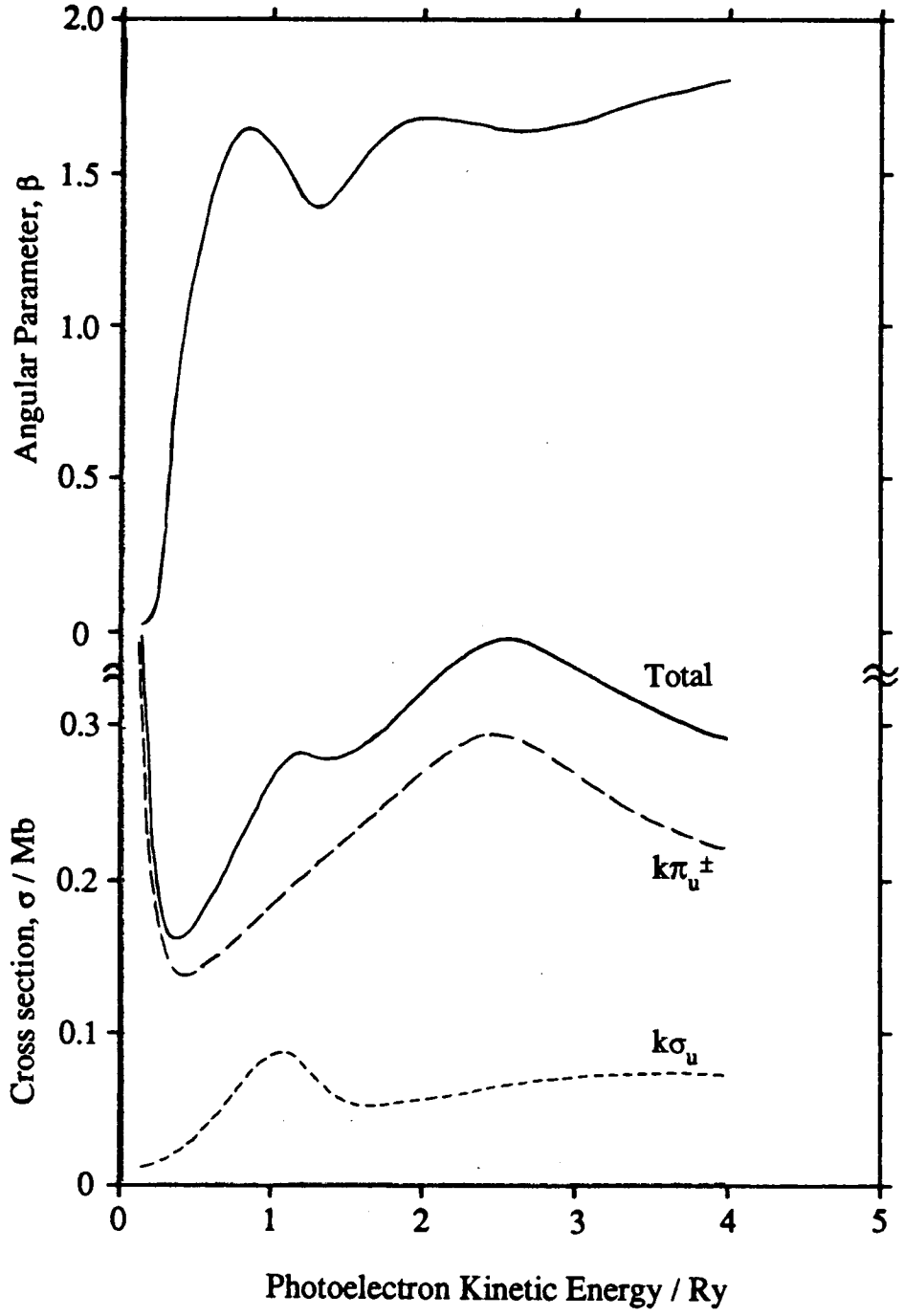

VII-1e. Calculated total and channel cross sections and angular parameter as a function of photoelectron kinetic energy for Cl_2 $1\sigma_g$.

Cl_2 $1\pi_u$ and $1\pi_g$

Cl_2's 3p lone pair orbitals are $1\pi_u$ and $1\pi_g$. The selection rules are

$$1\pi_u^+ \rightarrow k\sigma_g + k\pi_g^+ + k\delta_g^+ + k\delta_g^-, \text{ and} \qquad \text{Eq. VII-1}$$

$$1\pi_g^+ \rightarrow k\sigma_u + k\pi_u^+ + k\delta_u^+ + k\delta_u^-.$$

As seen in the Figures, σ_{tot} shows bumps due to SR not found in the atom's profile, and β is dragged down from the very high values which it achieves in chlorine 3p. Past 1 Ry, the curves are much like the atom's.In $1\pi_u$, the bump in σ_{tot} at about 0.6 Ry is due to an $l = 4$ SR in $k\pi_g$ and an $l = 4, 2$ SR in $k\sigma_g$. $k\pi_g$ and $k\delta_g$ virtually go to zero at the CM at 1.6 Ry.

$1\pi_g$ appears to have only one $l = 3$ SR in the $k\delta_u$ channel which pulls down β from the high values it has in the atom. Comparing the σ_{tot} curve with that for $1\pi_u$, however, turns up a much narrower minimum in $1\pi_g$-- σ_{tot} for $1\pi_g$ falls toward and rises away from the minimum faster than σ_{tot} for $1\pi_u$. $k\sigma_u$ in $1\pi_g$ is seen to have higher values than $k\sigma_g$ in $1\pi_u$ at energies just below the minimum. The $k\sigma_u$ eigenphase sum shows a slight bend at these energies indicating that a small SR is responsible for holding up $k\sigma_u$'s cross section. It also causes the hump in β below 1 Ry. In $1\pi_u$, $k\pi_g$ is at a minimum at 1.7 Ry, and $k\delta_g$ at 1.6 Ry compared to about 1.5 Ry in chlorine 3p. $\beta = 0$ at 1.8 Ry, and β is at a minimum at 1.9 Ry. In $1\pi_g$, $k\pi_u$ is lowest at 1.4 Ry and $k\delta_g$ at 1.6 Ry. $\beta = 0$ at 1.55 Ry (an energy between the two channels' minima), but β is lowest at 1.7 Ry.

[As an aside, let us use our method suggested in Chapter IV for finding the energy of the CM. We find the energy where

$$\beta' = \frac{\beta \text{ (maximum around CM)} + \beta \text{ (minimum around CM)}}{2} \qquad \text{Eq. VII-2}$$

and the energy where β is lowest, and locate the point midway between these energies. This point is a good estimate of the energy of the CM.

For $1\pi_u$, $\beta_{max} \approx 1.4$, $\beta_{min} \approx 0$. $\beta' = 0.7$ at $\varepsilon = 1.35$ Ry, and $\beta_{min} = 0$ at 1.9 Ry. Midway between these energies, $\varepsilon \approx 1.6$ Ry, is near the points where $k\pi_g$ and $k\delta_g$, are at minima. Similar "analysis" for $1\pi_g$ gives $\varepsilon \approx 1.5$ Ry as the location of its CM--between the channel minima.]

$\underline{Cl_2\ 2\sigma_g}$

The $2\sigma_g$ bonding orbital shows a mixture of SR and partial CM. Its selection rule is

$$2\sigma_g^+ \rightarrow k\sigma_u + k\pi_u^+ + k\pi_u^-. \qquad \text{Eq. VII-3}$$

$k\sigma_u$ has an $l = 1$, 5 SR at 1 Ry. At 1.6 Ry, where $k\pi_u$ goes through its minimum, $k\sigma_u$ makes up 80% of σ_{tot}. This latter behavior is much more like that in the atom than HCl's 2σ, where $k\sigma$ and $k\pi$ each are about 50% of σ_{tot} at the CM. This occurs because the major factor behind the partial CM in Cl_2 is the $l = 0$ character introduced by the molecular field into the atomic spheres (which are purely $l = 1$ in the atom). In HCl, this factor combines with the scattering amplitude from the hydrogen sphere--which contributes to different partial waves than does the amplitude from chlorine. In Cl_2, by the symmetry of the molecule, both atoms contribute to the same partial waves without "interference."

In Cl_2 $2\sigma_g$, the $k\sigma_u$ channel cross section near threshold is much smaller relative to $k\pi_u$'s than HCl or chlorine atom's pertinent $k\sigma$ channels'. This causes a narrower traverse in β near threshold, although $k\sigma_u$'s SR makes β wiggle around 1.2 Ry. Past 2.5 Ry, β rises from the CM and achieves values similar to β for chlorine 3p.

Cl_2 $1\sigma_g$ and $1\sigma_u$

Since $1\sigma_g$ and $1\sigma_u$ are primarily formed from the ns orbitals of the constituent halogens, we would do well to remember the ns behavior. It consists of: Cooper minima at or below threshold, cresting cross sections around 2 Ry, and energy independent $\beta = 2$ from the Cooper-Zare formula. Recall also that the chlorine atom's cross section crest is 0.45 Mb which is twice that for bromine and iodine.

Now to the Cl_2 $1\sigma_g$ and $1\sigma_u$. The pertinent selection rules are

$$1\sigma_g \rightarrow k\sigma_u + k\pi_u^+ + k\pi_u^-, \text{ and} \qquad \text{Eq. VII-4}$$

$$1\sigma_u \rightarrow k\sigma_g + k\pi_g^+ + k\pi_g^-.$$

The same pattern we have seen for Cl_2's other orbitals is apparent here: SR within 1 Ry of threshold mar the otherwise-atomic look of σ_{tot} and β. $1\sigma_g$ shows roughly atomic ns behavior: total cross section peaks at 0.36 Mb at about 2.5 Ry (versus 0.45 Mb at 1.6 Ry in chlorine 3s), and β rises rapidly from a low value at threshold to high values (nearly two) within 1 Ry of threshold. As anticipated, SR make their appearances. A little SR in $k\sigma_u$, due to $l = 1$, causes a bump in the total cross section and a downward wiggle in β around 1.1 Ry.

At 0.3 Ry, the total cross section shows a minimum and β rises rapidly, indicating the presence of a CM. Although the $k\pi_u$ channel cross section has a minimum, $k\sigma_u$'s minimum is masked by the SR in that channel at 1.1 Ry. Both channels of $1\sigma_u$ show SR at the energy of the CM, although the atomic 3s$\rightarrow$ kp matrix element changes sign; the CM is masked overall in $1\sigma_u$.

$1\sigma_u$ behaves atomically but for its SR. An $l = 0$ (with small $l = 4$ contribution) SR occurs in $k\sigma_g$ at 0.3 Ry, and an $l = 2$ SR in $k\pi_g$ occurs at 0.6 Ry. Although distinguishable in σ_{tot}, these are broad and close enough to cause wiggles in β. These

are difficult to break down further except to say that β differs from 2 in the region of these SR. The cross section "peak" is past 3 Ry but is now around 0.5 Mb large, up from 0.36 Mb in $1\sigma_g$. We attribute this difference to the differing *l* make up of initial and final states' g and u symmetries in all spheres. $k\sigma_g$ in the spectrum of $1\sigma_u$ holds closer to 1/3 σ_{tot} (the value of kpσ in Cl 3s PI) than $k\sigma_u$ does in $1\sigma_g$.

Bromine Molecule: Br_2

From Appendix III, for Br_2, we see eigenphase sum changes in the same channels as for Cl_2, but at different energies. For Br_2, the bends in the curves are softer than Cl_2's.

Figures VII-2a through VII-2e hold the results for cross section and β for the five outermost orbitals. Table VII-3 contains a summary of the shape resonances found in these orbitals and the partial waves responsible for them.

Br_2 $1\pi_u$ and $1\pi_g$

The effect of SR on Br_2's lone pair orbitals, $1\pi_u$ and $1\pi_g$, is smaller than their effect on Cl_2, as anticipated from Br_2's softer eigenphase sum curves. The β curves for Br_2's lone pairs closely resemble bromine 4p's, except that the lone pairs' β's are pulled down by about 0.2 near threshold.

Although the results seem atomic, the SR which are present are quite similar to those in Cl_2. $1\pi_u$ in Br_2 has SR in its $k\pi_g$ channel at 0.6 Ry due to $l = 4, 2$ and its $k\sigma_g$ channel at 0.4 Ry due to $l = 4$. $1\pi_g$ has a $k\delta_u$ SR at 0.2 Ry and a hard to detect $k\sigma_u$ resonance at about 1.2 Ry which holds σ_{tot} high and alters the β curve as we discussed for Cl_2 $1\pi_g$.

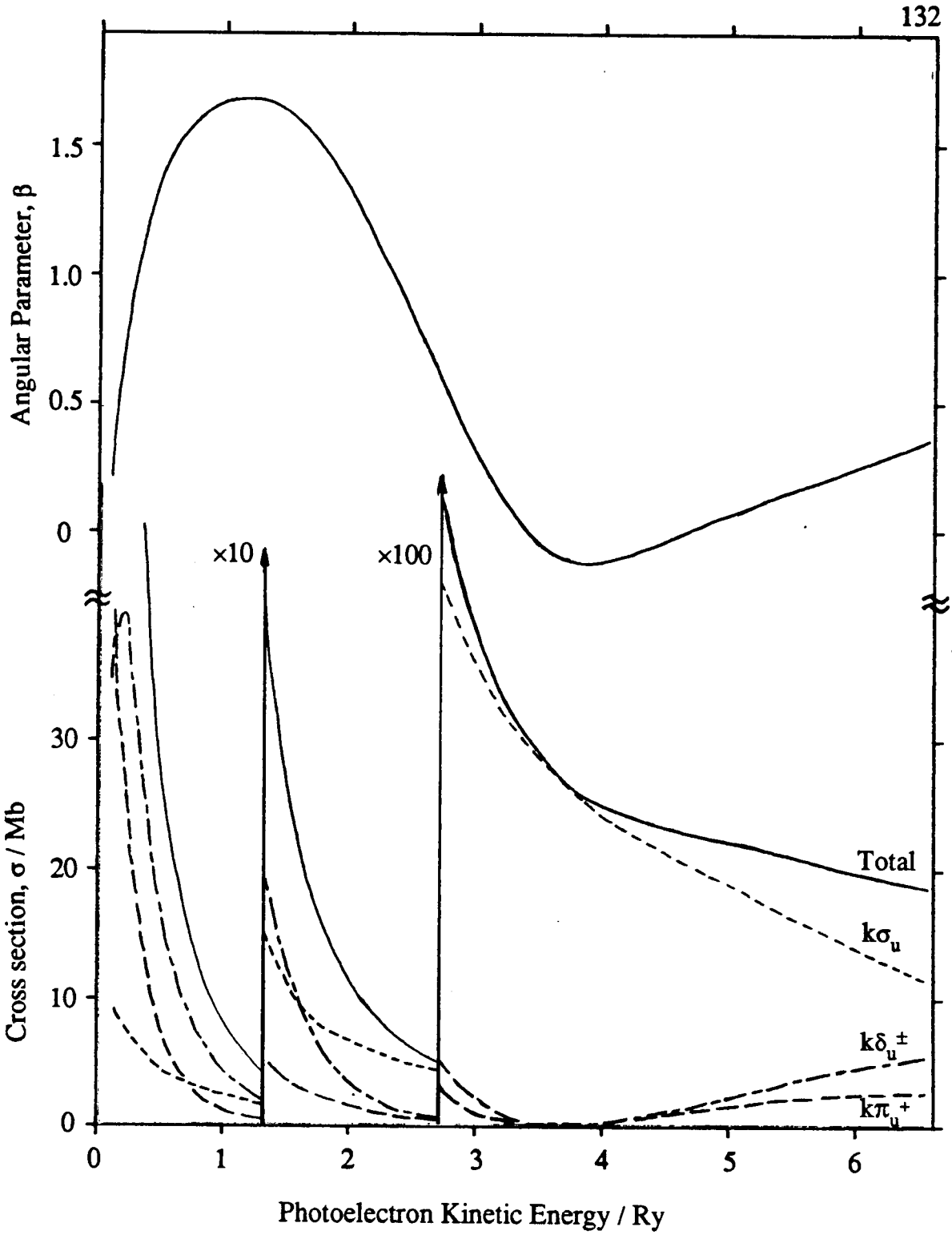

VII-2a. Calculated total and channel cross sections and angular parameter as a function of photoelectron kinetic energy for Br_2 $1\pi_g$.

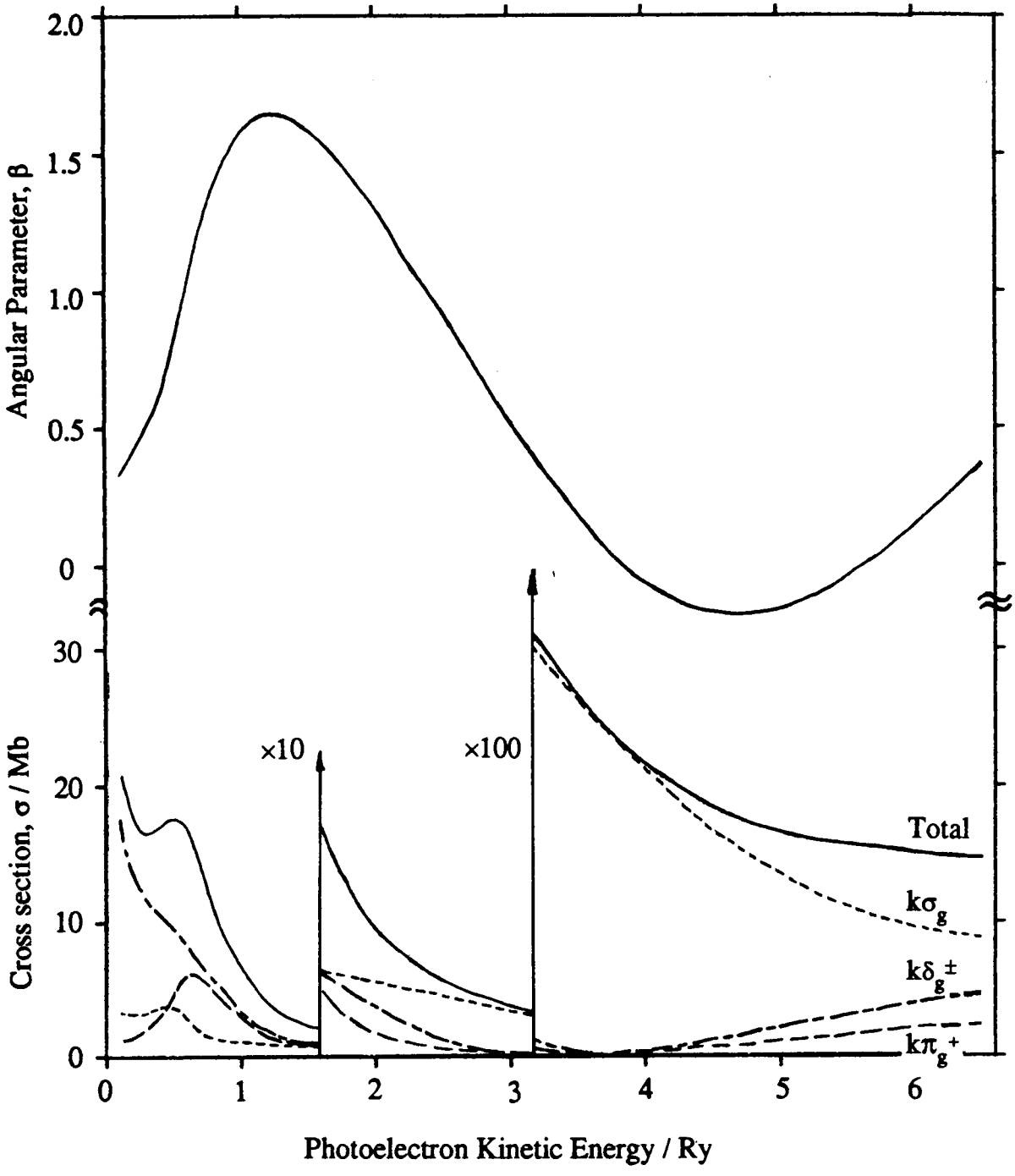

VII-2b. Calculated total and channel cross sections and angular parameter as a function of photoelectron kinetic energy for Br_2 $1\pi_u$.

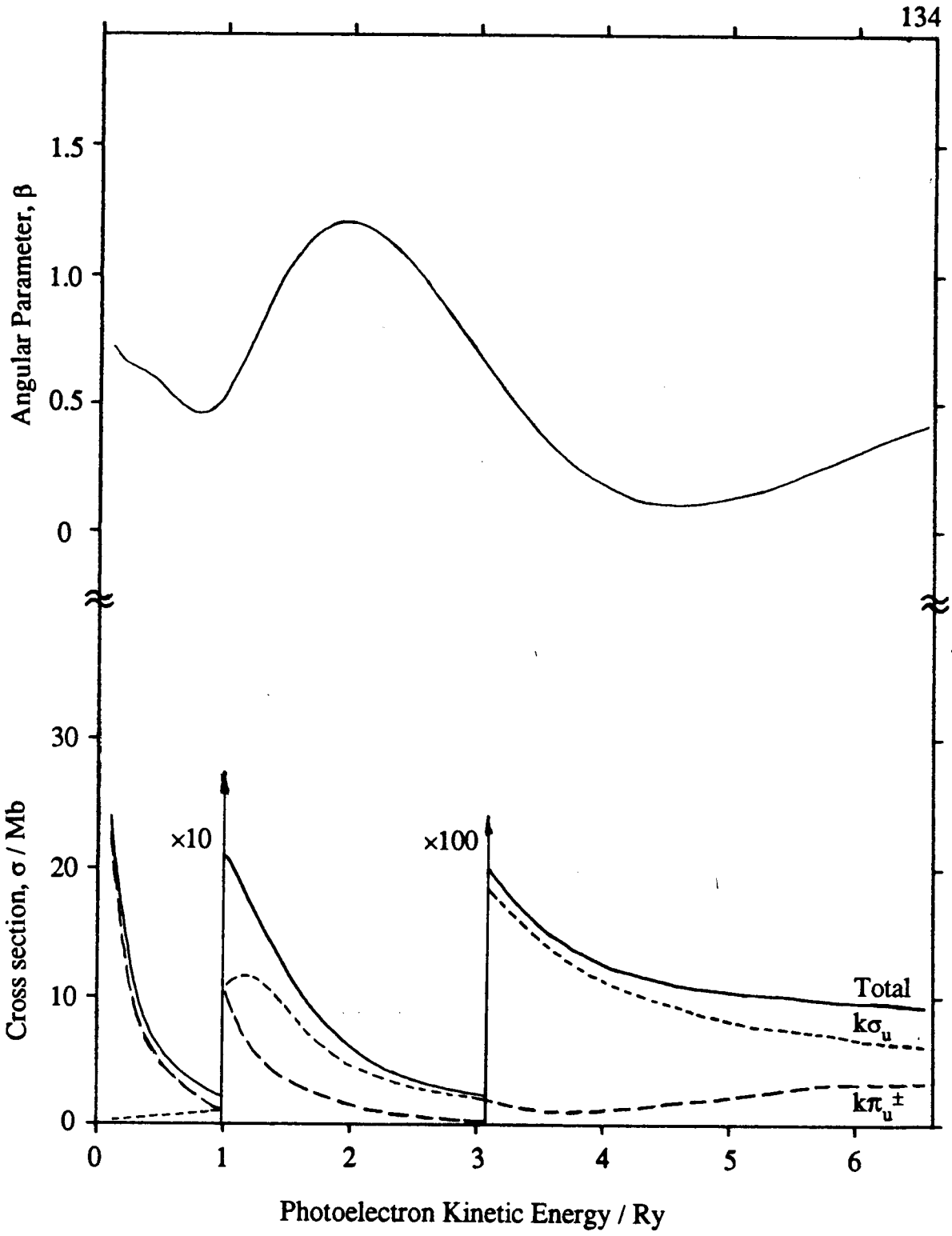

VII-2c. Calculated total and channel cross sections and angular parameter as a function of photoelectron kinetic energy for Br_2 $2\sigma_g$.

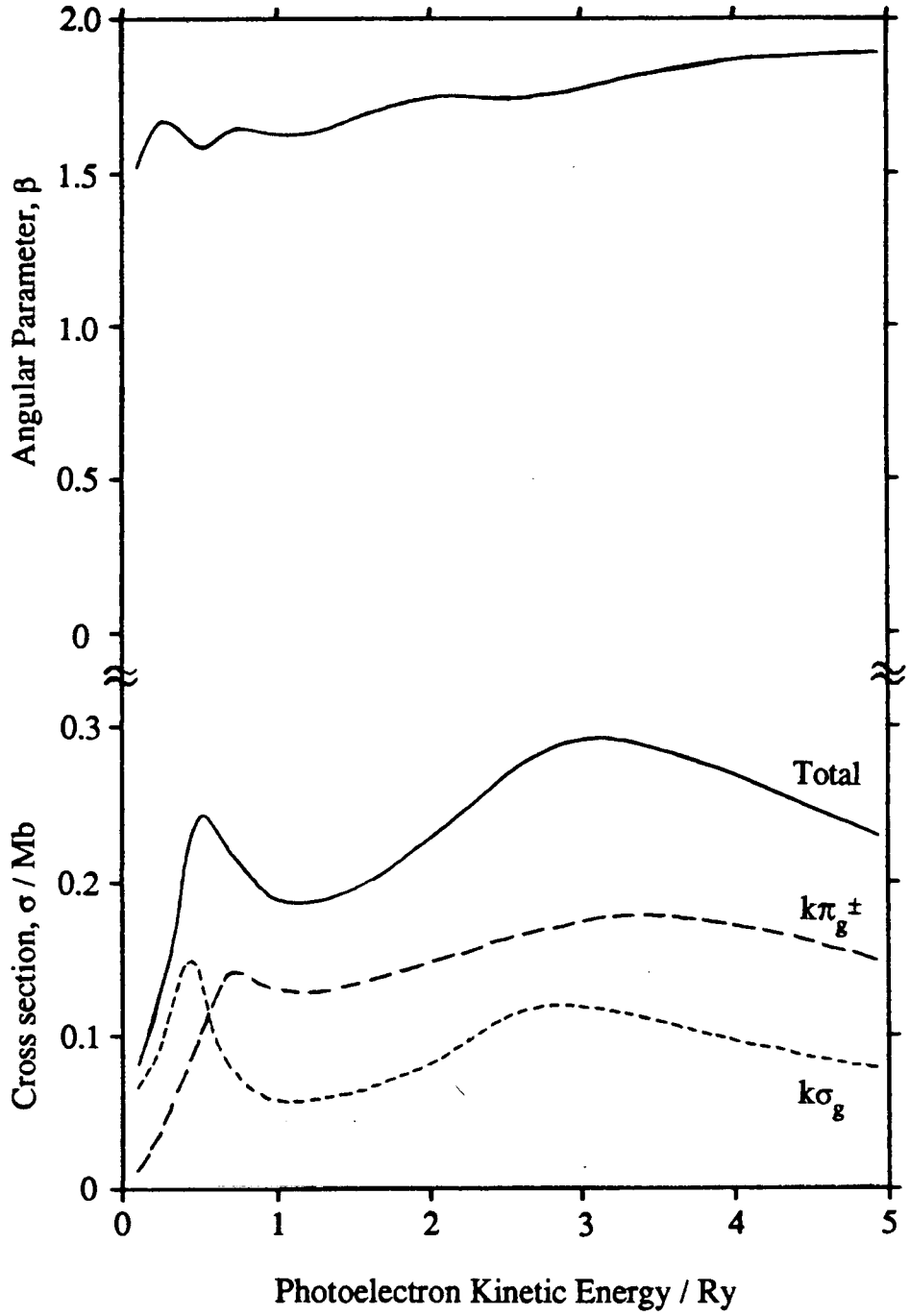

VII-2d. Calculated total and channel cross sections and angular parameter as a function of photoelectron kinetic energy for Br_2 $1\sigma_u$.

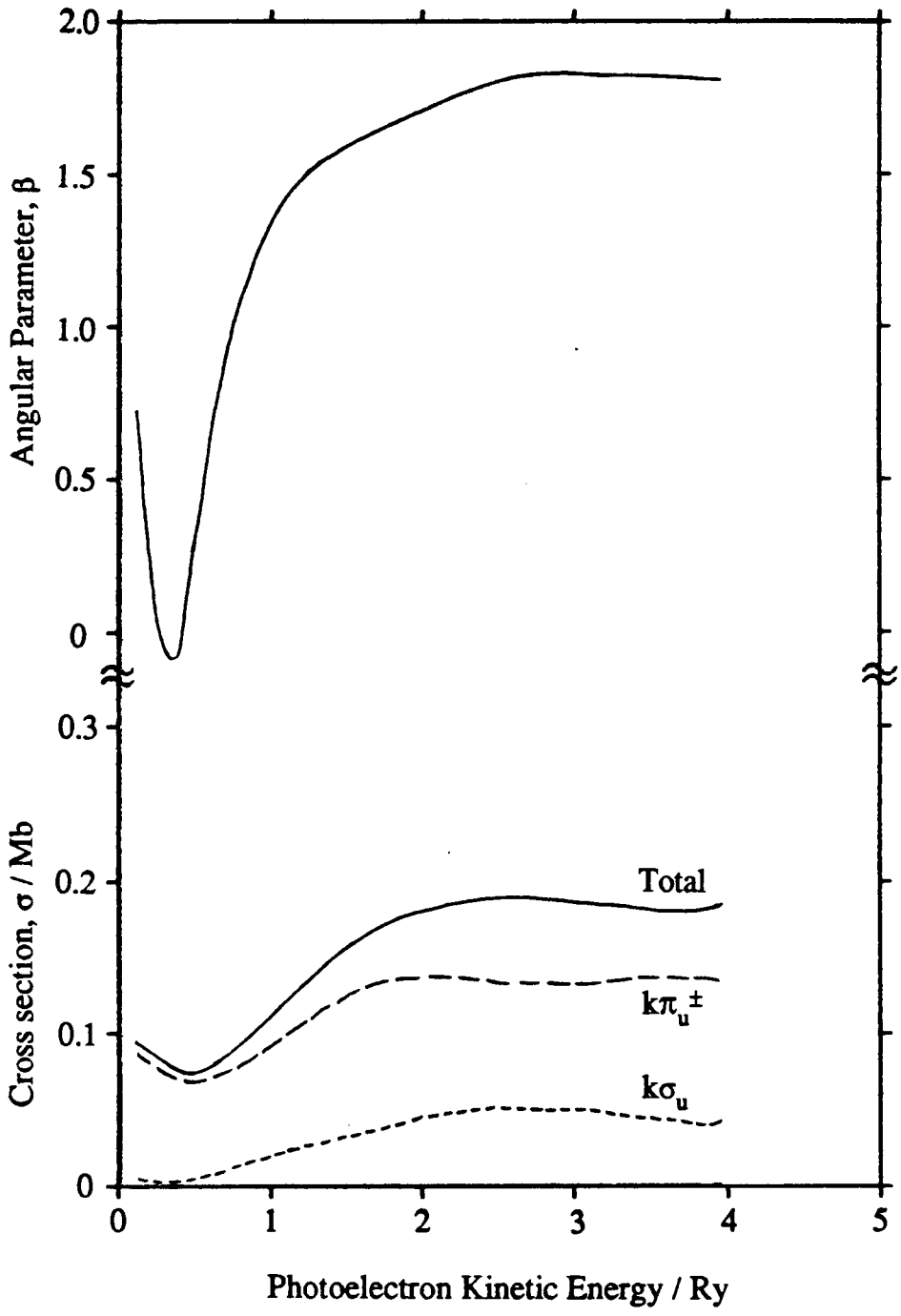

VII-2e. Calculated total and channel cross sections and angular parameter as a function of photoelectron kinetic energy for Br_2 $1\sigma_g$.

Table VII-3. Energy positions in rydbergs of shape resonances in bromine molecule. Numbers in parentheses indicate responsible partial waves. "n" means "no resonance in this channel."

	$k\sigma_g$	$k\pi_g$	$k\delta_g$	$k\sigma_u$	$k\pi_u$	$k\delta_u$
$1\sigma_g$	-.-	-.-	-.-	.n	.n	-.-
$1\sigma_u$	0.45 (0,4,2)	0.75 (2)	-.-	-.-	-.-	-.-
$2\sigma_g$	-.-	-.-	-.-	1.2 (1,5)	.n	-.-
$1\pi_u$	0.4 (4)	0.65 (4,2)	.n	-.-	-.-	-.-
$1\pi_g$	-.-	-.-	-.-	1.2 (?)	.n	0.2 (3)

$\underline{Br_2\ 2\sigma_g}$

Br_2's $2\sigma_g$ bonding orbital displays trends with respect to HBr 2σ and bromine 4p, similar to Cl_2's $2\sigma_g$ with respect to HCl 2σ and chlorine 3p.

The $k\sigma_u$ channel of Br_2 $2\sigma_g$ has an SR at 1.2 Ry due to $l = 1, 5$. In addition, $k\sigma_u$'s small cross section at threshold helps to pull down β from its value of almost two in bromine 4p. At 3.7 Ry where $k\pi_u$ undergoes a CM, $k\sigma_u$ is quite dominant and β dips almost to zero as opposed to HBr's 2σ which only achieves $\beta = 0.86$. Past the CM, cross sections (once occupation numbers have been accounted for) and β for Br_2 $2\sigma_g$ act similarly to bromine 4p.

Br_2 $1\sigma_g$ and $1\sigma_u$

Br_2 $1\sigma_g$ and $1\sigma_u$ behave similarly to their counterparts in Cl_2. $1\sigma_g$ has a CM about 0.3 or 0.4 Ry, $k\sigma_u$ is reduced relative to 1/3 σ_{tot} (the value of $kp\sigma$ in bromine 4s PI), and σ_{tot} reaches a peak of 0.19 Mb past 2.5 Ry compared to 0.21 Mb at 1.7 Ry in bromine atom. $k\sigma_u$ channel lacks a distinct SR which was present in Cl_2; as we have noted, the eigenphase sum curves are softer here meaning less pronounced SR.

$1\sigma_u$'s channels, $k\sigma_g$ and $k\pi_g$, show SR near threshold at 0.4 Ry due to $l = 0$, 4 and 0.8 Ry, due to $l = 2$ respectively. These are close enough and broad enough to show up as only one peak at 0.5 Ry in σ_{tot}. β wiggles in this energy range, but ranges mostly without mishap from 1.6 near threshold up towards 2.0 at higher energies. Again the peak in $1\sigma_u$'s σ_{tot} is past 3 Ry and is about 0.30 Mb high. This is about one and a half times the peak in $1\sigma_g$.

Iodine Molecule: I_2

The graphs of channel eigenphase sums in Appendix III show sharp and frequent resonances above threshold. $k\sigma_g$, $k\sigma_u$, and $k\pi_g$ have two resonances each. The potential is deep enough that $l = 4$ in the outer and $l = 3$ in the atomic spheres can have resonances.

The results for the outermost five orbitals are presented in Figures VII-3a through VII-3e. Table VII-4 contains a summary of the shape resonances found in these orbitals and the partial waves responsible for them.

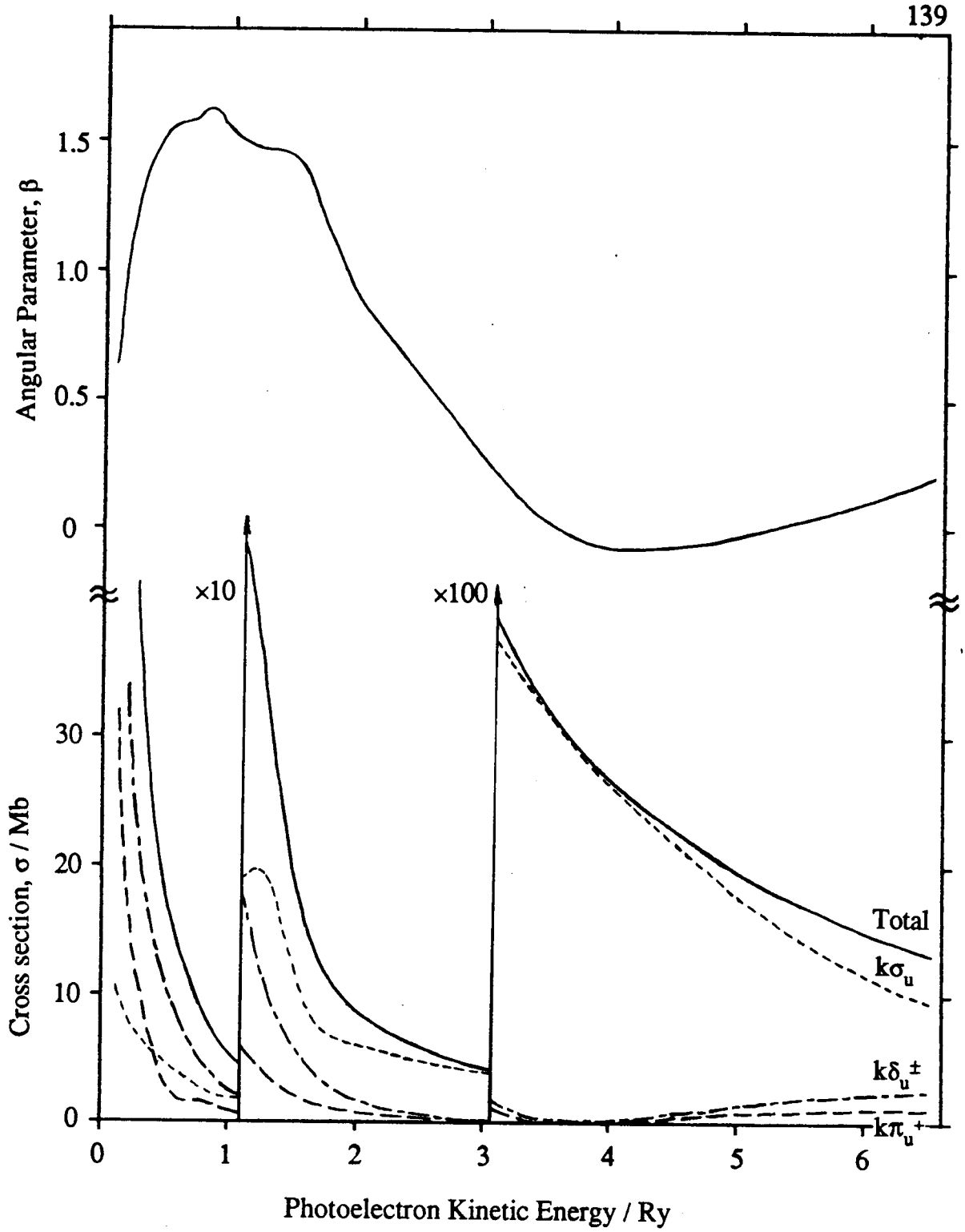

VII-3a. Calculated total and channel cross sections and angular parameter as a function of photoelectron kinetic energy for I_2 $1\pi_g$.

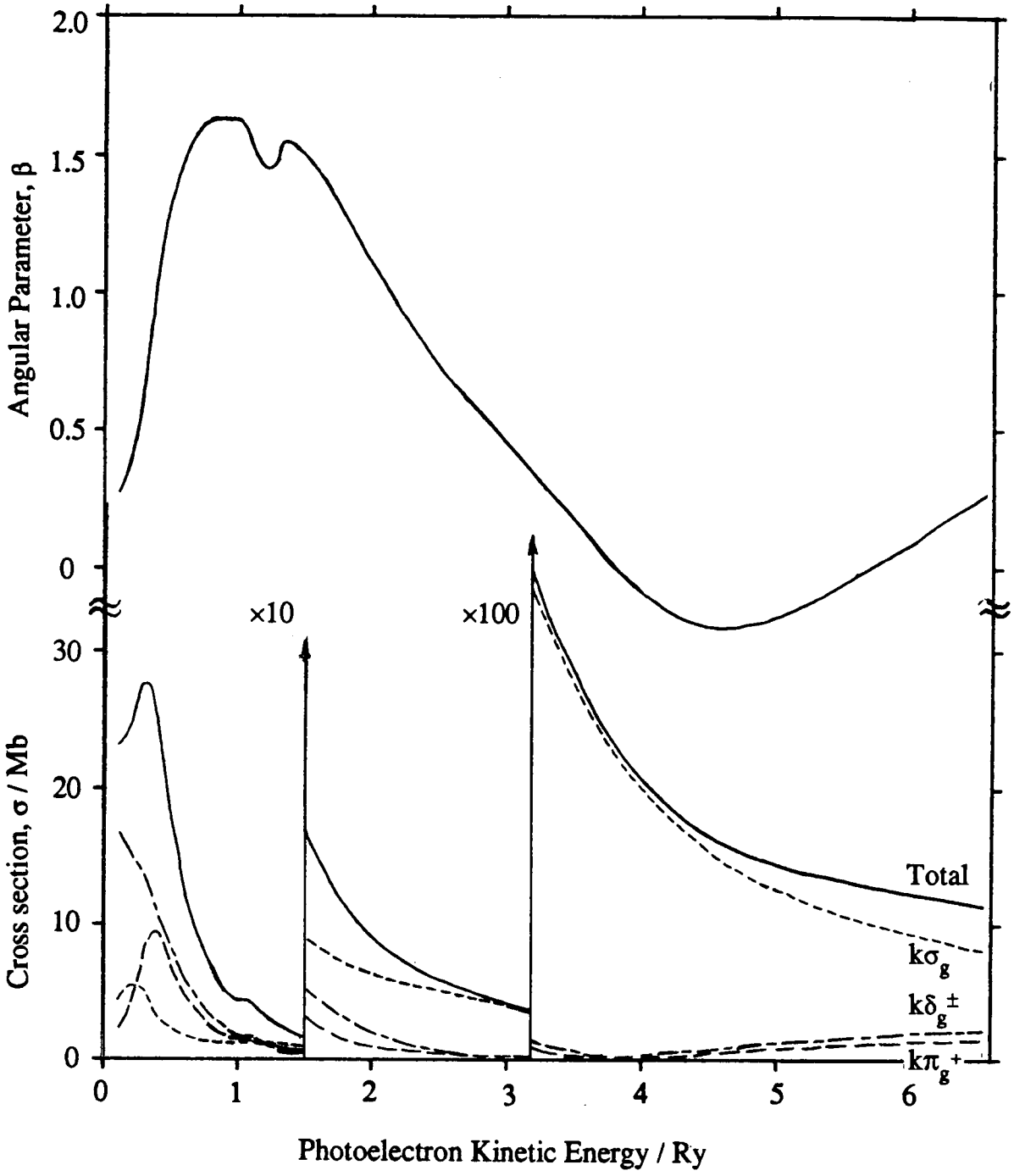

VII-3b. Calculated total and channel cross sections and angular parameter as a function of photoelectron kinetic energy for I_2 $1\pi_u$.

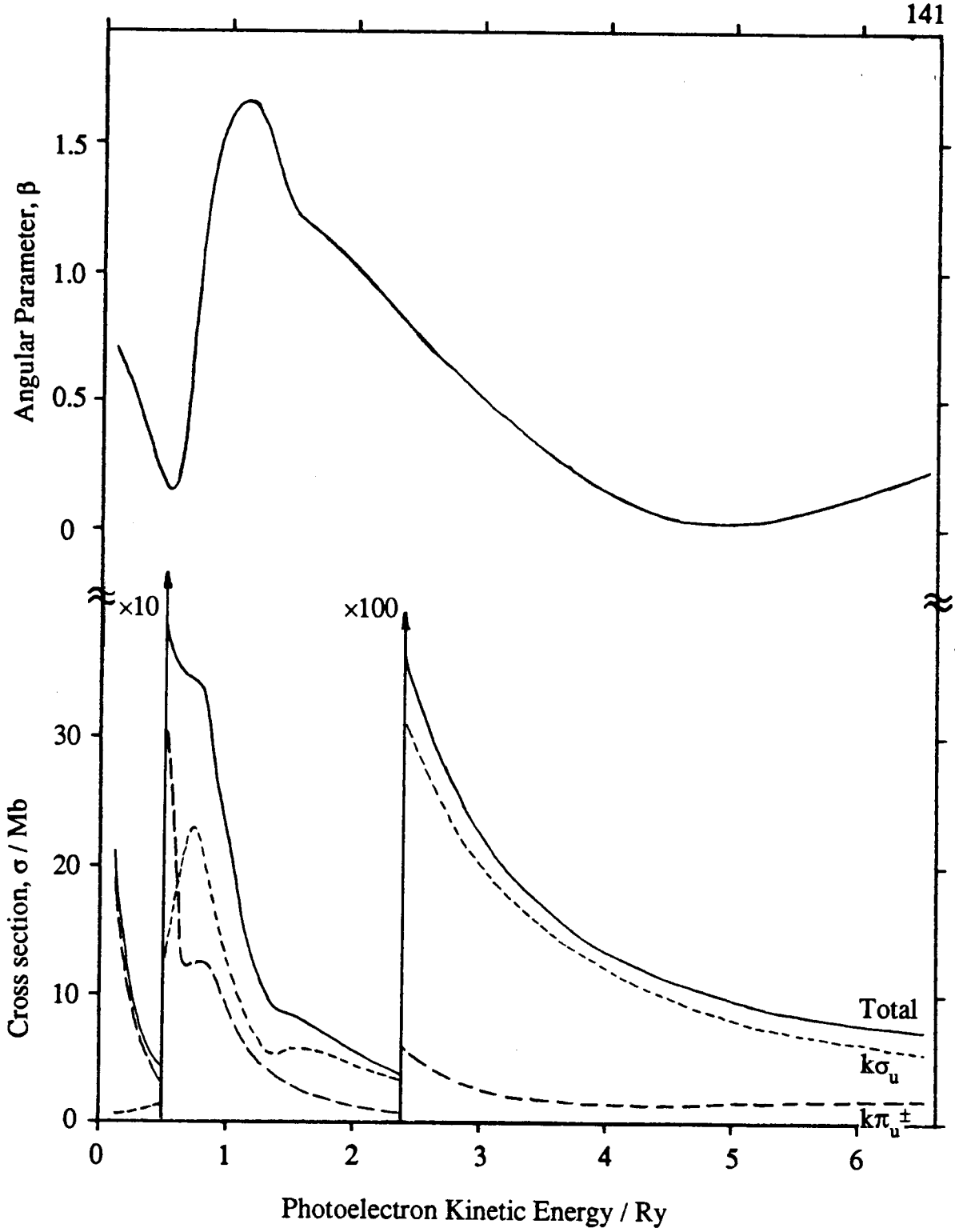

VII-3c. Calculated total and channel cross sections and angular parameter as a function of photoelectron kinetic energy for I_2 $2\sigma_g$.

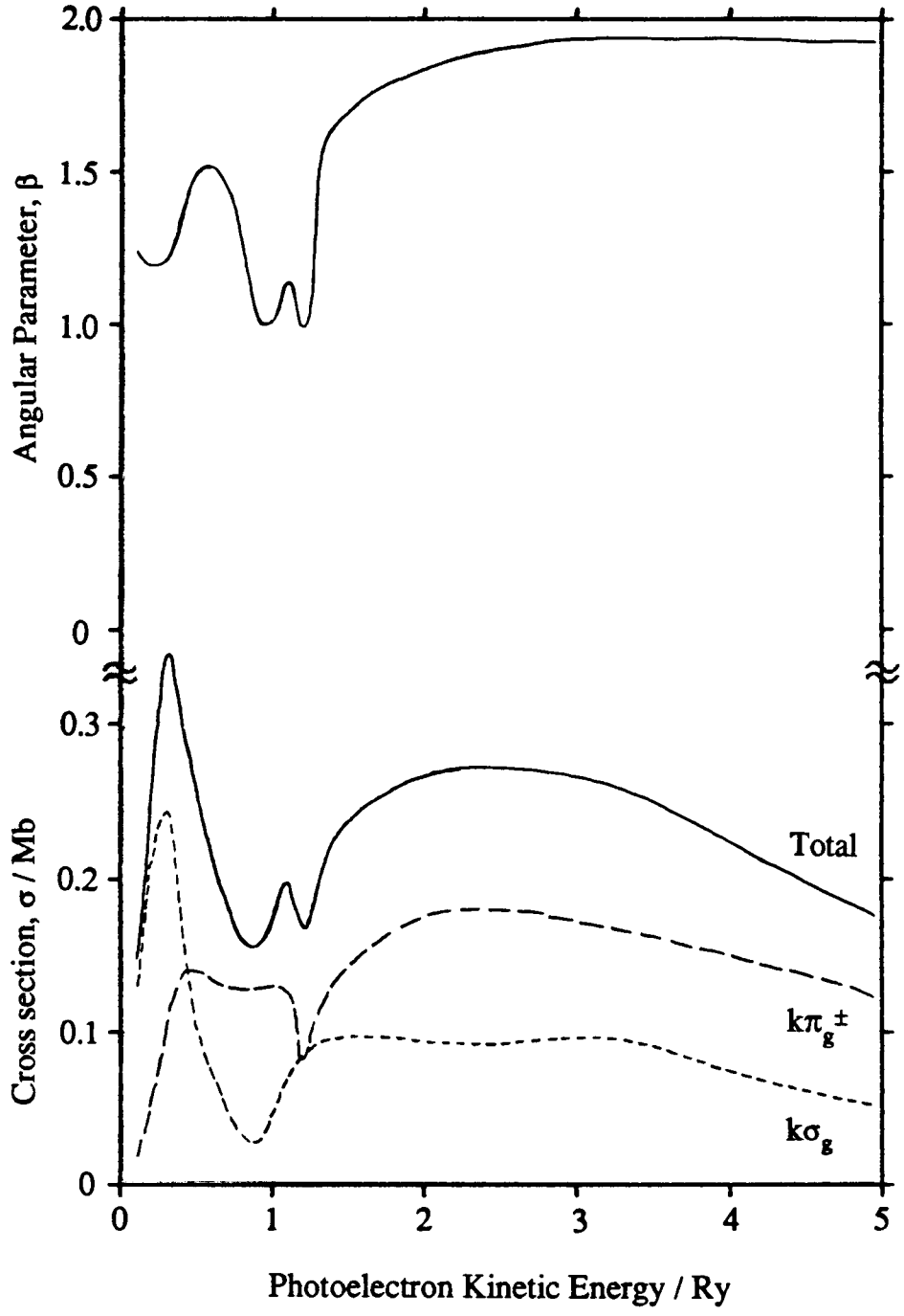

VII-3d. Calculated total and channel cross sections and angular parameter as a function of photoelectron kinetic energy for I_2 $1\sigma_u$.

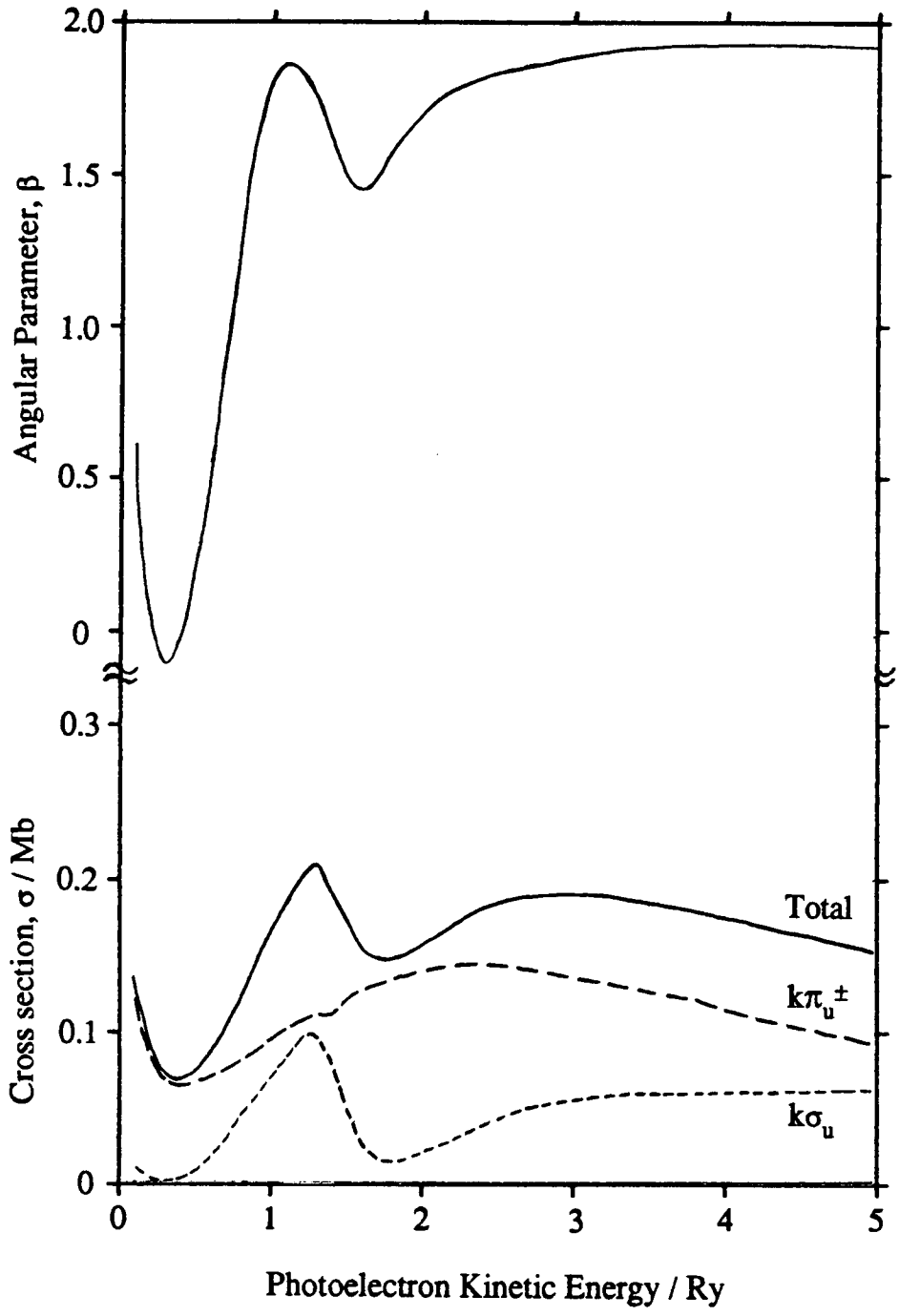

VII-3e. Calculated total and channel cross sections and angular parameter as a function of photoelectron kinetic energy for I_2 $1\sigma_g$.

Table VII-4. Energy positions in rydbergs of shape resonances in iodine molecule. Numbers in parentheses indicate responsible partial waves. "n" means "no resonance in this channel."

	$k\sigma_g$	$k\pi_g$	$k\delta_g$	$k\sigma_u$	$k\pi_u$	$k\delta_u$
$1\sigma_g$	-.-	-.-	-.-	1.25 (1,5)	.n	-.-
$1\sigma_u$	0.3 (4,0)	0.45, 1.2 (2,4), (?)	-.-	-.-	-.-	-.-
$2\sigma_g$	-.-	-.-	-.-	0.75, 1.6 (1,3,5), (1,3)	0.8 (3)	-.-
$1\pi_u$	0.2 (4)	0.4, 1.1 (4,2), (2,6)	.n	-.-	-.-	-.-
$1\pi_g$	-.-	-.-	-.-	1.2 (5)	.n	0.0 (3)

I_2 $1\pi_u$ and $1\pi_g$

As with Br_2, the I_2 lone pairs, $1\pi_u$ and $1\pi_g$, show β curves like iodine 5p's and σ_{tot} curves which are enhanced due to SR near threshold and which decrease monotonically past about 1 Ry. As with Br_2, the CM is masked by a rapidly falling $k\sigma_g$ or $k\sigma_u$ channel cross section.

In I_2's $1\pi_u$, the $k\pi_g$ channel displays an SR at 0.4 Ry due to $l = 4, 2$ and another at 1.1 Ry due to $l = 2, 6$. $k\sigma_g$ shows an SR at 0.2 Ry due to $l = 4$. There is a rise in $k\pi_g$'s cross section due to a $l = 4, 2$ SR at 1.1 Ry. This feature causes a dip in β.

In $1\pi_g$'s cross sections, we see that the $k\sigma_u$ SR at 1.2 Ry due to $l = 5$ has finally expressed itself in I_2. (It was distinguishable in Cl_2 and Br_2 not as a peak but only as a higher than expected channel cross section.) $k\pi_u$ shows a tiny SR at 0.8 Ry.

$\underline{I_2\ 2\sigma_g}$

I_2's bonding orbital, $2\sigma_g$, past 1.8 Ry acts more like its constituent atoms' np orbitals than do the $2\sigma_g$ in either Cl_2 or Br_2. SR in $k\sigma_u$ at 0.7 Ry due to $l = 1, 5$ and in $k\pi_u$ at 0.7 Ry due to $l = 3$ are responsible for the bump in σ_{tot} and for pulling down β from two near threshold. Another SR in $k\sigma_u$ at 1.6 Ry is due to $l = 1, 3$ and causes a small depression in the decreasing β curve. β reaches almost zero near the CM caused by $k\pi_u$'s minimum at 4.3 Ry.

$\underline{I_2\ 1\sigma_g \text{ and } 1\sigma_u}$

The 5s orbitals of I_2, $1\sigma_g$ and $1\sigma_u$, follow the pattern of Cl_2 3s and Br_2 4s orbitals. The CM in $1\sigma_g$ is now in the continuum at 0.4 Ry, $k\sigma_u$ has a large $l = 1, 5$ SR at 1.2 Ry, and σ_{tot} reaches a peak of 0.19 Mb at 3 Ry. β dips sharply at the CM and again less dramatically near the SR in $k\sigma_u$. At high energies, β tends towards two.

$1\sigma_u$'s channels, $k\sigma_g$ and $k\pi_g$, show SR due to $l = 4, 0$ at 0.3 Ry and due to $l = 2, 4$ at around 0.5 Ry, respectively. These two SR show up as only one peak in σ_{tot} which displays the normal humped ns behavior past 1 Ry. β is more strongly affected by the SR here than in Br_2, dipping to 1.0 around 1 Ry. β also tends towards two rather rapidly past 2 Ry.

The $k\pi_g$ feature at 1.2 Ry is related to the one we found in the $1\pi_u$ orbital of I_2 at 1.1 Ry. Examination of the eigenphase sums and comparison with other X_2

molecules make us wonder whether this is real or an artifact of our method--due to an unknown glitch. It has no counterpart in other X_2 molecules, and the change in the eigenphase sum which underlies it is sharper than any other feature in all the other channels' eigenphase sums. We would not normally be so suspicious of a spectral feature, except that it is manifested as a cross section decrease in the $k\pi_g$ channel.

Summary

Again, the molecular channels closely follow the atomic channels; $k\sigma$ is recognizable as ks, $k\pi$ as kp, and $k\delta$ as kd. The g and u labels do not affect the overall trends of behavior. The features of these molecules' orbitals can be explained in terms of atomic CM and molecular SR. In all the orbitals, the SR lie near threshold and enhance σ_{tot} compared to the atom, but lower β's value. Past about 2 Ry, these orbitals show normal behavior with respect to the atomic CM, or, in the case of the bonding orbitals, behavior appropriate for partial CM (narrowing of β's traverse, shallower σ_{tot} minima). $2\sigma_g$, $1\pi_u$, and $1\pi_g$ in Cl_2 (like 2σ and 1π in HCl) have minima in σ_{tot} which are washed out in the corresponding orbitals of Br_2 and I_2 (and HBr and HI).

Comparison with Experimental Results

Of the dihalogens, only Cl_2 has been studied by PED techniques. (P. Dowben[89] has performed absorbed molecule experiments on Br_2, but because these are systems of fixed orientation, comparison with our results will be complicated.) Carlson, et. al.,[20] have found cross sections and angular parameters for the first three bands ($1\pi_g$, $1\pi_u$, and $2\sigma_g$) of Cl_2. As with the hydrogen halides, the qualitative agreement of experiment and theory is quite good. The experimental cross sections all show

minima, and the $2\sigma_g$'s is the shallowest. The resonance in $1\pi_u$ near 0.6 Ry seems to be confirmed by the experiment, although the appearance of a cross section maximum depends on the value of only one experimental point. The energy placement of CM is different (higher in the theory), but the overall β curves display surprisingly consistent relative behavior between the orbitals. In both experiment and theory, the lowest dip in β belongs to $1\pi_g$, the highest to $2\sigma_g$. Below the energy of the minimum, the $1\pi_u$, reaches the highest values followed by $1\pi_g$ then $2\sigma_g$. At energies past about 3 Ry the β curves of the three orbitals merge in the manner of our results (as well as experimental points with scatter can merge). Thiel[59] shows that his analysis can predict the qualitative relative behavior of β around the CM for the first three bands of Cl_2.

CHAPTER VIII

SUMMARY

In the preceding chapters, we have presented a survey of MSXα calculations of energy dependent cross sections and angular parameters for the valence orbitals of some small halogen containing molecules. Special attention has been paid to the presence and behavior of Cooper minima and shape resonances.

An outstanding result of this work is that the analysis of the energy dependence of the photoelectron dynamics (PED) parameters, σ_{tot} and β, allows a distinction between bonding and nonbonding molecular orbitals. These molecular PED parameters show energy dependent features which may be discussed in terms of properties of the molecule's constituent atoms, and properties due to the formation of the molecular potential. Atomic behavior is plainly discernable in the nonbonding or lone pair orbitals, whereas bonding orbitals display different behavior due to their "multi-atomic" composition. Shape resonances result from the spatial extent of the molecular potential and modify the PED parameters' behavior in both bonding and nonbonding orbitals.

Our calculational method is based on a nonrelativistic, independent particle theory, and thus ignores the spin-orbit splitting of energy levels and electron correlation effects such as autoionization. Because of this, our method should not be expected to adequately treat situations in which these effects are important.

It would be a poor model, indeed, which did not find Cooper minima in molecules (one, for instance, which excluded the possibility for matrix elements to change sign). Nevertheless, considering the complexities of the description of the angular distribution of photoelectrons and the rapidity with which valence orbitals' matrix elements change with photon energy, the MSXα method has performed well in predicting the trends of the PED parameters within and among the molecules and orbitals presented.

Molecules consisting of atoms from the second, third, and fourth periods, as well as nonlinear polyatomics, and core orbitals,[90] may be treated reliably by our method. Calculations for CCl_4[19] and $SiCl_4$[25] have been completed and show the same agreement with experiment as those presented herein.

LIST OF REFERENCES

LIST OF REFERENCES

1. J.W. Davenport, Ph. D. Dissertation, The University of Pennsylvania, Philadelphia, Pennsylvania, 1976.

2. D. Dill and J.L. Dehmer, J. Chem. Phys., **61**(2), 692 (1974).

3. J.L. Dehmer and D. Dill in "Electron-Molecule and Photon-Molecule Collisions," edited by T. Rescigno, V. McKoy, and B. Schneider, Plenum Press, New York, 1979, p. 225.

4. K.H. Johnson in "Advances in Quantum Chemistry," **7**, edited by P.O. Löwdin, Academic Press, New York, 1973, p.143.

5. J.C. Slater, "The Self-Consistent Field for Molecules and Solids," Quantum Theory of Molecules and Solids, vol. 4, McGraw-Hill, New York, 1974.

6. K.H. Johnson, Ann. Rev. Phys. Chem., **26**, 2598 (1975).

7. D.A. Case, Ann. Rev. Phys. Chem., **33**, 151 (1982).

8. F.A. Grimm, T.A. Carlson, W.B. Dress, P. Agron, J.O. Thomson, and J.W. Davenport, J. Chem. Phys., **72**(5), 3041 (1980).

9. J.W. Cooper, Phys. Rev., **128**(2), 681 (1962).

10. T.A. Carlson, "Photoelectron and Auger Spectroscopy," Plenum Press, New York, 1975. M.O. Krause in "Synchrotron Radiation Research," edited by H. Winick and S. Doniach, Plenum Press, New York, 1980, p. 101.

11. A.F. Starace in "Handbuch der Physik," vol. XXXI, edited by W. Mehlhorn, Springer Verlag, Berlin, 1982, p. 1.

12. S.T. Manson, Adv. Electron Electron. Phys., **41** (1976).

13. S.T. Manson, Adv. Electron Electron. Phys., **44** (1977).

14. H. Bock and P.D. Mollere, J. Chem. Ed., **51**(8), 506 (1974).

15. U. Fano and J.W. Cooper, Rev. Mod. Phys., **40**(3), 441 (1968).

16. M. Roche, D.R. Salahub, and R.P. Messmer, J. Electron Spectrosc. Relat. Phenom., **19** (1980).

17. S. Katsumata, K. Mitani, and H. Shiromaru, Chem. Phys. Lett., **75**, 196 (1980).

18. T.A. Carlson, M.O. Krause, and F.A. Grimm, J. Chem. Phys., **77**(4), 1701 (1982).

19. T.A. Carlson, M.O. Krause, F.A. Grimm, P. Keller, and J.W. Taylor, J. Chem. Phys., **77**(11), 5340 (1982).

20. T.A. Carlson, M.O. Krause, F.A. Grimm, and T.A. Whitley, J. Chem. Phys., **78**(2), 638 (1983).

21. T.A. Carlson, M.O. Krause, F.A. Grimm, J.D. Allen, Jr., D. Mehaffy, P.R. Keller, and J.W. Taylor, J. Chem. Phys., **75**(7), 3288 (1981).

22. T.A. Carlson, M.O. Krause, A. Fahlman, P.R. Keller, J.W. Taylor, T. Whitley, F.A. Grimm, J. Chem. Phys., **79**(5), 2157 (1983).

23. T.A. Carlson, A. Fahlman, M.O. Krause, T.A. Whitley, and F.A. Grimm, J. Chem. Phys., **81**(12), 5389 (1984).

24. T.A. Carlson, A. Fahlman, M.O. Krause, P.R. Keller, J.W. Taylor, T. Whitley, and F.A. Grimm, J. Chem. Phys., **80**(8), 3521 (1984).

25. T.A. Carlson, M.O. Krause, W.A. Svensson, J.W. Taylor, F.A. Grimm, T.A. Whitley, unpublished results.

26. T.A. Carlson, M.O. Krause, W.A. Svensson, unpublished results.

27. T.A. Carlson, unpublished results.

28. T.A. Carlson, M.O. Krause, J.W. Taylor, P.R. Keller, M.N. Piancastelli, F.A. Grimm, and T.A. Whitley, IEEE Trans. Nuc. Sci., **NS-30**(2), 1034 (1983).

29. J.H.D. Eland, "Photoelectron Spectroscopy: an Introduction to Ultraviolet Photoelectron Spectroscopy in the Gas Phase," 2nd ed., Butterworths, London, 1984.

30. C.S. Johnson, Jr. and L.G. Pederson, "Problems and Solutions in Quantum Chemistry and Physics," Addison-Wesley, Reading, 1977.

31. E.P. Wigner, "Group Theory and its Application to the Quantum Mechanics of Atomic Spectra," Academic, New York, 1959.

32. J.R. Taylor, "Scattering Theory: The Quantum Theory of Nonrelativistic Collisions," Wiley, New York, 1972.

33. A. Messiah, "Quantum Mechanics," Wiley, New York, 1966.

34. P.G. Burke, "Potential Scattering in Atomic Physics," Plenum Press, New York, 1977.

35. C.N. Yang, Phys. Rev., **74**(7), 764 (1948).

36. J.A.R. Samson and A.F. Starace, J. Phys. B, **8**(11), 1806 (1975).

37. M.E. Rose, "Elementary Theory of Angular Momentum," Wiley, New York, 1957.

38. D. Dill and U. Fano, Phys. Rev. Lett., **29**(18), 1203 (1972).

39. U. Fano and D. Dill, Phys. Rev. A, **6**(1), 185 (1972).

40. D.R. Salahub, S.H. Lamson, R.P. Messmer, Chem. Phys. Lett., **85**(4), 430 (1982).

41. W. Kohn and L.J. Sham, Phys. Rev., **140**, A1133 (1965).

42. R. Gaspar, Acta Phys. Acad. Sci. Hung., **3**, 263 (1954).

43. K. Schwarz, Phys. Rev. B, **5**(7), 2466 (1972).

44. J.W.D. Connolly in "Semiempirical Methods of Electronic Structure Calculation, Part A: Technique," edited by G.A. Segal, Plenum Press, New York, 1977, p. 105.

45. S. Wallace, Ph.D. Dissertation, Boston University, Boston, Massachusetts, 1980.

46. E. Butkov, "Mathematical Physics," Addison-Wesley, Reading, 1968.

47. L. Noodleman, J. Chem. Phys., **64**(6), 2343 (1976).

48. J.L. Dehmer and D. Dill, Phys. Rev. Lett., **35**(4), 213 (1975).

49. J.L. Dehmer and D. Dill, J. Chem. Phys., **65**(12), 5327 (1976).

50. J. Macek, Phys. Rev. A, **2**(3), 1101 (1970).

51. D. Loomba, S. Wallace, D. Dill, and J.L. Dehmer, J. Chem. Phys., **75**(9), 4546 (1981).

52. H.A. Bethe and E.E. Salpeter, "Quantum Mechanics of One- and Two-Electron Atoms," Springer Verlag, Berlin, 1957.

53. A. Msezane and S.T. Manson, Phys. Rev. Lett., **35**(6), 364 (1975).

54. A. Msezane and S.T. Manson, Phys. Rev. Lett., **48**(7), 473 (1982).

55. J. Lahiri and S.T. Manson, Phys. Rev. Lett., **48**(9), 614 (1982).

56. D.J. Kennedy and S.T. Manson, Phys. Rev. A, **5**(1), 227 (1972).

57. S.T. Manson, J. Electron Spectrosc. Relat. Phenom., **1**(5), 413 (1973).

58. J. Cooper and R.N. Zare, J. Chem. Phys., **48**, 942 (1968).

59. W. Thiel, J.Electron Spectrosc. Relat. Phenom., **34**, 399 (1984).

60. R.G. Houlgate, J.B. West, K. Coding, and G.V. Marr, J. Phys. B, **7**(17), L470 (1974).

61. D.L. Miller, J.D. Dow, R.G. Houlgate, G.V. Marr, and J.B. West, J. Phys. B, **10**(16), 3205 (1977).

62. M.O. Krause, T.A. Carlson, and P.R. Woodruff, Phys. Rev. A, **24**(3), 1374 (1981).

63. W. Ong and S.T. Manson, Phys. Rev. A, **21**(3), 842 (1980).

64. K.N. Huang, W.R. Johnson, K.T. Cheng, At. Data Nucl. Data Tables, **26**, 33 (1981).

65. S.T. Manson and J.W. Cooper, Phys. Rev., **165**(1), 165 (1968).

66. W. Thiel, J. Electron Spectroc. Relat. Phenom., **31**, 151 (1983).

67. S.T. Manson, A. Msezane, A.F. Starace, and S. Shababi, Phys. Rev. A, **20**(3), 1005 (1979).

68. S.T. Manson and A.F. Starace, Rev. Mod. Phys., **54**(2), 389 (1982).

69. W. Ong and S.T. Manson, Phys. Rev. A, **19**(2), 688 (1979).

70. A. Zangwill and P. Soven, Phys. Rev. A, **21**(5), 1561, (1980).

71. G. Herzberg, "Molecular Spectra and Molecular Structure, I. Spectra of Diatomic Molecules," Van Nostrand, New York, 1950.

72. A. Fahlman, T.A. Carlson, and M.O. Krause, J. Phys. B, **16**, L485 (1983).

73. A. Fahlman, T.A. Carlson, and M.O. Krause, Phys. Rev. Lett., **50**, 1114 (1983).

74. A. Fahlman, M.O. Krause, and T.A. Carlson, J. Phys. B, **17**, L217 (1984).

75. K. Faegri, Jr., and H.P. Kelly, Chem. Phys. Lett., **85**(4), 472 (1982).

76. K. Faegri, Jr., and H.P. Kelly, Phys. Rev. A, **23**, 52 (1981).

77. P. Pyykko and J-P. Desclaux, Acc. Chem. Res., **12**, 276 (1979).

78. D.D. Koelling and B.N. Harmon, J. Phys. C., **10**, 3107 (1977).

79. T. Takeda, Z. Physik B, **32**, 43 (1978).

80. J.H. Wood and A.M. Boring, Phys. Rev. B, **18**(6), 2701 (1978).

81. C.Y. Yang and S. Rabii, Phys. Rev. A, **12**(2), 362 (1975).

82. J.L. Dehmer, D. Dill, and A.C. Parr in "Photophysics and Photochemistry in the Vacuum Ultraviolet," edited by S. McGlynn, G. Findley, and R. Huebner, D. Reidel Press, Dordrecht, Holland, 1983.

83. W. Thiel, Chem. Phys., **77**, 103 (1983).

84. W. Thiel, Chem. Phys. Lett., **87**(3), 249 (1982).

85. C.E. Brion and J.P. Thomson, J. Electron Spectrosc. Relat. Phenom., **33**, 287 (1984). C.E. Brion and J.P. Thomson, J. Electron Spectrosc. Relat. Phenom., **33**, 301 (1984).

86. S. Daviel, Y. Iida, F. Carnovale, and C.E. Brion, Chem. Phys., **83**, 391 (1984).

87. J.H. Moore, J.A. Tossell, and M.A. Coplan, Acc. Chem. Res., **15**, 192 (1982).

88. J. Kessler, Comments Atom Mol. Phys., **10**(2-3), 47 (1981).

89. P. Dowben, unpublished results.

90. T.A. Carlson, M.O. Krause, F.A. Grimm, P.R. Keller, and J.W. Taylor, Chem. Phys. Lett., **87**(6), 552 (1982).

91. P. Senn, Ph.D. Dissertation, University of Tennessee, Knoxville, Tennessee, 1983.

92. J.G. Norman, J. Chem. Phys., **61**, 4630 (1974).

93. R. Latter, Phys. Rev., **99**, 510 (1955).

94. J.E. Bloor, R.E. Sherrod, and R.A. Paysen, Chem. Phys. Lett., **54**(2), 309 (1978).

95. N. Rösch, W.G. Klemperer, and K.H. Johnson, Chem. Phys. Lett., **23**(2), 149 (1973).

96. K. Kimura, S. Katsumata, Y. Achiba, T. Yamazaki, and S. Iwata, "Handbook of HeI Photoelectron Spectra of Fundamental Organic Molecules," Halsted Press, New York, 1981.

APPENDICES

APPENDIX I

THE USE OF REAL SPHERICAL HARMONICS AND SELECTION RULES

[This Appendix is reprinted from the Ph.D. dissertation of Dr. P. Senn[91] almost in its entirety.]

The wave functions in the Xα program are expressed in terms of real spherical harmonics.

Let Y_{lm} denote the usual complex spherical harmonics; the real spherical harmonics are denoted by y_{lm}. These can be formulated as products of θ- and φ-dependent parts. [Refer to Rose[37] for a treatment of angular momentum and the spherical harmonics.]

$$Y_{lm}(\theta,\phi) = (-1)^m (2\pi)^{-1/2} X_m(\phi) Z_{lm}(\theta) \qquad \text{A-I-1}$$

$$y_{lm}(\theta,\phi) = (-1)^m (\pi(1 + \delta_{m0}))^{-1/2} x_m(\phi) z_{lm}(\theta) \qquad \text{A-I-2}$$

where

$$Z_{lm}(\theta) = [\, (2l + 1)(l - |m|)!/ (2(l + |m|)!) \,]^{1/2} \; P_l^{|m|}(\cos\theta). \qquad \text{A-I-3}$$

P_l^m represents associated Legendre polynomials. The φ dependent parts are:

$$\begin{aligned} X_m(\phi) &= \exp(im\phi) && \text{for } m\geq 0 \\ &= (-1)^m \exp(im\phi) && \text{for } m<0, \end{aligned} \qquad \text{A-I-4}$$

and

$$\begin{aligned} x_m(\phi) &= \cos(m\phi) && \text{for } m\geq 0 \\ &= \sin(-m\phi) && \text{for } m<0. \end{aligned} \qquad \text{A-I-5}$$

In writing the photoionization program, Davenport[1] had the option of either converting the Xα program to the usual complex spherical harmonics or to adopt the

conventions of the Xα program. He chose the latter. He had to convert the Gaunt integrals

$$I(L, L', L'') = \int Y_L^* Y_{L'} Y_{L''} \, d\theta \, d\phi \qquad \text{A-I-6}$$

to "real" Gaunt integrals

$$I_R(L, L', L'') = \int y_L y_{L'} y_{L''} \, d\theta \, d\phi \qquad \text{A-I-7}$$

where the L's represent pairs of quantum numbers l and m.

The dipole moment operator in the molecular frame is

$$\mathbf{A} = \sum_v \mathbf{a}^{(v)} \qquad \text{A-I-8}$$

where $$\mathbf{a}^{(v)} = (4\pi/3)^{1/2} (-1)^v \, \mathbf{O}(r) \, Y_{1v}(r) \, \mathbf{D}^{(1)}(A)_{0v} \qquad \text{A-I-9}$$

In Equation A-I-9, A represents the molecular orientation and **O** is an operator which will depend on the representation chosen for the dipole moment operator [in our case, the acceleration form]. $\mathbf{D}^{(1)}(A)_{0v}$ is the (0,v) matrix element of the $l = 1$ representation of the rotation group. If we are dealing with linear molecules, the initial wave function can be chosen such that it contains spherical harmonics of a fixed projection quantum number, either in terms of real spherical harmonics or in terms of complex spherical harmonics. (A "fixed" projection quantum number means that we don't take linear combinations of Y_{lm} and $Y_{l,-m}$.)

The essential features of bound Xα wave functions for linear molecules are reproduced by

$$\psi_\lambda(\mathbf{r}) = \sum_{lj} c_{lvj} \, G_l(r_j) \, Y_{lv}(r_j), \qquad \text{A-I-10}$$

where j is the index of summation over the sites. If real spherical harmonics are used instead of Y in Equation A-I-10, the expansion coefficients, c_{lvj}, remain the same for linear molecules.

In Davenport's notation, an individual partial wave of the continuum wavefunction becomes

$$|E_\varepsilon \, l'\lambda'> = \sum_{l''\lambda''j} c_{l'\lambda' l''\lambda''j} \, F_{l''}(r_j) \, Y_{l'\lambda'}(k_I)^* \, Y_{l''\lambda''}(r_j), \qquad \text{A-I-11}$$

where k_I is the propagation vector of the free electron. According to Davenport[1] and Johnson[4] we can write the secular equations as

$$\sum_{j\,L'} G_{LL'}^{ij}\, C_{L'} = 0 \qquad \text{A-I-12}$$

where it has been assumed that the initial state is a bound state. The quantities G^{ij} are structure constants between pairs of sites i and j. They can be formulated as

$$G_{L'L}^{ij} = 4\pi \sum_{L''} i^{l+l''-l'}\, I(L, L', L'')\, z_{L''}(kR_{ij})\, Y_{L''}(R_{ij}), \quad \text{for } i \neq j, \qquad \text{A-I-13}$$

where the functions z are spherical Bessel functions of different types depending on whether the outer sphere is involved in the pair of sites. Notice that L'' does not refer to the initial state in Equation A-I-13, but simply serves as a summation index (over final state L's).

Davenport wrote his dissertation as though he had used the usual complex spherical harmonics. If i = j, the structure constants contain a factor

$$\delta_{l\,l'}\, \delta_{\lambda\lambda'}. \qquad \text{A-I-14}$$

For a linear molecule, R_{ij} lies along the z-axis, such that we have $\lambda'' = 0$. In this case, the Gaunt integrals of the complex spherical harmonics are nonzero only if $\lambda = \lambda'$. With real spherical harmonics, the Gaunt integrals are nonzero only if $\lambda = \pm \lambda'$, because $y_{l\,m} = Y_{l\,m} \pm Y_{l\,-m}$.

In the nonzero matrix elements, the integral over ϕ can be factored out. For real spherical harmonics

$$\langle E_\varepsilon\, l'\lambda' |\, \mathbf{a}^{(v)} \,|\, \psi_\lambda \rangle = [\,(1+\delta_{\lambda'0})\,(1+\delta_{v0})\,(1+\delta_{\lambda 0})/\,8\,]^{1/2} \times \int x_{\lambda'}\, x_v\, x_\lambda\, d\phi \quad \langle \ldots \rangle, \qquad \text{A-I-15}$$

and for complex spherical harmonics

$$\langle E_\varepsilon\, l'\lambda' |\, \mathbf{a}^{(v)} \,|\, \psi_\lambda \rangle = \int X_{\lambda'}\, X_v\, X_\lambda\, d\phi \quad \langle \ldots \rangle, \qquad \text{A-I-16}$$

where $\langle \ldots \rangle$ is the same in both A-I-15 and A-I-16. $\langle \ldots \rangle$ involves the integral over θ, and the radial dipole matrix element integral. The integration in A-I-16 can be

performed analytically

$$\int_0^{2\pi} \exp(i(\lambda + \nu - \lambda')\phi)\, d\phi = 2\pi\, \delta_{\lambda',\lambda+\nu} \qquad \text{A-I-17}$$

which gives the selection rule

$$\lambda' = \lambda + \nu. \qquad \text{A-I-18}$$

Besides the integral of Equation A-I-17, the integral in A-I-16 also contains a factor of

$$(-1)^{(\lambda S_\lambda + \nu S_\nu - \lambda' S_{-\lambda'}) + \lambda} \qquad \text{A-I-19}$$

where S represents a modal quantity

$$\begin{aligned} S_n &= 0 \quad \text{for } n \geq 0 \\ &= 1 \quad \text{for } n < 0. \end{aligned} \qquad \text{A-I-20}$$

For real spherical harmonics, the integration over ϕ gives a factor

$$[\, 8/ (1 + \delta_{\lambda'0})\, (1 + \delta_{\nu 0})\, (1 + \delta_{\lambda 0})\,]^{1/2} \int_0^{2\pi} \mathbf{S}(|\, \lambda' |\, \phi)\, \mathbf{S}(|\, \nu \,|\, \phi)\, \mathbf{S}(|\, \lambda \,|\, \phi)\, d\phi \qquad \text{A-I-21}$$

where S is the sine or cosine depending on the S_n of each of λ', ν, and λ.

The selection rule obtained from A-I-21 is different from that of Equation A-I-18. If the integrand of A-I-21 is not an even function , the integral vanishes. This gives

$$\mathrm{sgn}(\lambda')\, \mathrm{sgn}(\nu)\, \mathrm{sgn}(\lambda) > 0. \qquad \text{A-I-22}$$

If one of the projection quantum numbers is zero, the following relations apply

$$\begin{aligned} \int_0^{2\pi} \sin(n\phi) \sin(n'\phi)\, d\phi &= \delta_{n\,n'}\, \pi\, (1 - \delta_{n\,0}) \\ \int_0^{2\pi} \cos(n\phi) \cos(n'\phi)\, d\phi &= \delta_{n\,n'}\, \pi\, (1 + \delta_{n\,0}) \end{aligned} \qquad \text{A-I-23}$$

From this, we obtain:

1. if $\lambda = 0$ then $\lambda' = \nu$,
2. if $\nu = 0$ then $\lambda' = \lambda$,
3. if $\lambda' = 0$ then $\nu = \lambda$. A-I-24

The selection rule, obtained when using real spherical harmonics, becomes

$$\lambda' = \pm\lambda \pm \nu, \text{ except } \lambda' \neq \lambda, \text{ if } \lambda \neq 0. \qquad \text{A-I-25}$$

Let us set up some notation. For an initial orbital with the quantum number λ, we draw arrows to the possible symmetries of the partial waves of the final states. The arrows pointing to the right indicate the accessible partial waves, when expressing them in terms of real spherical harmonics, and arrows pointing to the left indicate the accessible partial waves, when expressing them in terms of complex spherical harmonics. In addition, we also indicate in square brackets the values of the matrix elements, excluding the quantity denoted $< \ldots >$ in Equations A-I-15 and A-I-16. Finally, the components ν of the nonzero matrix elements will also be indicated. Using this notation, we obtain the following scheme for the photoionization of a σ orbital:

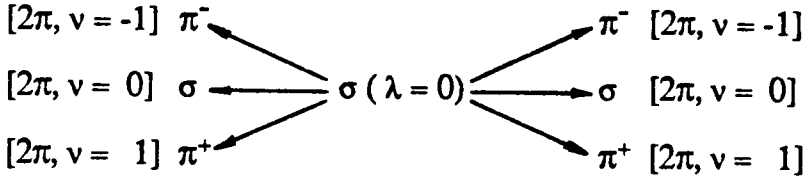

A-I-26

According to the above, the matrix elements obtained in the photoionization of σ orbitals are the same when using real or complex spherical harmonics.

For the photoionization of a π^+, orbital we obtain the following scheme:

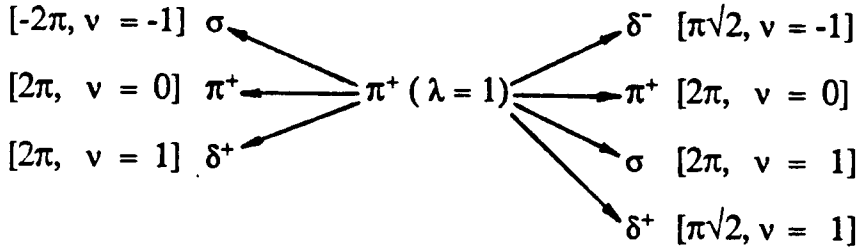

A-I-27

For the photoionization of orbitals with $|\lambda| \geq 2$, the following scheme arises:

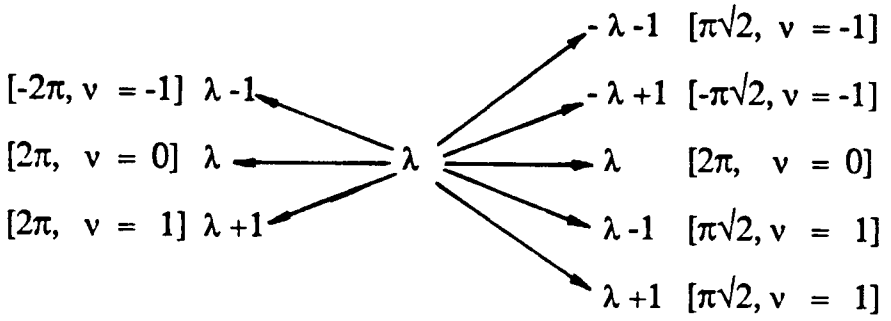

A-I-28

This gives us the selection rules for photoionization in linear molecules.

APPENDIX II

EXPERIMENTAL MEASUREMENT OF PHOTOELECTRON DYNAMICS PARAMETERS

In many modern PED experiments, photoelectrons are accepted for energy analysis over only a small solid angle due to the use of focusing slits. As pointed out in Chapter II, the photoelectron intensity, which is proportional to the differential cross section, is an angle dependent quantity from Equation II-19:

$$I(\theta, h\nu) \sim \left.\frac{d\sigma}{d\Omega}\right|_{\Omega=\Omega_1(\theta)} = \frac{\sigma_{tot}(h\nu)}{4\pi}\left[1 + \frac{\beta}{4}(1 + 3p\cos 2\theta)\right], \qquad \text{A-II-1}$$

where θ is the angle between the direction of the leaving electron and the major polarization axis of the incident photon beam measured perpendicular to the photon beam's direction of propagation (as shown in Figure II-3), and p is the polarization of the photon beam. $d\sigma/d\Omega$ is energy dependent.

Generally the proportionality constant relating experimentally measured intensity and the differential cross section is a function of angle:

$$I(\theta,h\nu) = C(\theta,h\nu)\left.\frac{d\sigma}{d\Omega}\right|_{\Omega=\Omega_1(\theta)}. \qquad \text{A-II-2}$$

$C(\theta,h\nu)$ results from the experimental geometry in-the-small and may be investigated by using an orbital for which $\beta(h\nu)$ is known at a given energy. (He 1s displays $\beta = 2$ very reliably.)

In principle, because only two parameters, $\sigma_{tot}(h\nu)$ and $\beta(h\nu)$, are being sought, intensity measurements at only two angles need be measured (aside from those needed to find the values of $C(\theta,h\nu)$ at these angles for this experimental set up). In practice, three measurements are made. $d\sigma/d\Omega$ has extrema at $\theta = 0$ and $\theta = \pi/2$ (regardless of the value of β) and varies least rapidly at angles surrounding these, i.e., its derivative

with respect to θ is zero at these points. Thus, experimental uncertainties in the detector angle and the effects of noise are minimized by measuring I(θ,hν) and I(π/2,hν) and taking the ratio at an energy hν:

$$R(h\nu) = \frac{I(0,h\nu)}{I(\pi/2,h\nu)} = \frac{C(0,h\nu)\ d\sigma/d\Omega|_{\Omega=\Omega 1(0)}}{C(\pi/2,h\nu)\ d\sigma/d\Omega|_{\Omega=\Omega 1(\pi/2)}}. \qquad \text{A-II-3}$$

If we set

$$R'(h\nu) = \frac{C(\pi/2,h\nu)}{C(0,h\nu)} R(h\nu) = C\,R(h\nu), \qquad \text{A-II-4}$$

then a little algebra brings us

$$\beta(h\nu) = \frac{4\,(R'(h\nu) - 1)}{3p\,(R'(h\nu) + 1) - (R'(h\nu) - 1)}. \qquad \text{A-II-5}$$

This is how β(hν) is measured experimentally. [In A-II-4 we have written C not as a function of energy, because most of the energy effects are common to all angles of measurement, that is, C(θ,hν) = C'(θ) K(hν). K(hν) includes the spectral dispersion of the light source, the collection efficiency for photoelectrons of a given energy, etc.]

Because β(hν) is a measured parameter subject to experimental error, as well as being energy dependent, it would be best to minimize its effect on the measurement of $\sigma_{tot}(h\nu)$. By examining Equation A-II-1, we see that for an angle such that

$$1 + 3p\cos 2\theta = 0, \qquad \text{A-II-6}$$

the differential cross section would be independent of angle. This is called the "magic angle," θ_m, and is given by

$$\theta_m = (1/2)\cos^{-1}(-1/3p). \qquad \text{A-II-7}$$

The relative energy dependence of $\sigma_{tot}(h\nu)$ may be measured at this angle without interference from β's influence:

$$I(\theta_m,h\nu) = C(\theta_m,h\nu)\ \sigma_{tot}(h\nu)/4\pi. \qquad \text{A-II-8}$$

The existence of the magic angle makes cross section measurement seem easier and more straightforward than β measurement, however, the difficulty of cross section measurement is buried in the energy dependence of $C(\theta_m,h\nu)$ whose complete treatment requires extensive and painstaking corrections.

Equations A-II-5 and A-II-8 relate the theoretically desired PED parameters to the experimentally measured intensities. Despite the formal simplicity of these equations and the straightforward intuitive appeal of the photoelectron intensity as a measured quantity, ample room for experimental error is available. Systematic and random errors involving the synchrotron light source include the time decay of the circulating electron beam causing decay of the output light intensity, and the critical experimental alignment due a high directional character of synchrotron radiation. Well-known random errors involved in counting the discrete photoionization events are present. Mostly systematic errors are introduced with the "efficiency" corrections for energy dependent monochromator transmission function, energy dependent efficiency of the electron energy analyzer, source region geometry and physics, and source region sample pressure variations.

The sympathetic reader will appreciate why in this dissertation we have compared theoretical and experimental <u>trends</u> in the PED parameters, rather than their <u>absolute values</u> at fixed energies.

Texts concerned with the experimental practice of electron spectroscopy[10,29] contain discussions of data analysis. As an example of the results of such analysis by one group--the ORNL group--we present in Figures A-II-1, 2, and 3 the first three bands of Cl_2, $2\pi_g$, $2\pi_u$, and $5\sigma_g$ from Reference 20. Bars indicate the (estimated) error limits of the PED parameters. It is difficult to determine a firm statistical interpretation of these error limits. It is fair to say that they represent a "high" confidence interval within which points are "expected" to lie. Points which do not lie within them are suspect and elicit either further investigation or "corrective" action. [These comments are not to be taken lightly. In designing an experiment and performing it for several years, a scientist develops an accurate sense of "acceptable" deviation.]

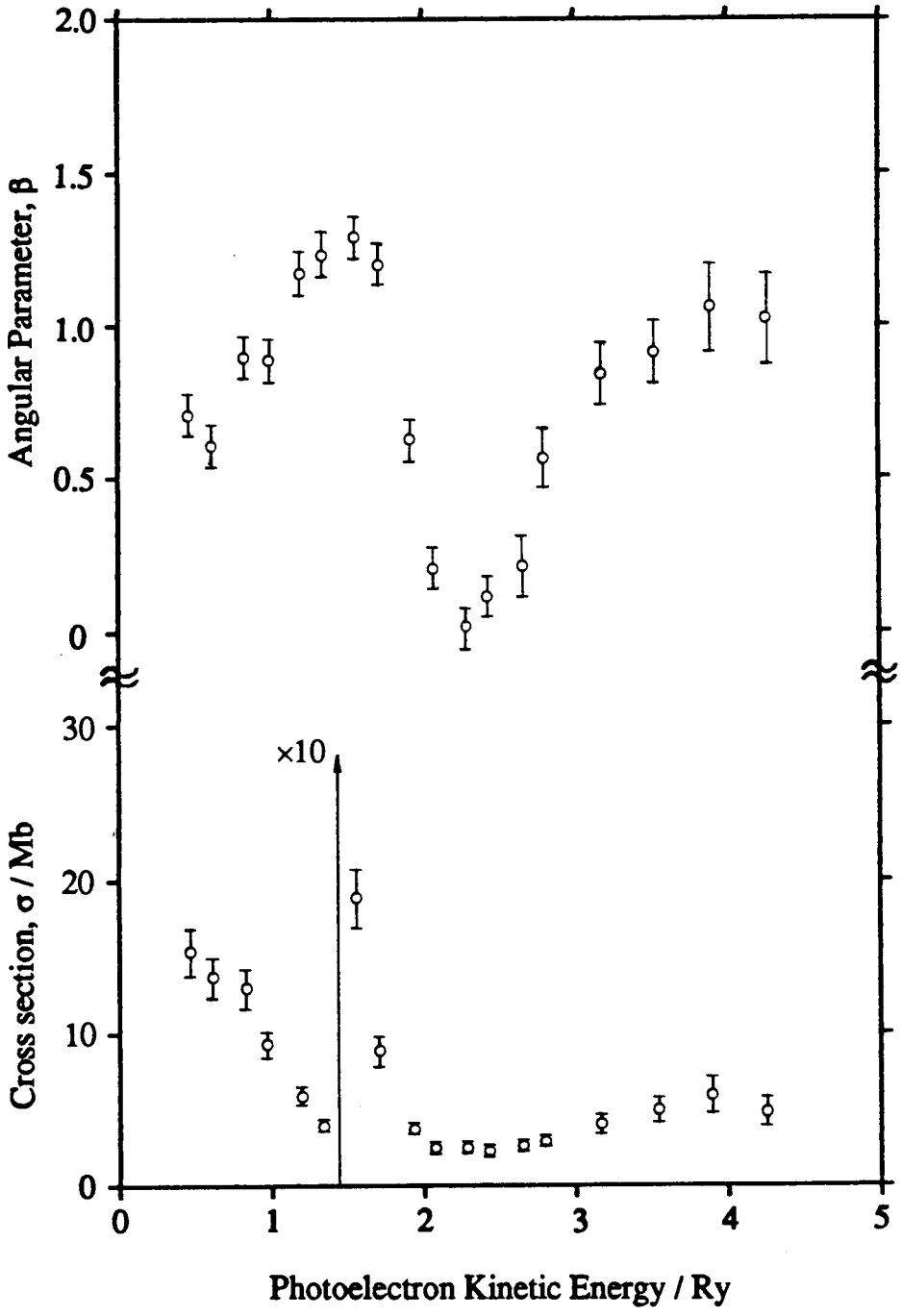

A-II-1. Experimental total cross section and angular parameter as a function of photoelectron kinetic energy for Cl_2 $1\pi_g$.

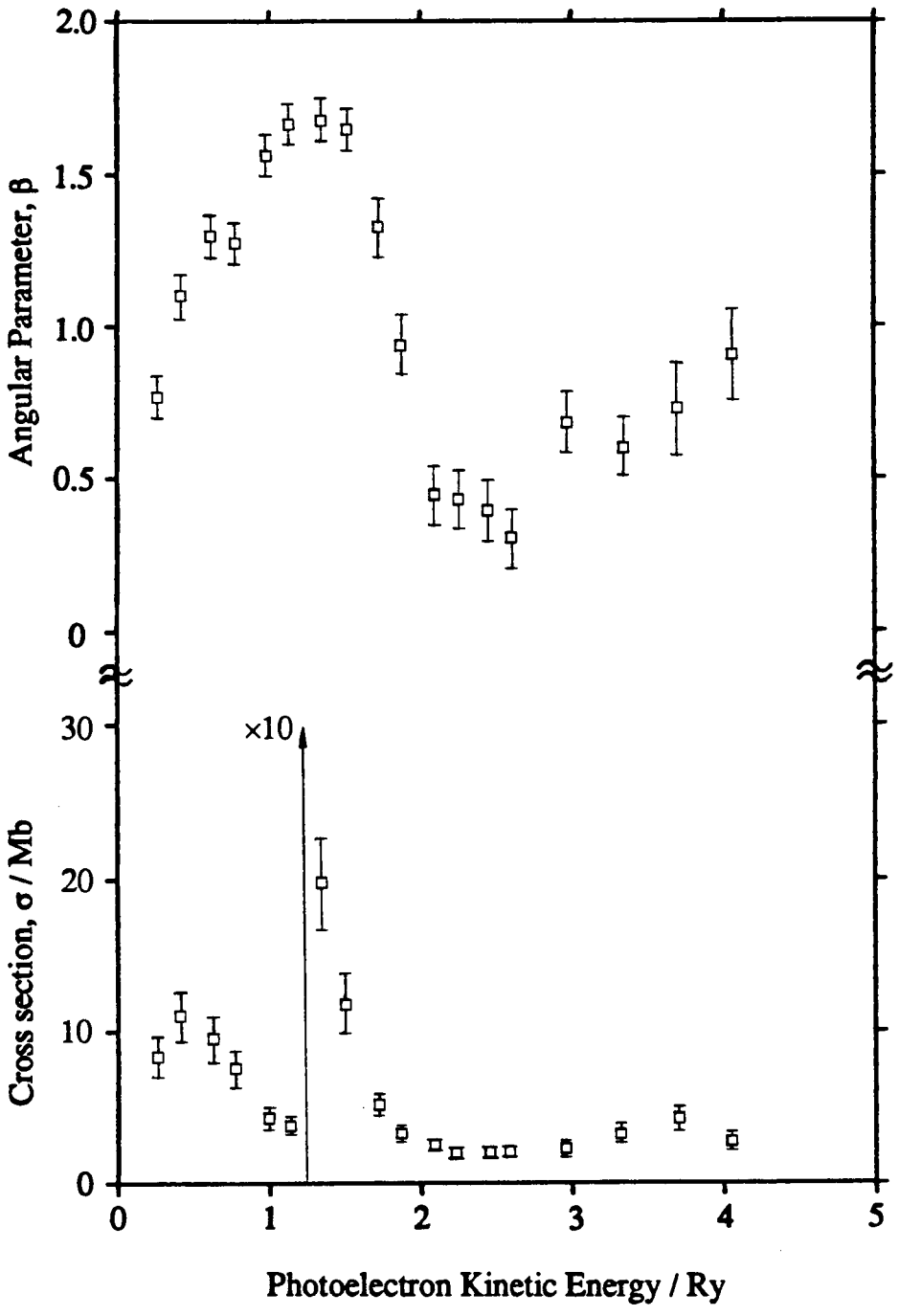

A-II-2. Experimental total cross section and angular parameter as a function of photoelectron kinetic energy for Cl_2 $1\pi_u$.

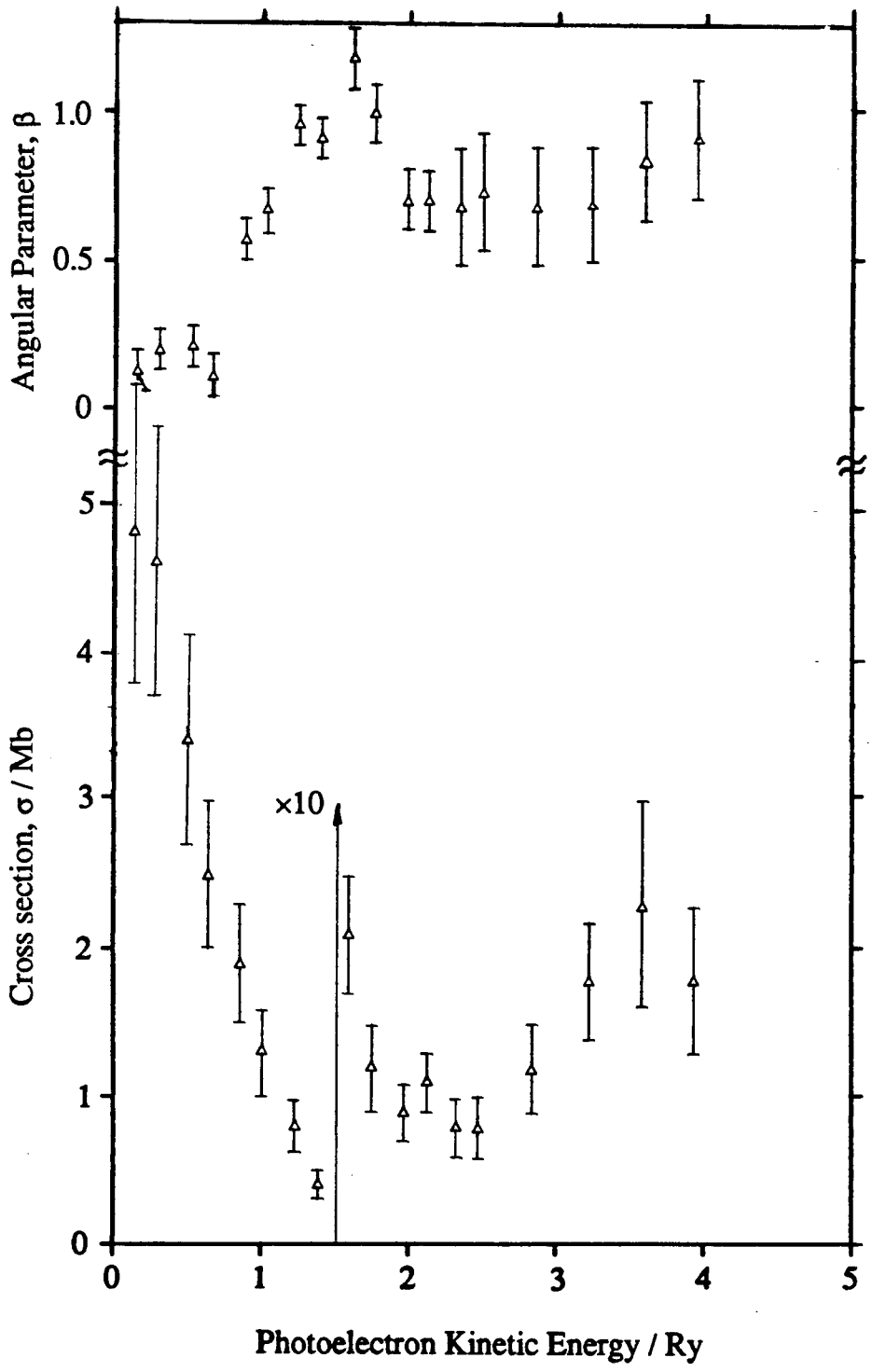

A-II-3. Experimental total cross section and angular parameter as a function of photoelectron kinetic energy for Cl_2 $2\sigma_g$.

APPENDIX III

EIGENPHASE SUMS AS A FUNCTION OF PHOTOELECTRON KINETIC ENERGY FOR THE ATOMS AND MOLECULES STUDIED

In the Figures are the unitless phase shifts, δ_ℓ/π, for the atoms and the eigenphase sums, $\mu_{sum} = \delta_{sum}/\pi$, for the molecules. All the "phases" have been shifted by units (δ_{sum} is shifted by π) in the Figures, so that they overlap as little as possible. The phases are determined only to the addition of a multiple of π.

The phase shifts for the halogen atoms are not presented. They closely resemble those for the noble gases.

Note that our phase shifts drop at resonances where others rise (References 50, 48, 49). This is due to Davenport's choice of outgoing wave normalization, i. e., there is a sign difference between our method and others'.

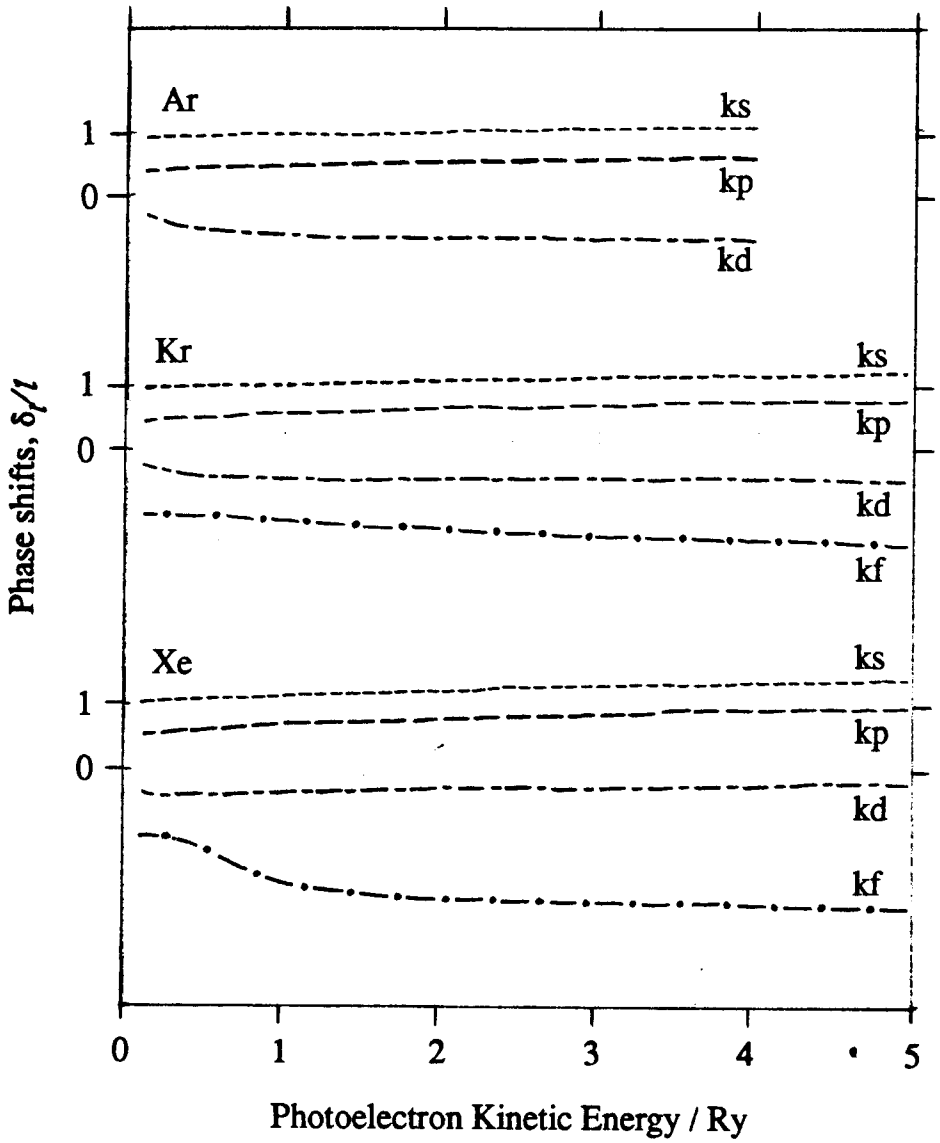

A-III-1 Phase shifts as a function of photoelectron kinetic energy for ks, kp, and kd channels of argon, krypton, and xenon.

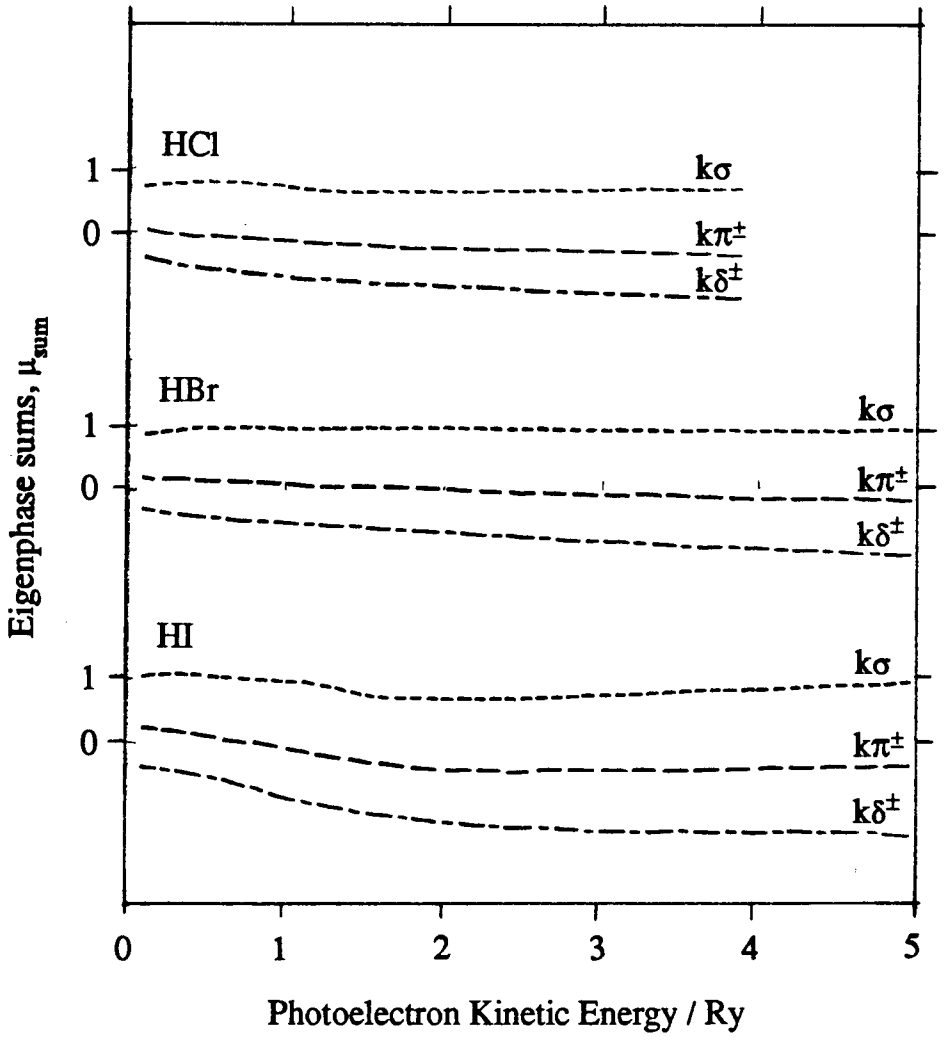

A-III-2. Eigenphase sums as a function of photoelectron kinetic energy for kσ, kπ, and kδ channels of HCl, HBr, and HI.

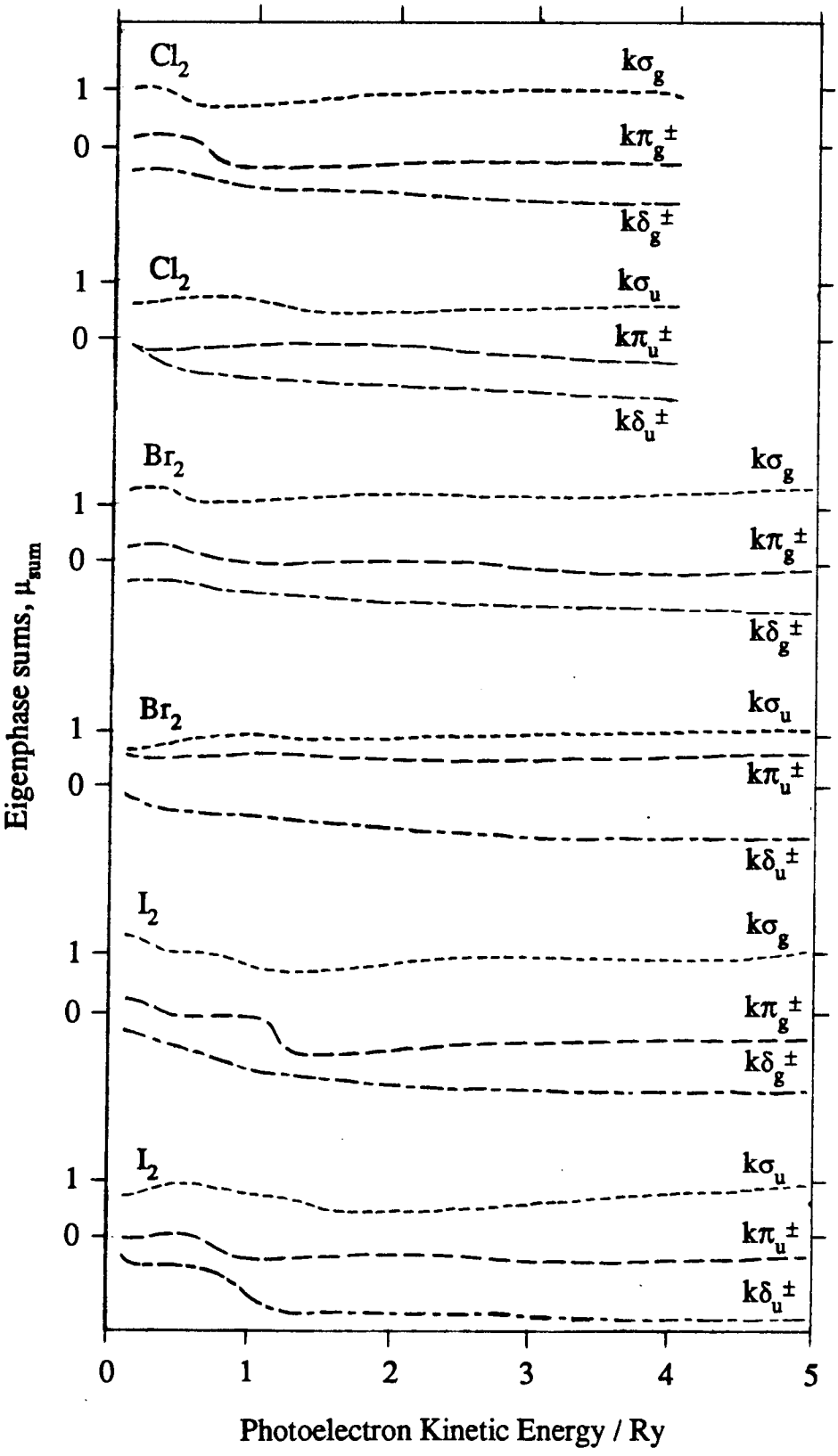

A-III-3. Eigenphase sums as a function of photoelectron kinetic energy for $k\sigma_g$, $k\pi_g$, $k\delta_g$, $k\sigma_u$, $k\pi_u$, and $k\delta_u$ channels of Cl_2, Br_2, and I_2.

APPENDIX IV

ATOMIC AND MOLECULAR ORBITALS WHICH DISPLAY COOPER MINIMA AND THEIR PROPER SYMMETRY LABELS

Orbitals which show Cooper minima are underlined.

Table A-IV-1. Atomic and molecular orbitals which display Cooper minima and their proper symmetry labels.

Noble Gases

Ar : $1s^2\ \underline{2s}^2\ 2p^6\ \underline{3s}^2\ \underline{3p}^6$

Kr : $1s^2\ \underline{2s}^2\ 2p^6\ \underline{3s}^2\ \underline{3p}^6\ 3d^{10}\ \underline{4s}^2\ \underline{4p}^6$

Xe : $1s^2\ \underline{2s}^2\ 2p^6\ \underline{3s}^2\ \underline{3p}^6\ 3d^{10}\ \underline{4s}^2\ \underline{4p}^6\ \underline{4d}^{10}\ \underline{5s}^2\ \underline{5p}^6$

Halogens

Cl : $1s^2\ \underline{2s}^2\ 2p^6\ \underline{3s}^2\ \underline{3p}^5$

Br : $1s^2\ \underline{2s}^2\ 2p^6\ \underline{3s}^2\ \underline{3p}^6\ 3d^{10}\ \underline{4s}^2\ \underline{4p}^5$

I : $1s^2\ \underline{2s}^2\ 2p^6\ \underline{3s}^2\ \underline{3p}^6\ 3d^{10}\ \underline{4s}^2\ \underline{4p}^6\ \underline{4d}^{10}\ \underline{5s}^2\ \underline{5p}^5$

Table A-IV-1. continued

Hydrogen Halides

HCl : $1\sigma^2_{Cl,1s}\ \underline{2\sigma^2}_{Cl,2s}\ 3\sigma^2_{Cl,2p}\ 1\pi^4_{Cl,2p}\ [\ \underline{4\sigma^2}_{Cl,3s}\ \underline{5\sigma^2}_{H\text{-}Cl}\ \underline{2\pi^4}_{Cl,3p}\ ]$

HBr: $1\sigma^2_{Br,1s}\ \underline{2\sigma^2}_{Br,2s}\ 3\sigma^2_{Br,2p}\ 1\pi^4_{Br,2p}\ \underline{4\sigma^2}_{Br,3s}\ \underline{5\sigma^2}_{Br,3p}\ \underline{2\pi^4}_{Br,3p}$

$6\sigma^2_{Br,3d}\ 3\pi^4_{Br,3d}\ 1\delta^4_{Br,3d}\ \ [\ \underline{7\sigma^2}_{Br,4s}\ \underline{8\sigma^2}_{Br,4p}\ \underline{4\pi^4}_{Br,4p}\ ]$

HI : $1\sigma^2_{I,1s}\ \underline{2\sigma^2}_{I,2s}\ 3\sigma^2_{I,2p}\ 1\pi^4_{I,2p}\ \underline{4\sigma^2}_{I,3s}\ \underline{5\sigma^2}_{I,3p}\ \underline{2\pi^4}_{I,3p}$

$6\sigma^2_{I,3d}\ 3\pi^4_{I,3d}\ 1\delta^4_{I,3d}\ \underline{7\sigma^2}_{I,4s}\ \underline{8\sigma^2}_{I,4p}\ \underline{4\pi^4}_{I,4p}\ \underline{9\sigma^2}_{I,4d}\ \underline{5\pi^4}_{I,4d}\ \underline{2\delta^4}_{I,4d}$

$[\ \underline{10\sigma^2}_{I,5s}\ \underline{11\sigma^2}_{H\text{-}I}\ \underline{6\pi^4}_{I,5p}\ ]$

Table A-IV-1. continued

Homonuclear Dihalogens

1s 2s 2p

Cl_2 : $1\sigma_g^2\ 1\sigma_u^2\ \underline{2\sigma_g^2\ 2\sigma_u^2}\ 3\sigma_g^2\ 3\sigma_u^2\ 1\pi_u^4 1\pi_g^4$

3s 3p

$[\ \underline{4\sigma_g^2\ 4\sigma_u^2}\ \underline{5\sigma_g^2\ 2\pi_u^4\ 2\pi_g^4}\ ]\ 5\sigma_u^0$

1s 2s 2p

Br_2 : $1\sigma_g^2\ 1\sigma_u^2\ \underline{2\sigma_g^2\ 2\sigma_u^2}\ 3\sigma_g^2\ 3\sigma_u^2\ 1\pi_u^4 1\pi_g^4$

3s 3p 3d

$\underline{4\sigma_g^2\ 4\sigma_u^2}\ \underline{5\sigma_g^2\ 5\sigma_u^2}\ \underline{2\pi_u^4\ 2\pi_g^4}\ 6\sigma_g^2\ 6\sigma_u^2\ 3\pi_u^4\ 3\pi_g^4\ 1\delta_g^4\ 1\delta_u^4$

4s 4p

$[\ \underline{7\sigma_g^2\ 7\sigma_u^2}\ \underline{8\sigma_g^2\ 4\pi_u^4\ 4\pi_g^4}\ ]\ 8\sigma_u^0$

1s 2s 2p

I_2 : $1\sigma_g^2\ 1\sigma_u^2\ \underline{2\sigma_g^2\ 2\sigma_u^2}\ 3\sigma_g^2\ 3\sigma_u^2\ 1\pi_u^4 1\pi_g^4$

3s 3p 3d

$\underline{4\sigma_g^2\ 4\sigma_u^2}\ \underline{5\sigma_g^2\ 5\sigma_u^2}\ \underline{2\pi_u^4\ 2\pi_g^4}\ 6\sigma_g^2\ 6\sigma_u^2\ 3\pi_u^4\ 3\pi_g^4\ 1\delta_g^4\ 1\delta_u^4$

4s 4p 4d

$\underline{7\sigma_g^2\ 7\sigma_u^2}\ \underline{8\sigma_g^2\ 8\sigma_u^2}\ \underline{4\pi_u^4\ 4\pi_g^4}\ 9\sigma_g^2\ 9\sigma_u^2\ 5\pi_u^4\ 5\pi_g^4\ 2\delta_g^4\ 2\delta_u^4$

5s 5p

$[\ \underline{10\sigma_g^2\ 10\sigma_u^2}\ \underline{11\sigma_g^2\ 6\pi_u^4\ 6\pi_g^4}\ ]\ 11\sigma_u^0$

APPENDIX V

INITIAL STATE ORBITALS' *l*-TYPE ANALYSES AND SUMMARY OF PARAMETERS AND OPTIONS USED IN CALCULATIONS

The following parameters and options were used in our calculations of the Xα-SW potentials presented in this dissertation.

Bond lengths were taken from Herzberg[71] and are presented in the following tables.

Values for α, the exchange parameter, were taken from Schwarz[43] and are presented in the following tables. In all calculations, one value of α was used for all regions, the value being that for the constituent atoms. For HX, the value of α for the halogen was used. When the same value of α is used in all regions, the virial theorem is satisfied, in principle. (See References 5, 92.)

A Latter tail potential[93] was used in the outer sphere region. In principle, this correction to the potential gives it the proper attractive Coulombic form at large distances. With this addition:

$V(r) = V(r)$ (as found by the Xα-SW method)

for all r such that $V(r) < -2/r_I$ (in Rydberg atomic units),

but

$V(r_I) := -2/r_I$

for all r_I such that $V(r_I) \geq -2/r_I$.

(We have used the notation ":=" to mean "is assigned the value of.")

Overlapping spheres and a transition state potential consisting of half an electron removed from the outermost orbital were used. (See References 94, 95, 92, 5.)

In the following tables:

1. Entries are percent *l*-type of the given orbital in a sphere. Within a sphere, for a given orbital, these should add up (across *l*) to 100% (within round-off error).

2. Entries in parentheses are the integrated percent charge for the given orbital in a sphere. These should add up (across spheres) to 100% (within round-off error).

3. The α values, sphere sizes, R_X, sphere locations along the z-axis, z_X (the outer sphere is centered at the origin of our coordinate system), and the bond lengths are shown.

4. Ionization energies for each orbital are shown. These may becompared to experimental values tabulated, for instance, in Reference 96.

5. "n" means less than 0.05.

6. "--" means not applicable, due to symmetry.

Table A-V-1. Atomic Initial State Orbitals' "l-type" analysis.

Noble Gas Atoms

		Ar		Kr			Xe		
		3p	3s	4p	4s	3d	5p	5s	4d
Orbital energies/Ry:		-1.15	-2.18	-1.01	-1.98	-6.57	-0.87	-1.61	-4.87
Atomic sphere	$l=0$	--	100.0	--	100.0	--	--	100.0	--
	$l=1$	100.0	--	100.0	--	--	100.0	--	--
	$l=2$	--	--	--	--	100.0	--	--	100.0
percent charge		(82.0)	(91.6)	(81.4)	(93.0)	(99.9)	(80.6)	(92.5)	(99.9)
Outer sphere	$l=0$	--	100.0	--	100.0	--	--	100.0	--
	$l=1$	100.0	--	100.0	--	--	100.0	--	--
	$l=2$	--	--	--	--	100.0	--	--	100.0
percent charge		(14.8)	(6.4)	(16.2)	(5.6)	n	(17.8)	(6.6)	n
Intersphere percent charge		(3.2)	(2.1)	(2.5)	(1.4)	n	(1.6)	(0.9)	n

$\alpha_{Ar} = 0.72177$ $\alpha_{Kr} = 0.70574$ $\alpha_{Xe} = 0.69$

$R_{Ar} = 2.30\ a_0$ $R_{Kr} = 2.60\ a_0$ $R_{Xe} = 3.00\ a_0$

Table A-V-2. Atomic Initial State Orbitals' "*l*-type" analysis.

Halogen Atoms

		Cl		Br			I		
		3p	3s	4p	4s	3d	5p	5s	4d
Orbital energies/Ry:		-0.99	-1.88	-0.90	-1.79	-6.26	-0.77	-1.44	-4.15
Halogen sphere	$l = 0$	--	100.0	--	100.0	--	--	100.0	--
	$l = 1$	100.0	--	100.0	--	--	100.0	--	--
	$l = 2$	--	--	--	--	100.0	--	--	100.0
percent charge		(74.5)	(86.9)	(77.9)	(91.4)	(99.9)	(74.6)	(89.4)	(99.9)
Outer sphere	$l = 0$	--	100.0	--	100.0	--	--	100.0	--
	$l = 1$	100.0	--	100.0	--	--	100.0	--	--
	$l = 2$	--	--	--	--	100.0	--	--	100.0
percent charge		(21.2)	(10.0)	(20.0)	(7.4)	n	(23.0)	(9.1)	n
Intersphere percent charge		(4.4)	(3.2)	(2.1)	(1.2)	n	(2.4)	(1.5)	n

$\alpha_{Cl} = 0.72325$ $\alpha_{Br} = 0.70606$ $\alpha_{I} = 0.69$

$R_{Cl} = 2.30\ a_0$ $R_{Br} = 2.60\ a_0$ $R_{I} = 3.00\ a_0$

Table A-V-3. Molecular Initial State Orbitals' "*l*-type" analysis.
Hydrogen Chloride Molecule

$\alpha = 0.72325$	$R_{Cl} = 1.901\ a_0$	$R_{out} = 2.500\ a_0$	
$R_{H\text{-}Cl} = 2.409\ a_0$	$R_H = 0.69\ a_0$		

		1π	2σ	1σ
Orbital energies/Ry:		-0.98	-1.10	-1.89
Chlorine	$l = 0$	--	4.5	99.6
sphere	$l = 1$	99.9	94.1	0.4
	$l = 2$	0.1	1.3	n
percent charge		(61.6)	(54.7)	(75.8)
Hydrogen	$l = 0$	--	98.5	96.4
sphere	$l = 1$	91.1	1.4	3.6
	$l = 2$	8.3	0.1	n
percent charge		(0.0)	(6.9)	(0.6)
Outer	$l = 0$	--	0.1	93.2
sphere	$l = 1$	93.4	97.2	5.9
	$l = 2$	6.3	1.4	0.8
	$l = 3$	0.4	1.3	n
	$l = 4$	n	n	n
percent charge		(18.7)	(19.3)	(9.1)
Intersphere percent charge		(19.6)	(19.0)	(14.5)

Table A-V-4. Molecular Initial State Orbitals' "l-type" analysis.
Hydrogen Bromide Molecule

$\alpha = 0.70606$	$R_{Br} = 2.2248\ a_0$	$R_{out} = 2.7933\ a_0$	
$R_{H\text{-}Br} = 2.6716\ a_0$	$R_H = 0.69\ a_0$		

		1π	2σ	1σ
Orbital energies/Ry:		-0.88	-1.00	-1.76
Bromine sphere	$l = 0$	--	3.3	99.6
	$l = 1$	99.9	95.0	0.4
	$l = 2$	0.1	1.4	n
percent charge		(63.3)	(56.0)	(80.2)
Hydrogen sphere	$l = 0$	--	98.9	95.4
	$l = 1$	92.6	1.1	4.4
	$l = 2$	7.0	n	0.2
percent charge		(0.0)	(6.8)	(1.3)
Outer sphere	$l = 0$	--	0.0	93.3
	$l = 1$	95.1	98.1	5.4
	$l = 2$	4.7	0.4	1.2
	$l = 3$	0.2	1.4	n
	$l = 4$	n	0.1	n
percent charge		(19.0)	(19.0)	(6.9)
Intersphere percent charge		(17.6)	(18.3)	(11.6)

Table A-V-5. Molecular Initial State Orbitals' "l-type" analysis.
Hydrogen Iodide Molecule

$\alpha = 0.69$	$R_I = 2.670\ a_0$	$R_{out} = 3.131\ a_0$	
$R_{H\text{-}I} = 3.031\ a_0$	$R_H = 0.561\ a_0$		

		1π	2σ	1σ
Orbital energies/Ry:		-0.78	-0.84	-1.44
Iodine	$l = 0$	--	2.2	99.6
sphere	$l = 1$	99.9	96.7	0.4
	$l = 2$	0.1	1.0	n
percent charge		(63.8)	(59.4)	(80.9)
Hydrogen	$l = 0$	--	99.4	97.8
sphere	$l = 1$	96.2	0.6	2.1
	$l = 2$	3.8	n	0.1
percent charge		(0.0)	(2.9)	(0.6)
Outer	$l = 0$	--	n	97.3
sphere	$l = 1$	97.8	99.2	2.1
	$l = 2$	2.2	0.1	0.5
	$l = 3$	n	0.7	0.1
	$l = 4$	n	n	n
percent charge		(21.8)	(21.9)	(8.6)
Intersphere percent charge		(14.4)	(15.8)	(9.9)

Table A-V-6. Molecular Initial State Orbitals' "*l*-type" analysis.

Chlorine Molecule

$\alpha = 0.72325$	$R_{Cl} = 2.0315\ a_0$
$R_{Cl\text{-}Cl} = 3.758\ a_0$	$R_{out} = 3.9105\ a_0$

		$1\pi_g$	$1\pi_u$	$2\sigma_g$	$1\sigma_u$	$1\sigma_g$
Orbital energies/Ry:		-0.87	-1.04	-1.13	-1.75	-2.00
Chlorine spheres	$l = 0$	--	--	4.2	96.8	94.8
	$l = 1$	99.3	99.1	94.1	2.7	4.3
	$l = 2$	0.6	0.8	1.7	0.4	0.8
	$l = 3$	0.1	0.1	n	0.1	0.2
percent charge		(74.7)	(68.2)	(80.9)	(85.9)	(85.4)
Outer sphere	$l = 0$	--	--	32.7	--	65.1
	$l = 1$	--	79.6	--	86.4	--
	$l = 2$	90.9	--	67.3	--	32.6
	$l = 3$	--	20.4	--	12.8	--
	$l = 4$	9.1	--	n	--	2.3
	$l = 5$	--	--	--	0.8	--
percent charge		(6.1)	(4.7)	(7.3)	(3.7)	(1.5)
Intersphere percent charge		(19.2)	(27.1)	(11.8)	(10.4)	(13.1)

Table A-V-7. Molecular Initial State Orbitals' "*l*-type" analysis.
Bromine Molecule

$\alpha = 0.70606$	$R_{Br} = 2.2248\ a_0$
$R_{Br\text{-}Br} = 4.312\ a_0$	$R_{out} = 4.3808\ a_0$

		$1\pi_g$	$1\pi_u$	$2\sigma_g$	$1\sigma_u$	$1\sigma_g$
Orbital energies/Ry:		-0.78	-0.91	-0.98	-1.66	-1.84
Bromine spheres	$l = 0$	--	--	3.1	98.2	97.2
	$l = 1$	99.5	99.4	95.5	1.5	2.3
	$l = 2$	0.3	0.5	1.2	0.3	0.4
	$l = 3$	0.1	0.1	0.2	n	0.1
percent charge		(71.2)	(64.5)	(76.5)	(86.4)	(84.3)
Outer sphere	$l = 0$	--	--	26.0	--	57.7
	$l = 1$	--	75.7	--	83.3	--
	$l = 2$	89.6	--	65.4	--	38.7
	$l = 3$	--	22.3	--	15.5	--
	$l = 4$	9.8	--	8.6	--	3.6
	$l = 5$	--	2.0	--	1.2	--
	$l = 6$	0.7	--	n	--	n
percent charge		(6.4)	(5.1)	(8.2)	(3.1)	(1.5)
Intersphere percent charge		(22.4)	(30.4)	(15.3)	(10.5)	(14.2)

Table A-V-8. Molecular Initial State Orbitals' "*l*-type" analysis.
Iodine Molecule

$\alpha = 0.69$	$R_I = 2.670\ a_0$
$R_{I\text{-}I} = 5.039\ a_0$	$R_{out} = 5.1895\ a_0$

		$1\pi_g$	$1\pi_u$	$2\sigma_g$	$1\sigma_u$	$1\sigma_g$
Orbital energies/Ry:		-0.69	-0.79	-0.85	-1.36	-1.51
Iodine spheres	$l = 0$	--	--	3.5	97.8	96.3
	$l = 1$	99.4	99.2	94.6	1.8	2.9
	$l = 2$	0.4	0.6	1.6	0.3	0.5
	$l = 3$	0.2	0.2	0.4	0.1	0.2
percent charge		(72.0)	(66.2)	(78.8)	(87.0)	(85.8)
Outer sphere	$l = 0$	--	--	27.1	--	55.7
	$l = 1$	--	72.3	--	81.9	--
	$l = 2$	88.7	--	63.8	--	40.5
	$l = 3$	--	25.3	--	16.7	--
	$l = 4$	10.6	--	9.2	--	3.8
	$l = 5$	--	2.4	--	1.4	--
	$l = 6$	0.7	--	n	--	n
percent charge		(5.6)	(4.3)	(7.6)	(2.9)	(1.3)
Intersphere percent charge		(22.4)	(29.5)	(13.6)	(10.1)	(12.9)

VITA

Timothy Alan Whitley was born on February 14, 1958, and raised in Memphis, Tennessee. He received his diploma from White Station High School in June 1976. The next September he entered Southwestern at Memphis (now named Rhodes College) as a Southwestern Scholar. In June 1980, he graduated cum laude with a Bachelor of Science degree in Chemistry.

He accepted a Graduate Teaching/Research Assistantship in the Department of Chemistry of the University of Tennessee at Knoxville and began his graduate studies in the fall of 1980. In the spring, he was awarded a three year Kodak Fellowship and joined the research group of Drs. Grimm and Carlson. He received the degree of Doctor of Philosophy in Chemistry in June 1985.

The author was married to Leslie Anne Ferda on September 1, 1984. He is a member of Phi Beta Kappa and the American Chemical Society. He is currently employed by the Tennessee Eastman Company.